The tensile properties of early age concrete and the experimental apparatus required for its determination

by

Diederick Dippenaar

Thesis presented in partial fulfilment of the requirements for the degree

Master of Structural Engineering at

Stellenbosch University

Supervisor: Mr R Combrinck

Co-supervisor: Prof WP Boshoff

Faculty of Engineering

Department of Civil Engineering

March 2015

Declaration

By submitting this thesis electronically, I declare that the entirety of the work contained therein is my own original work, that I am the authorship owner thereof (unless to the extent explicitly otherwise stated) and that I have not previously in its entirety or in part submitted it for obtaining any qualification.

Signature:

Date:

i

Summary

The early age cracking of concrete, which includes plastic shrinkage cracking (PShC) and plastic settlement cracking (PSeC), commonly occurs in flat concrete elements such as bridge decks and slabs or at the change of a concrete section depth. These cracks typically occur once the concrete has been cast and consolidated up to the final setting time, and initiate when the tensile stresses developed in the concrete exceeds its ultimate tensile strength or, alternatively phrased, when the restrained shrinkage induced strain in the concrete exceeds its tensile strain capacity. These cracks have a premature detrimental effect on the durability and strength of concrete structures as they allow deleterious materials to penetrate the concrete, which could cause the corrosion of steel reinforcing.

With this in mind, the objective of this study is to gain a fundamental understanding of the tensile properties of early age concrete, up to the point of final setting, as well as the variables that affect these properties. This is done to better understand, and ultimately reduce the risk of early age cracking. To achieve this, experimental assemblies found in literature were evaluated and built upon to create a multi-component uniaxial tensile testing setup that is able to capture the complete stress-strain behaviour of early age concrete, while still in a plastic state. The following significant findings were attained from this study:

- Reducing the coarse aggregate size in a concrete mix increases both the tensile strength and Young's modulus of early age concrete, while reducing both its fracture energy and fracture process zone (FPZ) characteristic length.
- The low volume addition of microfibres to a conventional concrete mix increases both the fracture energy and the FPZ characteristic length of early age concrete.
- The low volume addition of microfibres to a conventional concrete mix increases the strain capacity of early age concrete shortly before and after the initial setting time. This increased strain capacity is believed to be of great significance for the prevention of PShC.
- The addition of an accelerator to a conventional concrete mix accelerates the development of the tensile properties of early age concrete, while a retarder reduces it.
- The addition of a retarder to a conventional concrete mix increases the strain capacity of early age concrete shortly before and after the initial setting time. This provides a reason for the reduced PShC severity observed in retarded mixes in certain instances.

From this study it is concluded that the results from the tensile tests provide a greater understanding of the tensile properties of early age concrete as well as the variables that affect them. When interpreting these results in combination with those obtained from PShC experiments, it is suggested that it is possible to determine when and if PShC will occur.

Opsomming

Die vroëe-ouderdom kraking van beton, wat plastiese krimp krake (PKK) en plastiese versakkings krake (PVK) insluit, kom algemeen voor in plat betonelemente soos brug-dekke en blaaie, of by die die verandering in die deursnit diepte van betonelemente. Die krake kom tiepies voor vandat beton gegiet en gekompakteer is totdat dit die finale settyd bereik, en vind plaas sodra die trekspanning wat in die beton ontstaan sy treksterkte oorskry of, anders bewoord, wanneer die verhinderde krimp geinduseerde vervorming van die beton, die vervormings-kapasiteit van die beton oorskry. Hierdie krake het 'n voortydige nagelige uitwerking op die duursaamheid en sterkte van betonstrukture aangesien hulle toelaat dat skadelike stowwe die beton binnedring, wat die korrosie van staalbewapening veroorsaak.

Met dit ingedagte is die doel van die studie om fundamentele kennis rakende die vroëe-ouderdom trekeienskappe van beton, tot by die punt van finale set, asook die veranderlikes wat die eienskappe beinvloed, te verwerf. Om vroëe-ouederdom krake beter te verstaan en uiteindelik, te voorkom, is hierdie kennis nodig. Eksperimentele opstellings in literatuur is ge-evalueer en op voortgebou vir die bou van 'n multi-komponet eenassige terktoetsopstelling om die volledige spanning-vervorming gedrag van vroëe-ouderdom beton vas te vang. Die volgende bevindings het uit die studie aan die lig gekom:

- 'n Kleiner aggregaat grootte in n betonmeng verhoog beide die trekstrekte en Young se modulus van vroëe-ouderdom beton, terwyl dit beide die fraktuur-energie en die fraktuur proses sone (FPS) se karakteristieke lengte verminder.

- Die lae volume byvoeging van mikrovesels tot 'n betonmeng verhoog beide die fraktuur-energie en die FPS se karakteristieke lengte van vroëe-ouderdom beton.

- Die lae volume byvoeging van mikrovesels tot 'n betonmeng verhoog die vervormings kapasiteit van vroëe-ouderdom beton kort voor en na die aanvanklike settyd. Daar word geglo dat hierdie verhoogde vervormings-kapasiteit van groot belang is vir die voorkoming van PKK.

- Die byvoeging van 'n versneller tot 'n betonmeng versnel die ontwikkelingstempo van die trekeienskappe van vroëe-ouderdom beton, terwyl 'n vertrager dit verlaag.

- Die byvoeging van 'n vertrager tot 'n betonmeng verhoog die vervormings-kapasiteit van vroëe-ouderdom beton kort voor en na die aanvanklike settyd. Dit verskaf die rede vir die bevinding dat die byvoeging van 'n vertrager PKK in sekere gevalle verminder.

Hierdie studie het bevind dat die die trektoetse 'n groter begrip rakende die trek-eienskappe van vroëe-ouderdom beton, en die veranderlikes wat die eienskappe beinvloed, gelewer het. Wanneer die resultate van die studie tesame met PShC toetse geinterpreteer word, will dit voorkom dat dit moontlik is om te bepaal wanneer, en of PKK sal plaasvind.

Acknowledgements

I would like to thank the following people for their assistance and support during this study:

Table of Contents

List of Figures

List of Tables

Notations and Acronyms

Notations:

d	Fibre diameter [μm]
E	Young's modulus [MPa]
f_t	Tensile strength [kPa]
G_f	Fracture energy [J/m^2]
L	Fibre length [mm]
l_{ch}	Characteristic length [m]
P	Capillary pressure [Pa]
R_1	Maximum radius of water meniscus [mm]
R_2	Minimum radius of water meniscus [mm]
V_f	Volume fraction of fibres added to mix [%]
W	Crack opening displacement [mm]
W_c	Critical crack opening displacement [mm]
δ_c	Crack displacement [mm]
δ_0	Zero force transfer displacement [mm]
δ_e	Elastic deformation [mm]
δ_{ine}	Inelastic deformation [mm]
ε_c	Strain capacity [μ]
γ	Surface tension [Pa]
$\dot{\gamma}$	Shear rate [s^{-1}]
μ_p	Plastic viscosity [CP]
τ	Interfacial shear bond stress [kPa]

τ_0 Yield stress [Pa]

σ_{cu} Ultimate bridgind stress over unit crack area [Pa]

Acronyms:

COD	Crack opening displacement
C-S-H	Calcium Silicate Hydrate
FCM	Fictitious crack model
FPZ	Fracture process zone
LVDT	Linear variable differential transformer
LV-FRC	Low Volume - Fibre Reinforced Concrete
MA9	Mix Aggregate 9 mm
MA19	Mix Aggregate 19 mm
MF0.6	Mix Fibre 0.6 kg per cubic meter concrete
MF1.8	Mix Fibre 1.8 kg per cubic meter concrete
MR	Mix Reference
MSA	Mix Setting Accelerated
MSR	Mix Setting Retarded
NRMCA	National Ready Mixed Concrete Association
OPC	Ordinary Portland Cement
PSeC	Plastic settlement cracking
PShC	Plastic shrinkage cracking
SANS	South African National Standards
SAPY	South African Polypropylene Yarns

1. Introduction

The early age cracking of concrete often occurs in concrete elements with large exposed surface areas compared to concrete volumes, such as bridge decks and slabs, which are exposed to environmental conditions conducive to high evaporation rates, or over the change of concrete section depth. These cracks typically occur once the concrete has been cast and consolidated up to the final setting time. Early age cracking includes plastic shrinkage cracking (PShC) and plastic settlement cracking (PSeC) and are primarily caused by differential settlement and capillary pressure build-up, which are the mechanisms responsible for the development of stress in plastic concrete (Slowik, et al., 2008 & Wittmann, 1976). Crack onset occurs when the tensile stresses developed in the concrete exceeds its ultimate tensile strength or, alternatively phrased, when the restrained shrinkage induced strain in the concrete exceeds its tensile strain capacity. These cracks can have a premature detrimental effect on the durability and strength of concrete structures as it allows deleterious materials to penetrate the concrete which could cause the corrosion of reinforcing steel (Qi, 2003).

For this reason a fundamental understanding of the tensile properties of early age concrete and the variables that affect them are imperative in order to understand and reduce the risk of early age cracking. Ultimate tensile strength, tensile strain capacity and Young's modulus, all as a function of time, are the essential properties to be determined as they are required as input parameters to conduct a numerical analysis of early age concrete behaviour. This can ultimately be used to prevent and predict the early age cracking of concrete. The additional parameters of fracture energy and characteristic length are also required as they convey valuable information about the post-cracking behaviour of early age concrete.

The need for a greater fundamental understanding of the early age tensile properties of concrete has been apparent to the broader academic community for decades (Dao, et al., 2009). Despite this fact, there remains limited research available on this topic, specifically related to the measurement of the full stress-strain behaviour of early age concrete. A suggested reason for this is the substantial practical difficulties that need to be overcome in experimentally determining the early age tensile properties of concrete. The application of fracture mechanics to early age concrete fracture is also in its infancy.

With this in mind, the objectives of this study were:

- To provide an fundamental understanding of the tensile properties of early age concrete

- To build upon the experimental assemblies found in literature to allow the uniaxial tensile testing of concrete, while still in a plastic state, to capture the complete stress-strain curve of early age concrete specimens.

- To determine the effect of coarse aggregate size, the addition of microfibres in different volume fractions and the use of setting time altering admixtures on the ultimate tensile strength, strain capacity, Young's modulus, fracture energy and characteristic length of concrete.

- Finally, to interpret the results of the tensile test conducted in this study in combination with the results obtained from PShC tests, in order to gain a better understanding of the fundamental behaviour of PShC and how the tensile properties of an early age concrete affects its occurrence.

The following methodology was adopted to achieve the objectives of this study:

1. Gaining a fundamental understanding of the early age behaviour and tensile properties of concrete. This involved a background study on concrete rheology, setting and early age tensile properties and fracture mechanics. A literature review on early age cracking, which includes PShC and PSeC, was also conducted to identify their mechanisms and influencing factors. The fundamental concepts of low volume fibre reinforce concrete (LV-FRC) was also covered as it is of significance to this study.

2. The main emphasis of this literature study was gaining knowledge to better understand the period in which the early age cracking of concrete occurs and to identify the relevant material properties that need to be determined in order to understand the early age tensile behaviour of concrete. So as to determine the essential tensile properties required for this study, the acquisition of the complete stress-strain behaviour of early age concrete specimens was required.

3. Next, an experimental test setup to measure the complete stress-strain behaviour of early age concrete was constructed. This involved an extensive background study on the tensile testing of early age and mature concrete. This study considered direct tensile testing apparatus with the intension of determining, tensile strength, strain capacity and Young's modulus as well as apparatus with the purpose of determining fracture parameters. An initial test setup was also constructed.

4. Once a reliable test setup and experimental method had been established, test were conducted to determine the effect of coarse aggregate size, the addition of

microfibres in different volume fractions and the use of setting time altering admixtures on the tensile properties of early age concrete.

5. Finally, these results were evaluated in order to gain a fundamental understanding of the tensile properties of early age concrete and the variables that affects them.

This report has the following outline:

- In *Chapter 2* a background on the rheology and mechanisms causing setting is presented. After this the tensile properties of early age concrete and a review on fracture mechanics and its application in early age concrete is given.

- In *Chapter 3* provides a background study on the early age cracking of concrete, which include both PShC and PSeC. The mechanisms, influencing factors and precautionary measures associated with these cracks are discussed. Finally, low volume fibre reinforced concrete is also considered.

- In *Chapter 4* the experimental tensile test setup used in this study is discussed. Firstly, a background study on the various apparatus needed is presented. Next, an initial test setup is evaluated. Finally, the final test setup is described in detail.

- In *Chapter 5* the experimental programme and tensile testing method is discussed. Firstly, the objectives of the experimental work are presented whereafter the experimental programme and concrete mix designs are discussed. Finally, a detailed description of the experimental test procedure is presented.

- In *Chapter 6* the results with regards to the complete stress-strain curve of early age concrete is discussed.

- In *Chapter 7* the tensile properties of early age concrete with regards to pre-cracking behaviour is discussed.

- In *Chapter 8* the tensile properties of early age concrete with regards to post-cracking behaviour is discussed.

- In *Chapter 9* cracking and material behaviour are discussed and finally, a link is drawn between the results of this study and those of PShC tests.

- In *Chapter 10* the final conclusions and recommendations are presented.

- The *Appendices* contains details regarding the main components of the tensile testing setup, the full stress-strain curves of early age concrete specimens and a summary of the tensile properties of the various early age concrete specimens.

2. Background study on the tensile properties of early age concrete

This chapter discusses the early age tensile properties of concrete. Firstly, it provides an overview of the fresh concrete rheology and the mechanisms causing setting and the development of mechanical properties. Next, the tensile properties of early age concrete are discussed with regards to tensile strength, strain capacity as well as the Young's modulus. Finally, the field of fracture mechanics and its application to the tensile cracking of early age concrete is discussed.

In this study the term fresh concrete refers to concrete directly after it has been cast and consolidated while it is still workable and plastic, up to the initial setting time. Early age concrete, on the other hand, refers to concrete directly after it has been cast to the point of significant strength gain, which coincides with the final setting time. The period in which plastic settlement cracking (PSeC) and plastic shrinkage cracking (PShC) occur coincides with this early age period of concrete as defined in this study and is therefore of significant importance.

2.1 Rheology and setting of concrete

Immediately after the placing of concrete it is still in a plastic or at least semi-fluid state. The constituent materials are still able to move relatively freely. As initial setting commences the concrete changes into a rigid material which is unable to flow, while possessing little strength. For the material to gain significant strength, it must not be disturbed during this fragile period. With a further increase in time the material solidifies and stiffens further, with significant hardening and strengthening only occurring once the final setting time is reached (Illston & Domone, 2001).

This section first describes the rheological behaviour of fresh concrete, whereafter the process of setting and the mechanisms leading to the development of the mechanical properties of concrete are discussed.

2.1.1 Rheological properties

To better understand concrete in its plastic state, where it is in a phase between a liquid and a solid, the flow principles of rheology needs to be applied. Conventional fresh concrete behaves like a yield stress fluid. Where Newtonian fluids deform continuously under the influence of a shear stress, regardless of the magnitude of the stress, a minimum applied stress value exists for yield stress fluid at which irreversible deformation and flow occurs. For

this reason conventional fresh concrete stands as a heap, and only flows once a certain shear stress, defined as its yield stress, is applied (Illston & Domone, 2001).

The general consensus is that the yield stress model of fresh concrete is best described by the Bingham model as illustrated in Figure 2.1 (Illston & Domone, 2001).

Bingham behaviour: $\tau = \tau_0 + \mu_p \dot{\gamma}$

Bingham fluid

μ_p

Shear stress (τ)

Newtonian fluid

τ_0

Rate of shear strain ($\dot{\gamma}$)
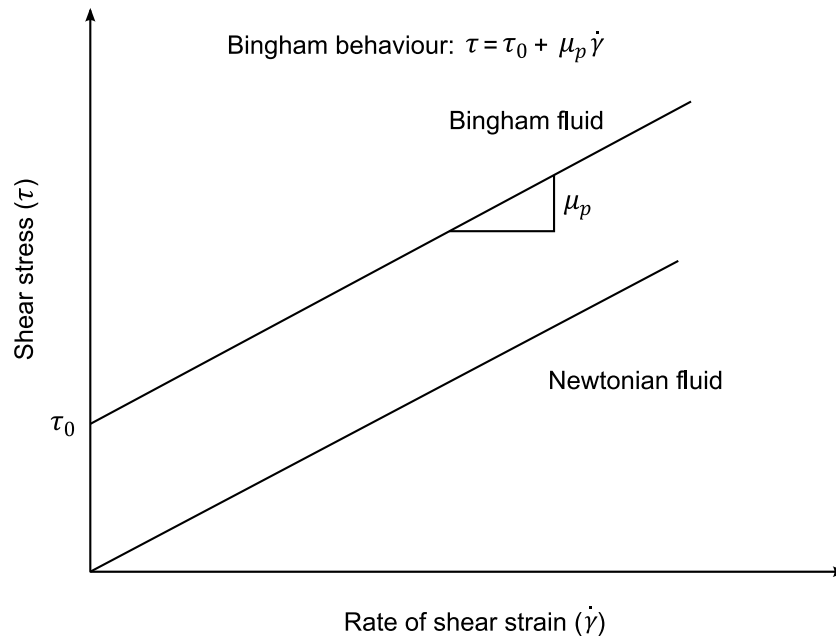
Figure 2.1: Flow curve of fresh concrete (Bingham fluid) and water (Newtonian liquid) (Illston & Domone, 2001)

For an approximate physical interpretation of the Bingham model, fresh concrete can be seen as a granular mixture consisting of cement or other binders, fine aggregates and coarse aggregates in a water suspension. For the purpose of this exercise, trapped air will be ignored. The minimum volume of water in the concrete can be seen as the volume that corresponds to that of the total porosity of the dry aggregate system. A concrete with no workability is thus a packing in which the system porosity is filled with water. Figure 2.2 illustrates a suspension with minimum water content. No shearing movement is possible without localised rupture of the particle structure (Ferraris & de Larrard, 1998).
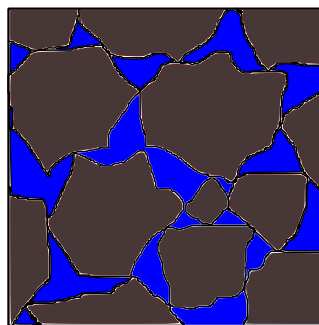
Figure 2.2: Concrete with minimum water content and zero workability (Ferraris & de Larrard, 1998)

5

If the water content in the system is increased to a higher than minimum volume, it results in the occurrence of water filled spaces between the solid particles. Sliding between particles can now be initiated, as illustrated in Figure 2.3. A deformation of the system will occur if an applied shear force is greater than the friction forces between solid particles. Consequently, the yield stress will be governed by the number and nature of the contact regions between solid particles. The excessive free water will influence the average distance between these solid particles. From this the deduction can be made that an addition of water above the minimum volume needed to fill all voids in the system will lead to a decrease in shear resistance and viscosity (Ferraris & de Larrard, 1998).
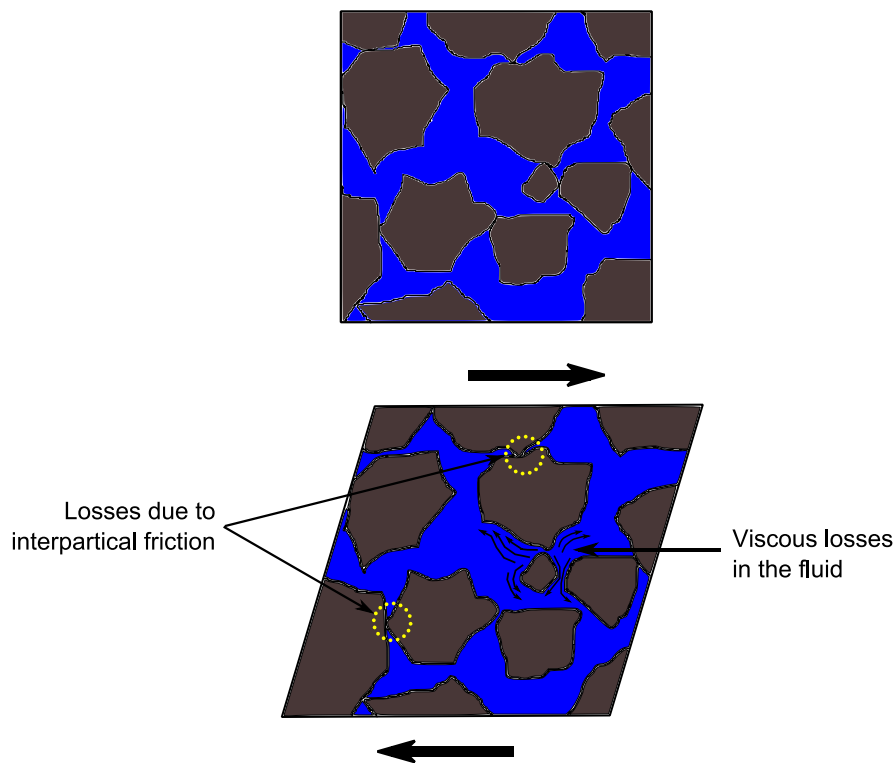
Figure 2.3: Concrete with more than minimum water content and a degree of workability (Ferraris & de Larrard, 1998)

When observing the microstructure of this material, the assumption can be made that the speed of an individual particle is the same as that of the macroscopic homogenised fluid, in this case fresh concrete. The contribution to shear resistance of the fluid is proportional to the global strain gradient of the system if one assumes a laminar flow regime for the fluid while flowing between the solid particles (Ferraris & de Larrard, 1998). This behaviour is described by the Bingham model as:

$$\dot{\gamma} = 0 \rightarrow \tau < \tau_0 \dots\dots\dots\dots\dots\dots\dots\dots\dots\dots\dots\dots\dots\dots\dots\dots\dots\dots\dots\dots\text{(Equation 2.1)}$$

$$\dot{\gamma} \neq 0 \rightarrow \tau = \tau_0 + \mu_p.\dot{\gamma} \dots\dots\dots\dots\dots\dots\dots\dots\dots\dots\dots\dots\dots\dots\dots\dots\dots\text{(Equation 2.2)}$$

6

The term τ_0 can be seen as the shear resistance contributed by the particle structure whereas the term $\mu_p.\dot{\gamma}$ defines the contribution of the suspended liquid.

To better visualise this, the vibration of a fresh concrete specimen can be seen as an applied shear stress. Flow of fluid takes place against frictional resistance offered by the immediate layer in contact with the moving layer and a velocity gradient exists along the transverse direction of laminar flow. The relevant flow property is viscosity. A cohesive concrete shall be more resistant to segregation under the effect of an applied shear stress as cohesiveness is governed by the shear strength of fresh concrete.

In reality, the full rheological behaviour of early age concrete is much more complex than the physical interpretation presented. It is a result of a multifaceted interaction between numerous physical phenomena which is currently only partially understood. At this early age the variety of multi-phase components of concrete causes at least four main interactions. These interactions include surface forces, Brownian forces, hydrodynamic forces and various contact forces between particles. The size of particles, the volumes fraction of constituent materials and external influences determine which of these interactions are dominant (Kovler & Roussel, 2011).

2.1.2 The Setting and hardening of concrete

This section gives an overview of the physical and chemical processes responsible for the stiffening, setting and hardening of early age concrete.

Hydration

Hydration is the chemical reaction between cement and water that is responsible for transforming concrete from a viscous suspension upon mixing, to a rock-like material, with the passing of time. Aluminates (C_3A) and silicates (C_3S and C_2S) are the compounds present in Portland cement that have the most significant influence on the hydration process. The rate at which aluminates hydrate is much greater than that of silicates. As a result, aluminates play a greater role in the stiffening and solidification stages of concrete, whereas silicates contribute primarily to the hardening and the ultimate strength of the concrete (Mehta & Monteiro, 2014).

A typical CEM I would compose of about 11.5% aluminates and 73.5% silicates whereas a CEM II would consist of 7.2% aluminates and 74.7% silicates. Because CEM II has comparatively lower aluminate content, it will set slower that the CEM I. The ultimate strength will however be nearly identical to that of the CEM I (Mehta & Monteiro, 2014)

In addition to the cement composition, the fineness of cement also affects its reactivity with water. The finer the cement, the more rapidly the hydration process will take place and consequently setting will occur earlier. Concrete with high water to cement ratios also typically requires a higher degree of hydration and consequently more time to achieve setting. This is primarily due to larger initial cement particle spacing that needs to be overcome for hydration products to interlock (Bentz, 2008).

Knowledge of the hydration reaction is of great significance as it determines the ultimate strength as well as the time of setting and hardening of concrete. Initially the hydration reaction must be slow enough for the concrete to be placed and finished. After this has occurred it is desired that the concrete hardens at a fast rate to ensure that it is not damaged during further construction and to allow the structure to support loads as soon as possible (Mehta & Monteiro, 2014).

Stiffening, setting and hardening

Stiffening is the process of plastic concrete losing its ability to flow. It commences directly after concrete has been mixed. Stiffening is typically associated with a loss of slump as the age of the fresh concrete increases. This process occurs as a result of the loss of free water from the concrete system as it is mainly free water that is responsible for the plasticity of fresh concrete, as described in the previous section. This loss is brought about due to evaporation, absorption by unsaturated aggregates or sub-grade as well as free water taking part in the hydration reaction to form hydration products. At this stage it is primarily aluminates (C_3A) that take part in the hydration process (Mehta & Monteiro, 2014).

When fresh concrete is left undisturbed it builds up an internal structure through the interlocking of hydration products. The most destructured state of concrete is directly after mixing (Kovler & Roussel, 2011). At a later stage surface adsorption by crystalline hydration compounds such as ettringite and calcium silicate hydrate (C-S-H), result in further stiffening and ultimately, the setting and hardening of the cement paste (Mehta & Monteiro, 2014).

Setting refers to the solidification of the plastic cement paste through hydration. The setting of a specific concrete is understood to start at its initial setting time and end at its final setting time. These setting times are determined by means of penetration resistance methods, usually using a Vicant apparatus. These penetration methods do not account for a specific change in the physical or chemical characteristics of the concrete but are rather defined by when the concrete microstructure offers some finite mechanical resistance to penetration or shear (Bentz, 2008). In the case of the initial setting time, it defines the time at which the concrete becomes unworkable. Concrete mixing, placement and compaction become problematic beyond this point. Cement paste does not solidify in an instant. Rather, it

requires a substantial amount of undisturbed time to become sufficiently rigid. The final setting time represents the point at which strength begins to develop at a significant rate. At this stage the hydration of C_3S and C_2S starts, increases rapidly and also continues for several weeks until either free water or silicates are no longer available to react with one another (Mehta & Monteiro, 2014). At the initial setting time it is still possible to form or mould the concrete paste without causing visible damage to the paste structure. At the final setting time this cannot be accomplished without visibly destroying the concrete paste structure (Combrinck, 2011). This is illustrated by Figure 2.4.
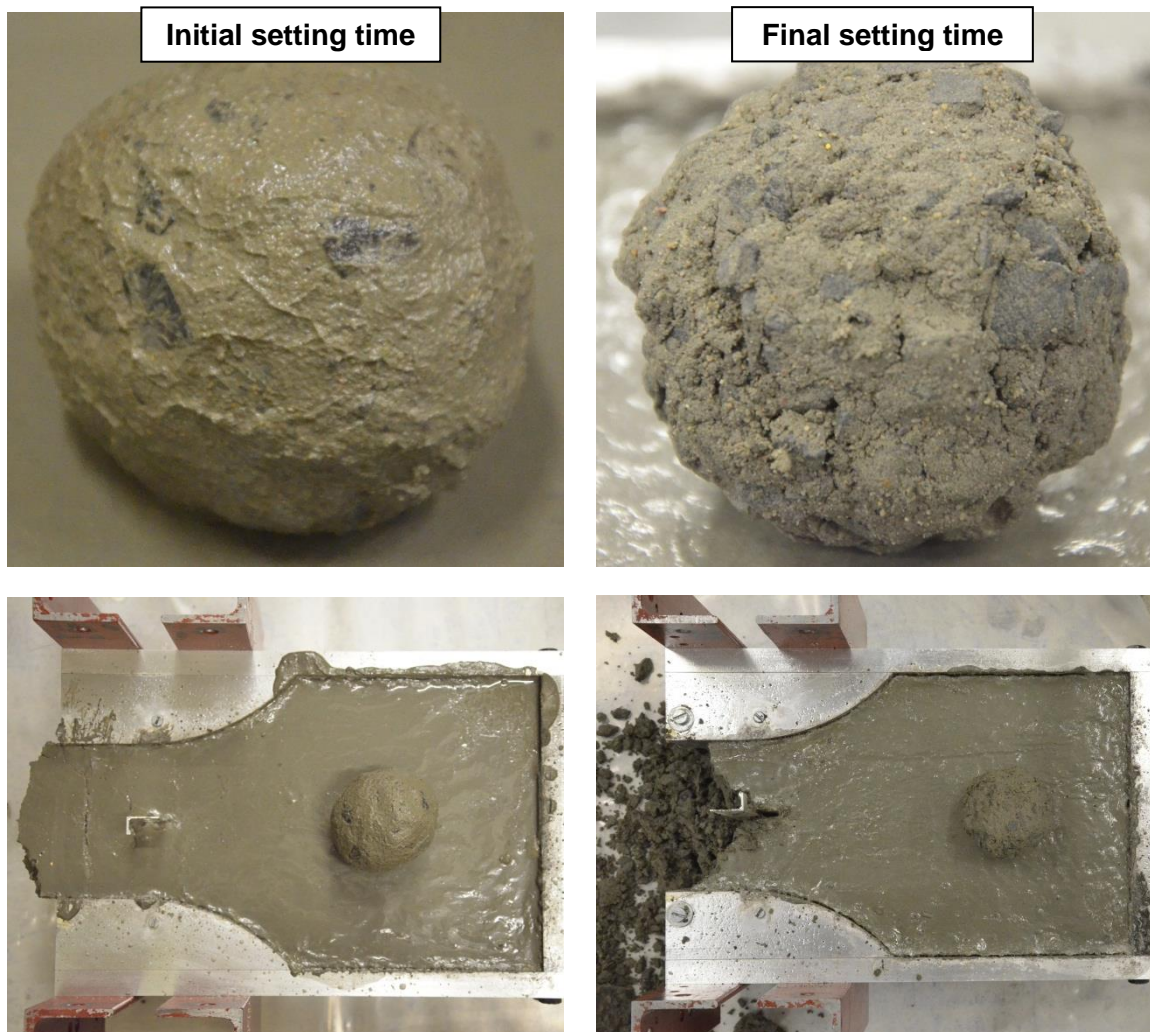
Figure 2.4: Concrete at initial and final setting times

The process of continual strength gain with time is referred to as *hardening*. The progressive filling of voids in the concrete matrix by hydration products and the interlocking of these hydration products results in a decrease of concrete permeability and porosity and a subsequently increase in its strength. This is shown in Figure 2.5. The development of the early age mechanical properties of concrete thus coincides with the development of a hydration product network. These mechanical properties are difficult to physically determine

9

in a reliable manner as they continuously evolve during the early stages of the hydration process and thus during the course of the measurement process (Bentz, 2008 & Gutsch, 2002).
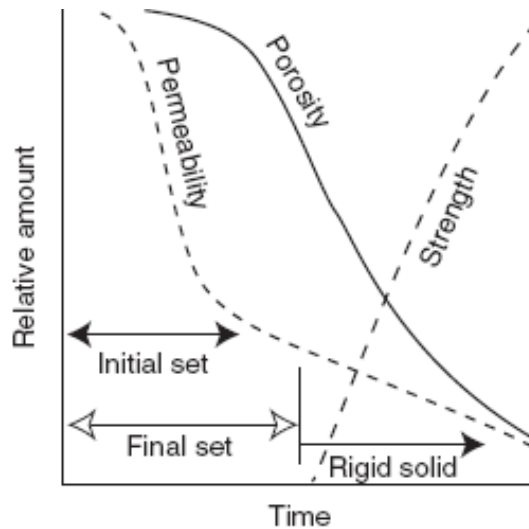
Figure 2.5: Hydration products formation influence on cement paste porosity, permeability, strength and setting time (Mehta & Monteiro, 2014)

To conclude, the respective phases of the setting of early age concrete are shown in Figure 2.6 and provide a summary of this section (Mehta & Monteiro, 2014).
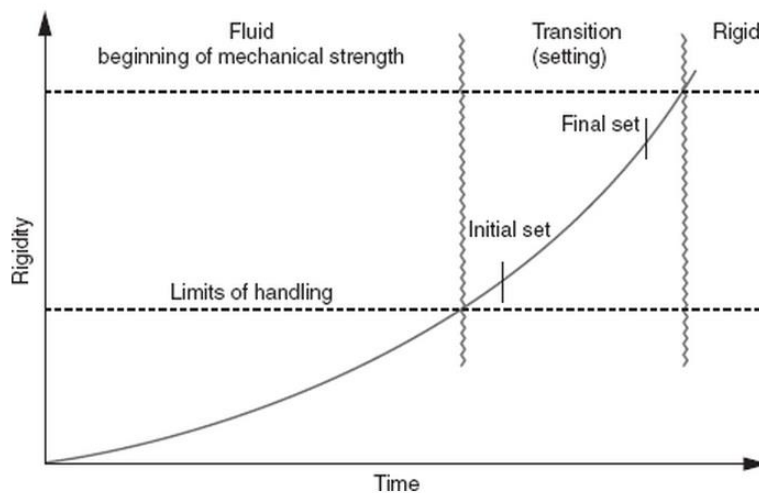
Figure 2.6: The stiffening, setting and hardening of early age concrete (Mehta & Monteiro, 2014)

Factors influencing setting time

This section discusses the most significant factors influencing the setting times of concrete, as well as the early age development of mechanical properties. These factors include water to cement ratio, cement type, concrete temperature and admixtures usage.

10

As setting is the result of the filling of interparticle gaps with hydration products, any factor that influences the water to cement ratio, will inevitably influence the setting times. Water loss from concrete can dramatically decrease its setting time as a direct result of the removal of excess free water from the concrete system, resulting in a subsequent reduction of the average interparticle distances between solids (Bentz, 2008).

The type of cement used in concrete will also significantly influence its setting times. As discussed previously, cement with higher aluminate content will set faster as it plays the primary role in hydration during the stiffening and setting phases of early age concrete. In addition to composition, the fineness of cement also affects its reactivity. The finer the cement type, the faster the hydration reaction will take place, resulting in a decreased setting time (Mehta & Monteiro, 2014).

Hydration is a temperature-dependent exothermic reaction. As a result, if more heat is released during hydration, or if the concrete constituents or the environment in which the concrete is cast is warm, hydration will accelerate and setting will occur faster (Mehta & Monteiro, 2014).

Finally, admixtures may also be used to alter the setting times of concrete. Accelerators increase the rate at which hydration takes place. Calcium chloride ($CaCl_2$) is effective in decreasing the initial and final setting times of concrete as well as increasing its early age strength. This effect reduces over time with the final strength of accelerated concrete being similar to that of un-accelerated concrete. As chloride accelerates corrosion of steel, these accelerators are not suitable for use in reinforced concrete. Retarders, on the other hand, increase the amount of time for setting to occur by altering and inhibiting the early hydration of cement. Retarders typically contain some form of sugar (Illston & Domone, 2001).

2.2   The tensile properties of early age concrete

As established in the previous section, the development of the early age mechanical properties of concrete such as, tensile strength, compressive strength, Young's modulus and fracture energy are a function of the degree of hydration and time (Gutsch, 2002). These tensile properties up to the final setting time are of particular relevance as their experimental determination is the focus of this study and as they correspond to the occurrence of early age cracking, which is discussed in Chapter 3.

Although the scientific community is aware of the need for improved knowledge in the field of the tensile properties of early age concrete within the first hours after it has been cast, there remains very little literature on this subject (Dao, et al., 2009). This is thought to be due to the

considerable practical difficulties that need to be overcome in order to experimentally determine these properties.

The aim of this section is to describe the tensile properties of early age concrete. Firstly, the stress-strain behaviour of early age concrete pertaining to the tensile properties of relevance before cracking has occurred is discussed. Finally, the fracture properties of early age concrete are discussed. The experimental setups used to determine these properties are discussed in detail in Section 4.1. Due to insufficient relevant literature on the tensile properties of concrete before the final setting time, the scope of this section is broadened to incorporate concrete up to an age of 28 days, as this is still considered as a relatively early age by most academics.

2.2.1 The stress-strain behaviour of early age concrete

The earliest literature found on the measurements of the tensile properties of early age concrete is that of Ravina & Shalon (1968). They conducted tests on various cement mortars specimens with different cement contents and water to cement ratios while varying ambient temperatures, relative humidity and wind velocity. The tensile strength that was measured was in the range of 1.67 and 18.2 kPa for specimens at ages between 2 and 4.5 hours after mixing.

Abel & Hover (1998) conducted tensile tests on concrete mixes with water to cement ratios varying from 0.3 to 0.7 and water contents between 194 and 220 kg/m^3. These tests showed that the tensile strength of concrete specimens initially developed very slowly, at an age of 5 hours reaching typical strengths of between 10 and 100 kPa. The test results for concrete mixes with a 194 kg/m^3 water content which were tested between 2 and 8 hours after mixing are shown in Figure 2.7.
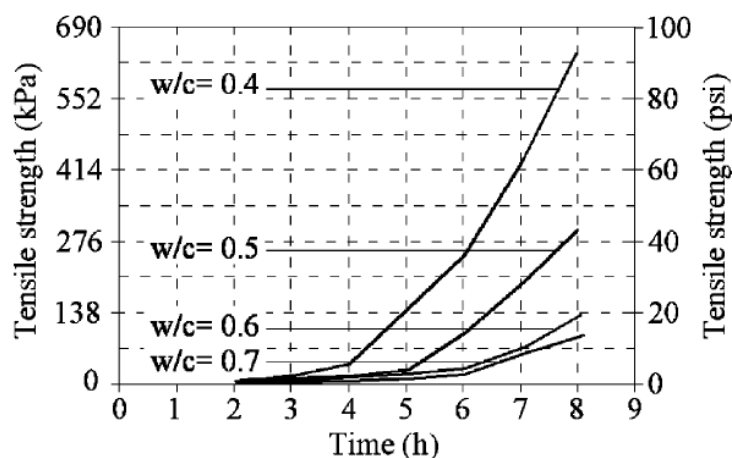
Figure 2.7: Tensile strength development over time for 194 kg/m^3 water content mixes (Abel & Hover, 1998)

12

This research only captured the tensile strengths and strains at failure. Important parameters such as Young's modulus and fracture energy, which are of great significance to the study of the early age cracking behaviour of concrete could not be determined from these test results. A complete ascending stress-strain curve is necessary to determine these parameters.

Kasai, et al. (1972) captured the ascending portion of the stress-strain behaviour of early age concrete up to the point of maximum tensile stress. Tests were conducted on concrete from two hours after mixing and onwards. It was found that with an increase in time the gradient of the ascending stress-strain curve increased as well. This was most pronounced in tests conducted on specimens with ages of 8 to 20 hours after mixing. The strain at maximum tensile stress was found to decrease rapidly with the passing of time. A minimum strain capacity, defined as the strain at peak stress, was reached in the order of tens of microstrains for concrete with ages of between 8 and 15 hours after mixing. However, with a further increase in time a slight increase to between 100 to 150 μ was observed. A displacement rate ranging from between 0.3 to 1.2 mm/min was used to conduct the tests under an ambient temperature of 20°C.

Possibly the first description of the complete stress-strain curve of early age concrete was provided by Hannant, et al. (1999). Two concrete mix designs were tested at hourly intervals ranging from 1 to 5 hours after mixing. The first was a concrete with a water to cement ratio of 0.5 with no admixtures, as shown in Figure 2.8. The 1 hour curve is hardly visible on the graph as it reached a maximum stress of merely 1.9 kPa at a corresponding strain of 8000 μ. Figure 2.9 shows the tensile stress-strain curve of the second mix. This was an extremely cohesive mix which was heavily retarded. It had a water to cement ratio of 0.29 and contained 9.6% microsilica and 1.75% superplasticiser by weight. A displacement rate of 0.75 mm/min was applied for both concrete mix designs, irrespective of the specimen age. The results from the two concrete mixtures firstly showed that fresh concrete's tensile strength increased at a slow rate initially up to an age of approximately 3 hours, after which an exponential increase was measured. When comparing the two concrete mixes, it was found that the strength of the 5 hour retarded mix was less than 20% of the normal mix at the same age, despite the fact that the 28 day compressive cube strength of the retarded mix was greater than 100 MPa. As can be seen from Figure 2.8 and Figure 2.9, the retarded mix possessed sufficient ductility for its complete stress-strain behaviour to be captured up to an age of 5 hours, while for the normal mix this could not be achieved as test specimens became too brittle for the apparatus to capture their descending stress-strain behaviour after failure had occurred. With regards to the tensile testing apparatus, it was found that fresh concrete could be tested from 1 hour after mixing up to 6 to 7 hours after mixing, depending on the rate of hydration, and thus the setting of the concrete. It should be noted that this

research was merely an initial test and focused more on the description of the test apparatus and procedure than the tensile properties of the early age concrete.
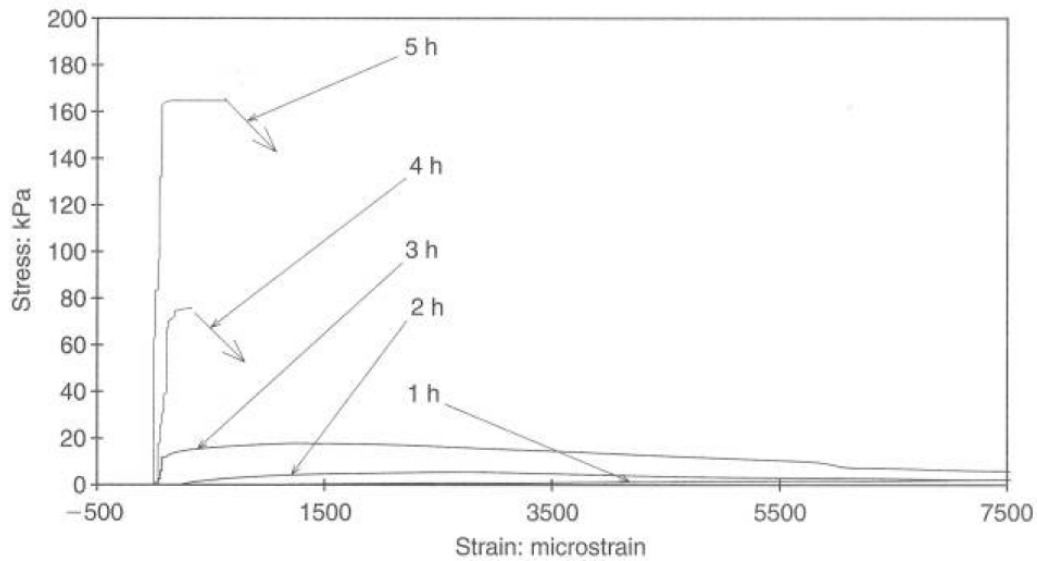
Figure 2.8: Tensile stress-strain curve of normal concrete with a water to cement ratio of 0.5 (Hannant, et al., 1999)
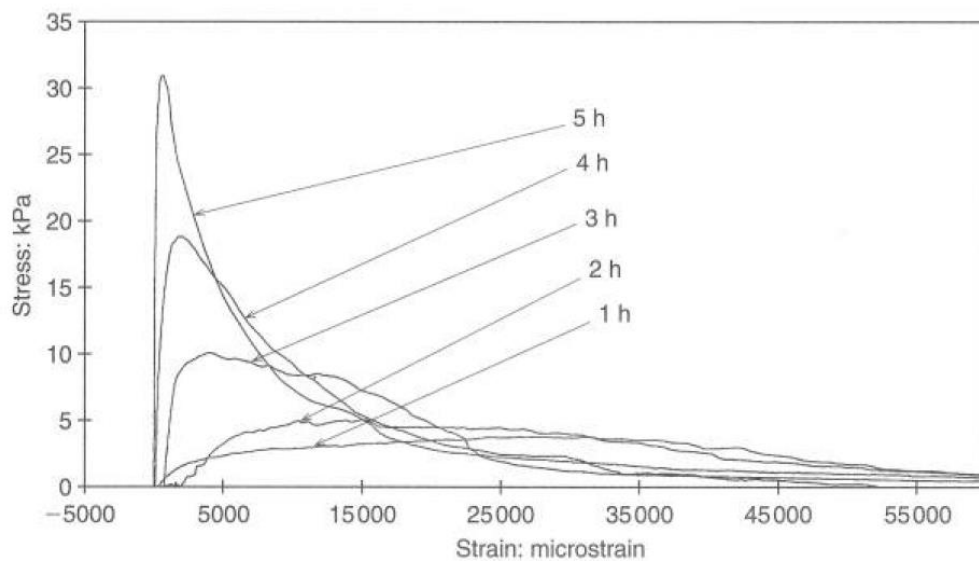
Figure 2.9: Tensile stress-strain curve of retarded high-strength concrete mix with a water to cement ratio of 0.29 (Hannant, et al., 1999)

Branch, et al. (2002) used the exact same test assembly as Hannant, et al. (1999) to conduct tensile tests on high-strength concrete which had a 28-day cube compressive strength in excess of 70 MPa. High strength concrete is more susceptive to the formation of plastic shrinkage cracks (PShC), due to its low water to binder ratio and the reactive nature of certain high-strength concrete constituents like silica fume. This causes an accelerated hydration rate and concrete temperature, which in turn increases the use and evaporation of

14

water in the concrete. The result is increased capillary pressure build-up within the concrete, which leads to the occurrence of PShC. This process is discussed in more detail in Section 3.1. These tests on early age concrete showed significantly greater variability than tests conducted on mature concrete. For this reason multiple stress-strain curve tests were conducted for each mix, at each age, to establish representative 95% confidence limits. Seven tests, at each age, were conducted on the control mix with a water to cement ratio of 0.53, while four tests, at each age, were conducted on the high strength mixes with water to cement ratios varying from 0.29 to 0.34.

Figure 2.10 shows a characteristic set of tensile stress-strain curves for a super plasticised high strength concrete mix. This mix had water to cement ratio of 0.29, a 28-day cube compressive strength of 85.5 MPa and an initial slump of 200 mm. As a result of its high superplasticiser dosage, causing retardation, it gained strength at a significantly lower rate than the other high strength concrete mixes that were tested. For this reason it was still possible to record full stress-strain curves at an age of 5 hours, where the other mixes became too brittle at an age of 4 hours for the test setup to record the descending portion of the full stress-strain curve. The increase of the concrete tensile strength and stiffness is apparent over the 5 hour period, as can be seen from Figure 2.10 (Branch, et al., 2002).
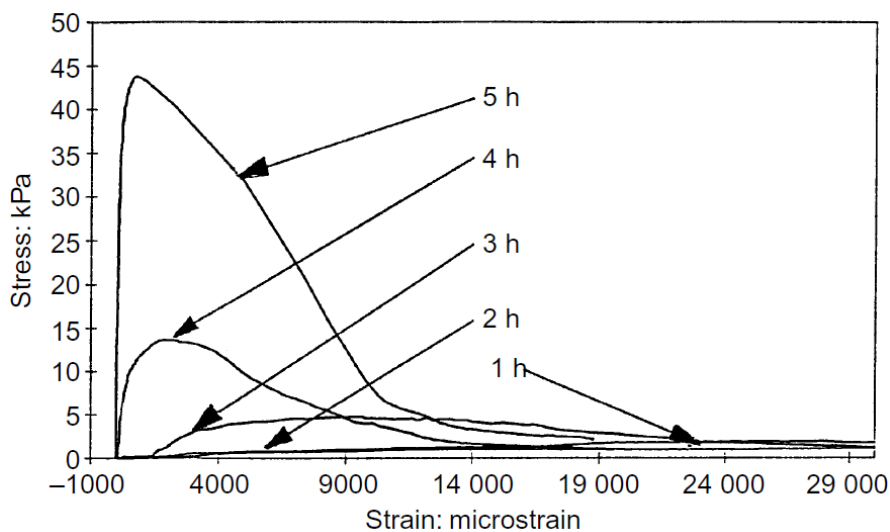
Figure 2.10: A characteristic set of tensile stress-strain curves for a highly retarded and superplasticized high strength concrete mix (Branch, et al., 2002)

For the majority of the tests conducted, the mode of tensile failure of the 1 hour and 2 hour specimens was arbitrary cracking across the tapered neck of the mould. A large amount of cement paste adhered to the surface of the aggregate particles. Typically from an age of 3 hours the failure mode became a single discrete crack through the tapered neck of the mould, which is described in Section 4.1. For this failure mode the aggregate surfaces

15

appeared to be relatively clean when compared to those of the 1 and 2 hour failure mode. From this it was deducted that the internal strength of the concrete paste rapidly became stronger than its bond strength with the aggregate. In addition to this, the strain at peak stress showed a rapid decrease as its age increased – typically exceeding 6000 µ at an age of 1 hour, decreasing to approximately 150 µ at an age of 4 and 5 hours (Branch, et al., 2002).

Figure 2.11 indicates the rate at which the maximum tensile stress increases and the corresponding rate at which the strain at maximum tensile stress decreases for the control concrete mix as well as the highly retarded and superplasticised high strength concrete mix, annotated as A (MS). It can be seen that the strain at maximum stress of the A (MS) mix is significantly greater than that of the control mix, whereas its rate of tensile strength gain is considerably less than that of the control mix. The great variability associated with these early age tensile tests is indicated by the large 95% confidence limits, as indicated in Figure 2.11. This was even more pronounced for the high strength concrete specimens (Branch, et al., 2002).
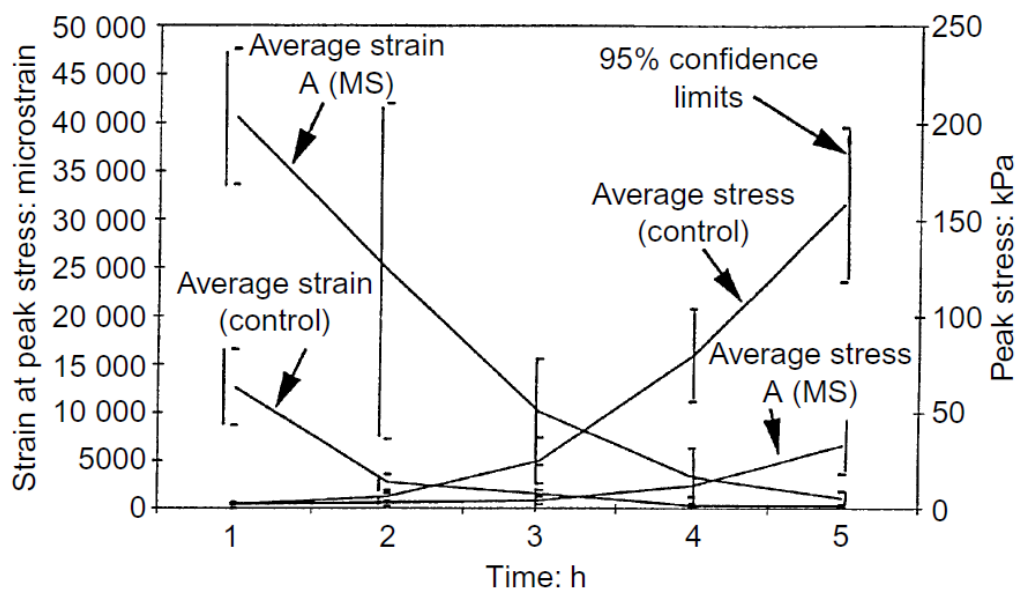
Figure 2.11: Peak stress and strain at peak stress over time of the control and highly retarded and superplasticised high strength concrete mixes (Branch, et al., 2002)

In addition, Branch, et al. (2002) also conducted tensile tests on specimens that were sealed from the atmosphere as well as specimens that were exposed to a 4 km/h wind. The wind was found to have a negligible effect on the stress-strain behaviour of the tested specimens up to a 5 hour specimen age. This implied that insufficient additional water was removed by the increased evaporation effect of the wind to have interfered with the hydration process of the concrete specimens. This result was inconsistent with the measured increase of negative

16

pore pressure in the wind exposed specimens, as they displayed a negative pore pressure twice that of the sealed specimens. In addition, the presence of microsilica in concrete mixtures and the rapid drying of specimen surfaces are also common denominators in specimens that displayed plastic shrinkage cracks (Combrinck, 2011).

Doa, et al. (2009) made further progress in the field of the tensile testing of fresh concrete, especially in terms of testing apparatus, which is discussed in Section 4.1. Tests were conducted on three concrete mixes designed to reflect those typically used for commercial concrete structures. A summary of the concrete mix designs is provided in Table 2.1. The 28 day compressive cube strength is indicated by the first term of the concrete mix notation, whereas the second term indicates the slump of the mix. The 32-80 mix utilised 0.7 l/m^3 of a water-reducing admixture as well as 0.25 l/m^3 of a water-reducing initial set retarder. An aggregate size of 10 mm or smaller was used to ensure that a fully developed fracture process zone would remain in the middle section of the concrete specimen.

Table 2.1: Summary of concrete mix design

Constituent	Unit	Concrete mix design		
		32-25	32-80	32-80
OPC cement	kg/m^3	385	380	460
Fly ash	kg/m^3	-	-	115
Total added water	kg/m^3	230	240	240
Water-reducing admixture	l/m^3	-	-	0.70
Water-reducing initial set retarder	l/m^3	-	-	0.25
10 mm aggregate	kg/m^3	525	520	935
5 mm aggregate	kg/m^3	435	435	-
Coarse sand	kg/m^3	490	490	350
Fine sand	kg/m^3	295	295	260

A displacement rate of 0.05 mm/min was used to carry out these tests. This was considerably slower than any of the displacement rates used in preceding studies. Tests were conducted from 1.5 to 6.5 hours after mixing had occurred, with the start of mixing taken as the zero age (Dao, et al., 2009).

The tensile strength of concrete specimens of the three mixes, tested at various times, is shown in Figure 2.12. Similar to previous studies, Doa, et al. (2009) also found that the tensile strength of early age concrete increased slowly at first, with a strength of approximately 10 kPa at an age of 3 hours, whereafter it increase rapidly, reaching approximately 100 kPa at an age of 6 hours. Due to the heterogeneous nature of the material tested, significant variability in the results were observed.

17
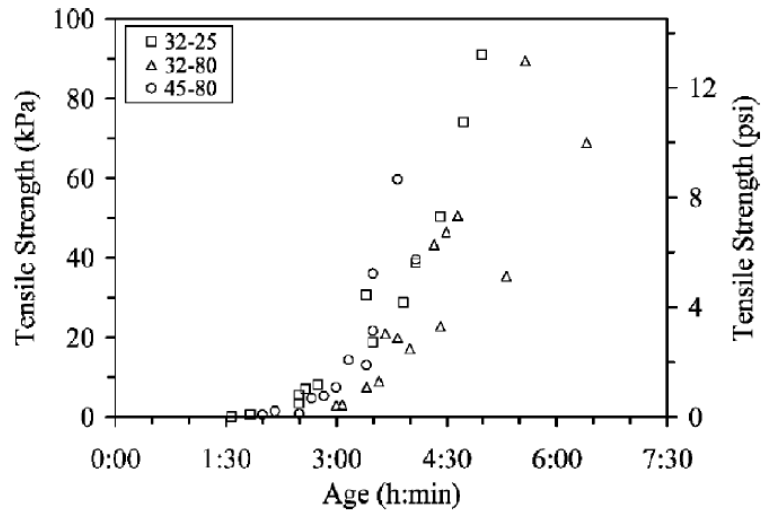
Figure 2.12: Tensile strength development with age (Dao, et al., 2009)

The Young's modulus of the specimens were determined by fitting a straight line to the initial ascending section of the stress-displacement curves. The results are shown in Figure 2.13. The development of Young's modulus with time was essentially similar to the development of tensile strength over time. There was however a larger amount of scatter, as a result of the subjective manner in which Young's modulus was determined. Despite this, a near linear relationship between the Young's modulus and the tensile strength of concrete specimens was found (Dao, et al., 2009).
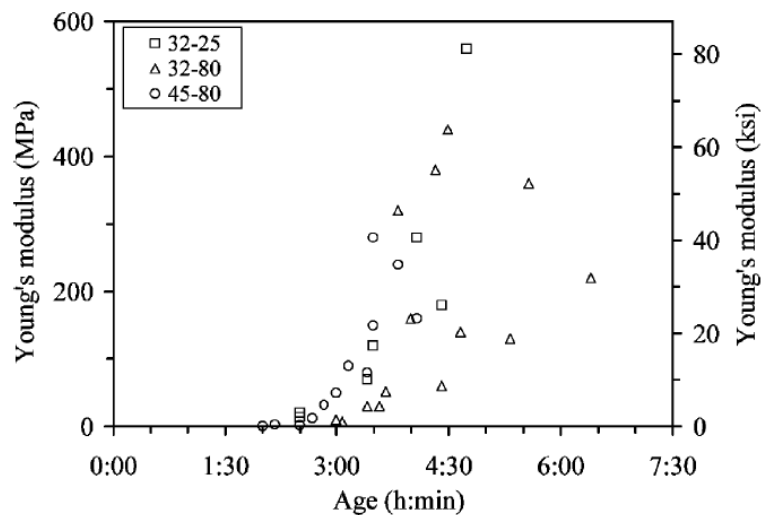
Figure 2.13: Young's modulus development with age (Dao, et al., 2009)

Furthermore, the results of the strain at peak tensile stress of the specimens, as shown in Figure 2.14, strongly agreed with those of Hannant, et al. (1999) as described earlier.
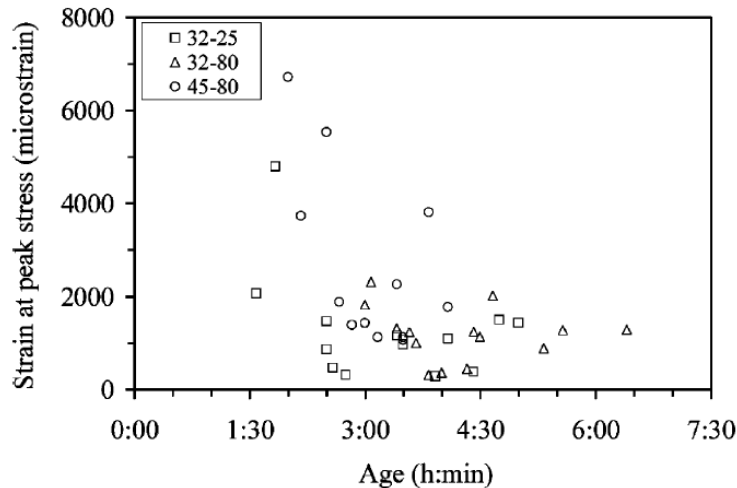
Figure 2.14: Strain at maximum tensile stress development with age (Dao, et al., 2009)

From the research presented in this section it is clear that both the tensile strength and Young's modulus of early age concrete increase with time as they are functions of the degree of hydration. However, the strain at maximum tensile stress behaviour is more complex. This literature study showed that upon casting the strain at maximum tensile stress is in the order of thousands of µ and with time decreases to an apparent minimum value in the order of tens of µ between the ages of 4 and 15 hours (Branch, et al., 2002, Dao, et al., 2009 & Swaddiwudhipong, et al., 2003). This minimum value corresponds with the period between initial and final setting times, as well as the period of initial strength gain. During this period the early age concrete goes from being a weak quasi-solid to a weak quasi-brittle solid with little capacity to undergo tensile straining. With a further increase in time, this strain capacity increases once again. Swaddiwudhipong, et al. (2003) determined that the strain at maximum tensile stress of 20 specimens of ages between 1 and 28 days was relatively constant, with an average of 120 µ. For mature concrete this value is 100 to 150 µ (Telford, 1992)

2.2.2 The fracture properties of early age concrete

Cracks initiate the moment the stresses in a material reach the material's strength limit. However, these cracks can only grow if the energy required to break the material further is provided. The field covering this energy criterion of cracking is called fracture mechanics, and came to be as a result of the work of Griffith (1920). Its most significant application has been the study of the brittle failure and fatigue failure of metal structures. Fracture mechanics have successfully been applied in the study of mature concrete cracking as well. However, there is limited literature available on its application to the cracking of early age concrete, particularly as early as the concrete specimens tested in this study. As stated before, this is

19

primarily the result of the numerous challenges in the experimental determination or the tensile stress-displacement of separation relationship of early age concrete.

This section first describes the fundamental concepts of fracture mechanics and how it applies to concrete. After this the application of fracture mechanics in the field of early age concrete cracking is discussed.

Background study on fracture mechanics

The Griffith energy theory can be used to describe the fracture of materials, which states that crack propagation is the unavoidable process of energy transfer from strain energy in an elastic material in equilibrium to fracture energy required for the formation of a crack surface, effectively achieving a state of least potential energy for a body at a given load level. Thus to develop a crack, a load has to be induced to deform a body to the point that the strain stored in the body is sufficient to provide the required fracture energy to cause the tip stress of the crack to reach a critical stress criterion, such as the maximum principle tensile stress criterion (Shi, 2009).

There are fundamental differences between the fracture of brittle-, brittle-ductile-, and quasi-brittle materials the likes of mature concrete. Figure 2.16 shows the fracture process zone (FPZ) for both ductile-brittle and quasi-brittle materials. Here F, N and L denote the fracture process-, non-linear- and linear zones in the materials. The FPZ is at the tip of a crack opening and is the transient zone in between the open crack and the undamaged, continuous material. The FPZ is the area in which a material undergoes softening damage in the form of tearing. For ductile-brittle materials hardening plasticity with perfect yielding takes place in this zone, which is relatively small. Whereas for quasi-brittle materials plastic flow is essentially absent and the nonlinear zone is nearly entirely filled by the FPZ as shown in Figure 2.15 (Bazant, 2002).
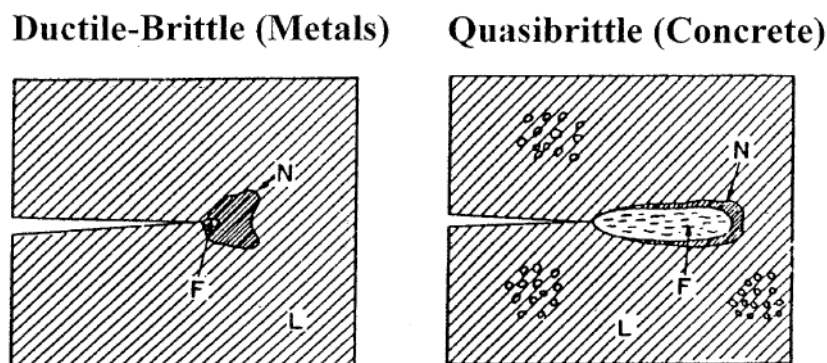
Figure 2.15: FPZ formation in brittle-ductile materials and quasi-brittle materials (Bazant, 2002)

The fracture process zone (FPZ)

Concrete is a heterogeneous material consisting of aggregates and cement paste that are bonded together at an interface called the interfacial transition zone. Due to inadequate bonding strength as well as numerous imperfections and microcracks that form in its structural matrix during hardening, concrete is very weak in tension. Its tensile strength typically ranges from 8 to 15% of its compressive strength. Under an external load in excess of the material's tensile strength, failure in the form of fracture will occur. As described in the previous section, a tension zone, known as the FPZ, forms near the crack tip. Within this FPZ complex microfailure mechanisms occur. They include microcracking, crack branching, crack coalescence, crack deflection and debonding of aggregate from the concrete matrix. These are all inelastic toughening mechanisms that occur when a crack originates and propagates (Shi, 2009).

A Typical FPZ is shown in Figure 2.16. It can be divided into a bridging and a microcracking zone. The bridging zone is a weak interface between aggregates and cement paste, and forms an important toughening mechanism in a concrete crack. Within the damaged microcracking zone the effective Young's modulus is reduced. For this reason the FPZ is modelled as a region of strain softening (Shi, 2009). It has been suggested that the fully developed FPZ of mature concrete is in the order of 3 to 12 times that of the maximum aggregate size in the concrete (Bazant, 2002).
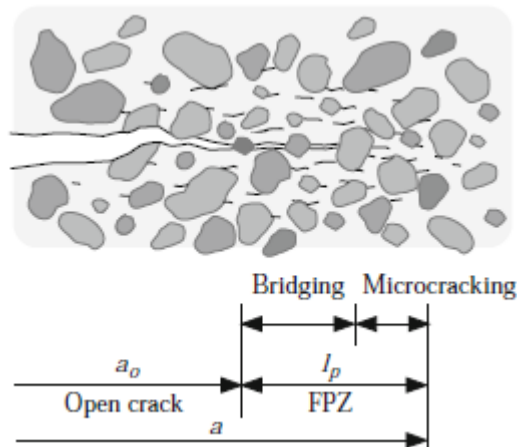
Figure 2.16: Typical FPZ in front of a crack opening (Shi, 2009)

Since the inelastic zone at a concrete crack tip is extensively developed, traditional linear elastic fracture models cannot be applied to the study of concrete fracture. Various other fracture mechanics models have been developed to define the FPZ in a concrete material. However, the fictitious crack model (FCM), as proposed by Hillerborg, et al. (1976), is widely

accepted as the standard nonlinear fracture mechanics model for the application of fracture mechanics to concrete structures. This is due to its simplicity and accuracy (Shi, 2009).

The fictitious crack model (FCM)

The FCM simplifies the complex inelastic material behaviour of the concrete FPZ as shown by Figure 2.17 (a)-(c). Figure 2.17 (a) represents the physical FPZ or micro cracked zone in front of a crack opening. During crack propagation in a concrete body the resistance provided by the cohesive stresses of the fictitious crack, shown in Figure 2.17 (b), against crack opening needs to be overcome. The relationship between the cohesive forces and the crack opening is show in Figure 2.17 (c), illustrating cracked concrete's characteristic strain softening behaviour. The energy consumed in this process of creating a cracked surface is the fracture energy which is equal to the area under the tensile stress - crack opening displacement (COD) curve (Shi, 2009).
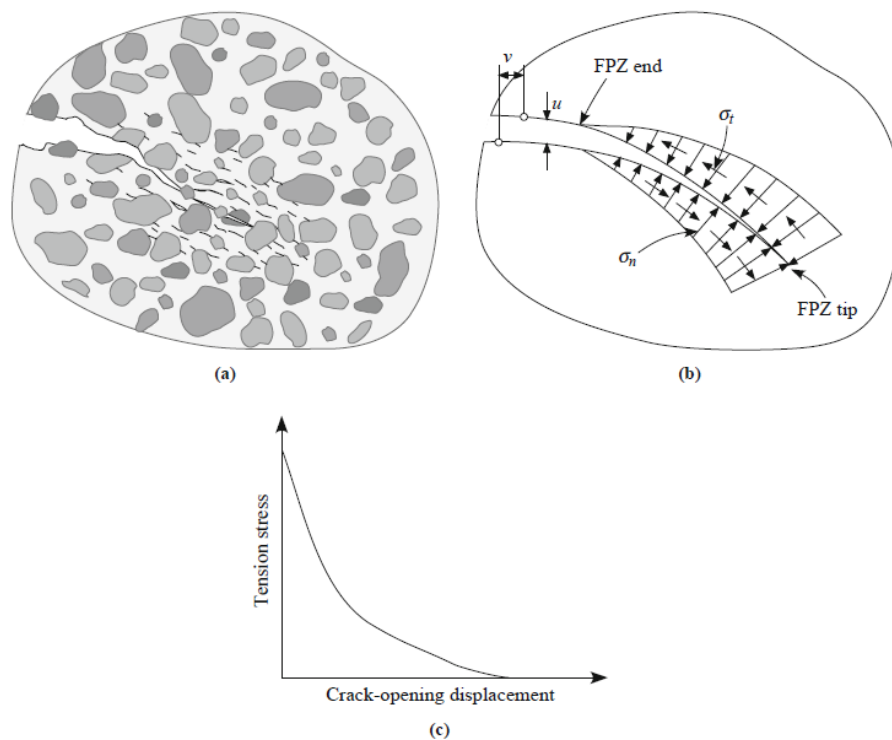
Figure 2.17: The fictitious crack model: (a) a typical crack in a concrete material, (b) an equivalent fictitious crack, and (c) the characteristic tension-softening behaviour of concrete (Shi, 2009)

As mentioned before, instead of the physical FPZ, Hillerborg, et al (1976), envisioned a fictitious crack in the place of the physical FPZ which is subject to closure tractions as illustrated by Figure 2.18. The closure stresses resulting from the bridging grains and microcracking zone has a maximum at the edge or tip of the FPZ. These closure stresses decreases to zero when the COD reaches its critical value, W_c, after which an open crack has formed. Known as the tension softening phenomenon, the relationship between the COD

22

and the closure tractions in the FPZ defines the fracture energy of concrete materials and describes the local material behaviour within the FPZ once fracture has occurred (Shi, 2009).
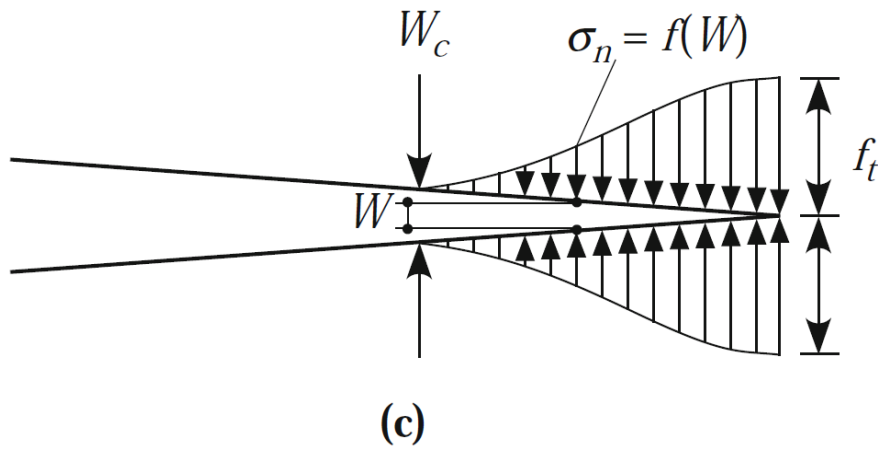
Figure 2.18: Tension-softening relation within the FPZ

Hillerborg, et al. (1976) developed these concepts from experimental evidence resulting from uniaxial tensile tests on concrete bars. These experiments showed that crack formation in a concrete material is an evolutionary process of strain build-up in the pre-peak zone, and strain localisation and the development of a visible crack in the post-peak zone. This process is illustrated in Figure 2.19 (Shi, 2009).
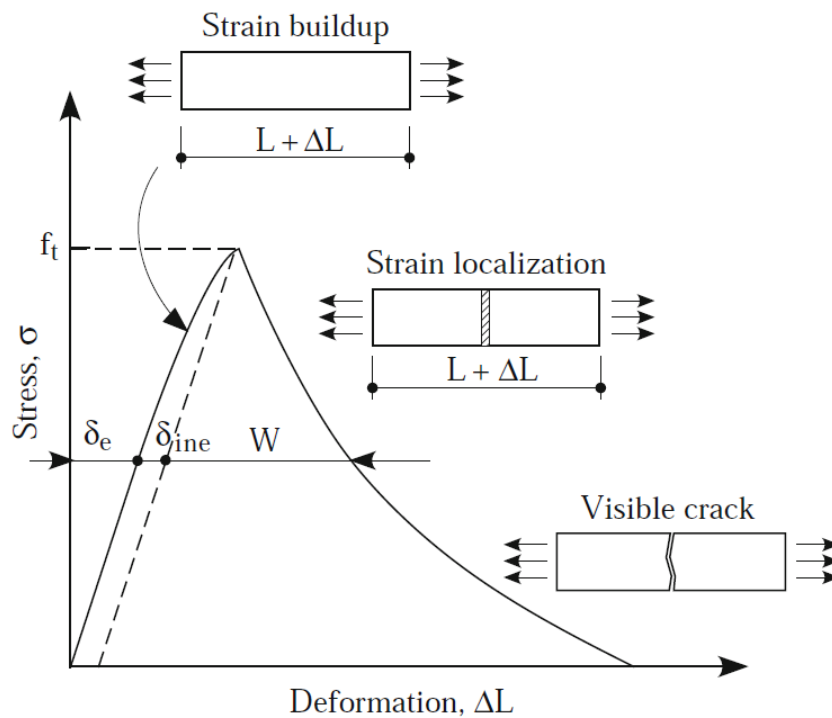
Figure 2.19: The evolution of crack occurrence (Shi, 2009)

With this in mind, Hillerborg, et al. (1979) modelled the zone of strain localisation as a fictitious crack that corresponds to a microcracked zone with some remaining ligaments of stress. Furthermore, it was suggested that this fictitious crack is a good reflection of reality and that stresses may develop in the FPZ providing that the corresponding displacement is small. From Figure 2.19 it can be seen that the total deformation for a bar of length L in the post-peak stress zone is given by:

$$\Delta L = \delta_e + \delta_{ine} + W \dots\dots\dots\dots\dots\dots\dots\dots\dots\dots\dots\dots\dots\dots\dots\dots\dots\text{(Equation 2.3)}$$

where δ_e represents the elastic deformation, δ_{ine} is the inelastic deformation and W is the crack opening displacement of the fictitious crack. For the initiated crack to propagate, the stress at the FPZ was assumed to reach the tensile capacity of the concrete. The assumption was made that the stress transmitted through the fictitious crack was dependent on W:

$$\sigma = f(W) \dots\dots\dots\dots\dots\dots\dots\dots\dots\dots\dots\dots\dots\dots\dots\dots\dots\dots\dots\text{(Equation 2.4)}$$

with $f(W)$ representing the tension-softening curve, as discussed previously. As W grows and reaches a critical value, W_c, the transmitted stress becomes zero and the fictitious crack becomes an open crack. For the sake of simplicity, Hillerborg, et al. (1979), made the assumption that δ_{ine} was negligible, resulting from the fact that the behaviour of the bulk material was linear elastic. Based on this assumption Equation 2.3 can be written as follows:

$$\Delta L = \delta_e + W = L\frac{\sigma}{E} + W = L\frac{f(W)}{E} + W \dots\dots\dots\dots\dots\dots\dots\dots\dots\dots\dots\dots\text{(Equation 2.4)}$$

with E being the Young's modulus of the concrete. If E and $f(W)$ are known, the complete post-peak stress-strain curve of a concrete material can be determined. Although simple, Equation 2.4 encapsulates the general principles for crack analysis in concrete. Firstly, it illustrates the importance of the tension softening law. In its absence, crack analysis cannot be performed. Secondly, it shows that post-cracking deformation in the cracked body consists of two components: the elastic deformation of the body and the crack opening width of the developing crack. Thirdly, the elastic body outside of the FPZ is subjected to the stress transmitted through the fictitious crack; hence its deformation is also a function of the crack opening width (COD). To summarise, the foundation of crack analysis is to determine the overall deformation of the cracked body after the occurrence of cracks. Once this is determined, stress-strain analysis can easily be carried out (Shi, 2009).

Although the assumption was made that the bulk material is linear elastic, as it makes the problem less complicated to solve, it is not an essential requirement for the crack analysis of concrete. The FCM can also be applied to nonlinear behaviour of the bulk material as

pointed out by Planas, et al. (1995). The following general hypotheses are used in the application of the FCM in the analysis of cracks in concrete (Shi, 2009):

1. The bulk material behaviour is isotropic linear elastic, and is thus defined by Young's modulus and Poisson's ratio.
2. A crack initiates at a point where the maximum principal stress reaches the tensile strength. The crack develops normal to the direction of the principal tensile stress.
3. As a crack develops and its crack opening grows, stress transfer occurs across the crack surface until the critical COD is reached. Pure mode-I crack opening stress transfer between cracked surfaces is a function of the COD, as described by Equation 2.4.

A crack may be subjected to three different modes of loading that cause the formation of crack surfaces. These are illustrated in Figure 2.20. A Mode I loading is applied normal to the plane of cracking and is responsible for crack opening. Mode II loadings represent in-plane shear and causes two cracked surfaces to slide over each other. Mode III loadings, refer to out-of-plane shear and tends to tear two crack surfaces apart (Shi, 2009).

Mode I
(Opening mode)

Mode II
(In-plane shear mode)

Mode III
(Out-of-plane shear mode)
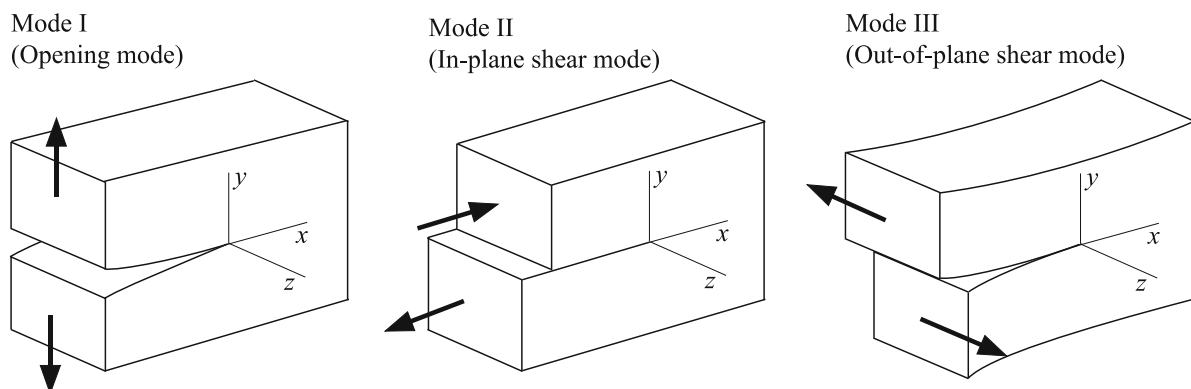
Figure 2.20: The three independent modes of deformation at a crack tip (Shi, 2009)

Fracture energy

As discussed earlier, the fracture of concrete originates in the FPZ at the edge of a crack opening by means of complex microfailure mechanisms. During this fracture energy is consumed to overcome the resistance of several toughening mechanisms to procedure an open crack at the end of the FPZ. The amount of fracture energy necessary to break a unit area of concrete is considered to be the material property that describes the fracture behaviour of concrete. Figure 2.21 shows the full tension softening relationship between the COD and the cohesive stresses along the FPZ as a crack develops. This tension softening

relationship is typically obtained by propagating an existing crack in a notched concrete specimen, but can also be derived from a direct tensile test, as is the case in Figure 2.21.
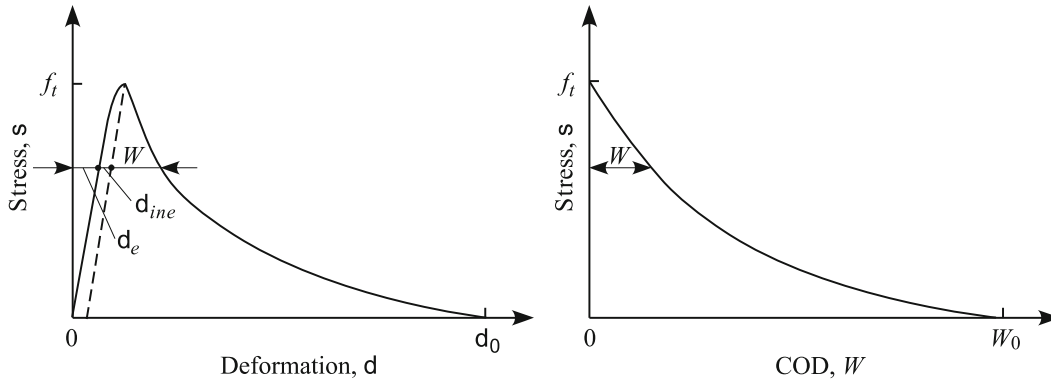
Figure 2.21: Stress-deformation relationship obtained from a deformation controlled uniaxial tension test and its derived stress-COD relationship (Shi, 2009)

The area enclosed by the $\sigma - W$ tension softening curve represents the exact fracture energy required to create and fully break a unit surface area crack. It is expressed as:

$$G_f = \int_0^{W_c} \sigma_n(W) dW \dots\dots\dots\dots\dots\dots\dots\dots\dots\dots\dots\dots\dots\dots\dots\dots\dots\dots\text{(Equation 2.6)}$$

In concrete fracture mechanics the term G_f is representative of the mode I fracture energy, which is generally simplified as fracture energy. When conducting uniaxial tensile tests to determine the fracture energy of concrete specimens, both early age and mature, friction should be eliminated as far as possible. A minor frictional force can significantly influence the tail portion of the tension softening curve, leading to a higher fracture energy value and unreliable results (Shi, 2009).

The fracture energy of mature concrete, determined by means of direct or indirect tensile testing typically varies from 40 to 150 J/m^2 (Elfgren, 1989 & Karihaloo, 1995). Factors that influence the fracture energy of concrete include aggregate size and quality, water to cement ratio, concrete age and loading rate during tests. Another significant factor is concrete tensile strength. Generally a higher concrete strength results in a higher fracture energy. This is in strong contrast to metals with elastic-plastic behaviour as their fracture energy decreases with an increase in ultimate tensile strength (Doa, et al., 2010). An increase in concrete fracture energy as a consequence of an increase in its tensile strength should however not be confused with an increase in concrete ductility. Fracture energy alone is not a sufficient indication of a material's brittleness or ductility. The parameter of characteristic length, l_{ch}, is used to make this distinction and is defined as (Karihaloo, 1995):

$$l_{ch} = \frac{E G_f}{f_t^2} \dots\dots\dots\dots\dots\dots\dots\dots\dots\dots\dots\dots\dots\dots\dots\dots\dots\dots\dots\text{(Equation 2.7)}$$

26

The smaller the characteristic length of a material, the more brittle the material. The characteristic length is also an indication of the FPZ length. Typical values of characteristic lengths are shown in Table 2.2 (Karihaloo, 1995).

Table 2.2: Typical characteristic lengths of concrete and related materials (Karihaloo, 1995)

Material	l_{ch} [mm]
Glass	10^{-6}
Silica fume densified cement paste	1
Hardened cement paste	5-15
Mortar	100-200
High strength concrete (50 - 100 MPa)	150-300
Normal concrete (aggregate size less than 20 mm)	200-500
Dam concrete (aggregate size of 38 mm)	700

From Table 2.2 it can be seen that the brittleness of concrete increases as its aggregate size decreases. Brittleness typically also increases with concrete strength. The more compact the microstructure of a concrete, the more brittle the concrete.

In spite of the successful application of fracture mechanics to mature concrete, its application to early age concrete is still in the early stages of development, as discussed in the next section.

Fracture properties of early age concrete

Zollinger, et al. (1993) conducted three point bending tests on concrete specimens aged 12 hours to 28 days. The results indicated an increase in both the critical stress as well as the characteristic length with an age. This indicated that early age concrete is more brittle that mature concrete.

Wedge splitting test for concrete specimens of ages from 1 to 28 days were conducted by Kim, et al (2004). It was found that the facture energy increased with age, with the most significant increase taking place at very early ages. An approximate fracture energy limit was reached at 28 days, after which the measured fracture energies no longer increase significantly. Similar trends were observed by Zollinger, et al. (1993).

Ostergaard, et al. (2004) also conducted wedge splitting tests on two high performance concrete mixes with w/c ratios of 0.31 and 0.48 and specimens ages varying from 8 hours to 28 days. From these tests it was revealed that the fracture energy of the concrete increased with age. This was also accompanied with an increase in tensile strength and Young's modulus. The ductility of the concrete specimens, as indicated by their characteristic length,

proved to decrease over time. The characteristic length as well as fracture energy development with age is shown in Figure 2.1.
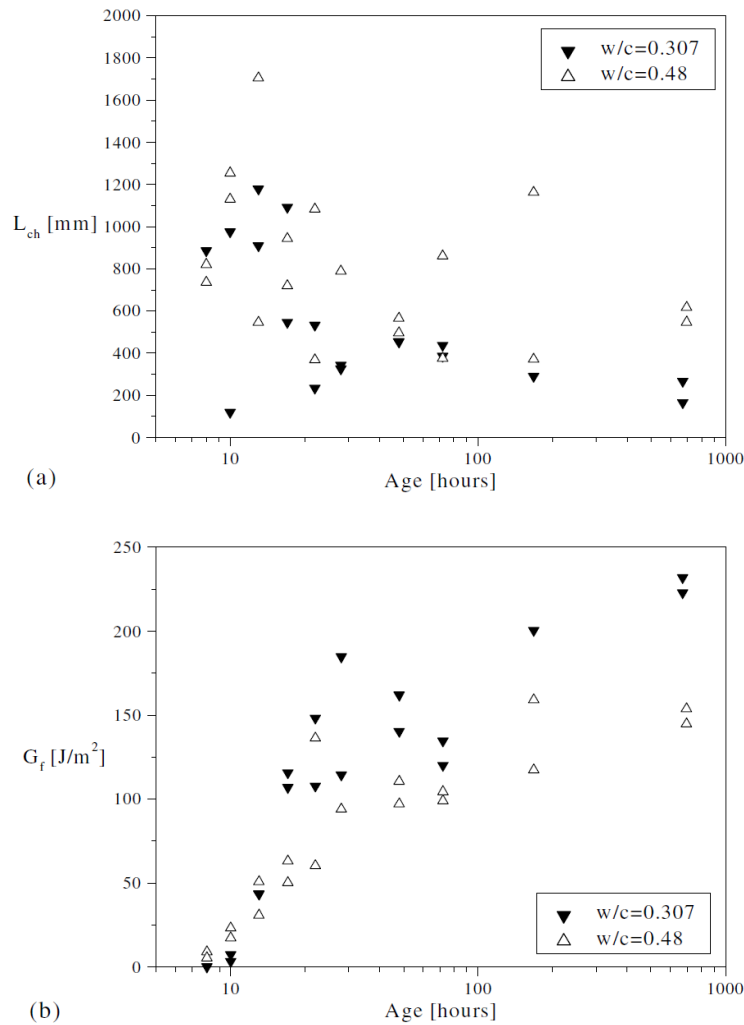
Figure 2.22: (a) The development of characteristic length, (b) The development of fracture energy (Ostergaard, et al., 2004)

The most recent contribution, and the only one that defines "early age" in the same way as this study, was made by Dao, et al. in 2009, as part of the same study discussed in the Section 2.2.1. Direct tensile test were conducted on three concrete mixes that were designed to reflect those typically used for commercial concrete structures, as described in Table 2.1. Although tests were conducted as soon as 95 minutes after the concrete had been mixed, the fracture energy of the specimens could only be determined when a certain degree of setting had occurred. For the faster setting 45-80 concrete mix this occurred as early as 120 minutes after mixing, while for the 35-25 the youngest specimen was 150 minutes in age and for the 35-80 the age was 180 minutes. The determined fracture energy of the respective concrete specimens is shown in Figure 2.23. It was found that the fracture energy initially assumed very small values and increased rapidly from 3 hours and onwards, reaching 50 to

28

80 J/m^2 at ages of approximately 6 hours. The development of fracture energy with time showed a similar trend to that of the material's Young's modulus and tensile strength (Dao, et al., 2009).
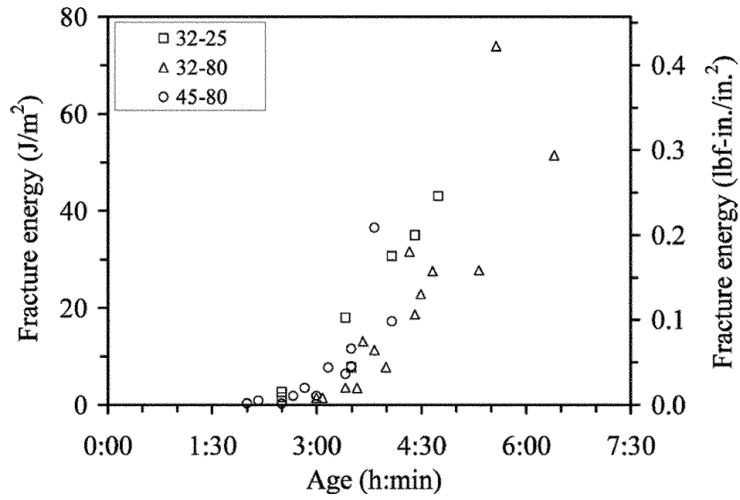
Figure 2.23: Fracture energy development with time (Dao, et al., 2009)

With regards to the characteristic lengths of the concrete specimens, great variation was observed, as can be seen in Figure 2.24. The most significant consequence was that for basically all cases the characteristic length of early age concrete was significantly higher than that of mature concrete, as shown in Table 2.2. This result is in accord with those of previous researches who found that the characteristic length decreases with an increase in age (Dao, et al., 2009).
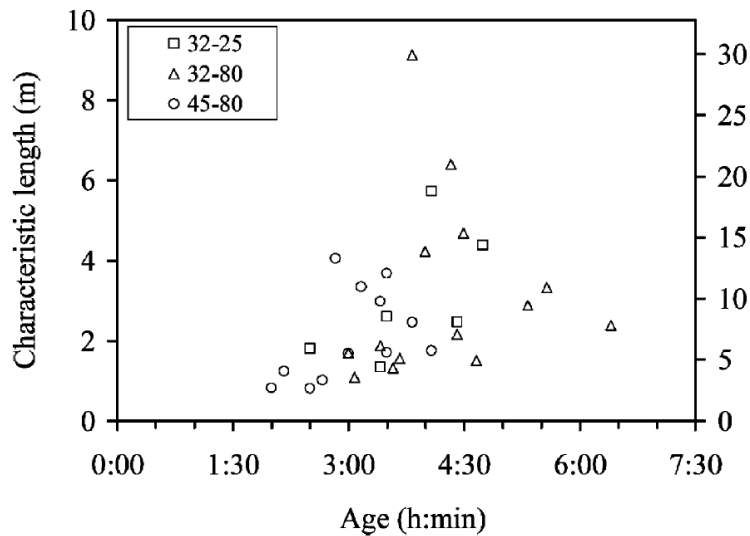
Figure 2.24: Characteristic length development with time (Dao, et al., 2009)

Doa, et al. (2010) proposed stress-COD relationships to model the softening behaviour of concrete at early ages. This included linear, bi-linear and a non-linear models as illustrated by Figure 2.25. In all cases least-square methods were implemented to determine best fits.
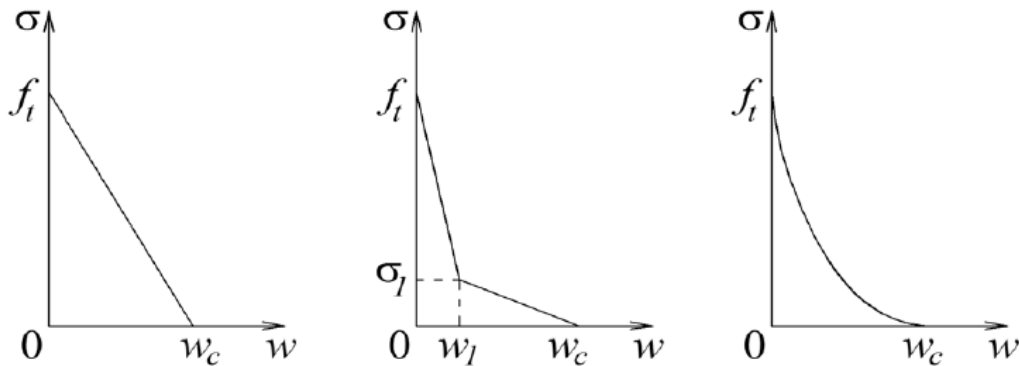
Figure 2.25: Idealized stress-COD relationships (Doa, et al., 2010)

It was found that the linear model was not suitable in describing the stress-COD relationship of early age concrete, as the results were inconsistent with that of the experimental work. Although the non-linear model was sufficient in its description of the stress-COD relationship the bi-linear model was preferred given that it was sufficiently accurate for practical purposes. The softening function for the bi-linear stress-COD relationship is given by:

$$\sigma = f_t - (f_t - \sigma_1)\frac{W}{W_1} \ for \ 0 \ \leq \ W \ \leq \ W_1 \dots\dots\dots\dots\dots\dots\dots\dots\dots\dots\dots\dots\dots\text{(Equation 2.8)}$$

and

$$\sigma = \sigma_1 - \frac{\sigma_1(W-W_1)}{(W_c-W_1)} \ for \ W_1 \leq \ W \ \leq \ W_c \dots\dots\dots\dots\dots\dots\dots\dots\dots\dots\dots\dots\text{(Equation 2.9)}$$

From Equation 2.6 the fracture energy is given by:

$$G_f = \frac{1}{2}(f_t - \sigma_1)W_1 + \frac{1}{2}\sigma_1(W_c - \ W_1) + \ \sigma_1 W_1 \dots\dots\dots\dots\dots\dots\dots\dots\dots\dots\text{(Equation 2.10)}$$

Using the experimentally determined value of 5 mm for W_c, the best fit values for W_1 were determined to be 0.808 mm, 0.558 mm and 0.308 mm for the corresponding σ_1 of $0.1f_t$, $0.15f_t$ and $0.2f_t$. This range of values proved to be consistent for the theoretical model as well as experimental stress-COD relationship obtained for early age concrete (Doa, et al., 2010).

2.3   Concluding summary

This chapter firstly describes the rheological behaviour of early age concrete. Then the physical and chemical processes responsible for the stiffening, setting and hardening of early

age concrete are discussed. The chemical process of hydration is identified as the main contributor in the evolution of early age concrete from a viscous suspension upon mixing, to a rock-like material with the passing of time. Next, the tensile strain and stress capacity as well as the Young's modulus are discussed. Despite the limited literature available on the topic, it is evident that both tensile strength and Young's modulus are dependent on the degree of hydration and increase with concrete age. The strain capacity however proved to be more complex in it prediction, reaching a maximum upon casting, decreasing to a minimum between the time of initial and final setting and then slightly increasing once again as the concrete matures. Finally, the fundamentals of fracture mechanics and its application in concrete cracking are discussed. Fracture energy determined from direct tensile testing is defined and the concept of characteristic length, which is both an inverse measure of brittleness and representative of the actual length of the FPZ, is introduced. From the studies described on relatively early age concrete it is apparent that fracture energy increases with concrete age and strength while characteristic length decreases. The next chapter focuses on the early age cracking of concrete.

3. Background study on the early age cracking of concrete

The early age cracking of concrete, as defined in this study, can occur once the concrete has been cast and consolidated up to around or just after the final setting time of concrete. These types of cracks include plastic shrinkage cracking (PShC) and plastic settlement cracking (PSeC). Crack onset occurs when the tensile stresses developed in the concrete exceeds its ultimate tensile strength or, alternatively phrased, when the restrained shrinkage strain of the concrete exceeds its tensile strain capacity.

Even though the cracks resulting from these phenomena are often internal and microscopic, further shrinkages as a result of chemical, drying and thermal shrinkages at later stages in the concretes design life may cause these cracks to open (Holt & Leivo, 2004). This not only contributes to aesthetic problems but could also lead to the intrusion of deleterious materials that attack the concrete paste and cause corrosion of the steel reinforcement. This has a premature detrimental effect on the durability, strength and ultimately the safety of concrete structures (Qi, 2003).

This chapter discusses both forms of early age cracking as well as low volume fibre reinforced concrete (LV-FRC), as it relates to the mitigation of PShC and is of relevance to the tensile tests conducted in this study.

3.1   Plastic shrinkage cracking (PShC)

Plastic shrinkage cracking occurs as a result of a rapid loss of water from a concrete element. This is typically a result of an unprotected concrete surface that is subject to evaporation. If the evaporation rate is greater than the rate at which surface water is replaced through bleeding, the concrete will shrink. This is referred to as plastic shrinkage. There generally exists some form of restraint to the concrete mass leading to restrained tensile strain in the surface region of the concrete. Due to the low tensile strength of the concrete at these early ages, cracks, known as plastic shrinkage cracks, occur (Illston & Domone, 2001).

These cracks mainly occur in concrete elements that have large exposed surfaces, for example: floors, slabs and bridge decks, which are exposed to environmental conditions conducive to high evaporation rates. Typical PShC are shown in Figure 3.1. These cracks can be identified by a meshed or parallel crack pattern and in some cases penetrate through the full depth of concrete elements (Owens, 2009). The length of cracks usually varies

between 50 and 1000 mm with their spacing being between 50 and 700 mm. The corresponding width of these cracks can be as wide as 2 mm (Slowik, et al., 2008)
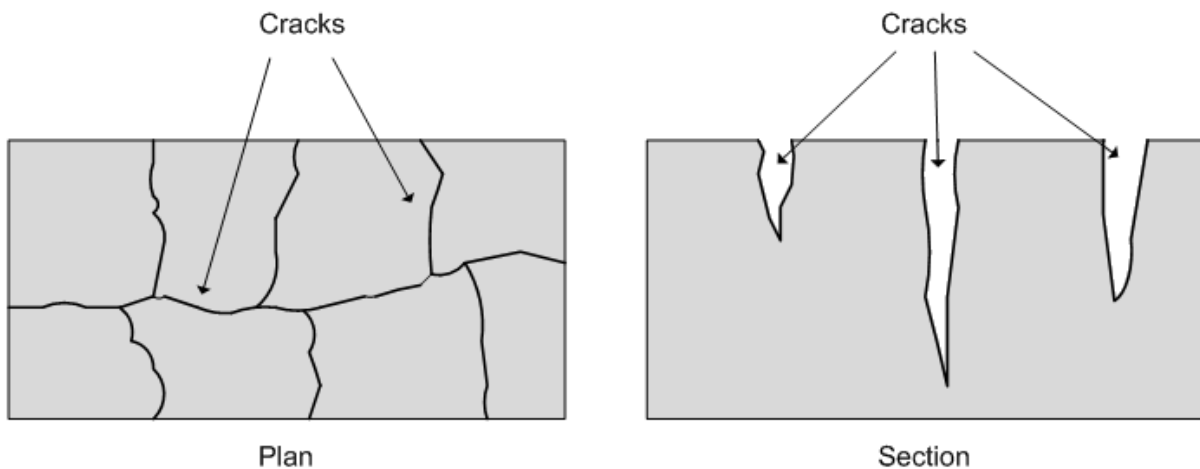
Figure 3.1: Typical plastic shrinkage cracks (Illston & Domone, 2001)

This section first describes the mechanisms causing PShC. This is followed by a discussion of the factors that influence PShC severity and its behavioural model. Finally, methods to reduce PShC occurrence and severity are presented.

3.1.1 PShC mechanisms

This section discusses the mechanisms that cause PShC, which include capillary pressure, air entry and restraint. In order for PShC to occur, all of these mechanisms are required to take effect on a concrete element.

Capillary pressure

It is widely accepted that the main mechanism causing PShC is capillary pressure (Wittmann, 1976; Bentz, 2008; Slowik, et al., 2008; Doa, et al. & 2010 Combrinck, 2011). Capillary pressure is defined as the difference between the pressure in the liquid and in the air immediately over the liquid surface (Doa, et al., 2010). The physical process responsible for the plastic shrinkage of concrete is capillary pressure build-up.

To better understand the process of capillary pressure build-up one needs to examine fresh concrete after it has been cast. Solid particles in the fresh concrete settle and water is transported to the concrete surface due to the effects of gravity. This effect, causing the thin film of surface water, is known as bleeding. The spaces between solid concrete particles form an interconnected pore system, practically completely filled with water. As a result of evaporation, the thickness of the surface water film is reduced. At a certain stage the solid surface particles will no longer be covered with water. Concave water surfaces known as

33

water menisci are now formed between the solid particles as a result of adhesive forces and surface tension, as shown in Figure 3.2. The curvature of the water menisci result in a negative pressure in the capillary water system of the fresh concrete. This negative pressure is illustrated in Figure 3.2 and described by the Gauss-Laplace equation, given as (Wittmann, 1976 & Slowik, et al., 2008):

$$P = -\gamma \left(\frac{1}{R_1} + \frac{1}{R_2} \right) \dots\dots\dots\dots\dots\dots\dots\dots\dots\dots\dots\dots\dots\dots\dots\dots\dots\dots\dots\dots\dots\dots\dots\dots\dots\text{(Equation 3.1)}$$

with P the capillary pressure, γ the surface tension, R_1 the maximum radius of water meniscus and R_2 the minimum radius of water meniscus.
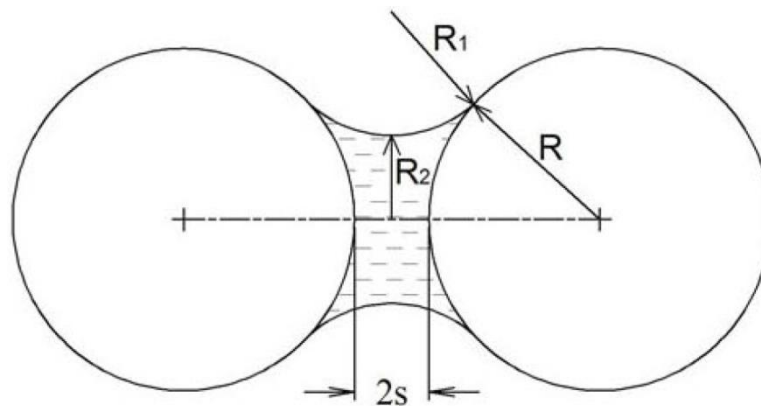
Figure 3.2: A simplified illustration of a water meniscus in a pore between two spherical particles (Doa, et al., 2010)

The two spherical particles in Figure 3.2 have an additional separation, 2s, to account for the surface roughness of the particles. The Gauss-Laplace equation states that the pressure value is inversely proportional to the radii of the water as well as directly dependent on the surface tension of the liquid. This negative pressure influences the surrounding solid particles, drawing them together and resulting in the contraction of the plastic concrete. As evaporation continues, so does the reduction of the main radii of the surface menisci resulting in a continual increase of the absolute capillary pressure as well as the strain of the concrete system. If the plastic shrinkage is in any way disturbed or restrained and the cohesive or tensile forces between solid particles are overcome, it will result in the cracking of the material (Slowik, et al., 2008).

Wittmann (1976) was the first to show that early age shrinkage can be related to the development of capillary pressure within the plastic phase of concrete. A typical plot of simultaneous capillary pressure build-up and plastic shrinkage of a concrete specimen, as a function of time, is shown in Figure 3.3.
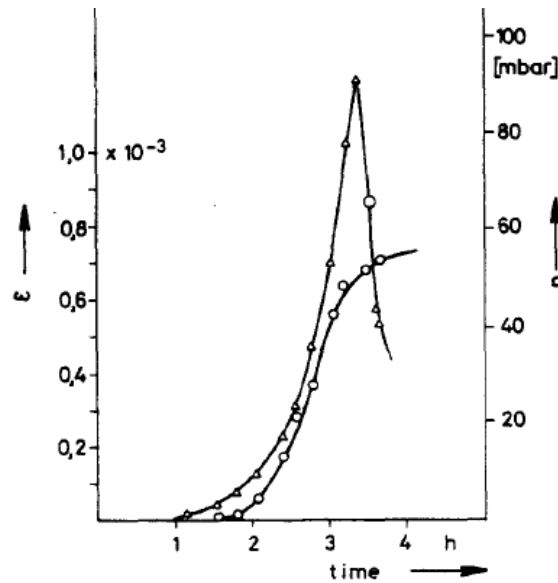
Figure 3.3: Plastic shrinkage and capillary pressure over time (Wittmann, 1976)

During the experiment illustrated by Figure 3.3 the ambient temperature was 20°C, the relative humidity 50% and the wind velocity 4 m/s. During the first hour the concrete surface was covered by a thin layer of bleed water. As a result the measured capillary pressure in the concrete system was close to zero. As evaporation continued, the capillary pressure increased, initially slowly and then at a higher rate after about 2.5 hours. This can be ascribed to the tendency of large pores to lose water before smaller pores. A maximum capillary pressure was reached at around 3.5 hours, whereafter a drastic fall was observed. Wittmann (1976) attributed this fall to the entry of air into the concrete system. This entry of air is discussed in more detail in the following section.

Air entry

The mechanism that indicates the onset of crack formation associated with plastic shrinkage is air entry. As described in the previous section, as evaporation continues the capillary pressure within the concrete also continues to rise. This proceeds till a certain pressure known as the "break-through" pressure is reached. At this point the main radii of the water menisci become too small to bridge the pore spaces between solid particles on the concrete surface. Air systematically and locally penetrates the system, starting with the largest pores. Because of the irregular arrangement and disparity in size of the solid particles on the concrete surface, not all pores between the surface particles are drained simultaneously (Slowik, et al., 2008).

The drained pores where air has entered the system are weak zones in the material. The contracting forces between solid particles in the air penetrated pores are notably smaller than those in the water filled pores. As a result, a localisation of strain occurs in these weak zones

35

of air filled pores which, when restrained, leads to cracks (Slowik, et al., 2008). Electron microscope images ilustrating the progressive development of air entry and crack formation along drained pores is shown in Figure 3.4.
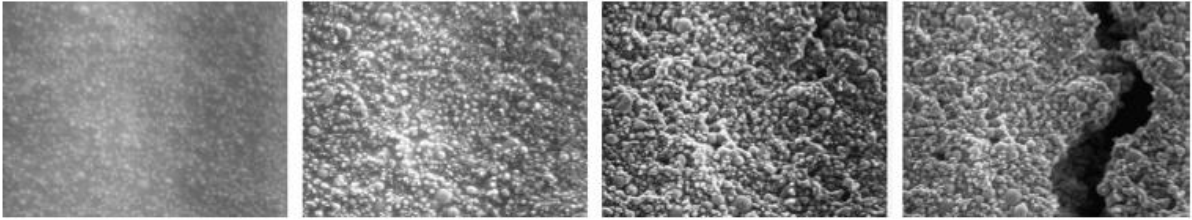
Figure 3.4: Air entry and crack formation along drained pores (Slowik, et al., 2008)

Restraint

As mentioned in the previous section, crack formation, in the case of PShC, can only occur once air entry had occurred. However, cracking is also not possible without the restraint of horisontal shrinkage in the concrete material (Slowik, et al., 2008). Once air entry has taken place in a specific zone, cracks do not automatically develop at this location and this is simply a zone with pores filled with air instead of water. If further plastic shrinkage alone occurs, the material will simply shrink uniformly, reducing its volume. If this shrinkage is restrained in any way, tensile stresses develop in the material. As soon as these tensile stresses exceed the tensile strength of the early age concrete, cracks will occur (Owens, 2012). Restraint is ever present in a concrete material, be it from external or internal sources.

Internal restraint is a result of a differential in volume reduction over the depth of a concrete element. The top portion of the concrete element experiences greater shrinkage than the lower portion due to surface evaporation and capillary pressure build-up. As a result, the free shrinkage of the top portion of the concrete is hindered by the bottom concrete layers, producing cracks on the concrete surface (Combrinck & Boshoff, 2012a).

External restraint of concrete elements is provided by physical boundary conditions which exert restraint on the concrete element boundaries. Formwork with irregular shapes or rough surfaces or dry sub-grade in which concrete is cast, all increase the effect of restraint on a concrete element. Reinforcing steel also provides a form of restraint (Combrinck & Boshoff, 2012a).

Plastic shrinkage cracking severity is typically increased with an increase in concrete restraint, as less free shrinkage is allowed and greater stresses develop within the concrete element.

36

PShC development summary

This section gives an overview of the mechanisms that lead to the occurrence of PShC. The six stages (A-F) in which the mechanisms of capillary pressure build-up, air entry and restraint take effect on a concrete element to produce PShC are shown in Figure 3.5.
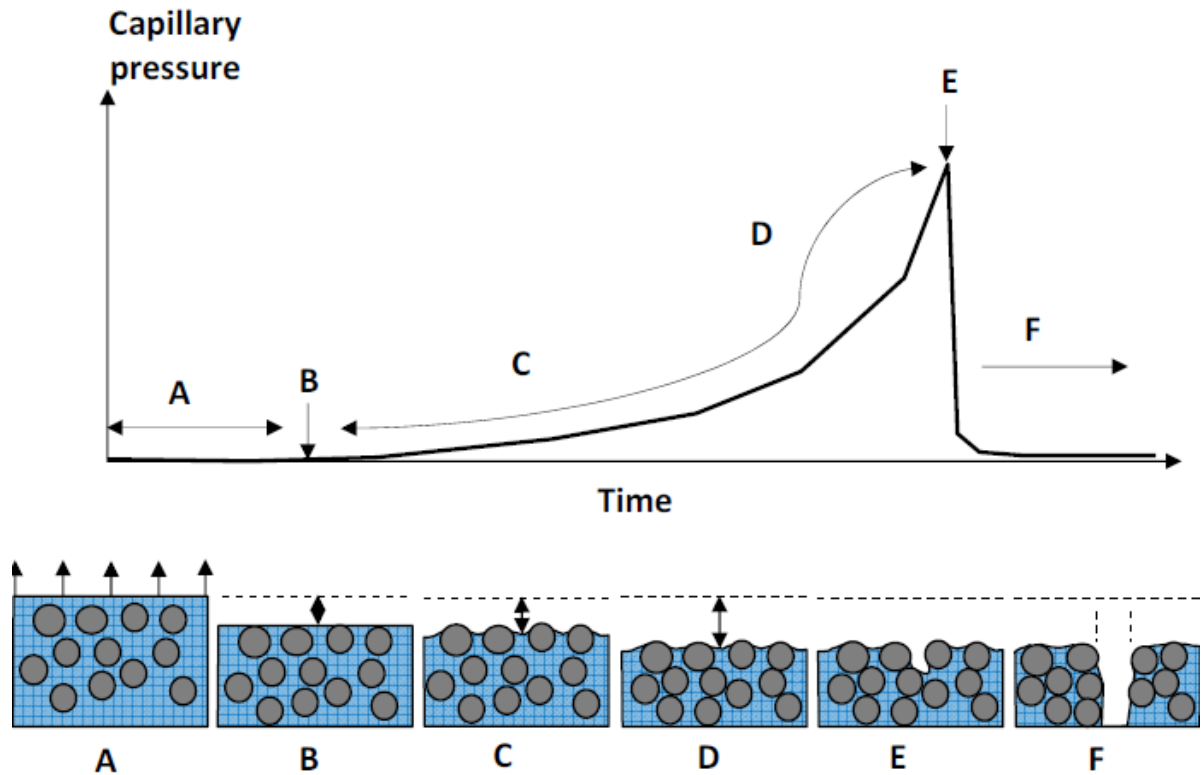
Figure 3.5: Stages of PSC development (Combrinck, 2011)

A:

During this stage a thin film of water is present on the concrete surface. The rate at which bleed water is transported to the surface is initially higher than the rate at which it evaporates. The result is an accumulation of bleed water on the surface.

B:

At this point there is no longer a thin film of bleed water on the concrete surface. The amount of bleed water that has been transported to the surface is equal to the water that has evaporated from the surface. This point indicates the start of capillary pressure build-up.

C:

As the evaporation rate exceeds the bleed rate, menisci gradually form between solid particles and result in an increasing contraction effect and a subsequent capillary pressure build-up.

37

D:

Capillary pressure has a vertical and horisontal component. At this stage the vertical component of capillary pressure forces the solid particles downwards. This results in the displacement of free water upwards, which has a decreasing effect on the capillary pressure (Powers, 1968). Despite this the rate of capillary pressure build-up is still on the rise (Slowik, et al., 2008).

E:

From this point onwards the vertical component of capillary pressure plays a minor role in the formation of PShC, as the maximum vertical settlement has been reached. Significant horisontal shrinkage initiates only once a considerable amount of vertical settlement has occurred, as can be seen in Figure 3.6 (Kronlöf, et al., 1995). This is a result of the horisontal component of the capillary pressure that plays a more significant role at this stage. Once the capillary pressure, known as the air entry or breakthrough value, is reached, the radii of the water menisci on the surface become too small to bridge the pore spaces between solid particles on the concrete surface and air entry occurs. The localised zones of air entry can be seen as weak points from a mechanical point of view (Slowik, et al., 2008).
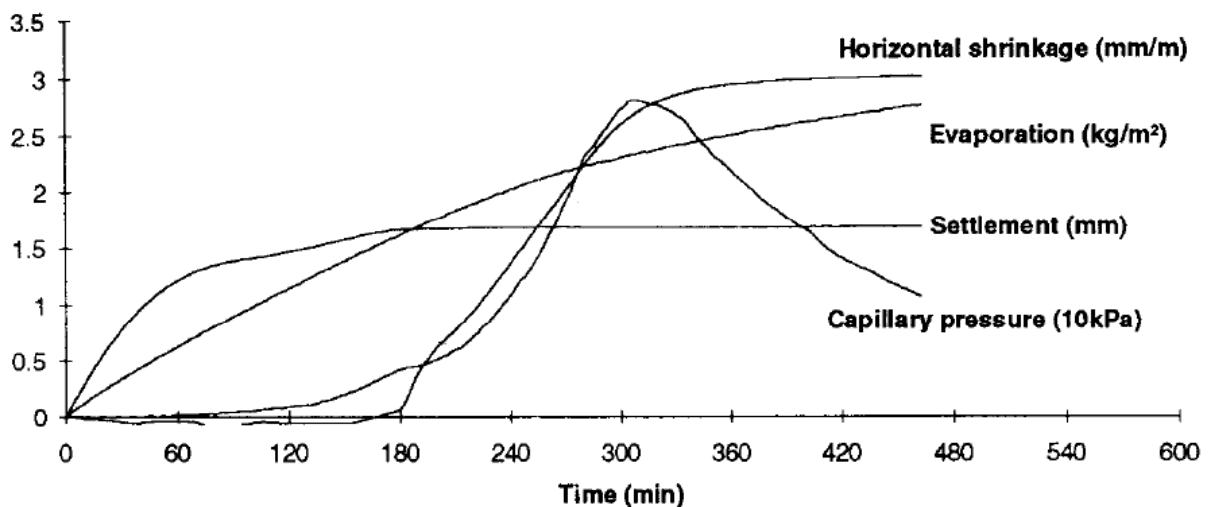
Figure 3.6: Relationship between horisontal shrinkage and vertical settlement (Kronlöf, et al., 1995)

F:

Between the weak zones of air entry the capillary pressure continues to build-up. Localisation of strain occurs in these weak zones as the concrete continues to shrink horisontally. When the shrinkage is restrained, tensile stresses build up until they inevitably exceed the tensile strength of the concrete over these weak zones, causing cracking.

38

3.1.2 Factors influencing PShC

PShC is a complex phenomenon that is influenced by many factors. The fact that many of these factors are interdependent and change over time, further contributes to the complexity of PShC. This section briefly discusses the most significant factors that influence PShC.

Evaporation rate

As previously discussed, capillary pressure, the principal mechanism responsible for PShC, is mostly caused by the evaporation of bleed water from the concrete surface. During evaporation active water molecules escape their liquid mass in the form of vapour through the absorption of heat or when the pressure above the liquid surface is less than that in the liquid. In a fresh concrete specimen the rate at which evaporation takes place is of great consequence because once the cumulative amount of evaporated surface water exceeds the cumulative amount of bleed water supplied to the surface, plastic shrinkage can occur. The factors that influence the evaporation rate are: wind velocity, relative humidity, concrete temperature and air temperature (Uno, 1998). These factors and their influence on evaporation are discussed briefly:

Wind velocity has a major effect on the evaporation rate. Wind continuously transports escaping water molecules from the liquid surface to the atmosphere. An increase in wind velocity leads to a significant increase in the rate of evaporation. As a result, one of the most effective ways to limit PShC is by limiting the exposure of a fresh concrete surface to wind (Uno, 1998).

Relative humidity refers to the level of water saturation of air at a specific temperature. It is given as a percentage of the actual amount of water vapour present in a unit volume of air over the maximum (saturation) amount of water vapour the air can hold at a specific temperature. The higher the air temperature, the higher is the air's capacity to hold water vapour (Uno, 1998). The consequence is that a sudden increase in air temperature would decrease the relative humidity of the air and this lower relative humidity, will increase the rate of water evaporation.

Concrete temperature actually refers to the concrete water temperature. The concrete water temperature is however influenced, through heat transfer, by the temperature of all the concrete constituents. A higher surface water temperature is an indication of water molecules with higher energy which leads to an increased evaporation rate (Uno, 1998). Heat produced by hydration within concrete also leads to an increase in the concrete temperature.

Air temperature has a significant effect on the rate of evaporation by influencing the relative humidity and the concrete temperature (Uno, 1998). Consequently, a higher air temperature leads to an increase in the rate of evaporation.

Bleeding

The rate as well as the cumulative amount of bleeding that takes place in a concrete element has a great impact on the occurrence of PShC. As mentioned previously, capillary pressure starts to builds up once the cumulative amount of evaporated water from the concrete surface exceeds that of the bleeding water on the surface.

Bleeding is the process of upward movement or displacement of water in fresh concrete. It can easily be identified by the formation of a thin film of water on the concrete surface shortly after it has been cast. In extreme cases this layer can amount to 2% or more of the total depth of the concrete section (Illston & Domone, 2001). Bleeding can either be categorised as normal bleeding or channel bleeding.

The mechanism causing normal bleeding is settlement. When observing a normal fresh concrete, the solid particles in concrete are denser than the concrete water. The effect of gravity displaces solid particles downwards while moving water upwards which then accumulates on the surface. This bleeding stops once no more settlement occurs (Powers, 1968). Settlement ceases once force equilibrium distances have been reached between solid particles or as a result of setting as the interparticle distances are bridged and fixed by the formation of hydration products (Slowik, et al., 2009). Channel bleeding occurs when channels form, allowing water to be transported from the interior of the concrete to its surface. This produces a significantly higher bleeding rate than normal bleeding and concrete mixes with insufficient cohesion or excess free water are most prone to its occurrence (Powers, 1968).

Numerous factors influence the rate and cumulative amount of normal bleeding. These factors include concrete permeability (Mehta & Monteiro, 2014), aggregate content and fineness, mix water absorption (internally or by its surroundings), capillary pressure build-up, hydration, vibration intensity and duration (Powers, 1968), mix water content and concrete element depth (Kwak & Ha, 2006). The effect of concrete permeability and aggregate fineness are briefly discussed.

Concrete permeability influences the rate at which water can move upwards within the porous media that is the concrete. Concrete with a high permeability will allow swift passage of water upwards, leading to a high bleeding rate. The permeability of fresh concrete is primarily decreased by an increase in fine content. Apart from making the concrete paste

40

less permeable, an increased amount of fine particles also increase the specific surface area of aggregates, which also reduces bleeding. Fines in the form of cement lead to an additional reduction in permeability due to hydration as the hydration products fill the interparticle pores systematically as the reaction commences (Powers, 1968).

Concrete composition

In this section concrete composition refers to the size and distribution of solid particles used in a concrete mix. The occurrence of PShC is notably reduced with an increase of average particle size. This is firstly a result of an increased bleed rate, as discussed in the previous section. The other reason is that smaller particles in near proximity to each other at the concrete surface have smaller menisci radii between them (Slowik, et al., 2009). This leads to an increase in the capillary pressure, as described in Section 3.1.1, increasing the risk of PShC.

Larger particles also have greater self-weight than those of smaller particles, which results in more stable particle structures, limiting particle mobility. This is a result of the gravitational force acting on the large particle being significantly greater than other inter-particle forces, such as van der Waals forces, electrostatic forces and Born repulsion. The greater mobility of smaller particles makes them more vulnerable to the effects of the horisontal component of capillary pressure. In a concrete element this would translate to greater strain localisations which may eventually lead to cracking (Slowik, et al., 2009). The result would be an increase in the occurrence and severity of PShC.

Restraint

This PShC influencing factor has already been described in Section 3.1.1 Plastic shrinkage cracks cannot occur without plastic shrinkage of the concrete material being restrained in some way. This will induce tensile stresses in the material, which when exceeding the tensile strength of the concrete material, leads to PShC. An increase in restraint, internal or external, will lead to a subsequent increase in the occurrence and severity of PShC (Combrinck & Boshoff, 2012a).

3.1.3 PShC behaviour model

This section describes the behaviour of typical PShC which include the important events leading to the occurrence of PShC. The model that is discussed was proposed by Combrinck (2011) and is shown in Figure 3.7, and the events shown in the figure are described chronologically.
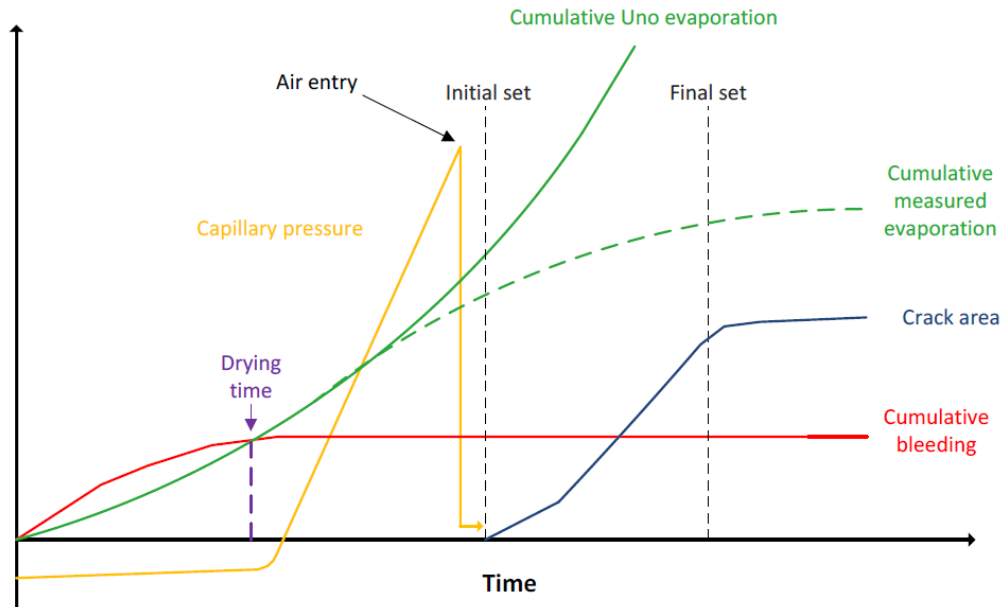
Figure 3.7: PSC behaviour model (Combrinck, 2011)

Drying time

At this point the concrete pore water starts to evaporate. This point signifies the start of tensile capillary pressure build-up. It should be noted that the concrete system's capillary pressure is typically in compression before this event due to its internal hydrostatic pressure provided by water (Combrinck, 2011).

The drying time can only be reached once the rate of evaporation is higher than the rate of bleeding and the cumulative evaporation exceeds the cumulative bleeding (Combrinck, 2011). The rate of bleeding is initially high, and then decreases with time until bleeding ceases and the cumulative bleeding becomes constant. The evaporation rate, in contrast, is initially low, and then increases over time as a result of an increasing concrete water temperature, leading to a continuously increasing cumulative evaporation. The Uno evaporation, shown in Figure 3.7, continuously increases with time due to the continuously increasing concrete temperature. In contrast, the measured evaporation decreases after a certain amount of time. The reason for this difference is that the Uno evaporation considers only open water evaporation, whereas the measured evaporation decreases as setting commences and bleed water transfer to the surface is reduced. However, these two evaporation curves are identical up until the drying time, which effectively is the end of open water evaporation.

Time of air entry

At this point air entry occurs locally at the concrete surface and the capillary pressure rapidly decreases. The concrete paste can no longer resist the capillary pressure, and air enters the

paste. It should be noted that the capillary pressure is usually measured at a localised point and air entry could occur at another location before a pressure drop is measured at the specific location (Combrinck, 2011).

Initial setting time

The occurrence of PShC is usually witnessed once the initial setting time has been reached. From this time onward the crack width increases and typically stabilises at the point of final setting (Combrinck, 2011).

Final setting time

After this point cracks may still widen, but at a considerably lower rate. Drying shrinkage and temperature changes may also cause cracking from this point onwards (Combrinck, 2011).

3.1.4 Preventing and mitigating PShC

The environmental conditions conducive to the occurrence of PShC are common across South Africa. As PShC can be detrimental to the durability, strength and ultimately the safety of concrete structures it is important to be aware of how to limit PShC occurrence and severity (Qi, 2003). The primary way to limit PShC occurrence and severity is by decreasing the evaporation rate and increasing the bleed rate and volume (Boshoff & Combrinck, 2013). External measure to limit evaporation and consequently PShC includes (Uno, 1998 & NRMCA, 1998):

- Wind breaks which reduce air flow over the surface of concrete,
- Curing of the concrete surface directly after casting by means of, vapour spray, curing compounds, damp surface covers or polyethylene sheeting,
- Wetting the subgrade or formwork prior to casing as to reduce the amount of water absorbed by them and subsequently removed from the concrete,
- If conditions are extremely conducive to the formation of PShC, schedule concrete casting to be done early in the morning or late in the afternoon to reduce evaporation.

Internal measures to limit PShC include (Uno, 1998; NRMCA, 1998 & Bentz, 2008):

- Adding evaporating retarders, such as aliphatic alcohol, to concrete,
- Avoiding the use of admixtures that reduce bleeding,
- Limiting the fine content of a concrete mix, in size or distribution, as this would reduce bleeding and increase capillary pressure build-up,
- Avoiding the excessive use of retarders as this delays setting and consequently prolongs the period in which PShC can occur. However, tests conducted by Combrinck & Boshoff (2012b) found the moderate addition of a retarder to a

reference mix reduced the severity of the induced PShC when compared to a reference mix.

- The addition of shrinkage reducing admixture which reduces the surface tension of the concrete,
- Adding a low volume of synthetic microfibres to the concrete mix.

Many of these precautionary measures do however pose difficulties with regards to successful implementation and cost. If these methods are not implemented correctly, it could lead to reduced effectiveness as well as decreased concrete quality. The use of synthetic microfibres is further discussed in Section 3.3, as they are of significance to this study and have proven to effectively limit PShC occurrence and severity (Hannant, 1978).

3.2   Plastic settlement cracking (PSeC)

Plastic settlement cracks occur while concrete is still in its plastic state, during the process of settlement. These cracks typically start to occur after the concrete has been cast till the concrete is no longer plastic, which generally corresponds with the initial setting time (Owens, 2009 & Combrinck & Boshoff, 2012).

Plastic settlement cracks can be distinguished from plastic shrinkage cracks by the characteristic crack pattern that typically mirrors the form of restraint that the concrete element is subjected to, for example steel reinforcing or a change in element section as shown in Figure 3.8 (Cement, Concrete & Aggregates Australia, 2005). Plastic settlement cracks can easily develop further by acting as weak zones for crack widening caused by subsequent volume changes related to plastic, drying, thermal, and chemical shrinkages (Holt & Leivo, 2004).
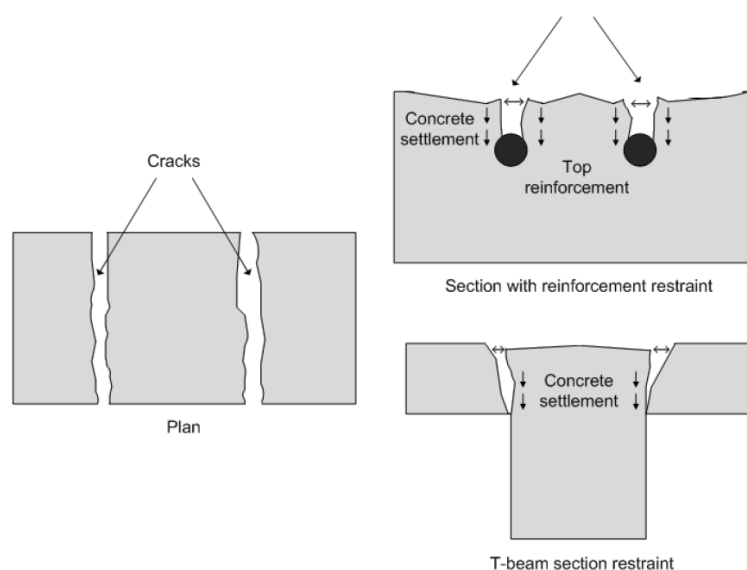
Figure 3.8: Typical plastic settlement cracks (Illston & Domone, 2001)

44

This section first discusses the mechanisms and development of PSeC. After this the interaction between PSeC and PShC is described, and finally, the methods to reduce PSeC occurrence and severity will be presented.

3.2.1 Mechanisms and development of PSeC

Plastic settlement cracks do not occur as a result of capillary pressure build-up or air entry, as is the case with plastic shrinkage cracks. Rather, it occurs as a product of a combination of vertical settlement and vertical restraint, resulting in differential settlement.

After fresh concrete has been cast, the effect of gravity causes the vertical settlement of the material. Bleed water moves to the surface while solid particles settle downwards. If no vertical restraint is present it merely results in a slightly lowered concrete surface. However, if the concrete is locally restraint from settling, while the adjacent concrete continues to settle, it gives rise to the development of stresses in the weak material. If these stresses exceed the strength of the fresh concrete, cracking or separation will occur in the material over the source of restraint (Mehta & Monteiro, 2014).

The differential settlement of fresh concrete around a reinforcing bar results in three distinctive defects, as shown in Figure 3.9. The first are the angled cracks that originate from the sides of the reinforcing bar to the concrete surface, as depicted in Figure 3.9 b), and referred to as shear cracks. The origin of these cracks corresponds with the border between the respective settlement zones. While these shear cracks are a result of tensile stresses, as shown by the rotated block with principal stresses in Figure 3.9 b), the source of these tensile stresses are shear stresses produced by the mechanism of differential settlement. The second defect is the formation of a tensile crack on the surface that propagates downwards to the reinforcing bar. These cracks are a product of direct tensile stresses, as shown in Figure 3.9 b), that also originate as a result of the differential settlement between the concrete at the sides of the reinforcing bar and the concrete above the reinforcing bar. The last defect is the development of water pockets under the reinforcing bar. This happens as a result of the settlement of concrete below the reinforcing bar and these water pockets form voids at a later stage (Combrinck & Boshoff, 2014).

It should be noted that restraint is essential for the occurrence of both types of early age cracking. Plastic shrinkage cracks require horisontal restraint for cracks to occur while plastic settlement cracks require vertical restraint (Combrinck & Boshoff, 2012a)
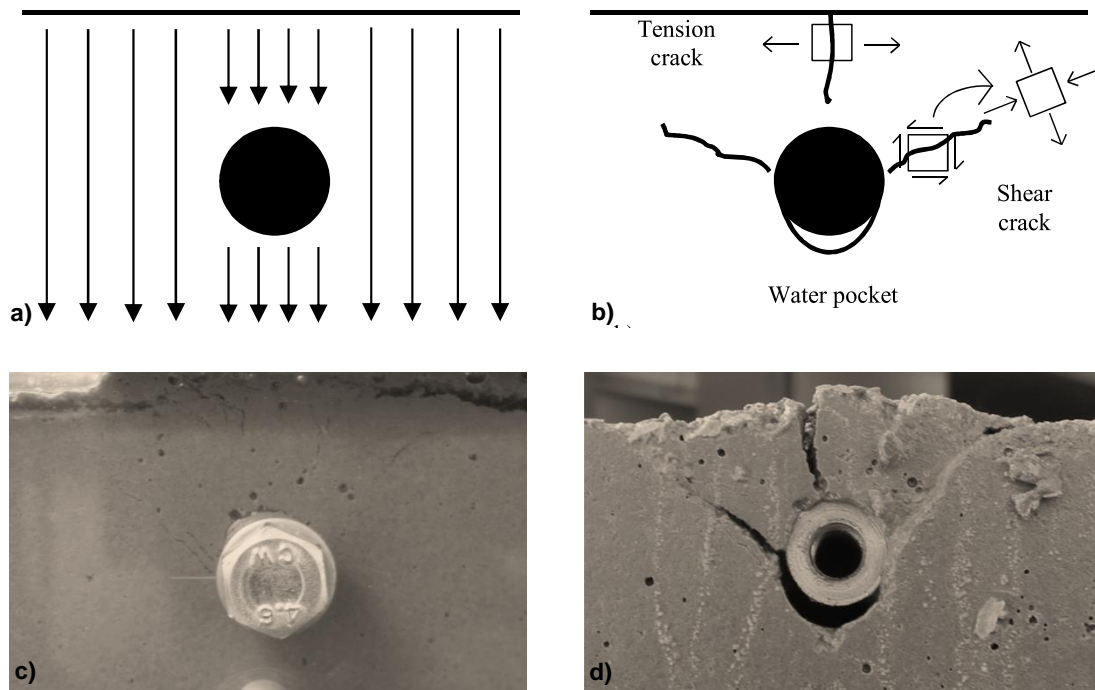
Figure 3.9: a) Respective settlement zones caused by reinforcing bar. b) Distinctive defects caused by differential settlement. c) Distinctive defects at initial setting time. d) Distinctive defects after final setting time (Combrinck & Boshoff, 2014)

Since differential settlement is the mechanism leading to the occurrence of plastic settlement cracking, concrete mixes that produce minimal settlement are less prone to the occurrence of these cracks. Bleeding is traditionally a good indication of settlement as a large amount of bleeding is usually indicative of a corresponding amount of settlement (NRMCA, 1998). However, it was found that low bleed concrete mixes that utilised a large amount of fine particles produced greater differential settlement than their high bleed counterparts. This is because these types of low bleed mixes lead to higher paste mobility and capillary pressure build-up and therefore also PShC. This causes an increase in PSeC that can only be ascribed to the vertical component of capillary pressure build-up that leads to an additional amount of vertical settlement (Combrinck & Boshoff, 2012a).

3.2.2 Interaction between PSeC and PShC

Combrinck & Boshoff (2012) carried out a study to determine the influence of restraint on early age cracking as well as the relationship between PSeC and PShC. These tests were conducted under conditions that were conducive to the development of both plastic PSeC and PShC. It was found that the first cracks occurred considerably earlier than the initial setting time and air entry. It is thus conclusive that the cracking was induced by differential settlement and not capillary pressure. Vertical plastic settlement as well as horisontal plastic shrinkage was responsible for the substantial crack growth up to the initial setting time. This was substantiated by the fact that the settlement was still occurring before the initial setting

46

time had occurred and capillary pressure build-up as well as air entry, leading to plastic shrinkage, was also witnessed during this time. The bulk of the cracking occurred long before it was expected due to the prior formation of plastic settlement cracks (Combrinck & Boshoff, 2012a).

It was determined that under environmental conditions with high evaporation rates, the occurrence of plastic settlement cracks could force the early and unanticipated development of the bulk of all early age cracking before the initial setting time had occurred. This "crack jump behaviour" is due to a combination of the following factors (Combrinck & Boshoff, 2012a):

- The plastic state of early age concrete,
- The practically fully developed capillary pressure build-up at the time of crack occurrence,
- The global pressure relaxation across the entire concrete element once the crack occurs, leading to all additional deformation being localised at the cracking position,
- The combined effect of PSeC and PShC working in agreement to open the crack further in both the vertical and horisontal direction.

3.2.3 Preventing and mitigating PSeC

The following measures can be taken to decrease the likelihood of PSeC occurrence and its severity (NRMCA, 1998):

- Use mixes with low settlement characteristics. Lower slumps and good cohesiveness are usually indications of this. Caution should however be exercised not to use an excessive fines content to achieve this as this will increase the vertical component of capillary pressure, leading to increased differential settlement (Combrinck & Boshoff, 2012a),
- Increase the ratio of concrete cover to reinforcement bar diameter. This will decrease the restraining effect of the reinforcement on the concrete. One can either achieve this by increasing the cover or decreasing the reinforcement bar diameter,
- Wetting the subgrade or formwork prior to casing to reduce the amount of water absorbed and subsequently removed from the concrete,
- Ensure that all formwork is installed accurately and securely so that no movement will take place during the casting of the concrete,
- Compact concrete sufficiently and ensure that prompt and proper curing takes place,
- Make use of sequential placement. Ensure that concrete is first cast into deep sections, like columns, and allowed to settle prior to casting and compacting of top

sections, like slabs. This should be done with care as not to cause cold joints (Kwak & Ha, 2006).

- Re-vibrating of the concrete just prior to its initial setting time in order to close the crack formed by PSeC (Kwak & Ha, 2006).

Although the addition of a low volume of synthetic microfibres reduces the occurrence and severity of PShC, it shows no significant influence on PSeC. PSeC usually occurs before the initial setting time of concrete. This is the time at which the interfacial shear bond stress between the microfibres and the concrete matrix start to develop. As a result, no significant additional resistance to PSeC is provided to the concrete with the addition of microfibres. This has been proven under environmental conditions conducive to a high evaporation rates and is still to be confirmed under other environmental conditions (Combrinck & Boshoff, 2012a).

3.3   Low volume fibre reinforced concrete (LV-FRC)

A conventional concrete which contains an addition of microfibres less than 0.2% of the entire concrete volume is defined as a low volume fibre reinforced concrete (LV-FRC) (Hannant, 1978). Microfibres refer to fibres with a cross section diameter in the same order as that of cement grains, typically less than 40 µm, with a length typically less than 25 mm (Mehta & Monteiro, 2014 & Illston & Domone, 2001). Usually synthetic fibres such as polyester, polyethylene and polypropylene are utilised in LV-FRC. These fibres characteristically have a low Young's modulus and a high percentage of elongation. These fibres are primarily available in two forms, monofilament fibres and film fibres (Hannant, 1978). This study considered and used monofilament polypropylene microfibres and when referring to fibres it should be assumed to be these fibres.

This section firstly discusses the advantages of LV-FRC, and identifies the mitigation of PShC as the most significant. Next, the mechanisms that control PShC in LV-FRC as well as the properties of fibres that influence PShC are described. Finally, the influence of fibres on bleeding is considered.

3.3.1 Advantages of LV-FRC

The addition of a low volume of synthetic microfibres to conventional concrete in an arbitrarily distributed manner has several advantages. LV-FRC has improved mechanical properties when compared to conventional concrete with regards to ductility and post-cracking behaviour. However, it should be noted that the tensile strength of LV-FRC is never more than that of conventional concrete. All fibres added to concrete only offer mechanical benefits once concrete cracking has occurred. For LV-FRC the tensile strength added by the fibres

after cracking, is insignificant when compared to the tensile strength of the concrete, and consequently does not contribute to the structural integrity of an element. However, the addition of a low volume of fibres does reduce the occurrence and growth of PShC (Illston & Domone, 2001 & Wongtanakitcharoen, 2005).

External methods of limiting PShC such as, sun shades, wind breaks, moisture retaining covers and sun sprays have the disadvantages of additional cost and labour associated with their erection or implementation. In some instances these methods cannot be utilised due to positional difficulties or construction limitations. However, the addition of fibres to concrete does not have these drawbacks and can be incorporated with or without the mentioned external methods to limit PShC.

Another advantage of the addition of fibres to concrete is an increased fire resistance. During a fire the evaporation of water inside the concrete occurs. Due to the greater volume of water vapour, expansion within the concrete occurs and consequently the spalling of concrete. This exposes steel reinforcing to the extreme heat of the fire, usually leading to the failure of the structure. With an LV-FRC the synthetic fibres combust, creating channels for steam to expand and escape and preventing the spalling of concrete, and therefore the exposure of steel reinforcing, to a great extent (Zeiml, et al., 2006).

3.3.2 Mechanisms controlling PShC in LV-FRC

It is clear that the addition of fibres to concrete decreases the occurrence and severity of PShC. However, the extent of this control is not fully understood. From a mechanical viewpoint the obvious explanation for the increased resistance to PShC occurrence and severity of LV-FRC is the additional post-cracking tensile strength provided by the bridging of fibres over a crack plane. The bonding of the concrete paste and fibres, referred to as the interfacial shear bond, is responsible for this additional tensile strength after cracking (Hannant, 1978). A typical fibre bridging over a crack is shown in Figure 3.10. The interfacial shear bond between the concrete paste and fibres is extremely weak in the case of fresh concrete (Wongtanakitcharoen, 2005). Due to this, it is believed that no significant additional resistance to PSeC is provided by fibre additions, as mentioned in Section 3.2.3. As time passes this bond continuously increases as solid contact points between the fibres and concrete paste increase due to the formation of hydration products. The initial setting time is an approximate indication of the point at which the interfacial shear bond between fibres and the concrete paste starts to increase (Combrinck & Boshoff, 2012a).

Since the interfacial shear bond increases with time and fibres only become effective once cracking has occurred, the time at which cracking initiates also influences the effect of fibres on PShC. From this it can be seen that to understand the exact time, means and degree in

49

which fibres control PShC, is a complex and multifaceted problem. At this stage no theory adequately describes the effects of fibres on PShC (Illston & Domone, 2001).
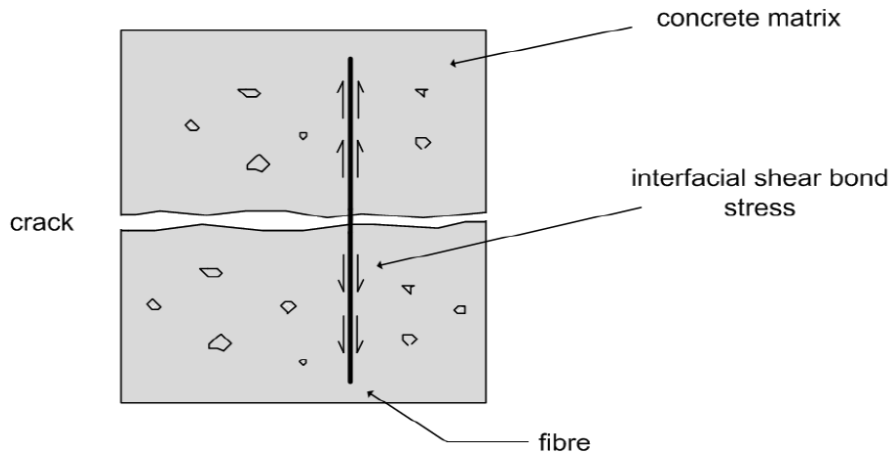
Figure 3.10 Fibre bridging over crack plane (Maritz, 2012)

3.3.3 Properties of fibres influencing PShC

After the initiation of cracking, the extent to which fibres can bridge a crack depends on the magnitude of the interfacial shear bond stress between the fibres and the concrete paste. Hannant (1978) proposed a model to determine the ultimate post-cracking stress sustained across a cracked plane of a composite by:

$$\sigma_{cu} = \frac{1}{2}\tau V_f \frac{L}{d} \dots\dots\dots\dots\dots\dots\dots\dots\dots\dots\dots\dots\dots\dots\dots\dots\dots\dots\dots\dots\text{(Equation 3.2)}$$

with σ_{cu} representing the ultimate bridging stress over the crack plane, τ the interfacial shear bond stress, V_f the volume fraction of fibres, L the fibre length and d the fibre diameter. The following assumptions apply to the model for all short, arbitrarily distributed fibres:

- the fibres pull out rather than break,
- the fibres are straight without hooks and,
- the fibres remain straight throughout the pull-out process.

This model was developed for mature concrete, but is still believed to be applicable to early age concrete. The factors that significantly impact the ultimate bridging stress are identified as interfacial shear bond stress, fibre volume and fibre aspect ratio. These factors are discussed in the following sections.

Interfacial shear bond stress

When considering fibres bridging the gap between two cracked surfaces, the interfacial shear bond stress between the fibres and the concrete paste is essential in order to transfer tensile stresses from the concrete paste to the fibres. Without this no tensile stress can develop in

the fibres, causing the strength of the concrete composite to be the same as that of the cracked concrete matrix (Johnston, 2001).

Combrinck (2011) conducted single fibre pull-out test to investigate the development of interfacial shear bond stress with time on polypropylene fibres. For specimens tested one hour after casting an interfacial shear bond stress value of 0.22 kPa was determined, while for the 5 hour test this value was 21 kPa. It is therefore assumed that the fibres in an early age concrete, as defined in this study, will not rupture when a tensile stress is applied, but rather pull out. The time dependant nature of the interfacial shear bond stress is made apparent as it increases as the degree of hydration increases. Figure 3.11 shows the fibres after they have been pulled-out from concrete at various ages. On the fibre surfaces a clear increase in frictional skid marks can be seen over time, indicating the increased frictional bond between fibres and concrete paste.
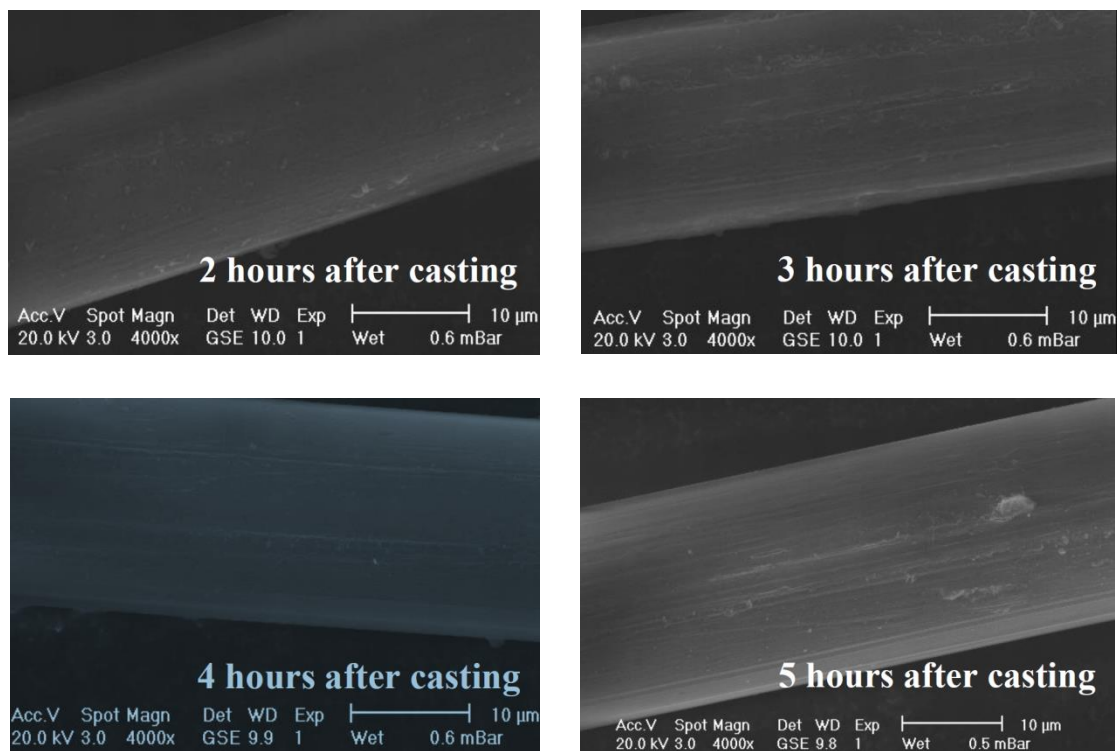
Figure 3.11: Electron microscope images of the effect of pull-out on fibres (Combrinck, 2011)

The pull-out mechanisms responsible for the shear bond stress between fibres and the concrete paste are adhesion, friction and mechanical anchorage. As the polypropylene fibres used in this study are smooth and straight, mechanical anchorage does not contribute to the pull-out resistance. Adhesion and friction however do occur. The sticking or joining together of two surfaces is referred to as adhesion. In this context it can either be classified as normal adhesion between fibre and concrete paste or chemical adhesion. Normal adhesion is a result of the attractive forces that exist between molecules whereas chemical adhesion

occurs when the fibre surface absorbs water that at a later stage takes part in the chemical reaction of hydration (Wongtanakitcharoen, 2005). The solid contact areas between the fibre and the concrete paste lead to interfacial friction once movement occurs. As the amount and magnitude of the contact areas increase, as hydration takes place, so does the magnitude of the friction. The magnitude of both the adhesion and friction is subject to primarily the surface texture and coatings of the fibres. A coarse surface texture would allow for increased friction and adhesion to develop. The effect of the surface coating differs considerably depending on the coating. They are most often applied to improve the adhesiveness of fibres, but can also result in a smoothened surface finish, reducing the fictional bonding potential of the fibre (Johnston, 2001).

Fibre volume

A typical commercial dosage of fibres is a 0.1% by volume addition (Illston & Domone, 2001). This addition significantly aids in the controlling of PShC while undesirably influencing other concrete properties to a lesser degree. The effect of different fibre volume additions on a concrete is of great interest to this study.

In theory an increase in the fibre volume in a concrete would correspondingly increase the amount of fibres bridging the crack plane, decreasing the area of stress transfer for the concrete matrix to the individual fibres, as shown in Figure 3.12. As the tensile stress transferred to each fibre decreases, the occurrence of fibre debonding is less likely. This results in a higher post-cracking load capacity, subsequently reducing PShC severity (Maritz, 2012).
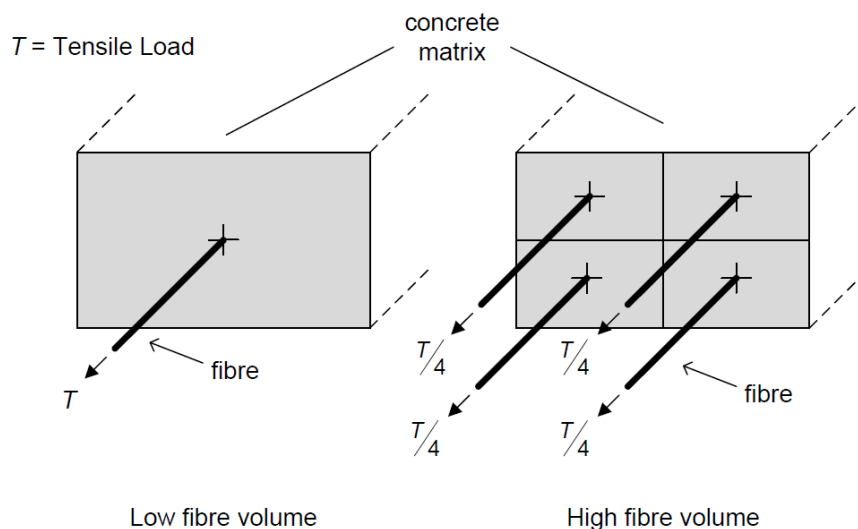
Figure 3.12: Effect of an increased fibre volume on the tensile load per fibre (Maritz, 2012)

Fibre aspect ratio

The ratio of fibre length, L, to fibre diameter, d, is defined as the fibre aspect ratio. For a fixed fibre length and volume fraction, the use of a smaller diameter fibre can be more effective in controlling PShC than larger diameter fibres. This is a result of the increased surface area provided by the smaller diameter fibres, that allows for increased interfacial shear bond stress area between the fibres and concrete paste, allowing improved stress transfer (Bagherzadeh, et al., 2011). The use of smaller diameter fibres, opposed to larger diameter fibres, also increase the amount of fibres bridging a crack plane. Due to this, the space between un-bridged areas in the concrete paste decrease, reducing stress concentrations and effectively the stress that is required to be transferred by the concrete paste to the fibres. The result is increased crack growth resistance. If the fibre diameter is further decreased it may become too small to allow for adhesion to and friction between the solid contact areas of the concrete, resulting in the development of insufficient interfacial shear bond stress.

It should also be noted that for a fixed fibre diameter and volume fraction, the influence of fibre length may have varying effects. The use of short fibres lead to an increased amount of fibres available to bridge the crack plane, limiting PShC in this manner. However, the use of longer fibres, although resulting in fewer fibres per volume fraction, may significantly increase the interfacial shear bond stress, also limiting PShC.

It is clear to see that in order to increase a LV-FRC resistance to PShC one cannot simply increase the fibre aspect ratio. Determining the optimal aspect ratio for a specific volume fraction of fibres is of great interest to the field of LV-FRC.

3.3.4 Influence of fibres on bleeding

Typically the addition of fibres lead to a reduction in the cumulative amount of bleeding as well as the bleeding rate. The presence of fibres in a concrete mix increases the stiffness and cohesion of the material, which in turn reduces settlement and subsequently bleeding (Qi, 2003). The increased fibre surface area could also cause a reduction in bleeding, particularly if the fibres are hydrophilic in nature (Uno, 1998). A larger fibre volume fraction addition or a smaller fibre diameter could further increase the bleeding reduction effect of fibres.

It should also be noted that in certain instances the addition of fibres may increase the bleeding of a concrete mix. This is a result of the fibres acting as channels whereby water can be transferred to the concrete surface (Qi, 2003).

As stated in Section 3.1.1, bleeding plays a significant role in the build-up of capillary pressure and the occurrence of PShC. As a result, the addition of fibres will also influence

53

the process of capillary pressure build-up. In the case where fibres will reduce bleeding, the capillary pressure build-up rate will increase, making the concrete more susceptible to the occurrence of PShC. This would unintendedly decrease the degree to which fibres control PShC.

3.4   Concluding summary

In this chapter PShC and PSeC are identified as two types of early age cracking. It is explained that capillary pressure together with air entry and horisontal restraint are responsible for the occurrence of PShC. The influencing factors of PShC are confirmed as the rate of evaporation, bleeding, concrete composition and restraint. Methods of limiting or preventing PShC are identified such as decreasing the concrete evaporation rate, increasing the amount and rate of bleeding, accelerating the setting time and the addition of a low volume of microfibres. PSeC was considered next. The primary mechanisms were determined to be differential settlement and vertical restraint. A strong interaction between PSeC and PShC is described. The measures to mitigate PSeC are then presented. Next, LV-FRC was defined and discussed. The advantages of fibres, the mechanism at work in LV-FRC that influence PShC, as well as the fibre properties that influence PShC are discussed. Finally, the influence of fibres on bleeding is considered. The next chapter discusses the design of the tensile testing setup used in this study.

4. Design of the experimental tensile setup

The early age cracking of concrete, as discussed in Chapter 3, occurs when a concrete has insufficient tensile strength and strain capacity to withstand its environment. These cracks typically occur after casting and consolidation up to the final setting time. The tensile material properties of early age concrete during this period are of great importance, not only for fundamental understanding but also the prevention of early age cracking. With this in mind, this chapter describes the design of the experimental setup used to determine the tensile properties of early age concrete during this period. This chapter first presents a review on apparatus used in literature for the determination of the tensile properties of early age concrete. The conditions for effectively determining both the ascending and descending portions of the stress-strain curve of early age concrete are discussed. Next, the initial test setup and results obtained from initial testing are discussed, highlighting its shortcomings and knowledge gained from it. Finally, the final test setup, designed utilising the knowledge gained from the literature review and the initial test setup, is described in detail.

4.1   Literature review

The methods used to determine the tensile properties of materials can either be categorised as direct or indirect tensile testing methods. The direct tensile testing of concrete, although of considerable theoretical and practical significance, has been given little consideration in the past by researchers. Indirect tensile testing methods are more commonly preferred for the study of the tensile properties of concrete due to its simplicity. In comparison, direct tensile tests provide results that are generally more reliable and coherent (Swaddiwudhipong, et al., 2003). However, due to the low degree of hydration present in early age concrete specimens during the period between casting and consolidation and final set, direct tensile methods are the only viable method of determining the tensile properties of this complex material which is in transition from a plastic suspension to a weak brittle solid. This review accordingly focuses on the literature relating to the direct tensile testing methods applicable to early age concrete. The aim of this literature review is to ultimately serve as a guideline for the development of a direct tensile testing setup and procedure to deliver reliable results from which the ultimate tensile strength, strain capacity, Young's modulus and fracture characteristics of early age concrete can be determined.

As stated before, because of the numerous practical difficulties associated with testing a material that cannot yet support its own weight without failure and since rheological and

mechanical properties of early age concrete are continuously evolving during the measurement procedure (Bentz, 2008), there is very limited literature available on this topic.

The earliest literature found on the measurements of the tensile properties of early age concrete is that of Ravina & Shalon (1968), as mentioned in Section 2.2.1. This study made use of a steel mould, a test setup much like that utilised for the ductility testing of bituminous materials and a proving ring for force measurement. However, it was not ideally designed to accommodate the testing of early age concrete. Abel & Hover (1998) made significant progress by conducting tensile tests on fresh concrete by using tensile moulds formed by two halves. These mould halves served as grips to transmit a tensile load to the concrete specimen inside the mould. Ball-bearing slides were used to minimise friction during the linear motion of the two halves moving apart while a frame loading structure was used to impose the tensile load responsible for pulling the mould halves apart.

As mentioned in Section 2.2.1, the first description of the complete stress-displacement curve of early age concrete was done by Hannant, et al. (1999). An illustration of the experimental setup used in this study is shown in the Figure 4.1.
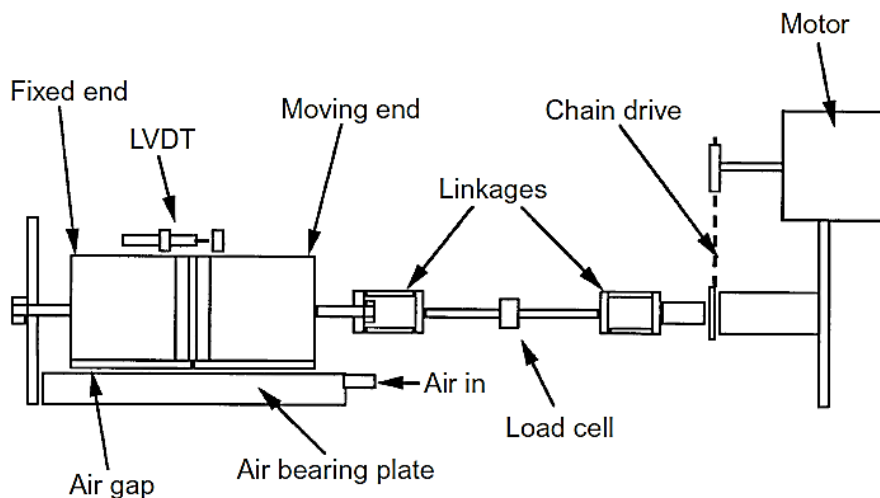
Figure 4.1: Tensile testing setup as used by Hannant, et al. (1999)

The following issues were identified by Hannant, et al. (1999) as key challenges to overcome for the reliable capture of the full tensile stress-displacement behaviour of early age concrete:

- The gripping of an early age concrete specimen to impose a tensile load,
- Elimination of the friction between the specimen mould and its vertical supports during horisontal movement,
- Limiting the damage to the concrete microstructure before the test is conducted,
- The placement of the specimen in the testing machine.

The tensile testing mould used by Hannant, et al. (1999) is shown in Figure 4.2. Since concrete in tension would easily slip out of a parallel-sided mould, gripping keys, indicated by (A) on Figure 4.2, were introduced to provide sufficient shear resistance at the concrete-mould interface. A 50 mm gauge length is indicated by (B), while (C) indicates the formation of a neck which reduces the section width from 100 to 70 mm, inducing cracking over the gauge length. In addition, 2 mm thick removable plates, indicated by (D), were used to reduce restraint cause by the neck to early age shrinkage. The measurement of strain on a wet material also proved to be troublesome. Hannant, et al. (1999) attempted to overcome this challenge by means of tapered sockets that were cast into the concrete and then connected to a linear variable differential transformer (LVDT) upon testing.
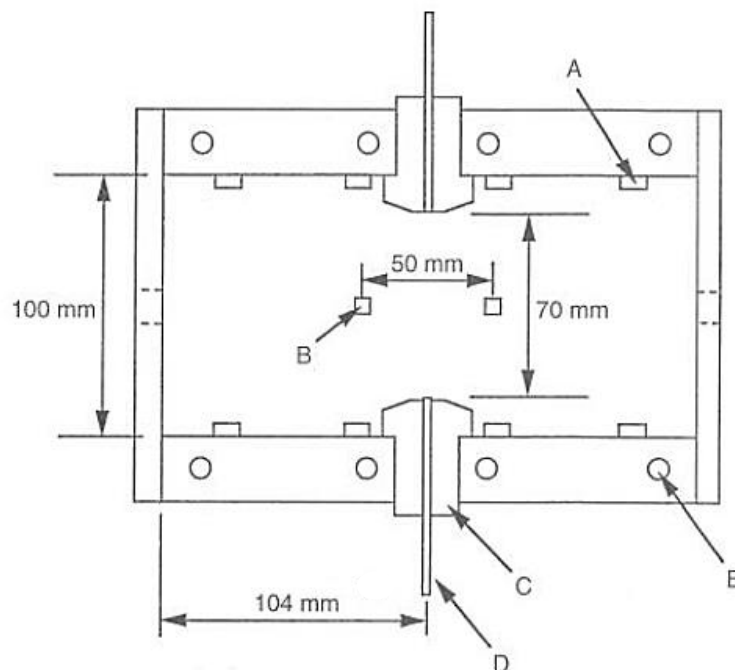
Figure 4.2: Plan view of the moulds used by Hannant, et al. (1999)

A major advancement from previous test setups was the use of an air-bearing. This allowed virtually frictionless movement between the moving mould halve and the air bearing surface. Due to the low tensile strength of the fresh concrete the elimination of friction is of great importance to ensure that reliable data can be obtained.

Special care was also taken not to disturb the test specimen after it was cast and consolidated. A lightweight tensile test setup was built, which could be placed around the test specimens. This resulted in minimum disturbance of the fragile concrete specimen prior to testing. Shortly before testing commenced the air bearing was pressurised, causing the specimen to float. A tensile force was then applied with a chain drive system while recording the corresponding force with a load cell and relative displacement over the gauge length with

the LVDT (Hannant, et al., 1999). From this initial study and a later one conducted by Branch, et al. (2002) it was determined that for this setup the early age concrete could be tested from 1 up to 7 hours after mixing, depending on the hydration rate of the concrete mix tested (Branch, et al., 2002).

Doa, et al. (2009) made further progress in the field of tensile testing of early age concrete. Their tensile test setup is shown in Figure 4.3. It is made up of an air bearing box as well as a lever arm, both attached to a small yet rigid steel frame. The lever arm was pin connected to the steel frame and was self-balanced in the test position. This allowed the direction, while not the magnitude of the applied force through the reference load cell, to be altered during testing. Four adjustable steel lugs were attached to the sides of the air bearing. This was done to prevent the sideways movement of the mould while setting up the test and during the test itself. Once the test specimen had been placed on the air bearing and floated, the one end was pin connected to the test load cell while the other end was connected to the lever arm. Although it is not stated it is assumed that this connection was also pinned as a fixed connection at the lever arm would result in unwanted vertical displacement. The reference load cell was also pin connected to the lever arm.
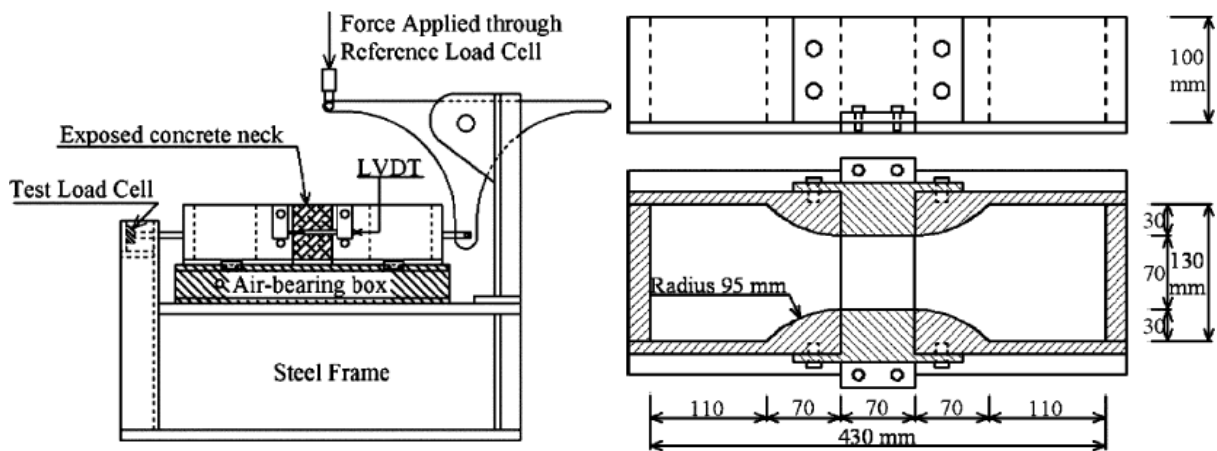
Figure 4.3: Tensile testing setup and mould as used by Doa, et al. (2009)

The most significant improvement, compared to previous research, was that of the mould design of the concrete specimens. The curved transitions, as seen on the right of Figure 4.3, promote failure in the middle section of the specimen. In contrast to the grips used in previous tensile test moulds, the use of this mould design allows for a tensile load to be transmitted to the specimen while eliminating any significant stress concentrations that could cause unintended cracking outside of the middle section. The effectiveness of this mould design was confirmed by both finite element analysis and by the occurrence of cracks in the middle section during testing. The sides of the middle portion of the mould were

58

removed prior to testing to expose the gauge length of the specimen. LVDT's were attached to the sides of the moulds to measure the displacement of the mould halves moving apart during testing. The measured displacement of the mould halves is not representative of the displacement of the concrete specimen inside the mould over its gauge length as a result of the deformation of the entire concrete specimen. However, the displacement over the 70 mm gauge length alone is required for analysis. To solve this problem, finite element analysis was implemented and determined that before the peak tensile stress, the deformation of the concrete over the gauge length is 50% of the measured mould displacement, while after the peak stress it is assumed as 90% of the measured mould displacement. These assumptions were utilised to obtain the resultant stress-displacement behaviour of the early age concrete specimens, from which all the needed tensile properties were determined (Dao, et al., 2009).

Figure 4.4, shows a typical stress-displacement curve of a semi-brittle concrete specimen determined as described above. The displacements measured by the LVDT's on the sides of the concrete specimen mould are indicated by Displacement 1 and Displacement 2 in Figure 4.4. The figure shows that the displacement measured on each side of the mould were different, indicating the skewing of the mould during testing. This is indicative of the formation of a crack in the side indicating a larger displacement. Despite the four adjustable steel lugs that were attached to the sides of the air bearing for the purpose of eliminating the sideways movement of the mould halves, a significant amount of skewing still took place during testing. It can be seen that at peak stress the one side of the specimen had displaced approximately 3 times the distance of the opposite side while at full separation it had achieved roughly twice the displacement of the opposite side.
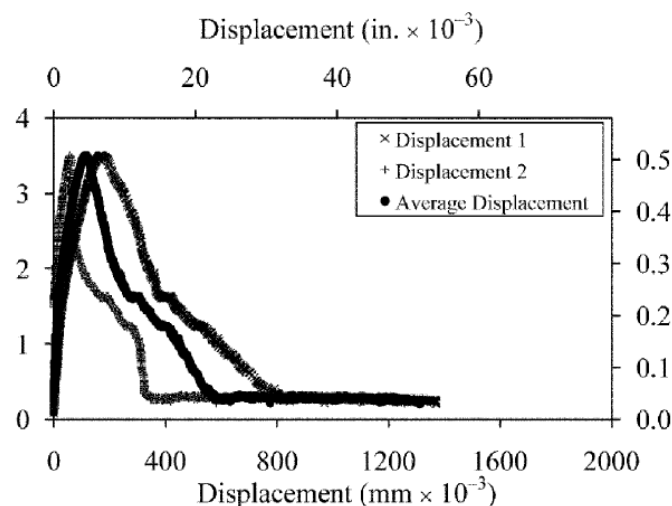
Figure 4.4: Typical stress-displacement curve indication skewing of the specimen (Dao, et al., 2009)

59

The average displacement of the two LVDT's was used to determine the various tensile properties of the early age concrete specimens. (Dao, et al., 2009). Although the fracture behaviour of specimens were determined from these experiments, this type of skewing as well as the boundary condition of the test setup loading platens are not desired for the reliable determination of the fracture behaviour of concrete, as will be described later on in this section.

Doa, et al. (2009) used a test procedure where the test moulds were filled in two equal layers and compacted by means of a vibration table. The specimens were then cleaned and placed in a room with controlled environmental conditions. At the time of testing, the specimen was placed on the air bearing and floated, whereafter it was connected to the lever arm and test load cell. Next, the side inserts of the mould were removed and LVDT's were connected on both sides of the mould. The experiment was initiated at a displacement rate of 0.05 mm/min. This was considerably slower than any of the displacement rates used in preceding studies, but gave results with better resolution of the post-peak behaviour. This slow rate did however result in undesirably long tests. As mentioned before, the rheological and mechanical properties of early age concrete continuously evolve during the measurement procedure and when using an extremely slow rate, as was the case with this study, this becomes even more pronounced. Using this test setup and test procedure, it was possible to conduct tests as early as 1.5 hours after mixing and onwards, depending on the degree of hydration of the test specimens.

Any experimental setup used for the measurement of fracture material properties, which include the ultimate tensile strength and the shape of the strain softening curve, related to the fictitious crack model (FCM), should be conducted using a stable deformation controlled uniaxial tension test between fixed loading platens. This is needed to achieve an almost simultaneous crack separation over the entire cross-section of the concrete test specimen, as illustrated by Figure 4.5. However, in practice this seldom occurs as specimens unavoidably skew and deform non-uniformly, resulting in the undesired propagation of cracks across the specimen cross-section (Bazant, 2002).

Reinhardt, et al. (1984) developed a direct tensile testing machine with the purpose of determining the fracture energy of hardened concrete dog-bone shaped specimens. The machine had a supporting frame to ensure that the two loading platens remained rigid and did not rotate during testing. The internal load cell configuration however caused a reduction in the rotational stiffness of the system as it could not be considered entirely fixed as some degree of rotation was permitted, depending on the crack formation in the concrete

specimens. The results of this study showed a great amount of variability in the stress-deformation behaviour of the concrete specimens that were tested.
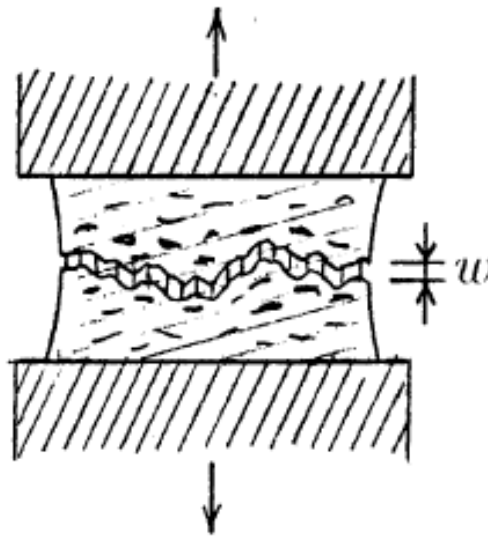
Figure 4.5: Approximately simultaneous crack separation of concrete specimen (Bazant, 2002)

Later studies by van Mier & van Vliet (2002) noted that the shape of the portion of the tensile stress-displacement curve of concrete is strongly dependent on the boundary conditions under which specimens are loaded. During tensile experiments on concrete using fixed load platens it was found that macroscopic cracking propagates from one side of the specimen as a result of the heterogeneous nature of concrete. As testing progressed, specimens were loaded more eccentrically, resulting in the development of a counteracting bending moment. This moment would obviously not have occurred in the case where freely rotating platens were utilised. This counteracting moment witnessed while using a test setup with fixed load platens resulted in the formation of a "bump" in the descending stress-displacement curve. In the case of freely rotating platens, a smooth descending stress-displacement curve is obtained. When comparing the fracture energies obtained using direct tensile test setups that utilise different boundary conditions, it is clear that a lower degree of rotational stiffness resulted in lower fracture energies.

However, for purely determining the ascending portion of the stress-strain behaviour of early age concrete, pin-fixed ends are preferred. If pin-fixed boundary conditions are used, secondary flexural stresses are avoided and the effects of bending moments that lead to large strength evaluation errors are decreased significantly (Kanakubo, 2006). It is clear that for an imperfect heterogeneous material, such as early age concrete, a compromise must be found in terms of boundary conditions to determine both the ascending and descending portions of the stress-strain behaviour sufficiently.

4.2   Initial tensile test setup

Taking the literature review presented in Section 2.2 and Section 4.1 into account and utilising the materials and apparatus available, an initial tensile testing setup was designed, assembled and used to conduct tensile experiments on early age concrete. This section firstly gives a description of the initial test setup and the method used to conduct experiments. Next, the results obtained from the tensile tests are presented. Finally, an evaluation of the setup and results is presented.

4.2.1   Description of initial test setup

The initial test setup is shown in Figure 4.6. The tensile testing mould, described in Appendix A, had its moving halve supported on four adjustable roller bearings while its fixed halve was bolted to a wooden box at the same height as the roller bearings. The wooden boxes on which both mould halves were supported could be adjusted individually in terms of height so that both mould halves were supported evenly and were level to one another. A pulley system in the form of a bicycle chain and gear was used to convert a vertical force provided by the loading machine into a horisontal force acting on the early age concrete specimen. Since the strength of early age concrete is extremely low and an extremely slow constant displacement rate is required to obtain accurate results, any slack in the pulley system or build-up of elastic strain energy in the entire system would result in a sudden jerk causing the specimen to fail abruptly or the results to be unreliable. The pulley system was connected to a load cell which measured the force exerted on the concrete specimen, as shown in the top right hand corner of Figure 4.6. A PC260 x 90 steel channel section was used as a base to ensure sufficient stiffness. All the components of the test setup were firmly mounted to this rigid base and the rigid base in turn was firmly mounted to a Zwick Z250 uniaxial testing machine which was used to apply the load through the pulley system.

LVDT's were used to measure the average displacement over the gauge length of the specimen as well as the mould halves moving apart. A LVDT was connected to each side of the mould, as shown in Figure 4.6, while four LVDT's were connected to the surface of the concrete, as shown in Figure 4.7. Since the material of the specimen at both the moving and fixed sides of the gauge length deforms during the application of tension, it was necessary to measure the displacement of both ends of the gauge length as the relative displacement between these points are needed in order to calculate the strain over the specimen gauge length. The two pairs of LVDT's were connected to freely rotating lightweight PVC pipes, to account for possible settlement of the specimen and to measure the movement of lightweight plastic placers, which had 25 mm long needles that were inserted into the specimen surface at the edges of the gauge length to track the displacement at these points.
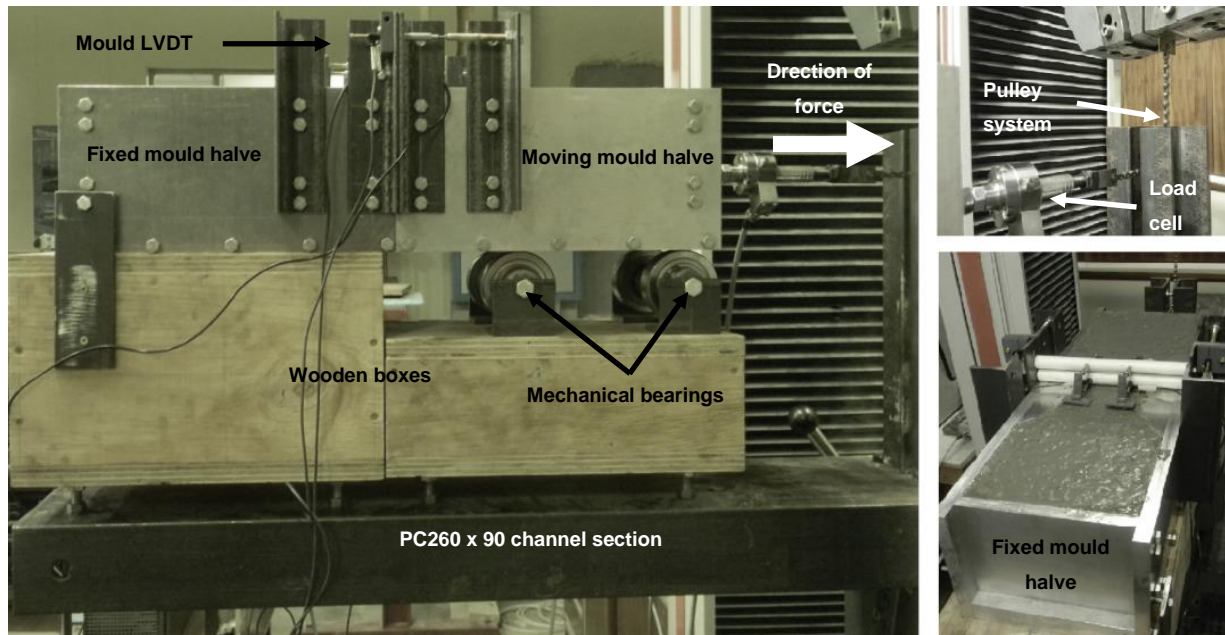
Figure 4.6: Supporting structure

Figure 4.7: LVDT displacement measurement setup over gauge length

4.2.2 Test procedure

All the constituents of the concrete mix were placed in a room with a controlled temperature of 23°C and a relative humidity of 60% at least 24 hours prior to testing. After the constituents were mixed sufficiently, the fresh concrete was placed in the prepared mould and compacted on a vibration table until air bubbles were no longer visible on the specimen surface. The mould was then carefully placed on the wooden box and mechanical bearings, as to disturb the specimen as little as possible, after which the LVDT's and load cell were connected to the specimen. A displacement rate of either 0.05 or 0.5 mm/min was used to perform the tests. The slower testing rate did however lead to undesirably long testing periods. The concrete mix design used in this initial study is shown in Table 4.1. This mix had a water to cement ratio of 0.4, a slump of 80 mm and was designed for minimum segregation and bleeding, and rapid setting.

Table 4.1: Mix proportions and constituents of the concrete mix design used for initial testing.

Constituent	[kg/m^3]
Water	205
CEM I 52.5N cement	513
13 mm Greywacke stone	631
Natural quarry sand	1105

4.2.3 Test results

Tensile tests were conducted on specimens from 1 to 4 hours after mixing had occurred. For this mix, the 1 hour test was a fresh concrete, still in a plastic state, while the 4 hour specimen was tested at the time at which final set had occurred. Before initial set had occurred, the hydrostatic force that the plastic concrete exerted on the inside of the mould combined with the weight of the pulley system, caused the slightest movement of the mould halves before the test was initiated. The tests before initial set could therefore not be successfully completed as the specimens were disturbed before the time of testing. This showed the need for a more rigid method of applying a tensile load that would be able to withstand the hydrostatic effect of plastic concrete. The stress-displacement curves of the tests conducted at 3 and 4 hours using displacement rates of 0.05 and 0.5 mm/min are shown in Figure 4.8 and Figure 4.9. From Figure 4.9 it can be seen that failure occurred before adequate data could be captured in the linear elastic region of the material's behaviour, despite the use of a data sampling rate of 50 Hz and an extremely slow displacement rate on some tests. The Young's modulus of the concrete specimen could thus not be determined. It is believed that the method of displacement measurement, i.e. the LVDT's which were weakly connected to the concrete surface, did not account for any significant deformation or cracks that may have occurred far below the concrete surface. Such deformation and cracks may have occurred before the LVDT's measured any deformation on the surface. This was more apparent on plastic fresh concrete specimens that displayed some shearing during testing, leading to the conclusion that a horisontal displacement gradient existed over the depth of the specimens. The cause of the abrupt failure of the specimens at final set can be accredited to the build-up of strain energy in the system, either at the fixed end of the wooden box or in the pulley mechanism. This can be seen in Figure 4.10, which shows that the 4 hour specimen which was tested at a rate of 0.5 mm/min reached its maximum tensile strength before any displacement was measured on the tensile testing mould. A sharp jump in the displacement shortly after the peak stress was reached, indicating failure, was measured. However, despite this the 4 hour specimens showed a maximum tensile strength of 9.6 and 8.1 kPa while the 3 hour specimens had a

maximum strength of 3.5 and 3.7 kPa, which are comparable with the results discussed in the Section 2.2.
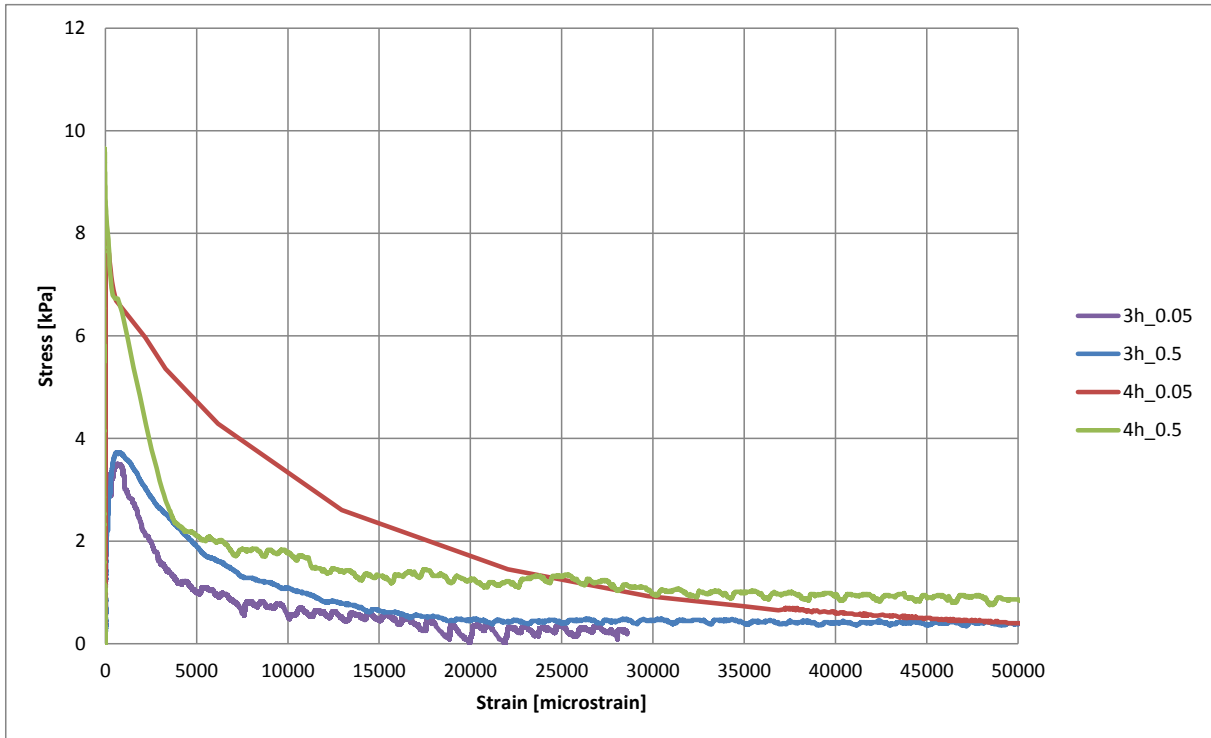
Figure 4.8 Complete sress-displacement curve of 3h and 4h specimens
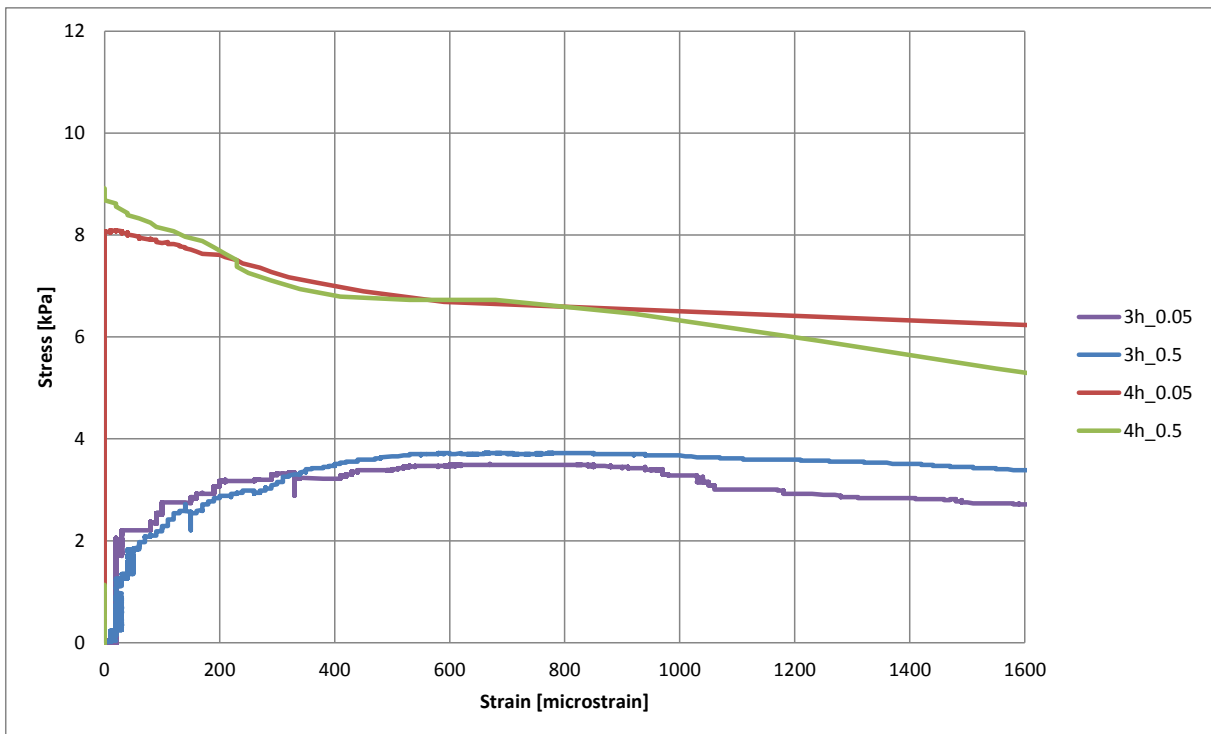
Figure 4.9: Initial section of the stress-displacement curve of 3h and 4h specimens

65
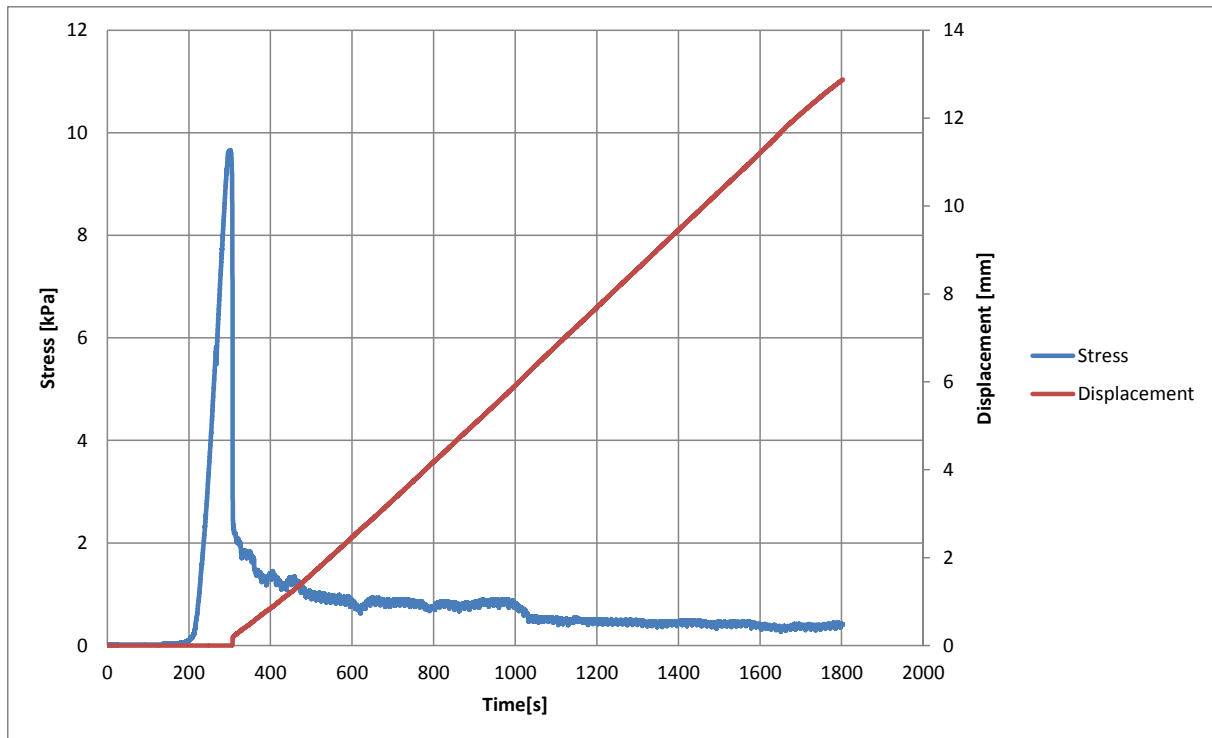
Figure 4.10: Stress and displacement measured on mould vs. time for the 4h specimens tested at a rate of 0.5 mm/min

4.2.4 Evaluation of initial tests setup and results

After critically evaluating the initial test setup and the results obtained, the following shortcomings and areas of improvements were identified:

- The method of load application through the loading machine and pulley system could not account for the influence of hydrostatic forces in a concrete specimen which has not reached the initial setting time.

- The method of load application and the fixing of the tensile testing mould were not rigid enough to capture the ascending part of the stress-strain curve and allowed for unwanted movement and strain build-up as illustrated by Figure 4.10.

- A rigid base is needed for the mounting of the tensile testing apparatus. The wooden boxes provided insufficient stiffness and caused slippage during testing that resulted in inaccurate results.

- The method of displacement measurement only accounted for deformation and cracking near the surface of the concrete. Assuming a displacement gradient exists in the depth of the plastic specimens, no reliable displacement can be captured using this method.

- It was cumbersome to align and level the fixed halve of the mould on the wooden box with the moving halve of the mould on the four mechanical bearings. A system where

66

both mould halves are on the same level and therefore simultaneously levelled would be ideal.

4.3   Final tensile test setup

From the evaluation of the literature review presented in Chapter 2 and Sections 4.1 and 4.2, a final test setup, shown in Figure 4.11, was designed and manufactured. This section describes the various components of this setup.
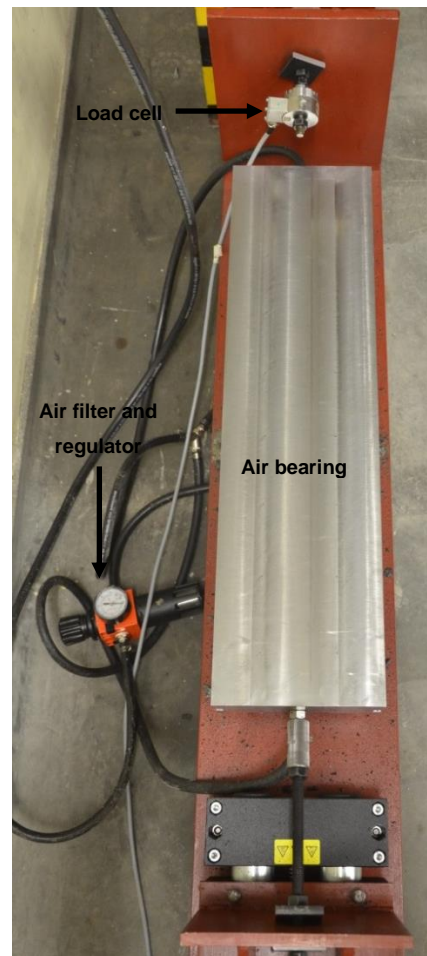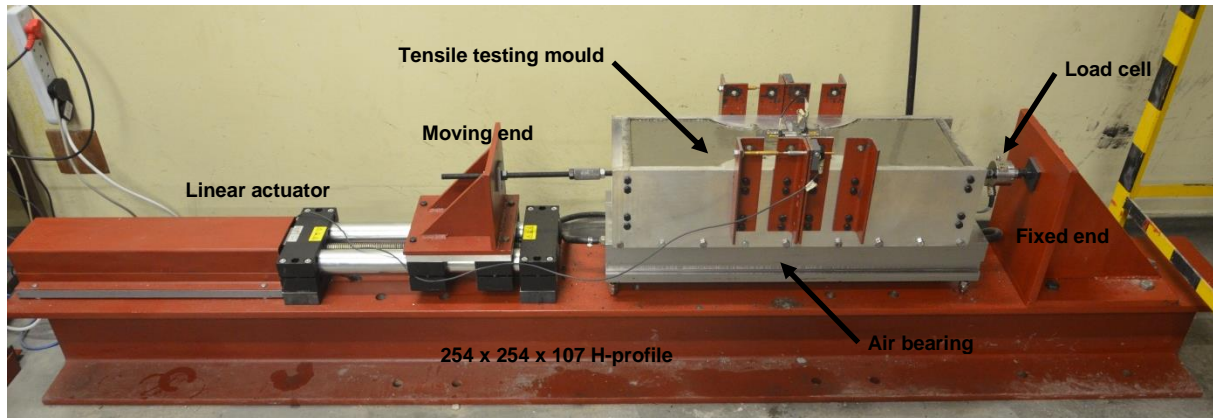
Figure 4.11: Final tensile testing setup

67

4.3.1 Tensile testing mould

The moulds used to conduct the tensile experiments in this study are referred to as tensile testing moulds. These moulds have the primary function of transferring a tensile force to the early age concrete specimen. The basic geometry of the moulds is based on the moulds used by Doa, et al. (2009). However, the moulds do have a few major differences. The first is the presence of mould sides supporting the concrete specimen over its constant gauge length during testing, whereas Doa, et al. (2009) utilised removable sides. This ensured that the specimen was not disturbed prior to testing by the removal of side inserts and that specimens that could not yet support their own weight could also be tested. Another noticeable difference to the moulds used by Doa, et al. (2009) is the fact that these moulds were scaled up by a factor of 1.43 to accommodate the testing of larger concrete specimens. This was done to ensure that a fully developed fracture process zone (FPZ) would be able to form over the necked gauge length section of a concrete specimen for mixes containing 19 mm coarse aggregate, as discussed in Section 4.1 (Bazant, 2002). The dimensions of the tensile testing mould, as shown in Figure A.3, together with details regarding the design, construction and performance of the tensile testing moulds are all presented in Appendix A.

4.3.2 Air bearing

The presence of friction during the linear motion required for testing will result in the overestimation of a specimens' tensile strength and Young's modulus pre-peak, and fracture energy post-peak because early age concrete is so weak. For this reason, an air bearing was used to facilitate the linear motion of the two mould halves moving apart. With a static friction coefficient of zero and a negligible kinetic friction coefficient, for which the only contributor is the viscous friction resulting from the shearing of an air film during motion, an air bearing is ideally suited for this application. The approximately 80 kg moulded test specimen could be floated on the air bearing at a pressure of 1.2 bar. The air bearing incorporated a threaded levelling system to allow for the accurate levelling of the air bearing surface. The dimensions of the assembled air bearing, as shown in Figure B.4, together with details regarding the design, components, construction and performance of the air bearing, are all presented in Appendix B.

4.3.3 Linear actuator

Sections 4.1 and 4.2 clearly identifies that a rigid method of load application is required for the tensile testing experiments in this study. For this reason, a displacement controlled linear actuator assembly capable of exerting a tensile force of 1.7 kN, at a stable constant rate as slow as 0.05 mm/min, was constructed. The linear actuator, together with its rigid connection system allowed for the capture of the full stress-displacement behaviour of early age

concrete specimens. Figure C.11, in Appendix C, indicates that the tensile testing moulds displace at a constant rate from the onset of the tensile stress measurement while utilising the linear actuator assembly to induce displacement. This is in contrast to the initial test setup which only measured an abrupt mould displacement once the peak tensile stress was measured, as shown in Figure 4.10. More details regarding the components, design, construction and performance of the linear actuator are presented in Appendix C.

4.3.4 Boundary conditions and connecting mechanisms

As discussed in Section 4.1, a compromise must be found in terms of boundary conditions to sufficiently determine both the ascending and descending portions of the stress-strain behaviour of early age concrete. When purely determining the ascending portion of the stress-strain behaviour, pin-fixed ends are preferred, while the requirement for determining solely fracture energy, based on the fictitious crack model, is a high degree of rotational stiffness in the end connections. For this reason, the boundary conditions for both the moving- and fixed end connections were made to be neither completely fixed nor pinned, as shown in Figure 4.12.
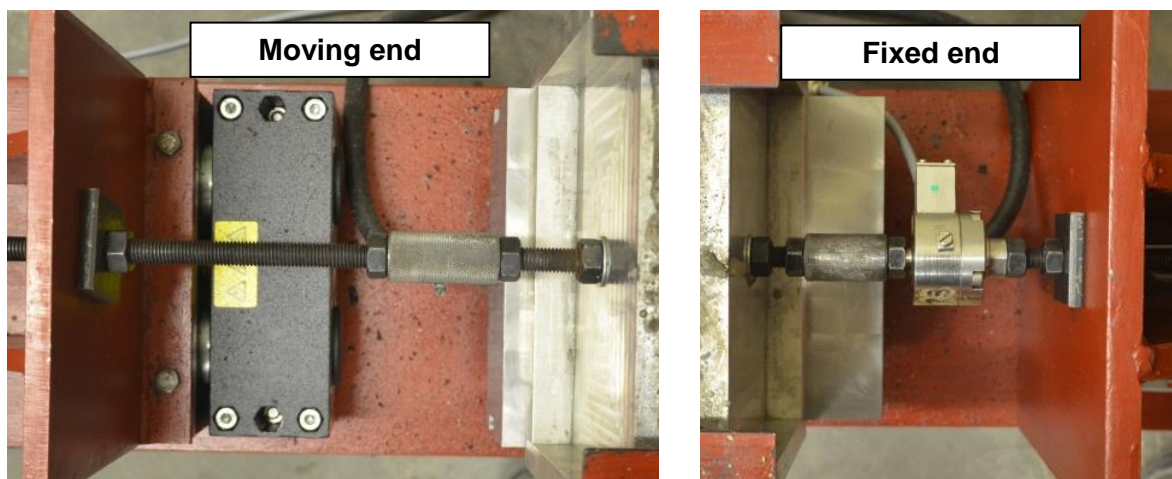
Figure 4.12: Moving and fixed end connections

The tensile testing mould, load cell as well as the moving- and fixed end structures, were all connected via M12 thread, nuts and coupling connectors. The threaded coupling connector is shown in Figure 4.13 a). 50 x 50 mm^2 plate washers were used to fix the tensile testing moulds to the moving- and fixed end structures, as shown in Figure 4.13 b). The nuts on both sides of the plate washers were fastened by hand as to create a boundary condition between fixed and pinned. When these end connections were tightened using leverage, resulting in a more rigid connection, skewing of the mould halves relative to each other occurred once displacement commenced. This is because the moving- and fixed end structure faces were not perfectly lined up.

69
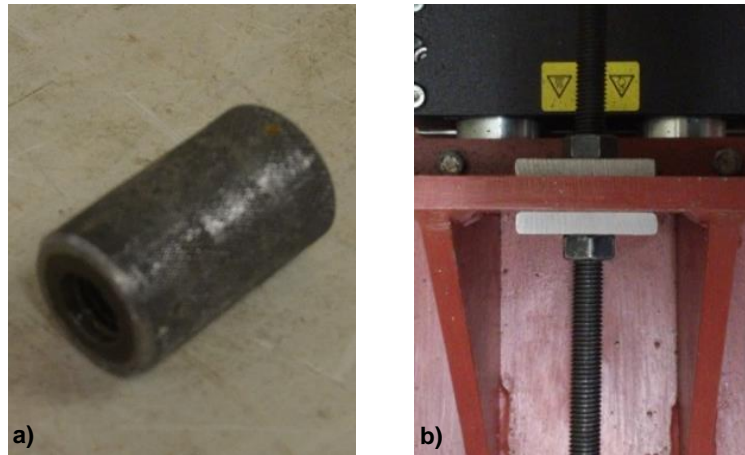
Figure 4.13: a) Threaded coupling connector. b) Moving end connection fixed by nuts and washers.

4.3.5 Displacement measurement

In this study it was required to measure the displacement of the insitu concrete specimen over its gauge length as well as the displacement of the mould halves relative to each other, as shown in Figure 4.14. HBM WI LVDT's were used to measure all displacements. These LVDT's had a nominal displacement range of 10 mm and a sensitivity of ± 40 mV/V.
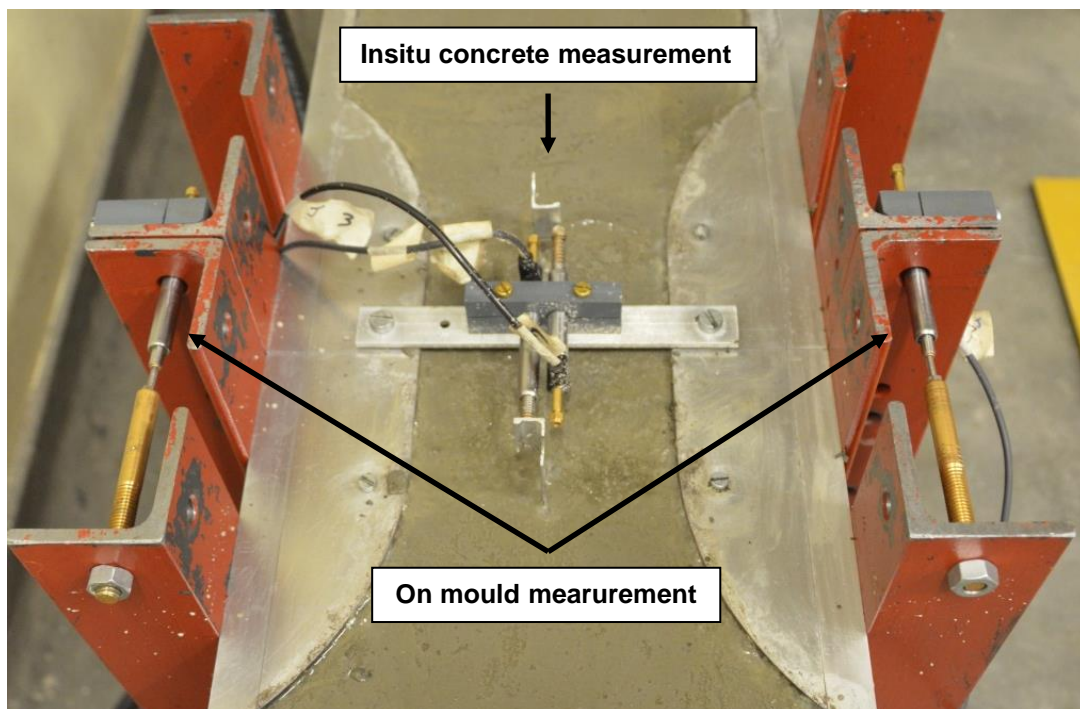
Figure 4.14: Displacement measurement systems

Insitu concrete measurement:

To capture the full stress-strain behaviour of early age concrete specimens, displacement measurement of the concrete specimen over the constant cross section gauge length was

70

required. A non-intrusive method of measuring the points on the edge of the gauge length of such a weak material would be ideal. However, because of the presence of a thin layer of bleed water on the surface of the concrete specimen, this was not possible. For this reason insitu aluminium pins, as shown in Figure 4.15, were cast into the concrete specimen at both edges of the 100 mm gauge length to provide measurement surfaces for the LVDT's.
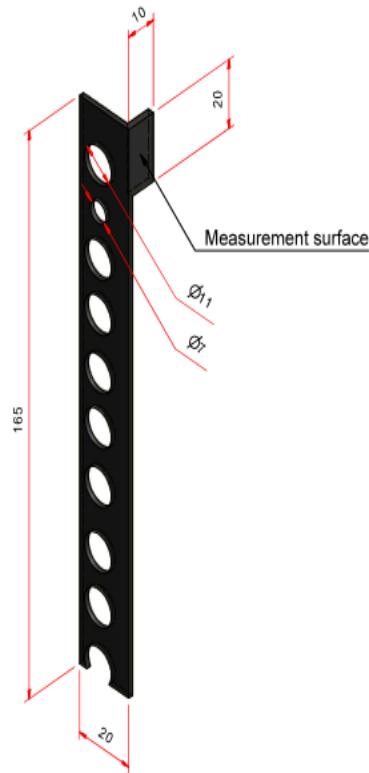
Figure 4.15: Insitu aluminium pin

These insitu aluminium pins have a thickness of 1 mm and a hole pattern that allows for the interlocking of concrete aggregate with the pins. Once installed prior to testing, as shown in Figure 4.16, these plates penetrated the depth of the concrete specimen to 5 mm from the mould bottom, while leaving its 20 mm high and 10 mm wide displacement measurement surface above and not in contact with the concrete specimen. The insitu pins were held in position during casting by 20 x 20 mm aluminium angle profiles, which were slotted and modified to allow for the perfect positioning and rigid clamping of these plates. This ensured that the insitu pins stayed on the edge of the gauge length and that the measurement faces lined up perfectly with the LVDT's. An early age concrete specimen directly after casting is shown in Figure 4.17.

Both mould halves were filled up simultaneously and evenly during casting to ensure that the pressure exerted by the fresh concrete on the insitu pins was approximately the same as to avoid possible movement of the pins.

71

Figure 4.16: Pre-casing setup of insitu concrete measurement system
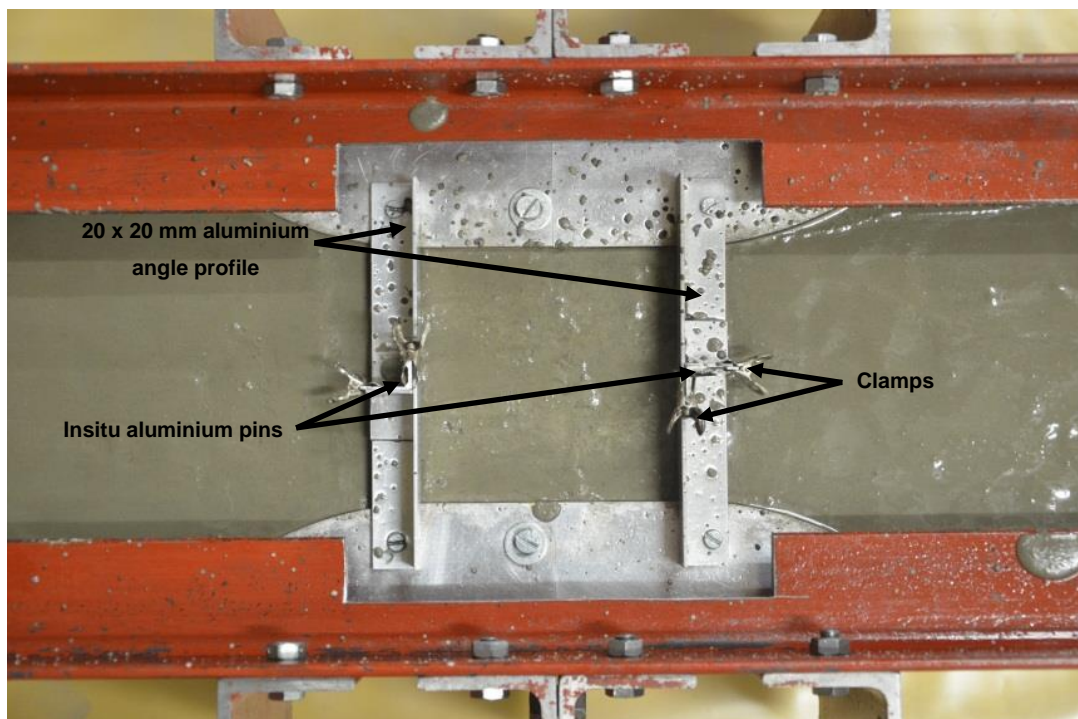
Figure 4.17: Post-casting setup of insitu concrete measurement system

Directly after casting and transporting the specimen to the testing venue, the clamps and 20 x 20 mm aluminium angle profiles were removed. Just before a specimen was tested, after it has been placed on the air bearing and all the other necessary pre-testing setups have been done, LVDT's, mounted on a bracket were attached to the fixed mould halve and placed in contact with the measurement faces of the insitu pin. The LVDT's were fitted with a spring and ball point probe to ensure that the LVDT ends were continuously in contact with the measurement faces of the insitu aluminium pins while causing minimum disturbance to the specimen. The complete insitu concrete measurement setup is shown in Figure 4.18.

72
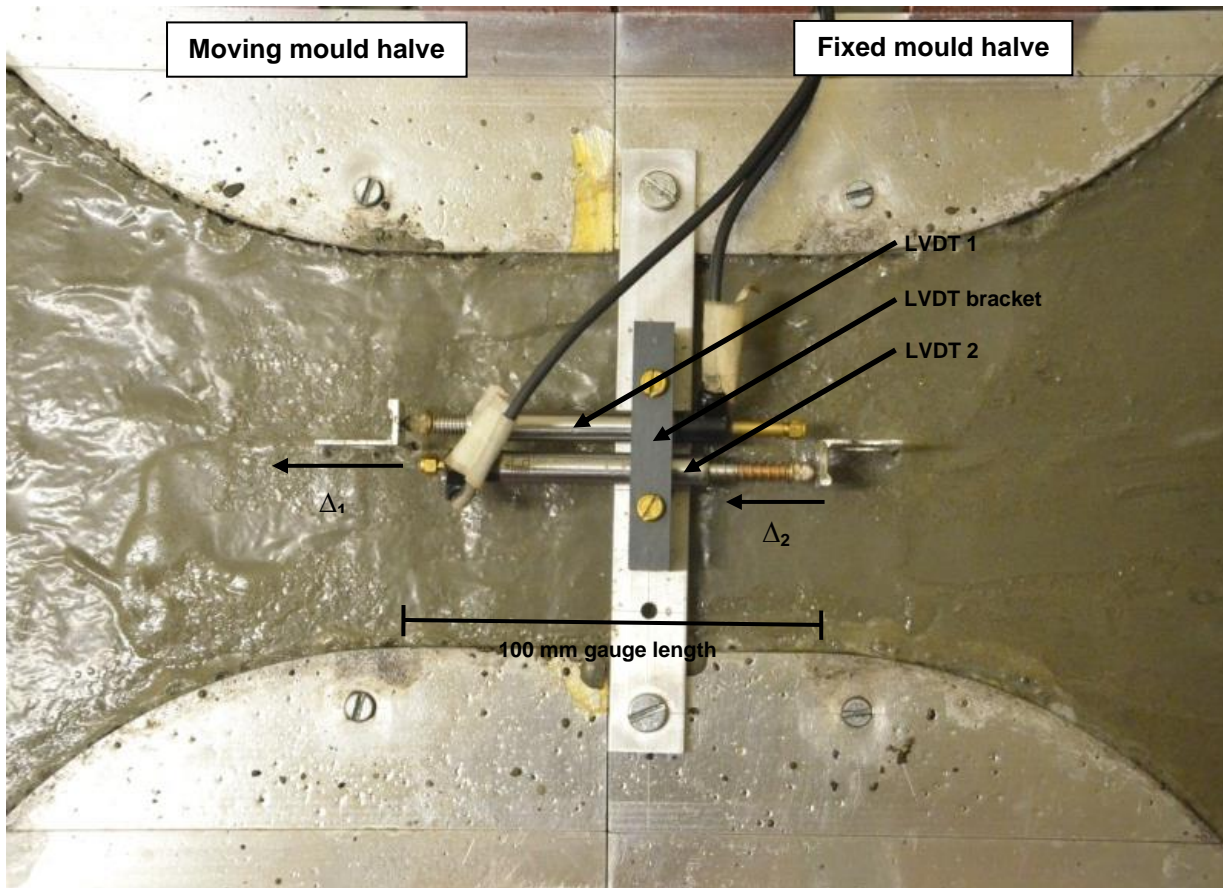
Figure 4.18: Complete insitu concrete measurement setup just prior to testing

The strain of the instu concrete specimen during testing can be calculated as follows:

$$\varepsilon = \frac{\Delta_1 - \Delta_2}{100}$$ ……………………………………………………………………..(Equation 4.1)

where Δ_1 represents the displacement measured on the edge on the specimens gauge length on the moving mould halve and Δ_2 the displacement measured on the edge on the specimens gauge length on the fixed mould halve.

On mould measurement

In order to verify the displacement of the mould halves and to determine if the actuator was displacing at a constant rate while applying an actively varying load, it was necessary to measure the displacement of the mould halves moving apart. To achieve this, the steel angle profiles connected to the tensile testing mould were modified to accommodate the attachment of LVDT brackets and threaded connectors, as shown in Figure 4.19. Just prior to testing the LVDT's were inserted and securely connected to the LVDT brackets, that were mounted on the steel angle profiles on the fixed mould halve. The threaded LVDT probes were then connected to the threaded connectors, which were in turn pin connected to the steel angle profiles on the moving mould halve. This was done on both sides of the mould.

The measurements at both sides of the mould were used to determine the average displacement of the moving mould halve.
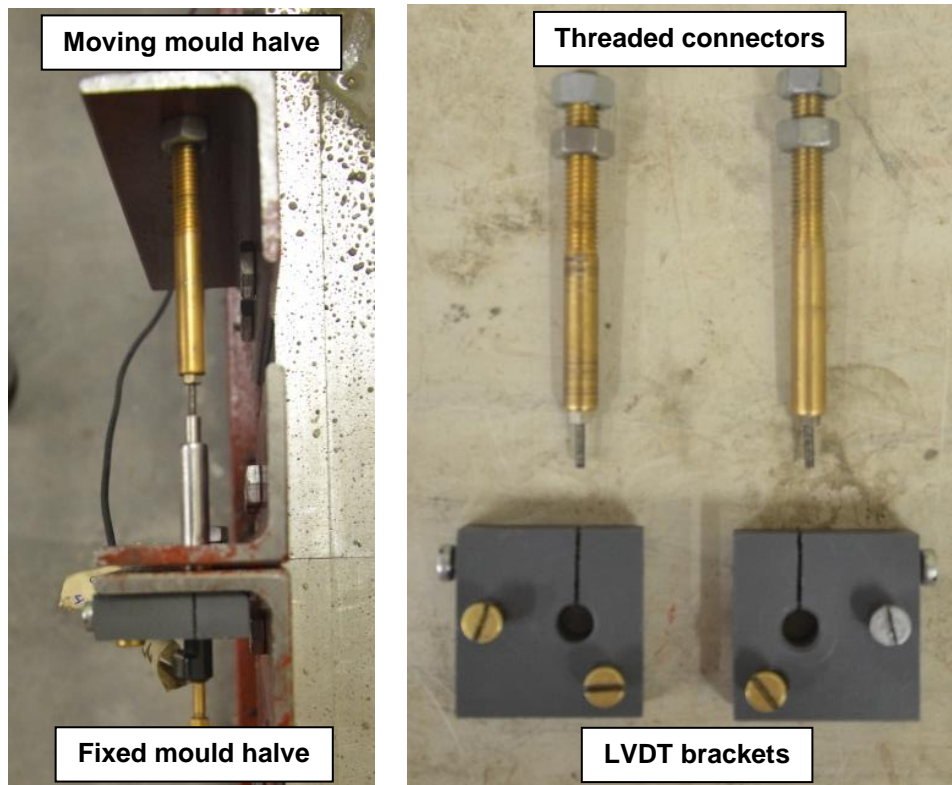
Figure 4.19: On mould displacement measurement setup

4.3.6 Force measurement

A HBM 1-U2B 2000 N load cell with a nominal sensitivity of ± 2 mV/V was used to measure the force transmitted through the early age concrete specimen. It was connected between the fixed end structure and the tensile testing mould as shown in Figure 4.12.

4.3.7 Base

A 2.5 meter long 254 x 254 x 107 H-profile served as a base to which the actuator and fixed end connection were bolted securely and the air bearing was levelled upon. The high rigidity of this beam made it well suited for this purpose as its deflections and deformation during testing was insignificant.

4.4 Concluding summary

This chapter focuses on the design of the experimental tensile test setup. Firstly, a literature review on the apparatus used for the determination of the tensile properties of early age concrete is presented. The conditions for effectively determining both the ascending and descending portions of the stress-strain curve of early age concrete are also discussed. Next, the initial test setup and the results obtained from initial testing are discussed,

highlighting its shortcomings and knowledge gained from it. Finally, the final test setup, designed using the knowledge gained from the literature review as well as the initial test setup is described in detail. The next chapter discusses the experimental program and tensile testing method.

5. Experimental programme and method

Whereas the previous chapter focusses on the experimental tensile test setup, this chapter provides a detailed description of the experimental test programme and the tensile test method used to conduct the tensile experiments on early age concrete. Firstly, a detailed description of the objectives of the experimental work is presented. Next, the test programme is described. The constituent materials of the various concrete mixes are then discussed whereafter the requirements, mix proportions and significant properties of the concrete mixes used in this study are described. Finally, a detailed description of the test procedure developed and used in conducting the tensile tests in this study, is provided

5.1   Experimental objectives

The background study on the tensile properties of early age concrete and early age cracking revealed the need for a greater fundamental understanding of the tensile properties of early age concrete, how these properties developed over time as well as the influencing factors. This knowledge is needed to better understand, predict and ultimately reduce the occurrence of early age cracking. With this in mind, the experimental tests were performed to achieve the following objectives:

Objective 1

Reliably capture the complete stress-strain behaviour of early age concrete specimens from one hour after casting and consolidation and onwards through the design and construction of a tensile testing setup.

This is the **main objective** of this study. Once achieved, all tensile properties of interest (ultimate tensile strength and strain capacity, Young's modulus, fracture energy and characteristic length), can be determined as a function of time as well as mix design influencing factors.

Objective 2

Determine the effect of **coarse aggregate size** on the tensile properties of early age concrete.

Objective 3

Determine the effect of the **addition of microfibres**, in different proportions, on the tensile properties of early age concrete.

Objective 4

Determine the effect of **setting time altering admixtures**, which are added to alter the initial and final setting times of concrete, on the tensile properties of early age concrete.

5.2   Experimental test programme

This section gives an overview of the different concrete mixes that were designed and the tensile tests conducted on these mixes in order to meet the objectives set out in the previous section. In total seven different concrete mixes were designed and used for tests. More details on the mix designs regarding materials, proportions and attributes are discussed in Section 5.3 and 5.4 respectively.

The reference mix, MR, was designed to be similar to mixes commonly used by ready-mix batch plants for industrial floor slabs, as these are the type of elements most prone to the occurrence of plastic shrinkage cracking (PShC). This mix was used for all initial tests of the tensile testing setup and the development of a test procedure to achieve Objective 1. All other concrete mixes were designed by altering the reference mix in order to achieve Objectives 2, 3 and 4.

To determine the effect of coarse aggregate size on the tensile properties of early age concrete, Objective 2, the size of the coarse aggregates in a reference concrete mix, which was 13 mm, was varied while keeping the content of all the other constituents the same. Both a 9 and 19 mm aggregate were used to replace the 13 mm aggregate used in the reference mix to create the MA9 and MA19 mixes respectively.

It has been shown that the addition of a low volume of microfibres to a concrete mix decreases the occurrence of PShC (Combrinck & Boshoff, 2012a). It is also reported that fibres increase the early age tensile strain capacity of concrete although no studies could be found in literature to substantiate this. To verify this two low volume fibre reinforced concrete (LV-FRC) mixes were designed. The first mix contained the minimum prescribed dosage of 0.6 kg microfibres per cubic meter of concrete while the second mix contained a higher dosage of 1.8 kg microfibres per cubic meter. These mixes were appropriately named MF0.6 and MF1.8 respectively.

The addition of a retarder to a concrete mix has in some cases shown to increases the occurrence of PShC, due to the slower setting and strength gain of these mixes (Uno, 1998), while other studies have found that it decreases PShC (Combrinck & Boshoff, 2012b).In order to better understand this and a retarders' effect on the tensile properties of early age concrete, the reference concrete mix was altered by the addition of a typical industrial dosage of a retarder to the reference mix, resulting in the MSR mix. The influence of an

accelerator on the tensile properties of early age concrete is yet to be confirmed. The reference concrete mix was altered by the addition of a low dosage accelerator. This accelerated mix is denoted as the MSA mix. The name, description and the objective to be achieved of the seven concrete mix designs are summarised in Table 5.1.

Table 5.1: Name, description and relevance of mixes used in this study

Name	Description	Relevance
MR	Reference mix – typical slab concrete with 13 mm aggregate	Standard / Control
MA9	Finer coarse aggregate – 9 mm	Effect of coarse aggregate size
MA19	Coarser coarse aggregate – 19 mm	
MF0.6	Lower volume polypropylene microfibre– 0.6 kg/m^3	Effect of microfibre addition
MF1.8	Higher volume polypropylene microfibre – 1.8 kg/m^3	
MSR	Setting time retarded– typical volume admixture	Effect of setting time altering admixtures
MSA	Setting time accelerated– typical volume admixture	

Tensile tests were conducted at hourly intervals for each of the seven concrete mixes. Tests started at one hour after the fresh concrete has been placed and consolidated to the time after the concrete specimen has reached its final set. Conducting these tests after the final setting has occurred, is believed to be of less significance with regards to the occurrence of PShC in concrete, since the initiation of these cracks typically ceases after this point (Combrinck, 2011).

5.3   Materials

This section describes the constituent materials used for the experimental tests. These materials include, fine aggregate, coarse aggregates, cement, fibres and admixtures.

5.3.1 Fine aggregates

The type of fine aggregates used in a concrete mix has a greater influence on the fresh concrete properties than the properties of the concrete in the hardened state. Two fine aggregates were utilised in the mixes used for the tensile experiments. The first was a natural quarry sand locally known as Malmesbury sand and the other a Greywacke crusher dust that was sieved through a 2 mm sieve to reduce the average particle size and therefore increase the fineness of the sand. The properties of the fine aggregates are shown in Table 5.2.

The quarry sand was formed by the natural weathering of rock resulting in sand with a rounded particle shape that does not contain a large percentage of fine particles. The Crusher dust was manufactured by the mechanical crushing of rock and therefore exhibits an

angular particle shape. The grading of the two sand types, as determined in accordance with SANS 1083 (2013), are illustrated in Figure 5.1.

Table 5.2: Fine aggregate properties

Fine aggregate	Fineness modulus – FM	Relative density – RD [kg/m^3]
Natural quarry sand	2.64	2.64
Greywacke crusher dust (2mm sieve)	2.40	2.60
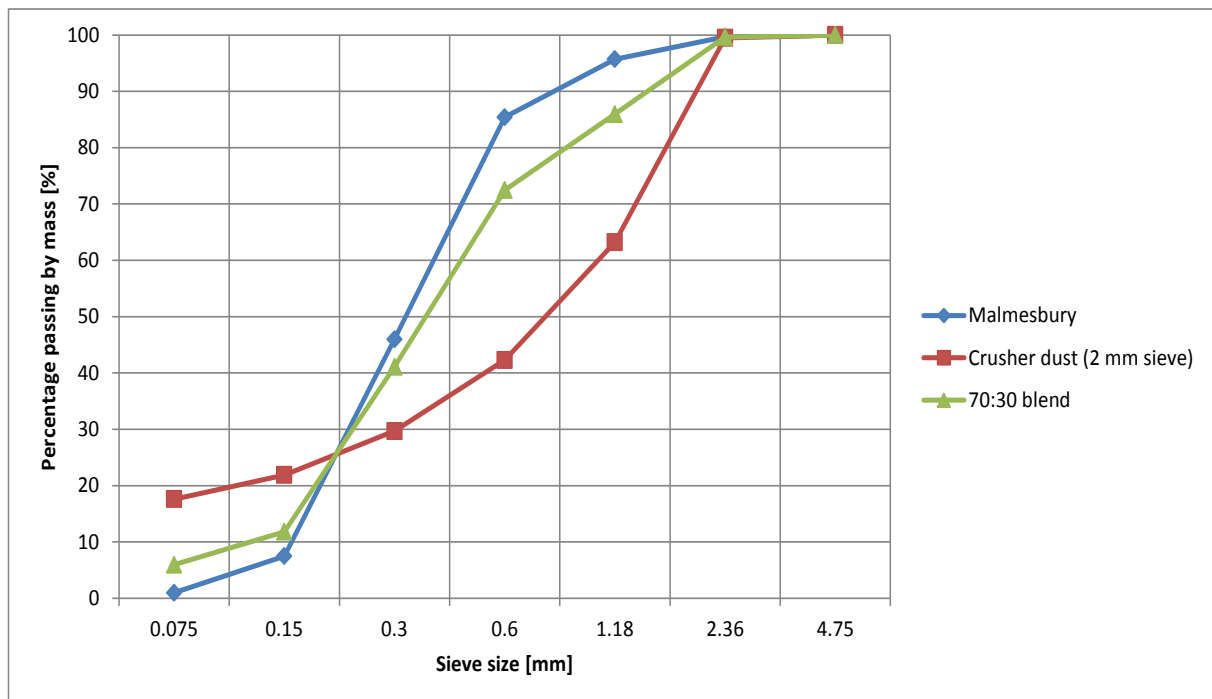
Figure 5.1: Fine aggregate grading

The quarry sand was used as a base material of the fine aggregates in these experiments due to its rounded particle shape. However, trial mixes containing the quarry sand alone exhibited an extremely high bleed rate and capacity. It also resulted in excessive slump measurements and insufficient cohesion when adding admixtures. The quarry sand was therefore blended with the crusher dust in order to increase the fine content of the concrete mixes as this would decreases bleeding and increase cohesion. A suitable blend was arrived at empirically by means of trial mixes. A 70:30 blend of quarry sand and crusher dust was chosen to be the most suitable fine aggregate for the objectives of this study, and was utilised in all the concrete mixes tested in this study.

5.3.2 Coarse aggregates

The coarse aggregate used in this study is known as Greywacke stone and is manufactured by the mechanical crushing of Malmesbury shale. The nominal sizes used were 9 mm, 13 mm and 19 mm. The stone has a relative density of 2.74 and the stone grading was done in accordance with SANS 1083 (2013).

5.3.3 Cement

A CEM II 52.5 N cement with a relative density of 3.14 was used for all experiments. This cement was supplied by PPC – Pretoria Portland Cement Co. Ltd.

5.3.4 Fibres

The fibres used in this study were polypropylene microfibres that were supplied by SAPY (South African Polypropylene Yarns) (Pty) Ltd. This fibre type is chemically inert and stable in an alkaline concrete environment. They do not absorb free water due to the hydrophobic nature of their surface area. As a result these fibres do not chemically adhere to the concrete paste, but rather bond mainly due to interfacial friction with the concrete paste, as described in Section 3.3.3. These fibres have a low Young's modulus and bond relatively poorly with the concrete paste (Wongtanakitcharoen, 2005). The fibres have a relative density of 0.91 kg/m^3, a fibre length of 12 mm and a diameter between 35 and 40 µm. A dosage of between 0.6 and 2.0 kg fibres per cubic meter of concrete is prescribed (SAPY, 2014).

5.3.5 Admixtures

The admixtures used in this study were supplied by Chryso SA (Pty) Ltd. The following section is a description of the accelerator and retarder used, as stated in the Chryso general catalogue (Chryso SA, 2007):

- **Xel A639** is an accelerating admixture that is based on calcium chloride. It is supplied as a clear solution, which instantly disperses in water. Xel A639 enhances the early stages of cement hydration, producing more rapid stiffening and hardening. This allows final finishing or mould stripping to begin at an earlier age without damaging the concrete surface.
- **Tard CE** modifies the hydrating reactions of the concrete and retards principally the time of initial setting. Tard CE does not increase the length of time between the beginning and end of setting. Therefore, concrete retarded with Tard CE will harden normally as soon as setting starts and high early and ultimate strengths can be obtained. This particularity means that with the use of Tard CE, a concrete mix can be obtained that remains workable for a long time and that has high early and ultimate strength. Tard CE has no surface tension effects.

The significant properties of the admixtures are given in Table 5.3.

Table 5.3: Admixture properties

Material	Relative density [kg/m³]	Prescribed dosage [litre / 100 kg of cement]
Accelerator (Xel A639)	1.35	1.6 – 3.0
Retarder (Tard CE)	1.25	0.3 – 2.0

5.4   Concrete mix designs

The requirements, mix proportions and significant properties of the concrete mix designs used in this study are discussed in this section. As mentioned in Section 5.2, the reference concrete mix used in this study was designed to simulate those commonly used by ready-mix batch plants for the casting of industrial floor slabs, as these are the type of elements most prone to the occurrence of early age cracking. All other mixes were achieved by simply varying the stone size or by the addition of fibres and admixtures. The reference mix was designed with the following requirements in mind:

- 28 day design compressive strength of 40 MPa
- 75 mm slump
- Minimum segregation
- Moderate bleeding

The reference mix design also had to make provision for the requirements of all the other concrete mixes as they were simply variations of the reference mix. The general requirements for all concrete mixes were:

- Slump values of between 50 mm and 110 mm
    - o Concrete specimens with slump values lower than 50 mm proved difficult to compact sufficiently when using the test method developed for this study.
    - o Concrete specimens with slump values in excess of 110 mm exerted a significant hydrostatic force on the inside of the mould and the fresh specimens also proved difficult to contain within the mould during testing.
- An adequate amount of bleeding:
    - o A mix with too much bleeding makes it difficult to see deformation and crack formation.
    - o A mix with too little bleeding would lead to capillary pressure build-up, as discussed in Section 3.1.2. and because the concrete specimens were not covered after it has been cast, a layer of bleed water on the surface is

81

required until final set has occurred to ensure that no plastic shrinkage occurred which could cause stresses to build up within the specimen.

The mix proportions of all seven mix designs are shown in Table 5.4.

Table 5.4: Concrete mix design proportions

Constituent	[kg/m³]						
	MR	MA9	MA19	MF0.6	MF1.8	MSR	MSA
Water	205	205	205	205	205	205	205
Greywacke crusher dust	244	244	244	244	244	244	244
Natural quarry sand	569	569	569	569	569	569	569
Cement (CEM II – 52.5 N)	342	342	342	342	342	342	342
13 mm Greywacke stone	1037	-	-	1037	1037	1037	1037
9 mm Greywacke stone	-	1037	-	-	-	-	-
19 mm Greywacke stone	-	-	1037	-	-	-	-
Polypropylene fibre	-	-	-	0.60	1.80	-	-
Retarder (Tard CE)	-	-	-	-	-	1.28	-
Accelerator (Xel A639)	-	-	-	-	-	-	8.30

The MA9 and MA19 mixes were achieved by simply exchanging the reference coarse aggregate size of 13 mm with 9 mm and 19 mm respectively.

The MF0.6 mix made use of the minimum prescribed dosage of polypropylene microfibres. This was done by simply adding 0.6 kg fibres to each cubic meter of the reference mix design. For the MF1.8 mix design a higher dosage of 1.8 kg fibres were added to each cubic meter of the reference concrete mix. Workability was the limiting factor in this case, as the MF1.8 mix had a minimum slump value of 50 mm.

The MSR as well as the MSA concrete mixes were produced by adding low additions of the retarder and accelerator respectively. The MSR mix made use of 0.3 litre of retarder per 100 kg of cementitious material, while the MSA contained 1.8 litre of accelerator per 100kg of cementitious material. These low dosages of admixtures achieved their objective of altering the setting times of the mixes, without altering other fresh concrete properties significantly.

The slump, 28 day compressive strength and setting times of each mix are shown in Table 5.5. The 28 day compression strength of the respective concrete mixes were determined in accordance with SANS 5863-1 (1994) and the average of 3 specimens were determined. The slump of each concrete mix was determined in accordance with SANS 5862-1 (2006).

The initial and final setting times were determined by means of a Vicat apparatus, illustrated in Figure 5.2, in accordance with SANS 50196-3 (2006). The initial setting time was reached when the penetration of the 1.1 mm diameter initial setting time needle decreased to 6 ± 3 mm from the base of the plate. Furthermore, once the final setting time needle fails to create a ring indentation on the specimen surface, the final setting time has been reached. The concrete used for the setting time test was vibrated through a 4.75 mm sieve to remove the coarse aggregate from the concrete paste. During testing the specimens remained covered to prevent evaporation and drying. The final setting time for the reference mix was found to be 6 hours, thus every mix design was tested to an age of at least 6 hours, where the zero time was taken as the time at which the concrete specimen has been placed and consolidated. Due to the retarded setting times of the MSR mix, the amount of tests conducted on this mix design was increased. The retarded mix had a final setting time of 8 hours, and consequently was tested to an age of 8 hours. Despite its final setting time occurring after 5 hours, the accelerated mix was also tested to an age of 6 hours.

Table 5.5: Concrete mix design properties

Property	Concrete mix						
	MR	**MA9**	**MA19**	**MF0.6**	**MF1.8**	**MSR**	**MSA**
28 day Compression Strength [MPa]	37.5	39.4	39.5	44.5	43.0	44.5	39.8
Slump [mm]	70/65	50/55	85/90	55/50	60/60	115/105	95/100
Initial setting time [hour]	3.5	-	-	-	-	4.5	3
Final setting time [hour]	6	-	-	-	-	8	5

Figure 5.2: Vicant apparatus

83

5.5 Test procedure

This section provides a detailed description of the test procedure developed and used to conduct the tensile tests in this study. The test procedure aims to be repeatable and therefore eliminate variability as far as possible. This section firstly describes the preparation needed in terms of the environmental conditions as well as the air bearing and moulds. Next, the mixing and casting and consolidation are described, followed by a discussion regarding the pre-testing setup. Finally, the testing of the early age concrete specimens is described.

5.5.1 Environmental conditions during test

The rate of hydration and therefore also the setting and hardening of concrete is greatly influenced by the temperature of a concrete sample. It was therefore very important to ensure that all concrete test specimens were at the same temperature once placed in the tensile testing moulds.

With this in mind, all concrete constituents were placed in a climate controlled room with an ambient temperature of 23°C and a relative humidity of 60% at least 24 hours prior to testing. The tensile testing moulds were permanently stored under these same conditions. The only stage where the moulds and constituents were exposed to an external environment was for a period of approximately 20 minutes during the mixing, compaction and finishing stages of the test procedure. In this manner it was ensured that the temperature for all concrete specimens used for tests were approximately the same upon casting.

5.5.2 Air bearing

It is necessary to clean and coat the air bearing surface with a thin layer of lubrication oil before the tensile tests can be conducted. This is done to ensure that the air bearing operates effectively and that the apparatus is protected against corrosion and hydrating concrete deposits that can damage the surface of the air bearing or cause the contamination of its orifice restrictors. Although the air bearing can float the concrete specimen and mould at a pressure of 1.2 bar, all tests were conducted at a pressure of 2 bar. This was done to ensure that the air bearing would still be able to float the specimen in the event that the effectivity of the air bearing or air supply system deceased for some reason.

5.5.3 Moulds

The first step in preparing the tensile testing mould halves was to ensure that they are completely clean. Any solid deposits on the bottom surface decreases the effectivity of the air bearing while concrete deposits on the inside of the mould results in unwanted friction and interference with the early age concrete specimen during testing. Once the mould was cleaned, both mould halves were then floated on the air bearing at an air pressure of 0.5 bar.

84

The mould halves were connected and the mould assembled on the air bearing by fastening its steel supporting structure, as described in Section A.2.1 . If the mould halves did not float without friction at this pressure it was an indication that the bottom surface of the moulds were not sufficiently clean. If this was achieved and the completely assembled mould failed to float, it indicated that the faces of the mould halves were not flush and most likely not sufficiently clean and smooth, as shown in Figure 5.3.
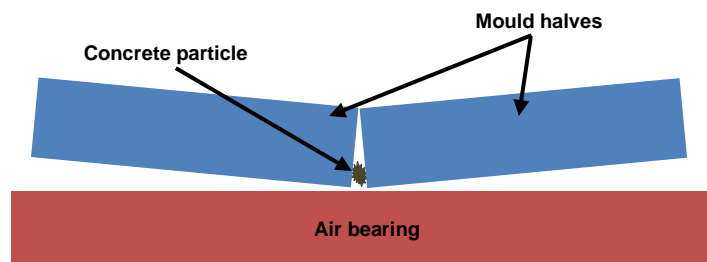
Figure 5.3: Elevated view of insufficient contact between mould faces due to the presence of concrete particles

About an hour before casting the concrete specimens in the moulds, the interface between the two moulds halves were sealed from the inside by a thick layer of bearing grease. This was done to ensure that the mould is impermeable and as a result, water or mould lubricant cannot escape from the mould and cause possible adhesion between the contact surfaces of the interface of the mould halves. In addition, if free water is removed from the test specimen it would lead to unreliable results as the rheology of the fresh concrete test specimen would be influenced as well as the setting and capillary pressure build-up after the initial setting time. The inside of the mould was then coated with a lubricant to decrease friction and adhesion between the mould and the early age concrete specimen and to assist in the demoulding of the specimen after testing. Finally, insitu aluminium pins were installed, as described in Section 4.3.5, to allow for the strain measurement over the gauge length of the specimen.

Directly after a test was completed, the concrete specimens were demoulded by rocking the upside-down mould continuously and with great care not to cause any damage to the mould. The mould halves were then cleaned with a high pressure water hose, and dried by hand with disposable towels to ensure that there were no concrete residue on the inside or the outside of the mould that could cause any contamination of the next specimen or the tensile test setup. The mould halves were then left to dry completely. All remaining coarse concrete residues on the inside of the mould halves were then carefully scraped with a paint scraper. Care was taken to ensure that no damage was caused to the aluminium mould halves. After this was completed the inside of the mould was sanded clean and smooth with various sandpapers to an acceptable final smoothness with P600 sandpaper with a grit size of

25.8 μm. The faces of the mould halves, that form the interface between the mould halves, were sanded to an acceptable final smoothness with P1000 sandpaper with a grit size of 18 μm. The mould halves were then blown clean with compressed air.

5.5.4 Mixing, compaction and casting

The mixing, compaction and casting was the only stage of the testing procedure that did not take place under controlled environmental conditions and special care was taken to ensure that the concrete constituents, moulds and finished fresh concrete specimens were not unnecessary exposed to unregulated environmental conditions.

The concrete was mixed in accordance with SANS: 5861-1 (1994). Directly after this, the freshly mixed concrete was transferred into the tensile testing mould on a vibration table. Due to the immense size and weight of the full mould it was necessary to use a poker vibrator to compact the concrete sufficiently. The concrete was compacted in two layers: the first filled two thirds of the mould, the second was filled up to approximately 5 mm from the top of the mould. The entire filling, compaction and finishing process took 6-8 minutes per mould. The concrete specimens with greater slump values, e.g. the retarder mix, took about 6 minutes to finish, whereas the stiffer mixes containing microfibres required more compactive effort and consequently approximately 8 minutes to finish. A freshly moulded specimen is shown in Figure 5.4.

Figure 5.4: Finished fresh concrete specimen on vibration table with protective cover

The finished specimens were then immediately transported on a trolley to the controlled environment where the tensile tests were performed. The profiles and clamps that kept the

insitu aluminium pins in position during the casting, compaction and finishing of the fresh concrete specimen were then carefully removed without disturbing the pins or specimen. The specimens in this state are shown in Figure 5.5.

Figure 5.5: Undisturbed specimens prior to testing

As mentioned in Section 5.4, the zero time, from where the age of the concrete was determined, was taken as the moment that the fresh concrete specimen had been compacted and finished. From this moment up until 15 minutes prior to the testing, the specimen was left undisturbed for hydration products to form and for it to gain strength.

5.5.5 Test setup

With the air bearing entry pressure set to 2 bar the moulded specimen was placed on the air bearing. At this pressure all specimens easily floated without friction over the air bearing surface. The mould ends were then connected to the M12 threaded rods, loosely attached to the fixed ends on the test setup, by using the threaded rod couplings, as described in Section 4.3.4. The mould was then lined up to ensure that the specimen was in the correct position on the air bearing. The treaded rods were then fastened at the fixed ends on the test setup to hold the mould securely in place. This was done by tightening the bolts on both sides of each mould end connection structure. The mould is fastened in such a way that the connection structures exert a compressive force of approximately 100 N on the mould halve. This was done; firstly to prevent the separation of the mould halves due to the hydrostatic pressure exerted by the plastic concrete in the mould that takes effect once the two horisontal supporting angle profiles were removed. Secondly, to ensure that the two halves did not move relative to each other as a result of the friction between the moulds faces, and disturb

87

the specimen during the setup of the LVDT's on the mould. Once this was done, the two horisontal supporting angle profiles, which were effectively friction grip connections, were removed. The displacement measurement of both the insitu concrete and the mould halves were then set up as described in Section 4.3.5. The bolts that were fastened by hand to keep the mould halves together were then also removed. At this stage the mould halves were held in place by the 100 N compressive force that the supporting structure exerted on them alone. This process took approximately 10 minutes. The progressive setup of the early age concrete specimen to the point just prior to testing is shown in Figure 5.6
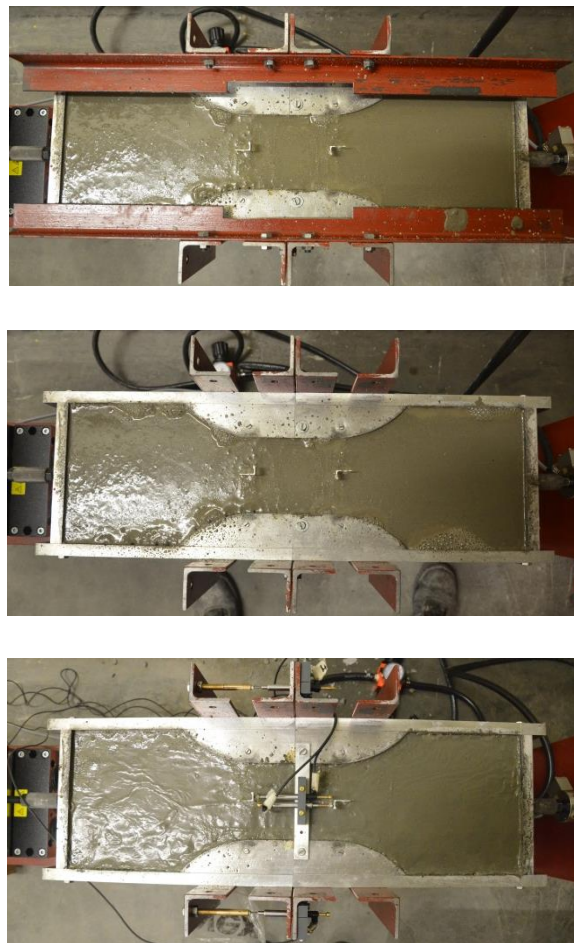
Figure 5.6: The progressive setup of the early age concrete specimen prior to testing

5.5.6 Testing

At the correct time the tensile test was initiated and the actuator displaced the moving halve of the mould at a constant rate of 0.25 mm/min relative to the stationary halve. This was chosen as the appropriate displacement rate as it is slower than the 0.75 mm/min rate used by Hannant, et al. (1999), which in their study did not deliver adequate post-peak behaviour, but faster than the rate used by Doa, et al. (2009) of 0.05 mm/min, which resulted in undesirably long testing periods. It is believed that during these extensive testing periods the

tensile properties of the early age concrete would develop significantly, during the measurement process (Bentz, 2008). The LVDT and load cell data was simultaneously captured on a computer using a data acquisition system. The tests were conducted from 28 to 32 minutes till an insitu concrete displacement of at least 6.5 mm, which coincides with the bridging distance of the 13 mm reference aggregate, was measured over the gauge length. Stiffer specimens typically produced shorter testing periods. This 6.5 mm was also roughly the measurement limit as the LVDT's can measure a maximum displacement of 10 mm, which could have occurred on one side of the mould had excessive skewing taken place. Furthermore, a displacement of 6.5 mm was more than sufficient to ensure the full separation of all specimens except the 19 mm aggregate specimens, which also showed practically zero resistance at this stage. The testing process is illustrated by Figure 5.7.
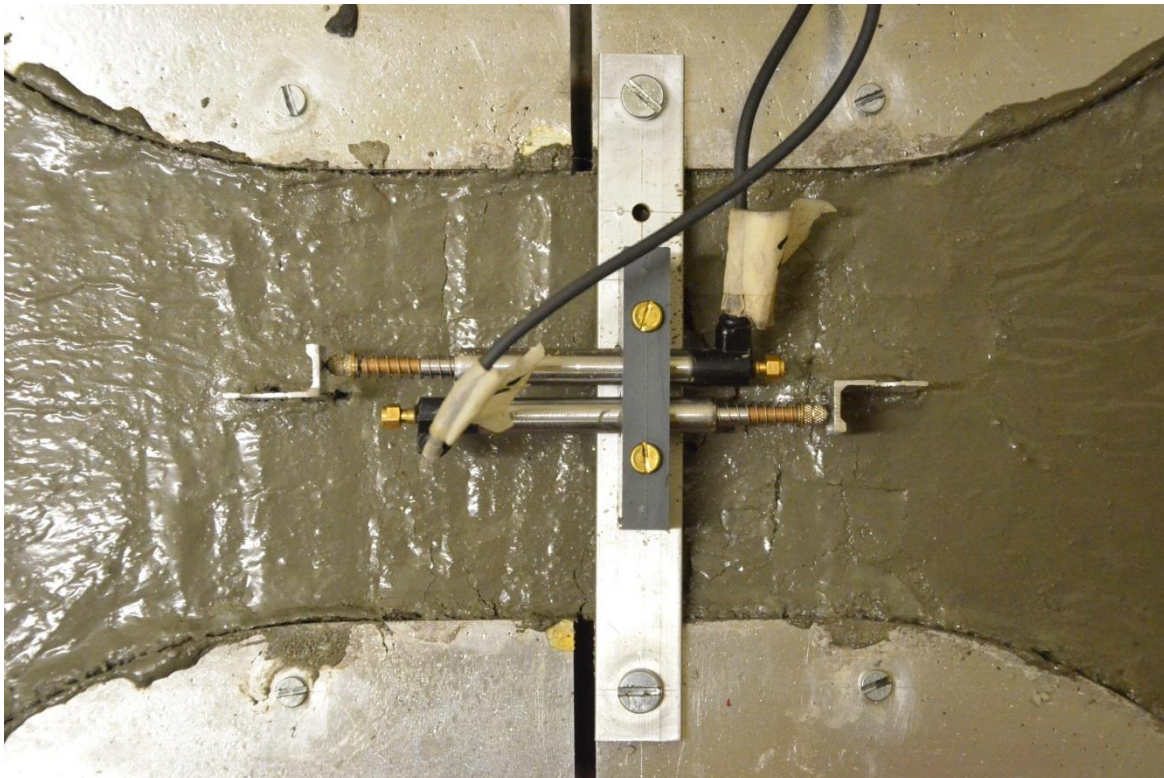
Figure 5.7: Specimen during testing

5.6   Concluding summary

This chapter focusses on the experimental programme of the tensile testing experiments conducted in this study. Firstly, a description of the objectives of this study is provided. Next, the test programme of the tensile tests is defined. The constituent materials of the various concrete mixes are then discussed. Next, the requirements, mix proportions and significant properties of the concrete mixes used in this study are described. Finally, a detailed

description of the test procedure developed and used in conducting the tensile tests in this study is provided. The next chapter presents the results obtained for Objective 1.

6. Experimental results and discussion: Objective 1

This chapter focuses on the results obtained for Objective 1, the reliable capture of the complete stress-strain behaviour of early age concrete specimens from one hour after casting and consolidation and onwards, through the design and construction of a tensile testing setup. The results of the tensile testing experiments performed on the seven concrete mixes described in Section 5.4. are presented. The methodology used to determine the strain of the early age concrete specimens before the initial setting time, as well as after the initial setting time is then described. Finally, the insitu method of strain determination for concrete specimens after the initial setting time is compared with the method used by Doa, et al. (2009) and evaluated.

6.1 Experimental results for Objective 1: The complete stress-strain curve of early age concrete

The complete stress-strain curves of the 1 - 6h MR test specimens are shown in Figure 6.1. The complete stress-strain curves of all seven concrete mix designs from one hour after casting and consolidation to the time of final set are presented in Appendix D.
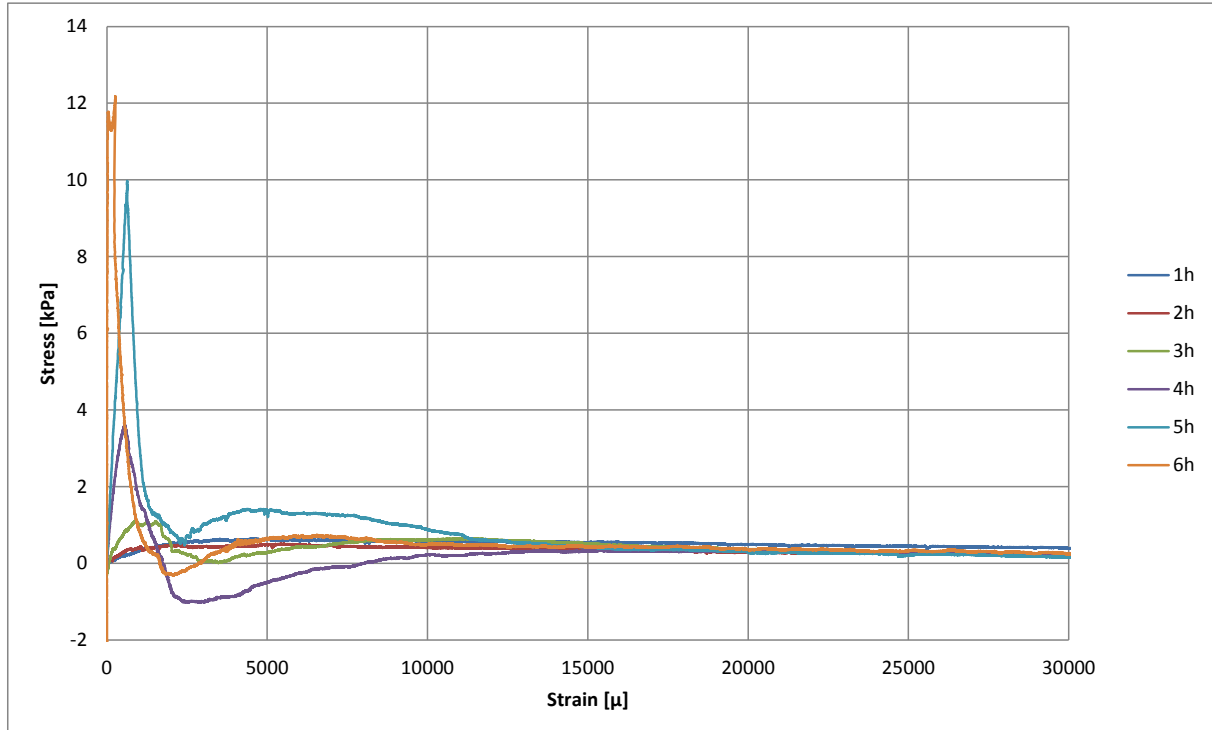
Figure 6.1 Stress-strain curves of the MR mix

6.2 Strain determination methodology

The insitu displacement measurement system was not successful in reliably capturing the displacement over the gauge length of the specimens before the initial setting time had occurred. This was because the plastic concrete could not yet hold the insitu aluminium pins over the gauge length in position under the influence of the minor force produced by the spring loaded LVDT's. Δ_2, as defined in Figure 4.18, would often displace in the direction opposite to that of the applied force during testing as a result of the force exerted on it by LVDT 2. The blue curve in Figure 6.2 is an extreme example of this behaviour, which often occurred in tests on specimens with an age of 1 hour. This led to great variability and unreliable displacement results of test specimens before the initial setting time had occurred.

In order to achieve a better estimation of the displacement of the fresh concrete specimens over its gauge length, the approach used by Doa, et al. (2009) was adopted. Via FEM analysis Doa, et al. (2009) determined that the displacement of the two mould halves ,relative to each other, before the peak stress has been reached, was 50% of that of the specimen over its gauge length and 90% afterwards. The initial portion of the stress-strain curves for the 1h and 3h reference specimens is shown in Figure 6.2 andFigure 6.3 respectively. The blue curves represent the strain determined using the insitu concrete displacement over the gauge length, while the red curve denotes the strain determined using the displacement measured on the mould halves and the green curves the strain determined using the factored on mould measurements, as proposed by Doa, et al. (2009).
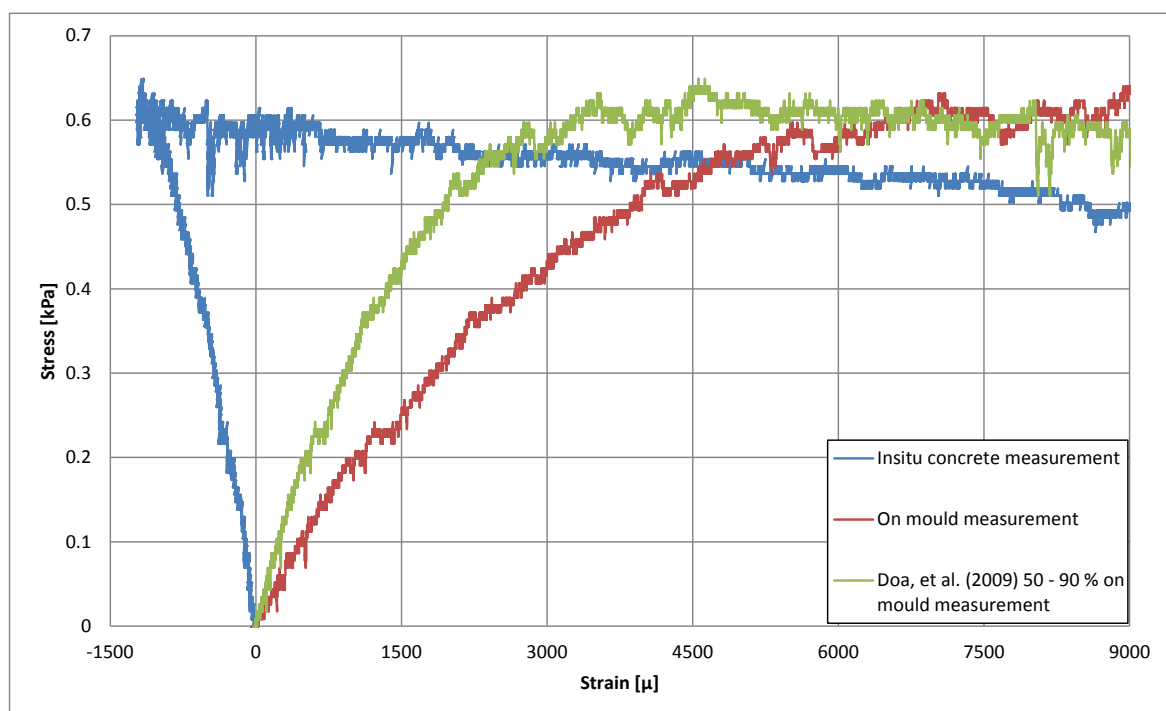
Figure 6.2: Displacement measurement for 1h MR specimen

92
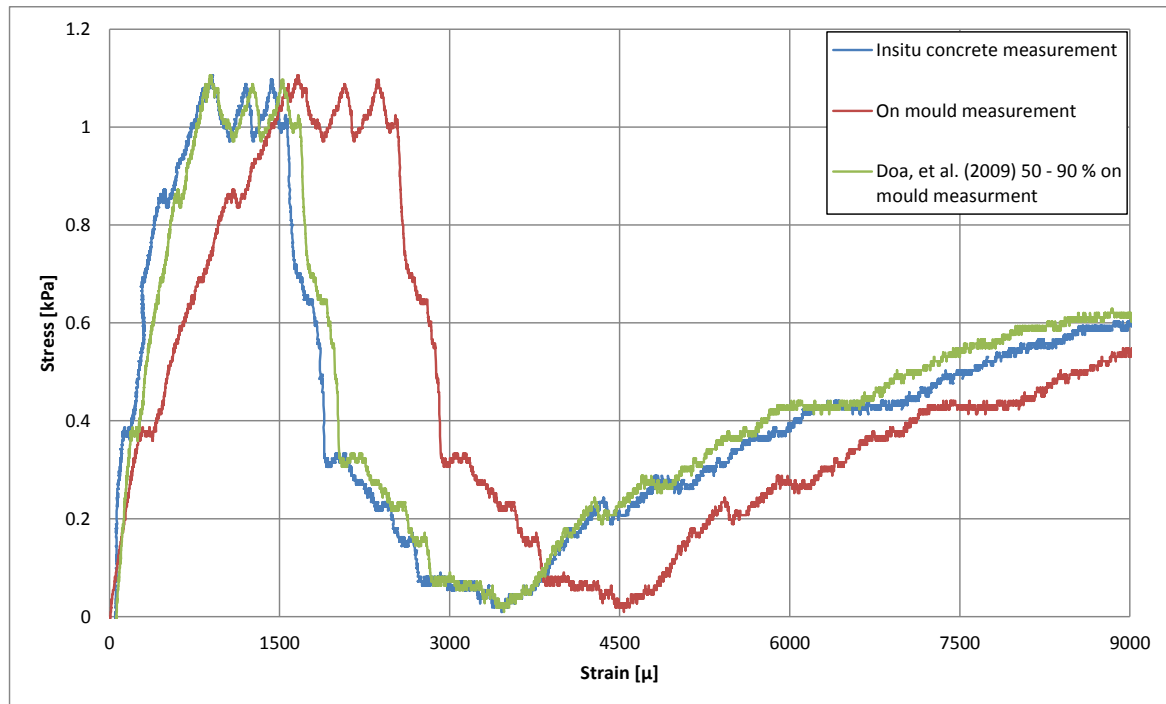
Figure 6.3: Displacement measurement for 3h MR specimen

It was found that the Doa, et al. (2009) 50 - 90% on mould displacement method of determining the specimens' displacement provided reliable and comparable results for the fresh concrete specimens. At an age of 3 hours the insitu concrete and Doa, et al. (2009) 50 - 90% on mould strain curve converged for almost all mixes with an initial setting time of 3.5 hours.

After the initial setting time of the specimens has been reached, the insitu concrete measurement method proved to be sufficient and delivered reliable results. At this stage, the insitu aluminium pins had become securely anchored in and interlocked with the concrete specimen and the effect of the minor force exerted by the LVDT's proved to have no effect on the movement of the insitu aluminium pins just prior to and during testing. For this reason, the strain of specimens tested after initial setting time was determined via the insitu concrete measurement method.

Thus for all the specimens that were tested before they had reached the initial setting time, the Doa, et al. (2009) 50 - 90% on mould displacement method was used to determine the strain and for all the specimens that were tested after they had reached the initial setting time, the insitu concrete measurement method was used. This is illustrated in Figure 6.4.

Fresh concrete specimens exert a slight hydrostatic force on the inside of the mould. As setting commenced and the specimens solidified, this hydrostatic effect diminished. This is

illustrated by Figure 6.5 that shows the average displacement of the mould halves with the corresponding tensile resistance of the 1-6h MR specimens.
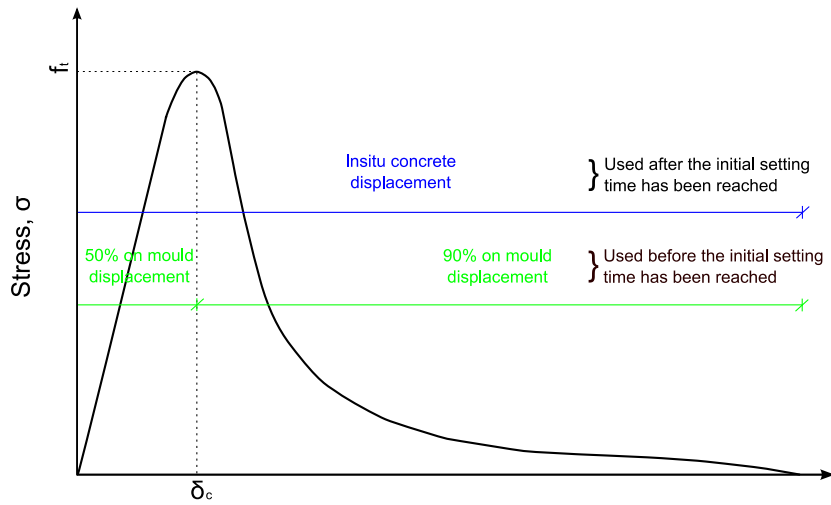
Figure 6.4: Stress-displacement curve illustrating the means of displacement determination
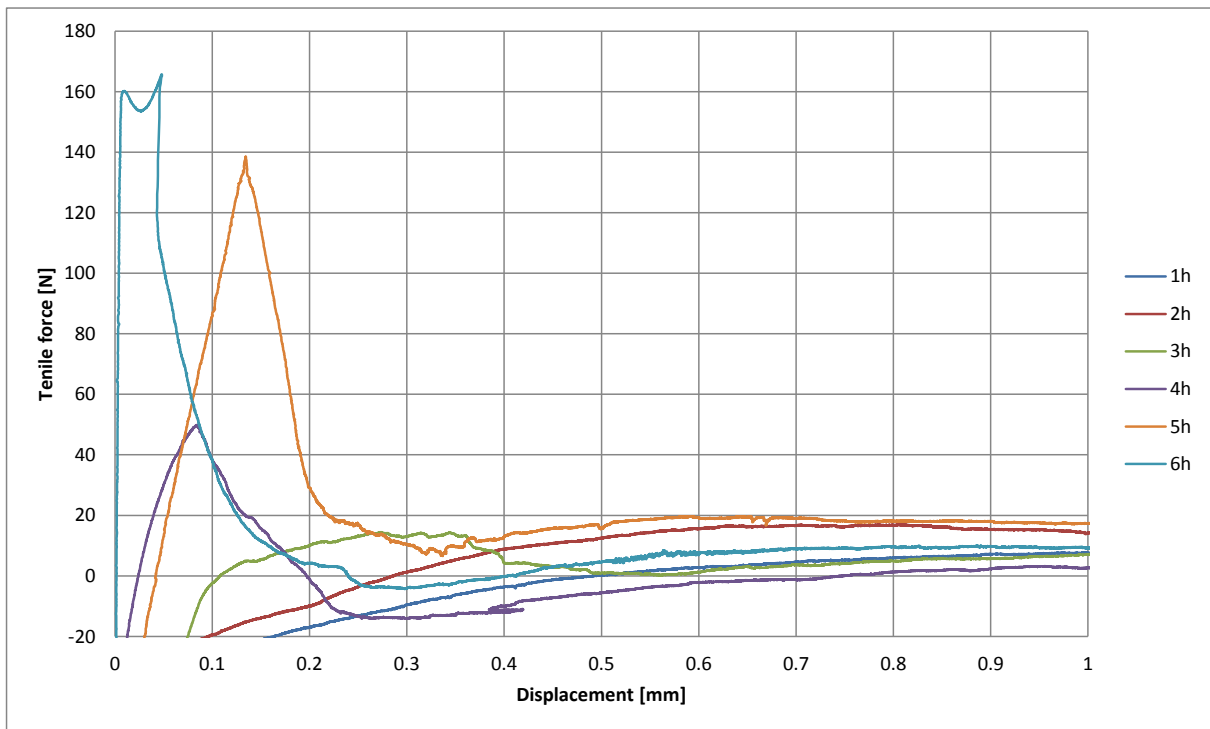
Figure 6.5: Displacement of moulds with corresponding tensile resistance of MR specimens

As can be seen, a tensile force was only transferred to the 1h MR specimen after the mould halves had moved approximately 0.5 mm apart. This distance typically decreased with age. The 6h specimen was so rigid that a significant tensile force was transferred virtually directly after displacement was initiated. During the data processing procedure, the displacement

94

zero point was taken as the onset of tensile force transfer in the specimens, as can be seen in Appendix D.

6.3   Evaluation of post-initial setting time strain determination

The Doa, et al. (2009) 50 - 90% on mould displacement method delivered realistic strains values for the concrete specimens before the initial setting time. This was confirmed by the large amount of deformation that occurred outside of the gauge length for the test conducted before initial setting and the convergence of the displacement as determined by the insitu concrete displacement- and the Doa, et al. (2009) 50 - 90% on mould displacement methods, as shown in Figure 6.3. However, after the initial setting time had occurred and the stiffness and strength of the specimens started to increase significantly, the displacement relationship proposed and used by Doa, et al. (2009) no longer gives a reliable estimation of the displacement behaviour of the concrete specimen over its gauge length.

The Doa, et al. (2009) 50 - 90% on mould displacement method severely underestimated the strain measured over the gauge length of the specimens tested after the initial setting time. This underestimation became more apparent with an increase in specimen age, as the concrete gained strength and stiffness. For the 5h MR test specimen the insitu concrete method of displacement measurement determined the strain capacity to be 631.3 μ while the Doa, et al. (2009) 50 - 90% mould displacement method found it to be 464.1 μ, as shown in Figure 6.6. This resulted in a 26.5% underestimation of the strain capacity.
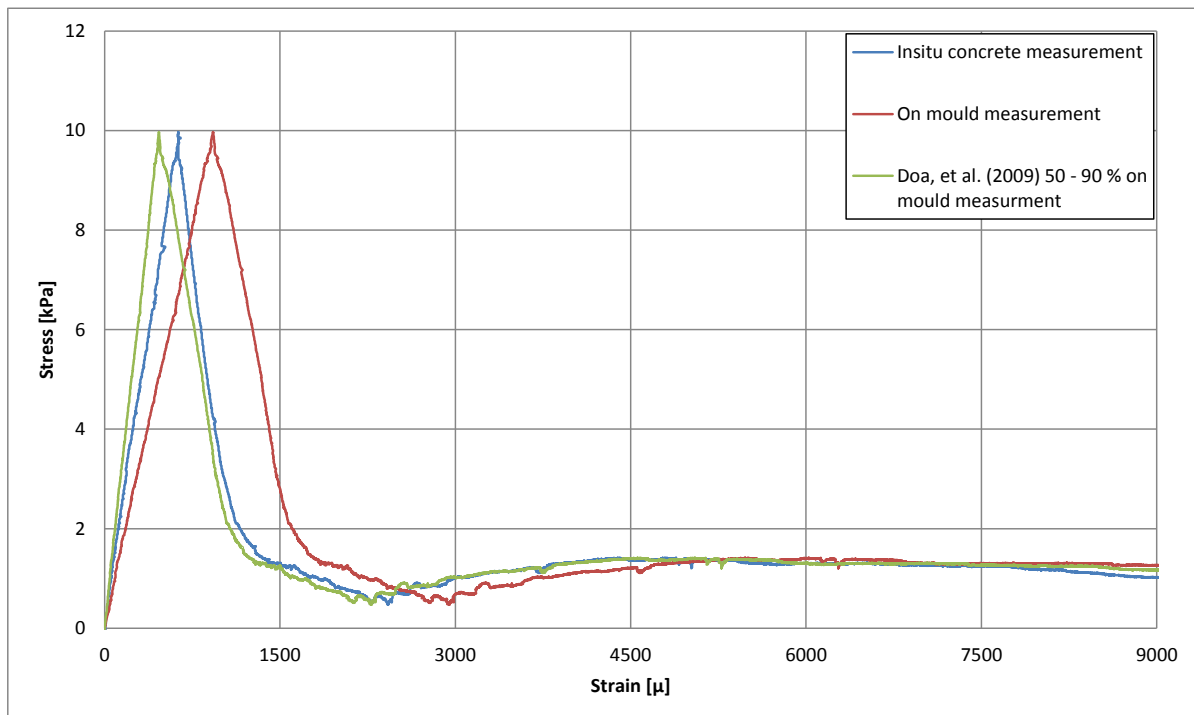
Figure 6.6: Displacement measurement for 5h MR specimen

95

Typically it was found that the older the tests specimens were, the greater the Doa, et al. (2009) 50 - 90% on mould displacement method underestimated their strain capacity. This is illustrated by Table 6.1, which compares the insitu concrete- and Doa, et al. (2009) 50 - 90% on mould displacement methods for the oldest test specimens tested for the various concrete mixes. The 6h MR test specimen is not shown in Table 6.1 as this specimen was an outlier in terms of strain capacity, as is discussed in Section 7.2.

Table 6.1: Insitu concrete and Doa, et al. (2009) 50 - 90% on mould strain capacity comparisons

Specimen	Insitu concrete ε_c [μ]	Doa, et al. 50 - 90% on mould ε_c [μ]	Under estimation [%]
6h MA19	650.0	540.6	16.8
6h MA9	675.0	389.1	44.0
6h MF0.6	1656.3	828.1	50.0
6h MF1.8	406.3	298.4	26.6
6h MSA	931.3	706.3	24.2
8h MSR	406.3	318.8	21.5

From the results presented in Table 6.1, it is clear that the displacement relationship proposed and used by Doa, et al. (2009) based on the displacement of the mould halves, does not account for the continuously evolving material behaviour of early age concrete after it has reached its initial setting time. For this reason the insitu concrete measurement method, as used in this study, is believed to deliver more reliable displacement results.

6.4   Concluding summary

This chapter focused on the full stress-strain behaviour of early age concrete, as presented in Appendix D. It is found that the insitu method of strain determination cannot be successfully carried out on fresh concrete specimens due to the plastic nature of these specimens. The Doa, et al. (2009) 50 - 90% on mould measurement method was adopted in order to approximate the displacement over the gauge length of the early age concrete specimens which have not yet reached the initial setting time. For the early age concrete specimens tested after the initial setting time the insitu concrete measurement method proved to be sufficient and delivered reliable results as the aluminium pins are securely anchored and interlocked with the concrete specimen at this phase of setting. Finally, it is shown that the Doa, et al. (2009) 50 - 90% on mould measurement method does not sufficiently account for the increased stiffness and strength of early age concrete specimens after the initial setting time has occurred. The following two chapters present and discuss the tensile properties of the early age concrete test specimens for the ascending and descending

portions of their stress-stain behaviour respectively, in other words, before and after material failure or cracking occurs.

7. Experimental results and discussion: Ascending stress-strain section

This chapter describes the ascending portion of the stress-strain behaviour of early age concrete, which comprises of the section from the onset of a tensile force transferred through the specimen, up to the point that the peak stress is measured. First the data processing methodology is discussed and the outliers are described. Next, the results are presented according to the objectives of this study: the effect of coarse aggregate size, the effect of the addition of microfibres and the effect of setting time altering admixtures on the tensile properties of early age concrete.

7.1   Data processing methodology

In this chapter the term "tensile strength" is an indication of the measured peak stress of a concrete specimen. Strain capacity is defined as the strain at peak stress. After this point in the stress strain curve, it is assumed that the test specimen has failed and a crack surface has begun to form. These fracture properties are described in Chapter 8.

The Young's modulus of the specimens was determined by fitting a straight line to a portion, assumed to be linear, of the ascending stress-strain curve. This was done by means of linear regression. Gutsch (2002) conducted tensile tests on concrete specimens with an age of 24 hours and presented a model suggesting a linear elastic stress-strain relationship from 0 to 50% of the tensile strength, whereafter plastic deformation occurred up to the point where the specimens' tensile strength was reached. This was found to be valid for most specimens that had already reached initial set, with the linear region typically extending even further, as can be seen in Appendix D. However, this was not the case for fresh concrete specimens. For specimens tested before the initial setting time, the linear region was very small, if present at all. It was decided to assume that the region spanning from 25 to 33% of tensile strength was linear elastic and to use it to determine these specimen's Young's modulus. Some specimens however did not exhibit true linear elastic material behaviour. The Young's modulus determined from these tests typically had lower R^2-values, indicating a lesser degree of a linear relationship between stress and strain. After the initial setting time, the region spanning from 25 to 50% of the tensile strength exhibited a near linear relationship between stress and strain. This larger interval over which the Young's modulus was determined resulted in greater resolution as well as much higher R^2-values that were determined for the straight lines fitted to this interval, which therefore describes the material's Young's modulus more accurately. This is discussed in more detail later on in this section.

Figure 7.1 illustrates how the Young's modulus was determined from the stress-strain curve of the specimens that were tested before the initial setting time while Figure 7.2 illustrates this for specimens tested after the initial setting time. The tensile strength, f_t, and strain capacity, ε_c, are also indicated.
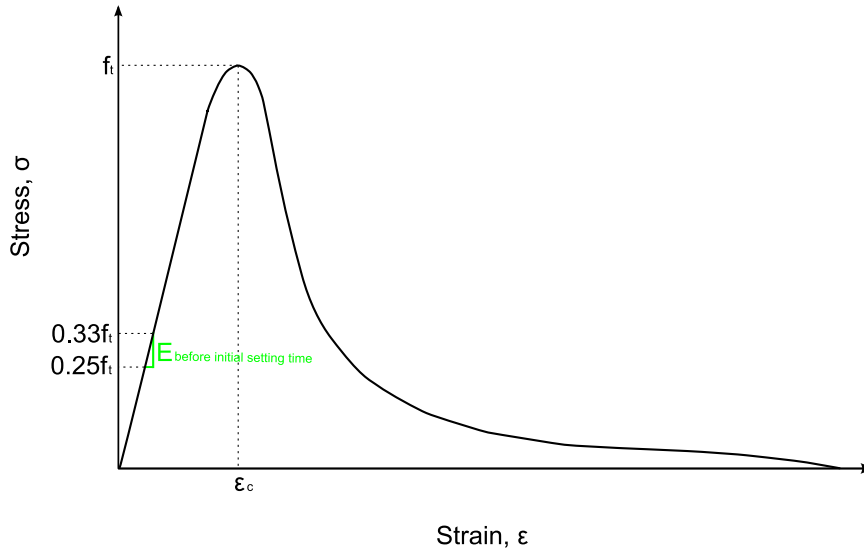
Figure 7.1: Determination of Young's modulus for a specimen tested before the initial setting time
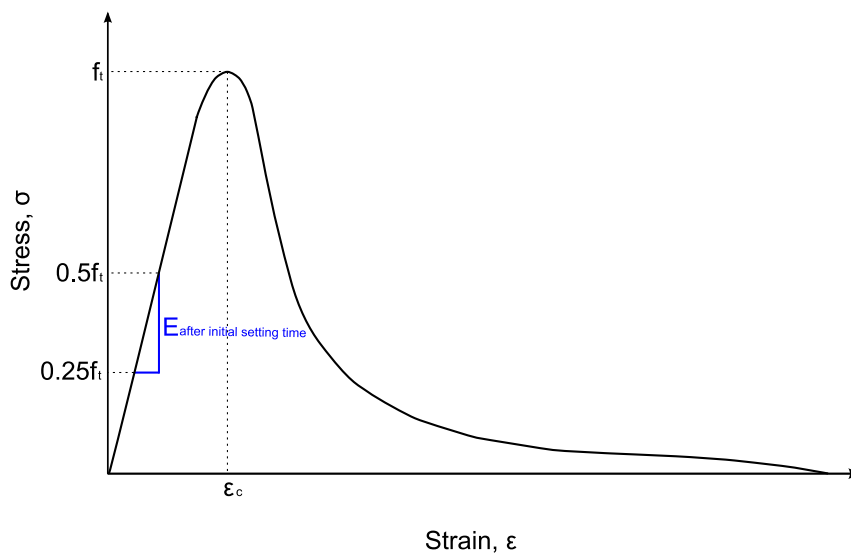
Figure 7.2: Determination of Young's modulus for a specimen tested after the initial setting time

It should be noted that the Young's modulus determined for a specimen is strongly dependent on the interval over which it was determined. An example of this is presented in Table 7.1 that shows the Young's modulus and corresponding R^2-values for the 8h MSR test specimen, determined over various intervals. While determining the Young's modulus over a small interval, for instance from 25 to 33% of the tensile strength, the resolution of the LVDT's became a problem as indicated by the low R^2-values. The highest R^2-value was

achieved over the 25 to 75% of tensile strength interval, which was the limit of the linear region for this specific specimen. The R^2-value typically increased as the interval over the linear stress-strain portion of specimens was enlarged. For each specimen, an optimum R^2-value can be determined, which in many instances can lead to a value that produces a better fit for the expected linear relationship between Young's modulus and tensile strength, to be discussed later on in this chapter. In order to process the results as objectively as possible, the 25 to 50% tensile strength interval was used to determine the Young's modulus for specimens tested after the initial setting and the 25 to 33% tensile strength interval for all specimens tested before the initial setting time. However, this approach did not always yield results with the optimal R^2-value, which would best describe the linear elastic behaviour of the test specimens.

Table 7.1: Young's modulus determined over different intervals for the 8h MSR test specimen

Interval [% of tensile strength]	Young's modulus [MPa]	R^2-value
25 - 33	111.6	0.379
25 - 50	293.2	0.797
25 -75	199.8	0.909
0 - 33	540.9	0.701
0 - 50	522.0	0.873
0 - 75	338.5	0.885

7.2   Variability and outliers

As only a single specimen of each mix at a specific age as tested no characteristic values or confidence intervals could be established for the specimens tested in this study. This made it problematical to establish trends and draw clear conclusions, especially given the heterogonous nature of the material tested. The large confidence intervals shown in Figure 2.11 indicating the tensile strength and strain capacity of early age concrete specimens from the study conducted by Branch, et al. (2002) and the large degree of scatter observed in the results of the study conducted by Doa, et al. (2009) convey this point strongly.

From the 44 tensile tests used for the analysis of early age concrete properties, there was only one specimen for which its Young's modulus and strain capacity could not be reliably determined. Three specimens produced significant outliers in terms of Young's modulus, according to the definition described in the previous section, as well as strain capacity. Taking into account the heterogeneous nature of the early age concrete specimens, together with all the factors that can influence test results, this is believed to be acceptable. This

section described these outliers along with the typical linear elastic behaviour of early age concrete.

Figure 7.3 shows the initial ascending portions of the stress-strain curves of the 4h, 5h and 6h MR test specimens. The 4h and 5h test specimens produced virtually straight lines up till the peak stress was reached. In contrast, the 6h specimen produced an extremely steep initial section, reaching an initial peak stress of 11.77 kPa at 18.75 µ. Throughout this initial section of the 6h MR test the strain measured by means of the insitu concrete measurements resulted in great variability with initial strain fluctuation between negative and positive values. After flatting out, the stress-stain curve reached in ultimate peak stress of 12.17 kPa at a strain of 265.5 µ, representing its tensile strength. More typical and expected linear behaviour for 6h test specimen is indicated by the straight black line in Figure 7.3. This irregular behaviour was thought to be a combination of a multifunction in the physical isitu concrete measurement system as well as the LVDT's that were responsible for measuring the displacement over the specimen gauge length. For this reason, the strain capacity, Young's modulus, and consequently also the characteristic length of the 6h MR test specimen, could not be determined.
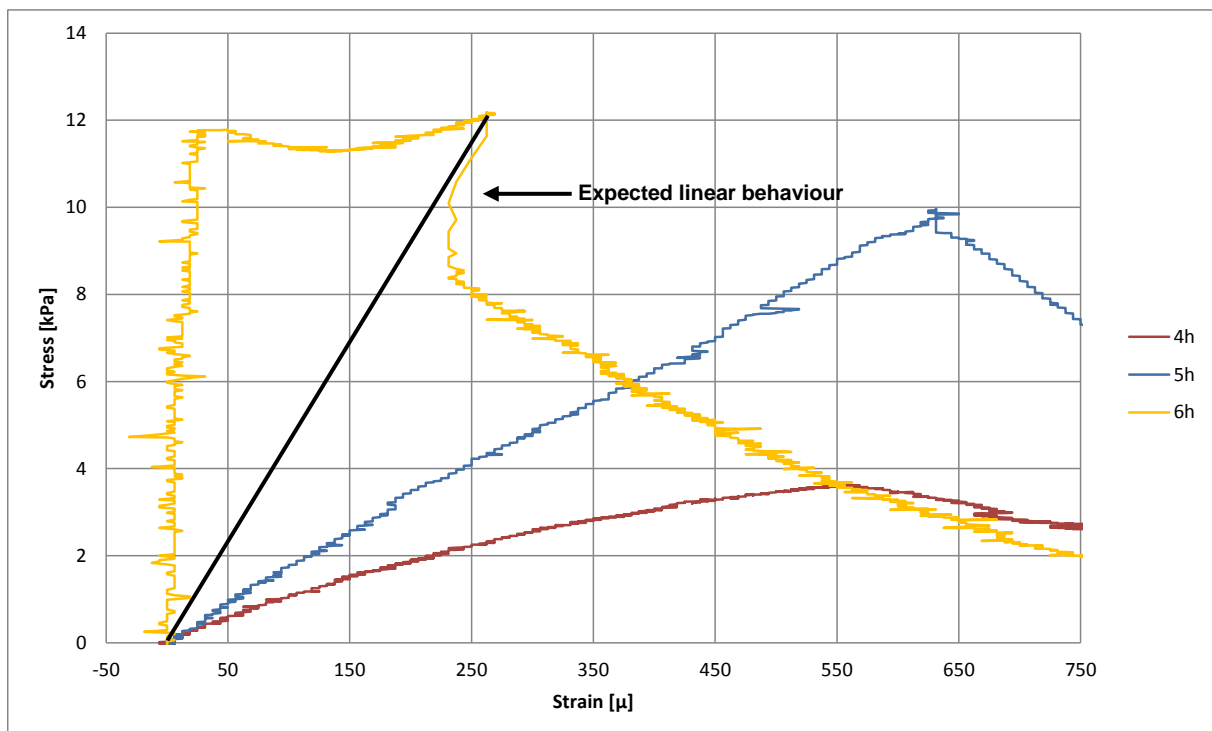
Figure 7.3: Irregular behaviour of 6h MR test specimen

It should also be noted that the linear region of the stress-strain curve often extended past the 50% of peak stress limit as predicted by Gutsch (2002). The 5h MR specimen is a good

example of this as it displayed a linear relationship between stress and strain virtually up to the point where its tensile strength was reached, as shown in Figure 7.3.

The 8h MSR test specimen also proved to be an outlier, as shown in Figure 7.4. This test specimen was extremely stiff and produced a very steep initial linear section and an unusually long plastic region leading up to its tensile strength.
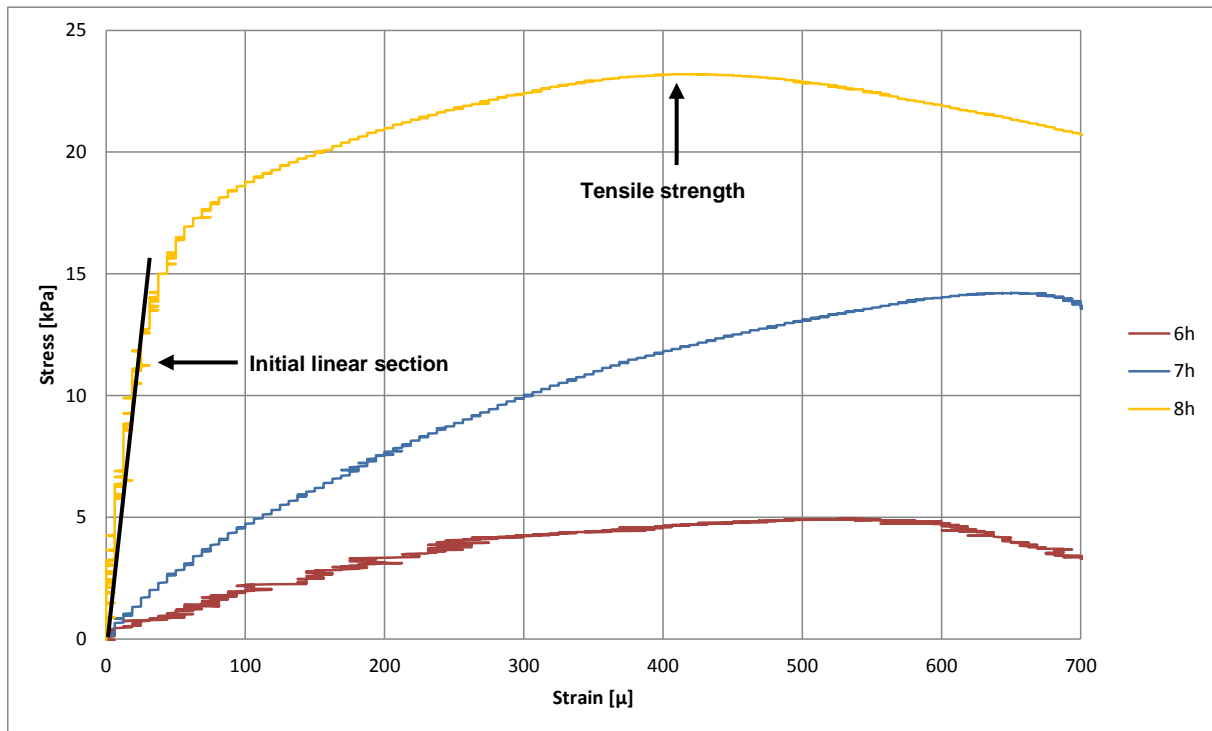
Figure 7.4: Irregular behaviour of 8h MSR test specimen

Using the method described earlier in this section of determining the Young's modulus of a test specimen after the initial setting time, it was determined to be 293.19 MPa. This is significantly higher than the Young's modulus of any other MSR specimen, which can be expected seeing that this was the oldest specimen tested, and displayed the highest tensile strength. However, the trend of a linear relationship between Young's modulus and tensile strength was not adhered to by this specimen, as can be seen for Figure 7.17. Consequently this test specimen is a clear outlier.

Figure 7.5 shows the irregular stress-strain behaviour of the 5h MF1.8 test specimen. As with the 8h MSR test specimen, this specimen produced a very steep initial linear section and an unusually long plastic region leading up to the point of its tensile strength. As a result, the trend of a linear relationship between Young's modulus and tensile strength was not adhered to by this specimen, and it is also considered an outlier in terms of Young's modulus and strain capacity.
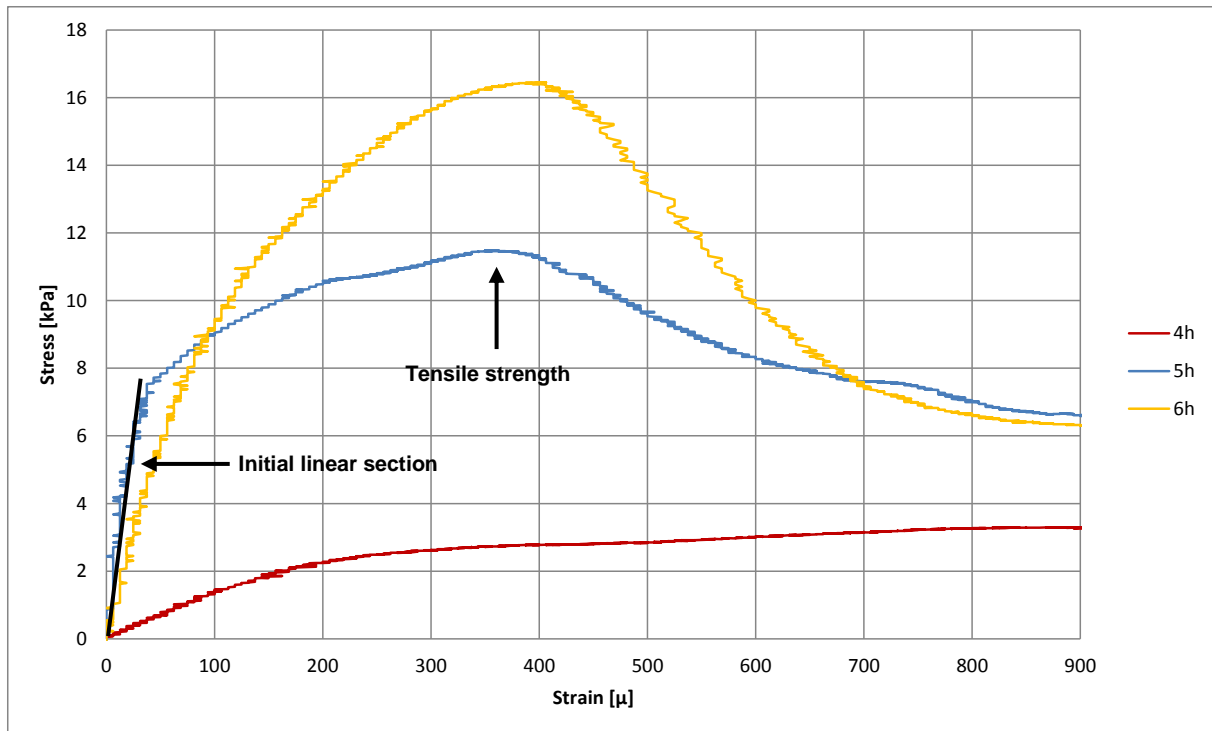
Figure 7.5: Irregular behaviour of 5h MF1.8 test specimen

The last significant outlier with regards to the Young's modulus and strain capacity of early age concrete was the 6h MF0.6 test specimen, as shown in Figure 7.6. In contrast to all the other outliers, this specimen produced a significantly lower than expected Young's modulus, as well as a considerably higher strain capacity. The region marked by the blue circle indicates the presence of slippage in the tensile application system, as a slight drop in the applied tensile stress was observed without failure occurring. Another exception observed for this test specimen is the small linear region ranging from 0 to 3.7 kPa. Although the interval used to determine the Young's modulus did not fall completely within the approximate linear region, it did not include the region of slippage and is still believed to be valid for the chosen definition of Young's modulus although it might not provide the most accurate representation of the material's linear elastic behaviour. Another irregularity observed in this test is the large flat region of the stress-strain curve from 1200 to 1800 µ just prior to the point of its tensile strength. The result is a significantly higher strain capacity than any other specimens, including all mixes, after the initial setting time has occurred. This did not agree with the trend, as the strain capacity usually decreased to a minimum at an age of around 5 – 6 hours.

The ascending stress–strain tensile properties of early age concrete for all 44 test specimens is presented in Table E.1 in Appendix E.

103
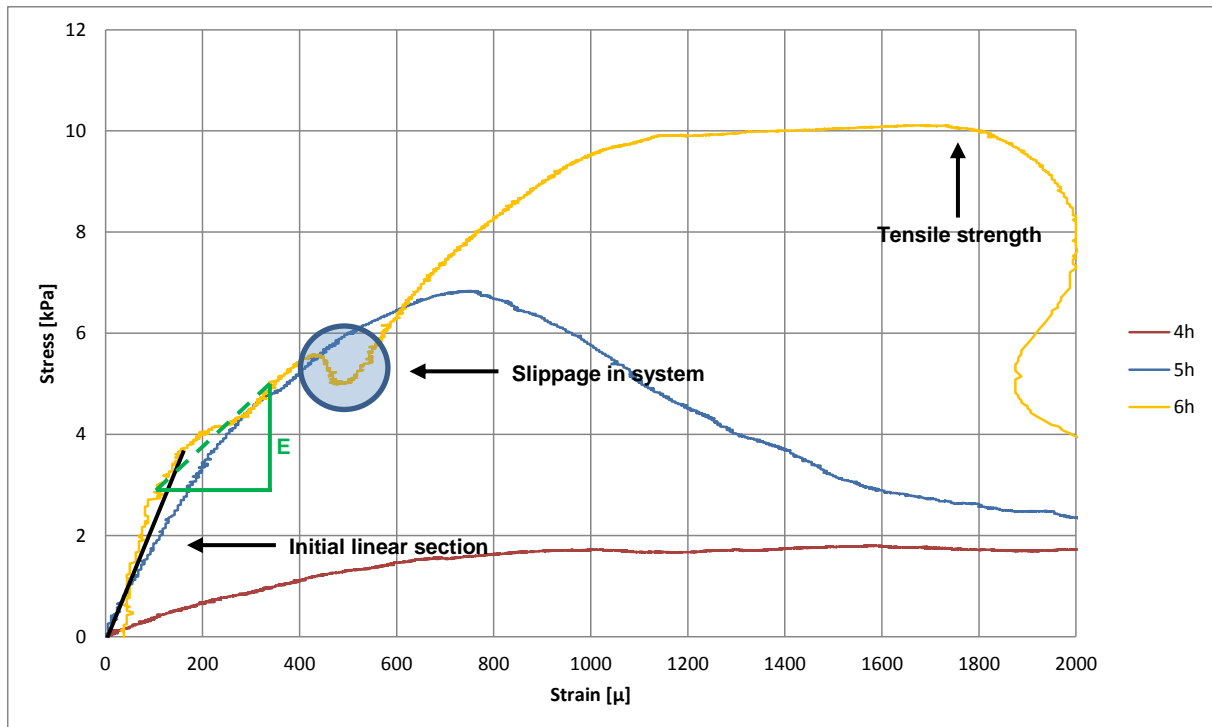
Figure 7.6: Irregular behaviour of 6h MF0.6 test specimen

7.3   Experimental results for Objective 2: Effect of coarse aggregate size on the tensile properties of fresh concrete

This section graphically presents the ascending tensile properties for the MR, MA9 and MA19 concrete mixes.

7.3.1 Tensile strength

The results of the tensile strength versus age of the MR, MA9 and MA19 mixes are shown in Figure 7.7. All three mixes display similar tensile strength measurements while in its fresh concrete state over the first three hours. After the initial setting time the strength of the specimens increase rapidly. The tensile strength of the MA19 test specimens is significantly lower that both the MR and MA9 test specimens, except for the four hours specimens, where the MA9 test specimen provided a lower than expected tensile strength. Assuming that the 5h and 6h MR test specimens were irregularly strong and the 6h MA9 test specimen was weaker than expected, the conclusion can be made that a reduction in coarse aggregate size leads to an increase in the early age tensile strength of concrete. This is supported by the tensile strength results of the 5h and 6h MA19 test specimens, which are considerably lower than those of the corresponding MR and MA9 test specimens which made used of smaller coarse aggregates.
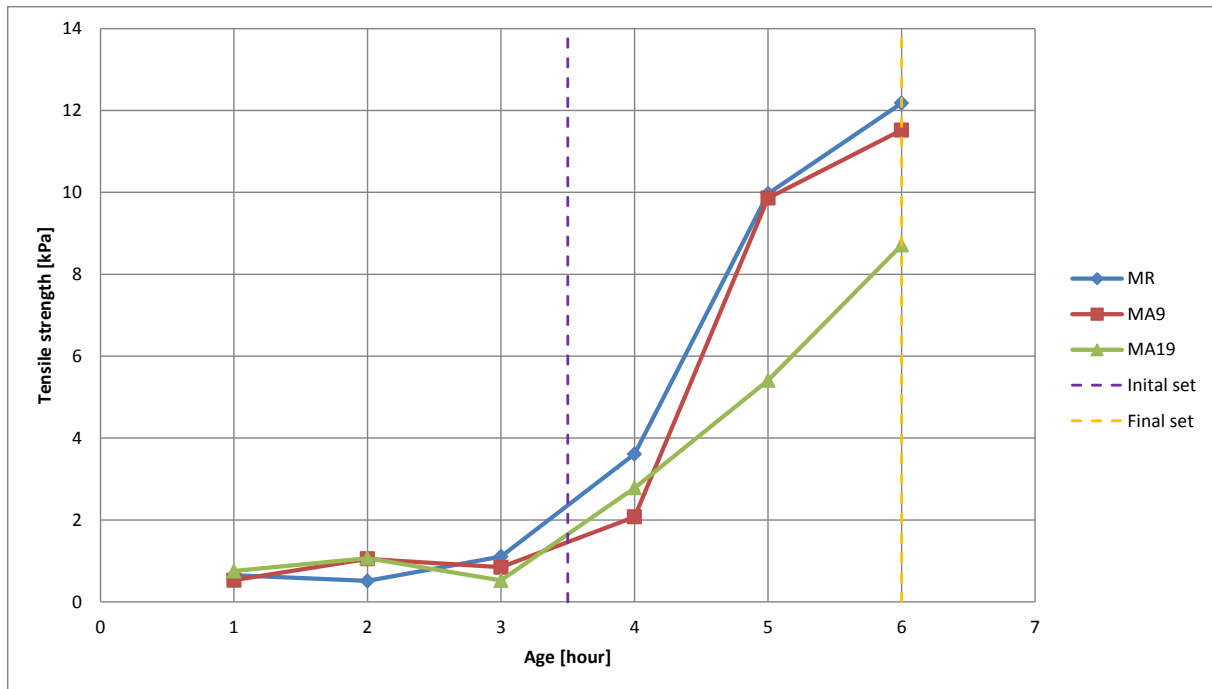
Figure 7.7: Tensile strength vs. age of MR, MA9 and MA19 mixes

7.3.2 Tensile strain capacity

The results of the strain capacity versus age of the MR, MA9 and MA19 mixes are shown in Figure 7.8. Assuming the strain capacity of the 2h MR test specimen is abnormally high and can be considered irregular strain behaviour, it is apparent that the strain capacity of the specimens decreases with time to a minimum in the order of 500 μ at an age of 5 hours. Coarse aggregate size does not clearly influence the strain capacity of early age concrete.

7.3.3 Young's modulus

The Young's modulus versus age of the MR, MA9 and MA19 mixes are shown in Figure 7.9. Initially the Young's modulus of the specimens is very low and gradually increases with time before initial setting time has occurred. However, after initial setting time has occurred, the Young's modulus increases rapidly. From the results presented it is deduced that a decrease in aggregate size leads to an increase in Young's modulus for early age concrete.

The Young's modulus vs tensile strength of the MR, MA9 and MA19 mixes are shown in Figure 7.10. Each mix produced a relatively straight curve as the two properties develop, signifying a linear relationship between Young's modulus and tensile strength. A clear influence of coarse aggregate size on the gradient of the Young's modulus - tensile strength curve is not observed.
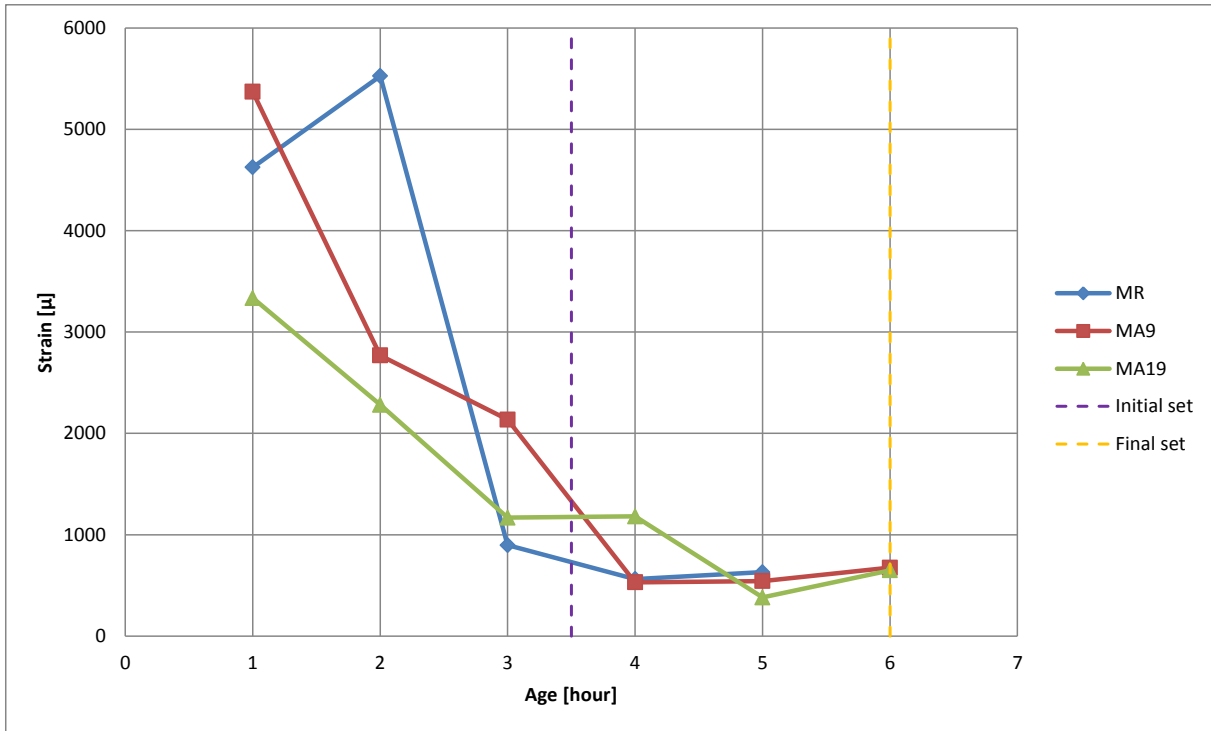
Figure 7.8: Strain capacity vs. age of MR, MA9 and MA19 mixes
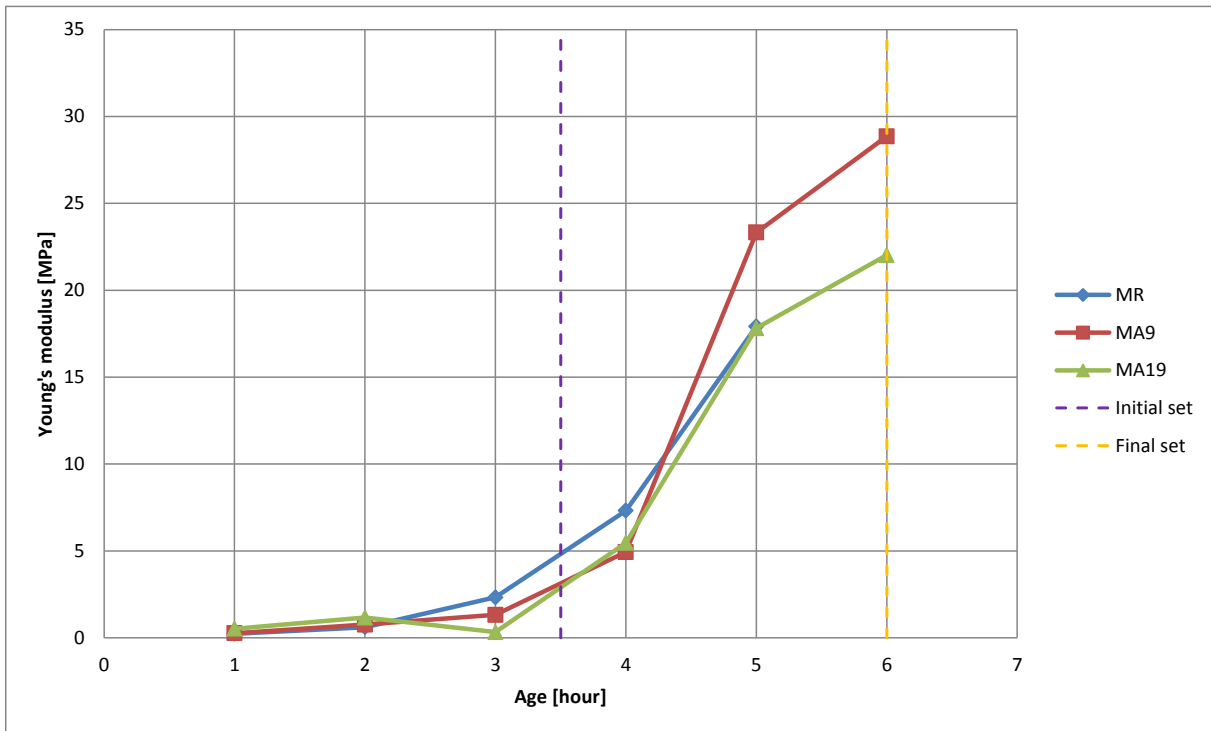
Figure 7.9: Young's modulus vs. age of MR, MA9 and MA19 mixes

7.3.4 Concluding remarks for Objective 2

From the result presented in this section it is found that a reduction in the coarse aggregate size of a concrete mix led to an increase in the early age tensile strength of the concrete. The

influence of coarse aggregate size on the strain capacity of concrete appears to be negligible. A reduction in coarse aggregate size leads to an increase in Young's modulus. A reduction in the coarse aggregate size also results in an increase in cohesiveness, while decreasing the slump value of the concrete mix in its fresh state. This could be a possible explanation for the greater strength and stiffness observed for the mixes utilising smaller coarse aggregates. With regards to the relationship between Young's modulus and tensile strength, all mixes, regardless of coarse aggregate size, display a linear relationship, with coarse aggregate size playing a seemingly insignificant role in the gradient of this relationship.
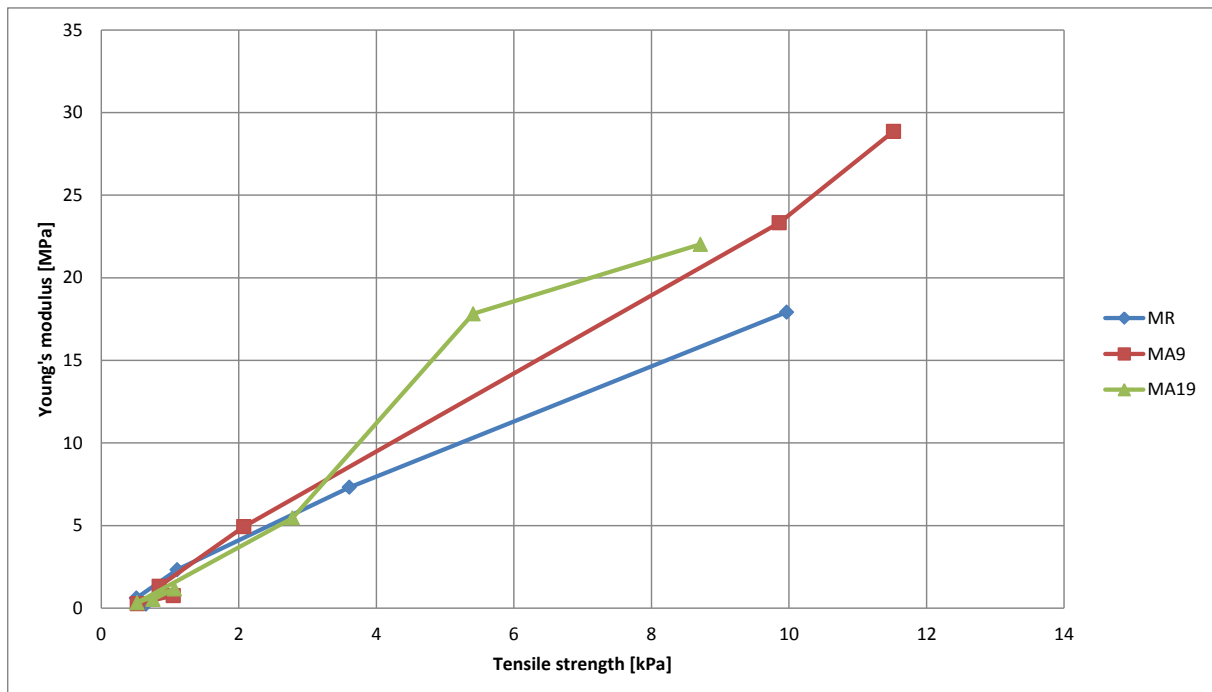
Figure 7.10: Young's modulus vs. tensile strength of MR, MA9 and MA19 mixes

7.4   Experimental results for Objective 3: Effect of the addition of microfibres on the tensile properties of fresh concrete

This section graphically presents the ascending tensile properties for the MR, MF0.6 and MF1.8 concrete mixes.

7.4.1 Tensile strength

The tensile strength versus age of the MR, MF0.6 and MF1.8 concrete mixes are shown in Figure 7.11. The tensile strength of the specimens is very low before the initial setting time has occurred. However, after the initial setting time has occurred, the tensile strength increases rapidly. For the fresh concrete specimens, which are the specimens tested before the initial setting time, an increase in fibre content leads to a slight increase in the measured

tensile strength. It should be noted that this increase in strength is strongly related to a decrease in the slump value of the fresh concrete mixes, showing that a more cohesive and less workable concrete mix would consequently have higher tensile strength as a fresh concrete. After the initial setting time was reached, the MF0.6 mix consistently supplied the lowest tensile strength values, while the MF1.8 mix provided the highest. Consequently, no apparent relationship between fibre content and early age tensile strength could be determined after the initial setting time had occurred. Rather, the results indicate that the addition of a low volume of fibres does not significantly influence the tensile strength of early age concrete after the initial setting time.
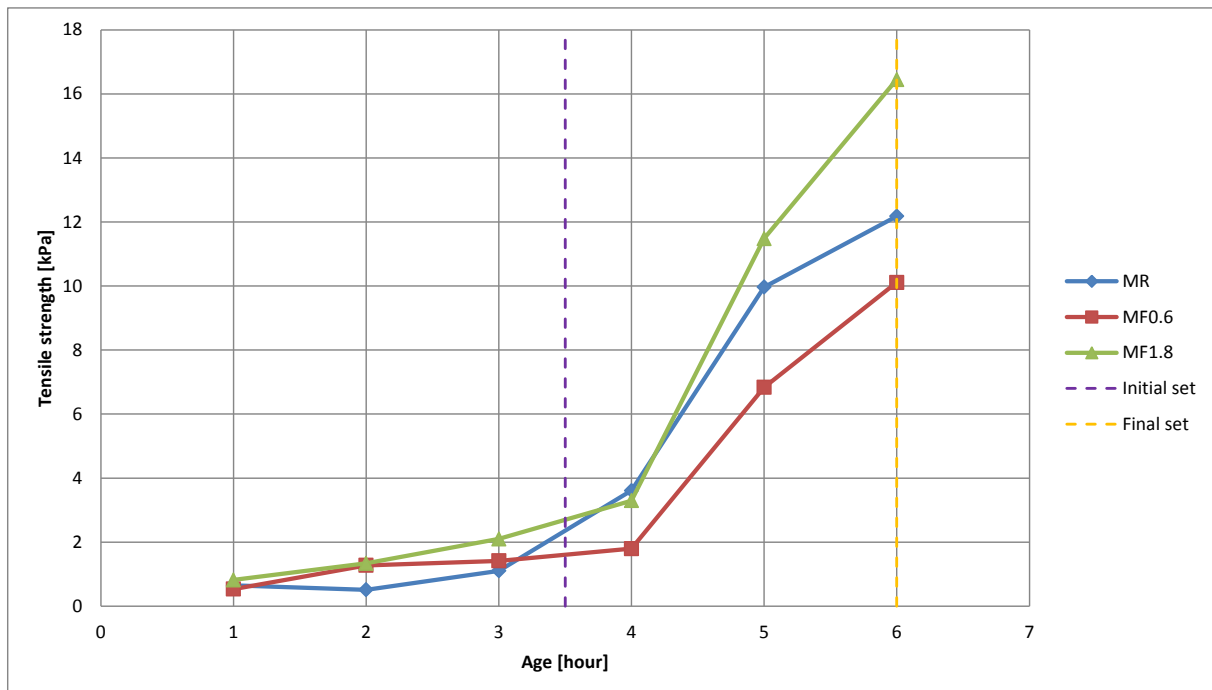
Figure 7.11: Tensile strength vs. age of MR, MF0.6 and MF1.8 mixes

7.4.2 Tensile strain capacity

The strain capacity versus age of the MR, MF0.6 and MF1.8 concrete mixes are shown in Figure 7.12. The strain capacity decreases with time to a minimum value at an age of 5 and 6 hours. As a result of the large viability during the first two hours, no clear correlation between fibre content and strain capacity could be identified for the these early ages. However, around the initial setting time the mixes containing fibres displayed significantly more strain capacity, when compared to the reference mix. For the 5 and 6 hour ages, no clear conclusion could be drawn since the 6h MR test specimen's strain capacity could not be reliably determined and the 6h MF0.6 and 5h MF1.8 test specimens were seen as outliers in this regard, as described in Section 7.1.
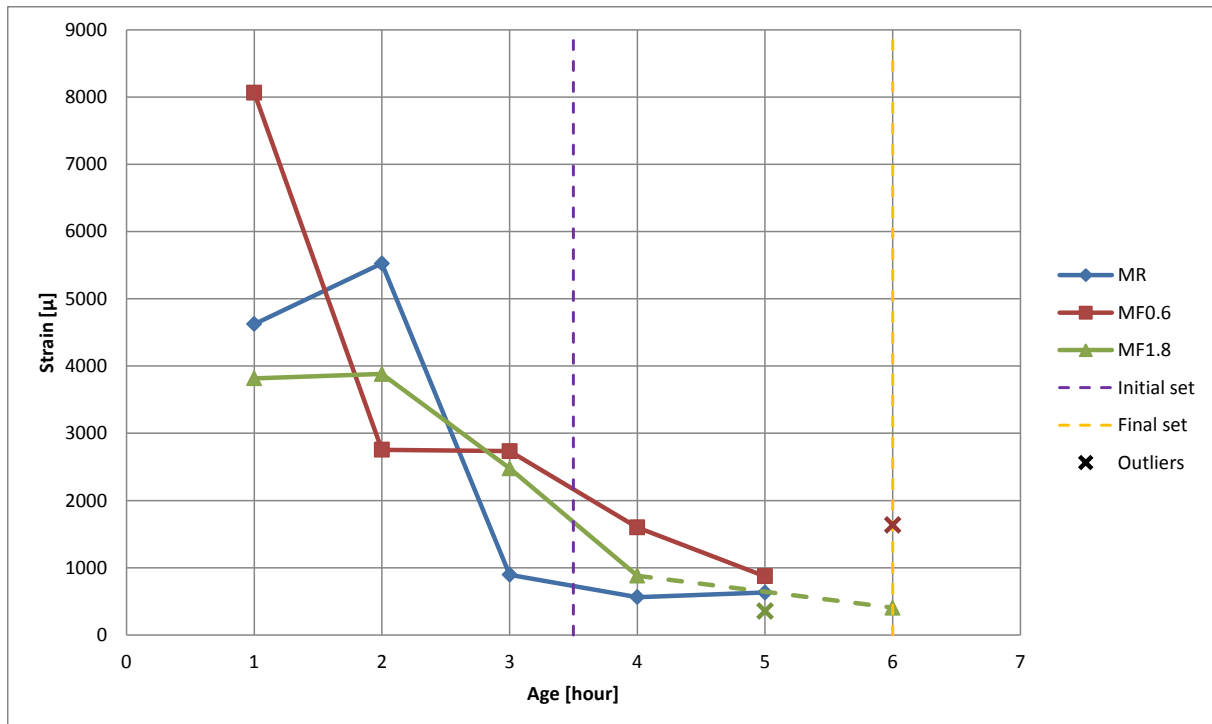
Figure 7.12: Strain capacity vs. age of MR, MF0.6 and MF1.8 mixes

7.4.3 Young's modulus

The Young's modulus versus age of the MR, MF0.6 and MF1.8 concrete mixes are shown in Figure 7.13. Initially the Young's modulus of the specimens is very low and gradually increases with time before the initial setting time has occurred. However, after initial setting time has occurred, the Young's modulus increases rapidly. The 5h and 6h MF1.8 test specimens displayed abnormally high Young's modulus values, with the 5h specimen being a clear outlier, as described in Section 7.1. Contrastingly, the 6h MF0.6 test specimen produced a low Young's modulus, also clearly an outlier, as described in Section 7.1. Consequently, no clear correlation between fibre content and early age Young's modulus could be determined, although tentatively it seems as if fibres may increase the Young's modulus of early age concrete to a certain degree, based on the results of the MF1.8 test specimens. This could also be due to the reduction in slump values and increase in cohesion caused by an addition of fibres.

The Young's modulus versus tensile strength of the MR, MF0.6 and MF1.8 concrete mixes is shown in Figure 7.14. After the initial setting time has occurred, the MF1.8 test specimens deviated from the assumed linear relationship between Young's modulus and tensile strength if the 5h outlier is taken into account. This is also the case for the MF0.6 mix if its 6h outlier is taken into consideration. However, if the outliers are ignored an almost linear relationship

109

between Young's modulus and tensile strength is observed. It appears as if an addition of fibres may cause a slightly steeper gradient to this almost linear relationship.
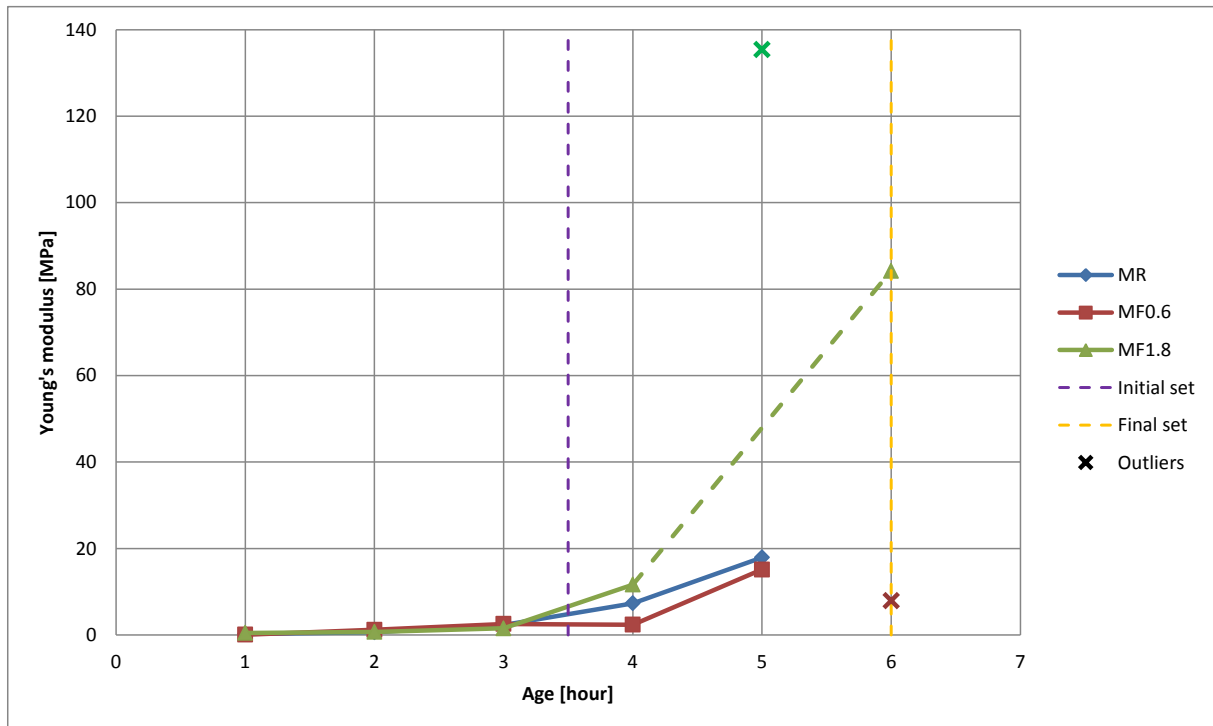
Figure 7.13: Young's modulus vs. age of MR, MF0.6 and MF1.8 mixes
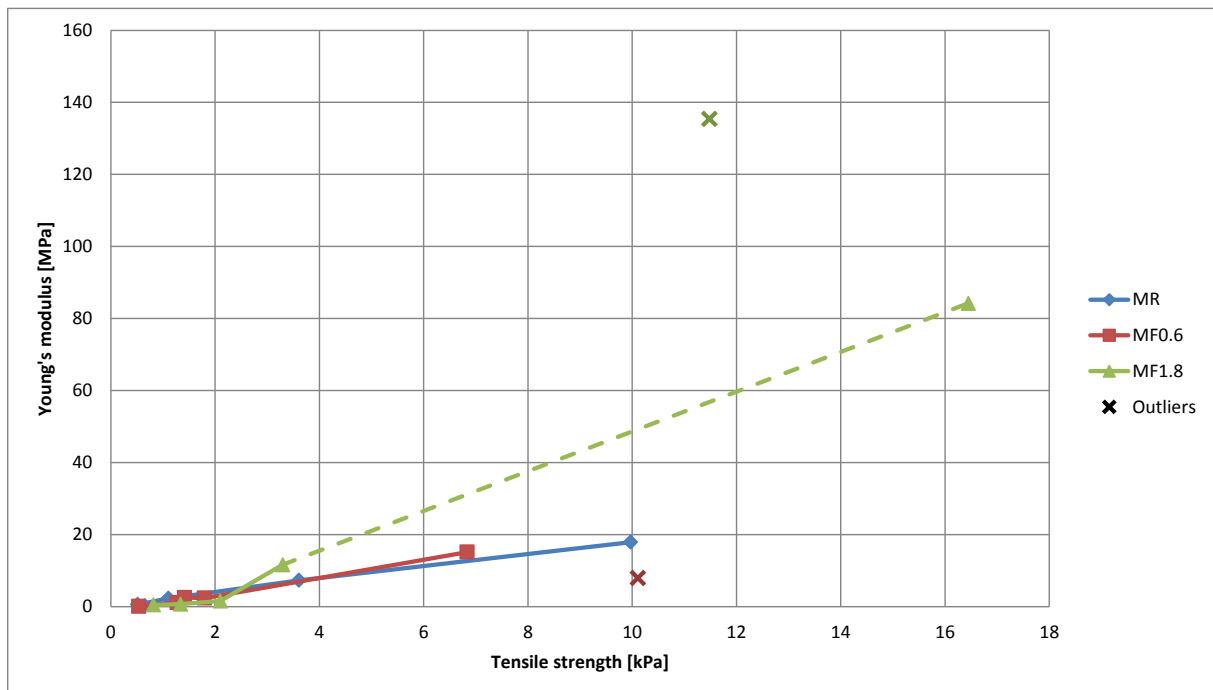
Figure 7.14: Young's modulus vs. tensile strength of MR, MF0.6 and MF1.8 mixes

110

7.4.4 Concluding remarks for Objective 3

For the fresh concrete specimens, tested before the initial setting time, an increase in fibre content leads to a slight increase in strength. This is thought to be a result of the lower slump values and increased cohesion associated with an addition of fibres to concrete. No clear relationship between fibre content and the tensile strength of early age concrete after the initial setting time exists. With regards to strain capacity, no clear relationship between fibre content is observed during the first two hours. However, at the ages of 3 and 4 hours, either side of the initial setting time, mixes containing fibres display increased strain capacity in comparison to the reference mix. This is of significance as the initiation of PShC typically occurs around the initial setting time. As both the MF0.6 and MF1.8 mixes displayed similar strain capacities for these tests specimens, it is believed that the fibre volume added to the reference concrete has an inconsequential effect on strain capacity within the range of fibre volume additions tested in this study. The strain capacity of 5h and 6h test specimens appear to be unaffected by the addition of fibres. No clear correlation between fibre content and early age Young's modulus is observed, although it appears as if an addition of fibres may lead to a minor increase. This could also be due to the reduction in slump value and increased cohesion associated with an addition of fibres. When ignoring outliers, an almost linear relationship between Young's modulus and tensile strength is observed. It appears as if an addition of fibres causes a slightly steeper gradient to this almost linear relationship.

7.5 Experimental results for Objective 4: Effect of setting time altering admixtures on the tensile properties of fresh concrete

This section graphically presents the ascending tensile properties for the MR, MSA and MSR concrete mixes.

7.5.1 Tensile strength

The tensile strength versus age of the MR, MSA and MSR concrete mixes are shown in Figure 7.15. The tensile strength of the MSA is closely related to that of the MR mix. This is unexpected as the MSA mix has an initial setting time of 3 hours and a final setting time of 5 hours, while the RM mix has an initial and final setting time of was 3.5 hours and 6 hours respectively. The only exceptions are the MR 5h test specimen, which was substantially stronger that the 5h MSA test specimen and the MSA 6h test specimen were considerably stronger than the MR specimen of the corresponding age, which could be expected as the MSA mix had reached its final setting time an hour earlier. These results support the notion that the MR 5h specimen displayed an abnormally high tensile strength, as stated previously. The tensile strength of the MSR specimens was found to be negligible up to an age of 5 hours, well after the initial setting time of 4.5 hours. After this point its strength increased

extremely rapidly, producing the highest measured tensile strength of all concrete mixes at its final setting time of 8 hours. From the results presented it can be concluded that for a specific concrete mix the initial and final setting times do not necessarily represent a specific tensile strength when making use of admixtures to alter the setting time of the mix.
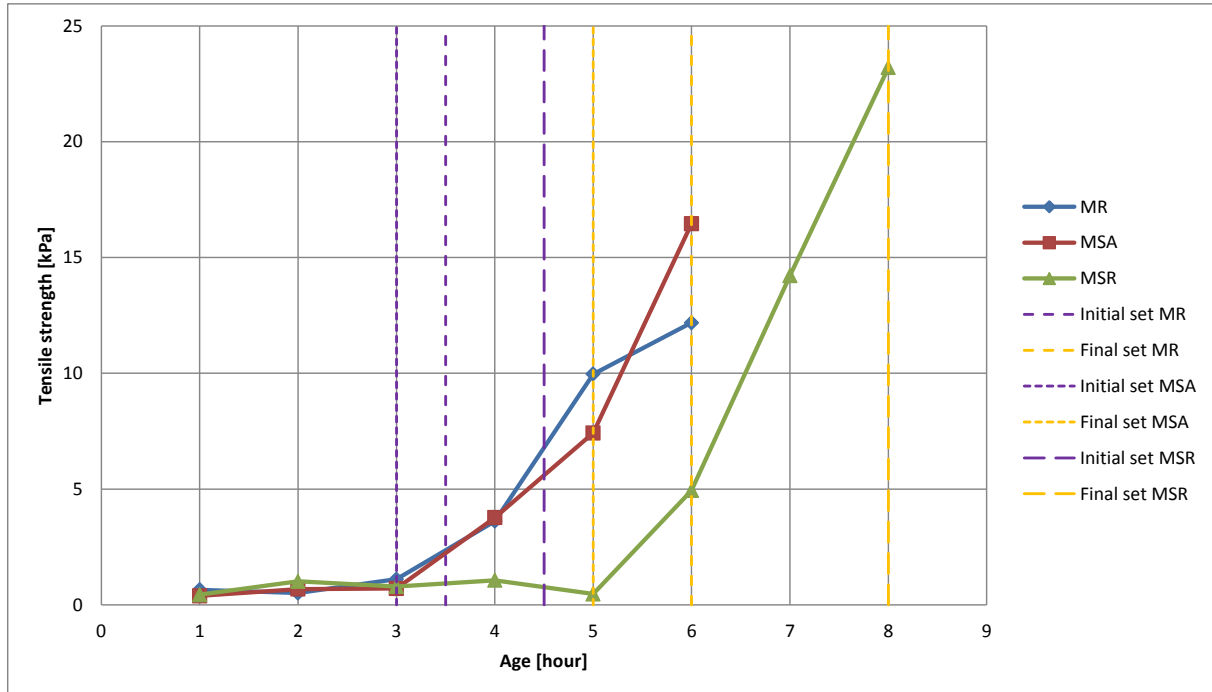
Figure 7.15: Tensile strength vs. age of MR, MSA and MSR mixes

7.5.2 Tensile strain capacity

The strain capacity versus age of the MR, MSA and MSR concrete mixes are shown in Figure 7.16. The strain capacity decreases with time to a minimum value at an age of 5 hours for the MR and MSA mixes and 6 hours for the MSR mix. As a result of the viability during the first 3 hours, no clear correlation between setting time altering admixtures and strain capacity could be identified for the fresh concrete specimens. However, the retarded mix displayed significantly more strain capacity around the initial setting time. After the point of initial setting the MSA mix displayed a slight increase in strain capacity when compared to the MR mix, while the MSR mix displayed a slight decrease in strain capacity during this corresponding setting phase.

7.5.3 Young's modulus

The Young's modulus versus age of the MR, MSA and MSR concrete mixes are shown in Figure 7.17. For the MSA mix the Young's modulus of the specimens was initially very low and gradually increased with time to the point of initial set. From after the initial setting time, 4h, to the point of final setting, 5h, the Young's modulus was slightly lower than that of the
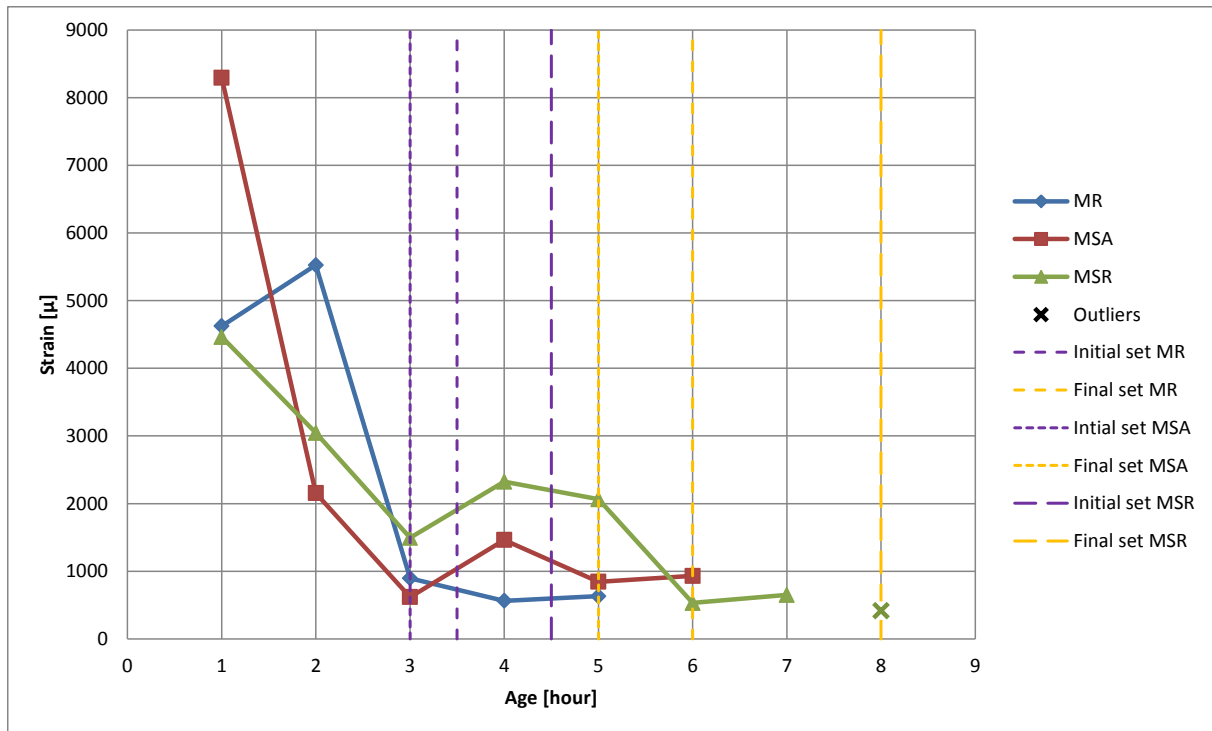
Figure 7.16: Strain capacity vs. age of MR, MSA and MSR mixes

corresponding MR specimens. However, after initial setting has occurred, the Young's modulus still increased rapidly. From the results presented it is concluded that the use of an accelerating admixture decreases the Young's modulus of early age concrete. The Young's modulus of the MSR specimens was found to be negligible up to an age of 5 hour, which unexpectedly was after the initial setting time. From an age of 6 hours its Young's modulus rapidly increased to 30.27 MPa at an age of 7 hours, and 293.19 MPa at an age of 8 hours, which was considered to be an outlier, as discussed in Section 7.1. The results indicate that the use of a retarding admixture decreases the Young's modulus of an early age concrete, when compared to the MR mix. Taking into account that the MSA and MSR mixes had the highest slump values and was the least cohesive of all the mixes, it provides an explanation for the reduction in the early age Young's modulus of these specimens.

The Young's modulus versus tensile strength of the MR, MSA and MSR concrete mixes are shown in Figure 7.18. All mixes displayed a nearly linear relationship between Young's modulus and tensile strength if the 8h MSR outlier is ignored.

7.5.4 Concluding remarks for Objective 4

It was found that the addition of an accelerator slightly increases the development of the ascending tensile properties of early age concrete, while a retarder decreased it, as would be expected. However, the initial and final setting times does not necessarily represent a

113
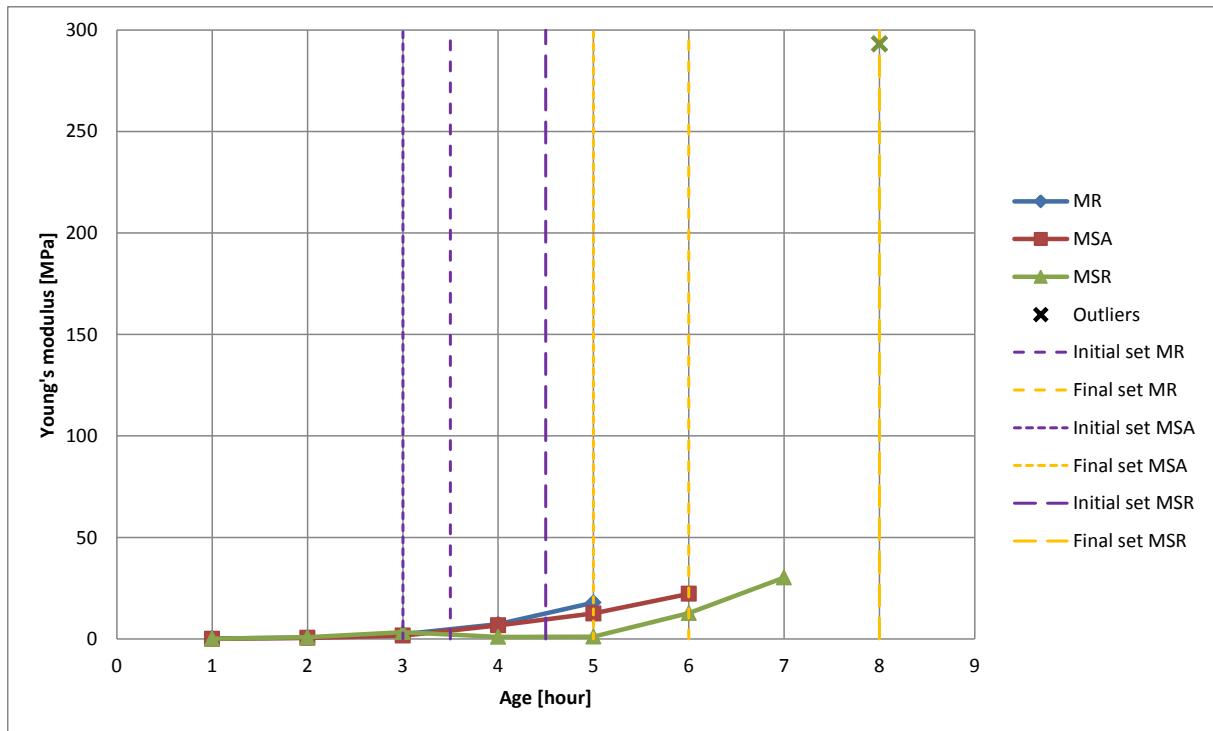
Figure 7.17: Young's modulus vs. age of MR, MSA and MSR mixes
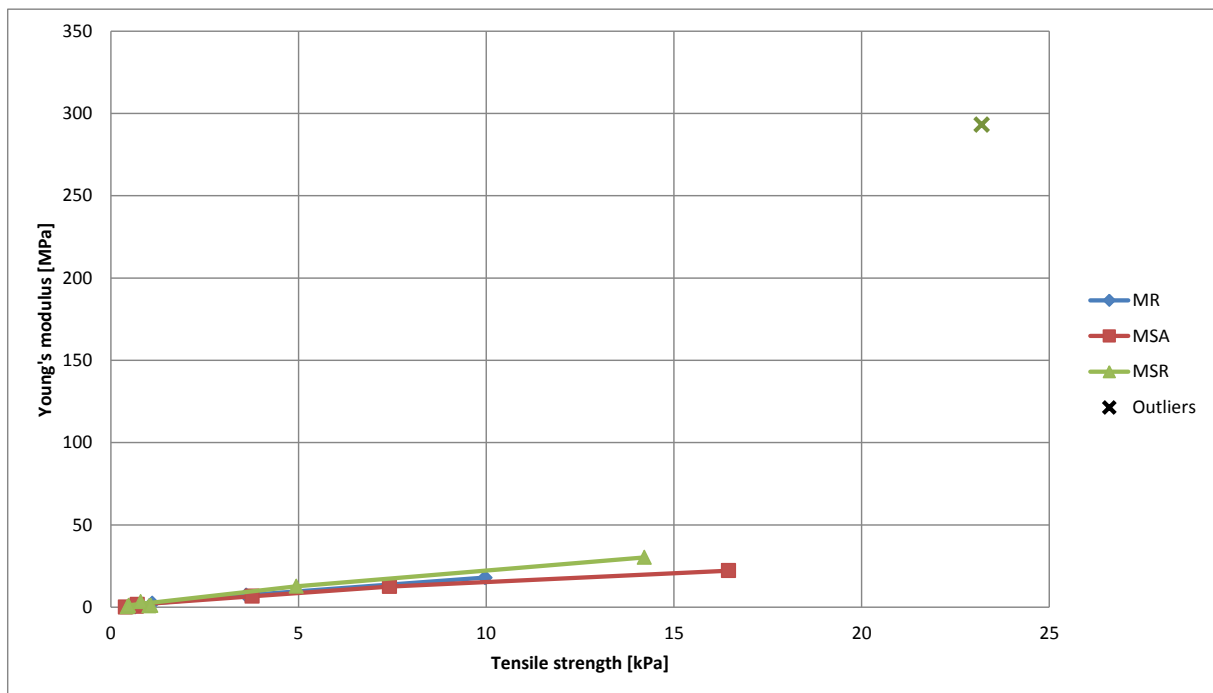
Figure 7.18: Young's modulus vs. tensile strength of MR, MSA and MSR mixes

specific tensile strength for mixes that utilised admixtures to alter their setting times. No clear correlation between setting time altering admixtures and strain capacity could be identified during the first three hours of testing. The MSR mix displayed significantly more strain capacity when compared to the MR mix around the initial setting time. This could be a

possible explanation for the reduction in PShC severity observed by Combrinck & Boshoff (2012) when comparing the induced PShC of a retarded mix with that of a reference mix. With regrads to Young's modulus, it was found that both the addition of an accelerator and retarder led to a reduction in Young's moduls for early age concrete when compared to the MR mix.

7.6   Concluding summary

This chapter describes the ascending portion of the stress-strain behaviour of early age concrete, which includes the section from the onset of a tensile force transferred through the specimen up to the point of the peak stress. First the data processing methodology is discussed. Next, the outliers with regards to Young's modulus and strain capacity are described. Finally, the results are presented and discussed according to the objectives of the study: the effect of coarse aggregate size, the effect of the addition of microfibres and the effect of setting time altering admixtures on the tensile properties of early age concrete. The next chapter describes the descending portion of the stress-strain behaviour of early age concrete, in other words, the post-cracking behaviour of early age concrete.

8. Experimental results and discussion: Descending stress-strain section

This chapter describes the descending portion of the stress-strain behaviour of early age concrete from the point of the peak stress, where the tensile strength of the specimen has been exceeded and cracking initiates, to the point of approximate full crack separation. First the data processing methodology is discussed as well as reasons for the occurrence of outliers. Nex,t the results are presented according to the objectives of this study: the effect of coarse aggregate size, the effect of the addition of microfibres and the effect of setting time altering admixtures on the tensile properties of early age concrete.

8.1   Data processing methodology

The fracture energy of specimens is defined as discussed in Section 2.2.2 as the energy required to create and fully break a unit surface of crack area. It is represented by the area enclosed by the stress-crack opening curve, or assuming that all specimens exhibit linear elastic material behaviour, the area indicated on the stress-displacement curve in Figure 8.1. As is shown in Appendix D, the stress-strain curves of all the specimens tested after the initial setting time has occurred, except that of MF1.8 specimens, converged to a resistance of approximately zero Newton at 30000 μ. This translates to a displacement of 3 mm over the gauge length of the concrete specimens and as the closure stresses deceased to approximately zero Newton after this displacement, it was chosen as the critical crack opening displacement. For the specimens that had reached the initial setting time, this displacement signified the formation of a discrete open crack. Simpson's rule was used to numerically integrate the area under the stress-displacement curve from the displacement point at peak stress where crack initiation occurs, δ_c, to the zero force transfer displacement, δ_0, of 3 mm. When the fracture energy obtained from the numerical integration method was compared to the fracture energy of the MR test specimens determined by means of hand calculations, a difference of less than 9% was attained. This confirms the validity of this numerical integration method.

In order to gain a better understanding of the brittleness or ductility of the early age concrete specimens, the characteristic length, l_{ch}, was also determined according to Equation 2.7. Characteristic length is a function of the ascending properties of tensile strength and Young's modulus as well as fracture energy. For this reason, the outliers in terms of Young's modulus, as described in Section 7.2, also resulted in outliers with regards to characteristic length. The smaller a materials characteristic length, the more brittle the material.
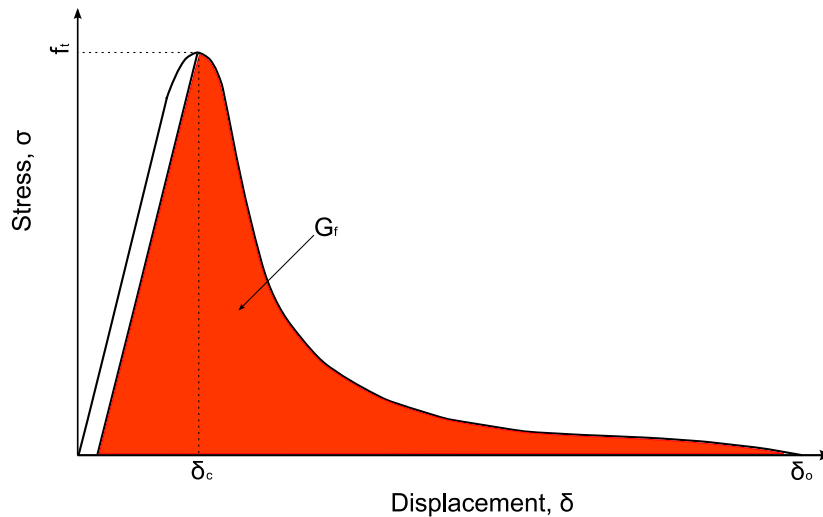
Figure 8.1: Determination of Fracture energy from a stress-displacement curve

The descending stress–strain tensile properties of early age concrete for all 44 test specimens are presented in Table E.2 in Appendix E.

8.2 Effect of skewing on descending stress-strain behaviour

Section 4.1 states that for determining the ascending portion of the stress-strain behaviour of early age concrete, pin-fixed loading platens are preferred. This avoids the effects of secondary flexural stresses and the development on bending moments, giving rise to significant stress evaluation errors. However, to effectively determine the fracture energy of concrete specimen according to the fictitious crack model it is required that crack separation over the entire concrete specimen is achieved almost simultaneously, as illustrated by Figure 4.5. However, as mentioned, in practice this seldom occurs as specimens unavoidably flex sideways and deform non-uniformly, resulting in the undesired propagation of cracks across the specimen cross-section (Bazant, 2002). During testing, the heterogeneous nature of concrete causes cracking to typically propagate or initiate from the weaker side of the specimen cross-section. As a result the specimen becomes eccentrically loaded. When fixed loading platens are used, a counteracting bending moment develops within the specimen resulting in the formation of a "bump" in the descending stress-displacement curve. In the case of freely rotating loading platens, no counteracting bending moment can develop and the result is a smooth, rapidly descending stress-displacement curve. This results in an underestimation in the fracture energy of the concrete specimen. The extent of the underestimation depends on the rotational stiffness of the loading platens.

As the aim of this study was to determine both the pre- and post-peak tensile properties of early age concrete, a compromise in terms of the boundary conditions of the loading structures was made. The boundary conditions chosen could not be considered completely

117

pinned or fixed. However, during testing this resulted in skewing of several test specimens. An extreme example of this is illustrated in Figure 8.2, which shows the displacement over time as measured by the on mould LVDT's, spaced 270 mm apart, during the testing of the 4h MR test specimen.
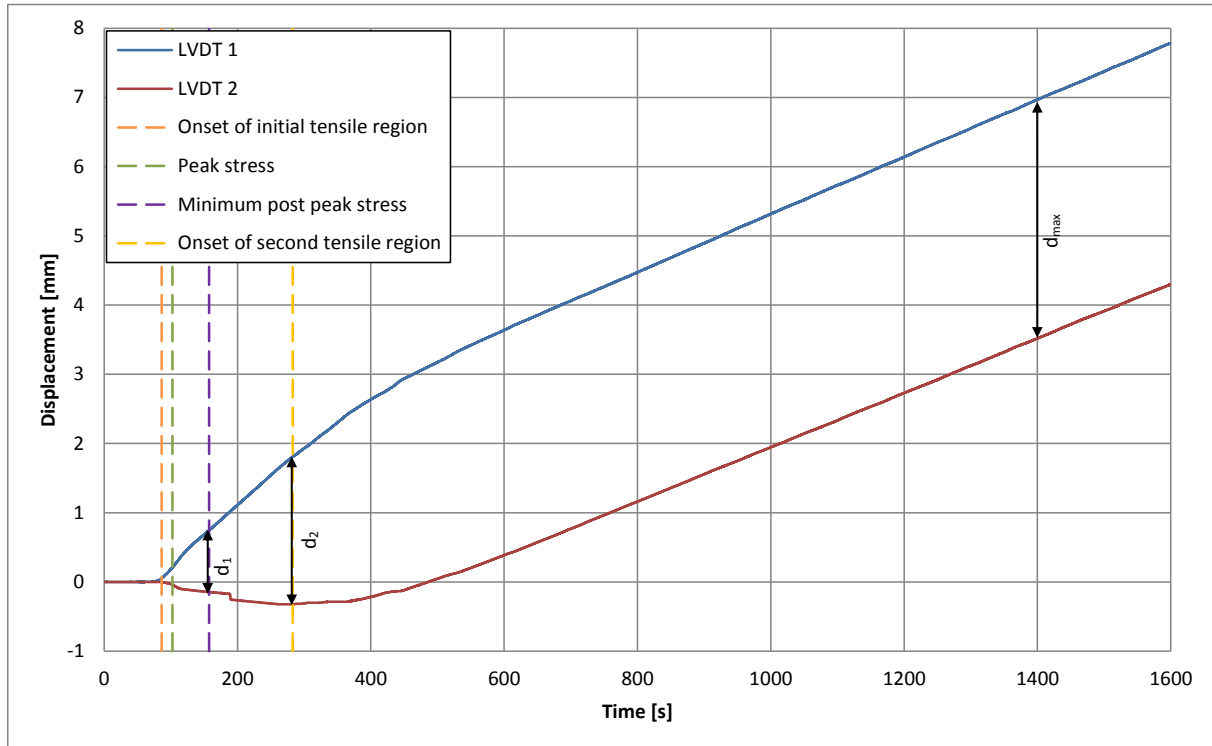
Figure 8.2: Displacement over time of the on mould LVDT's during the 4h MR test

Figure 8.3 shows the tensile stress over time as measured for the 4h MR test specimen. The time of the onset of the initial tensile region, the peak stress, minimum post-peak stress and the onset of the second tensile stress region are indicated on both figures. Although the average displacement of the specimen remained constant and positive throughout the test, this was not the case for the individual points on the mould that LVDT 1 and LVDT 2 measured during the displacement period. From the onset of the initial tensile region, LVDT 2 indicated a displacement in the direction opposite to the application of the tensile force, a clear indication that the sides of the mould did not open at the same rate. This skewing continued throughout the course of the test with the displacement difference between LVDT 1 and LVDT 2 continually increasing until full separation of the specimen had occurred. This took place at approximately 1000 seconds and after this point the displacement difference remained constant. The displacement difference at the minimum post-peak stress, denoted by d_1, was determined to be 0.8 mm, while the displacement difference at the onset of the

second tensile region, indicated by d_2, was approximately 2 mm. The maximum displacement difference, d_{max}, was determined to be 3.5 mm.
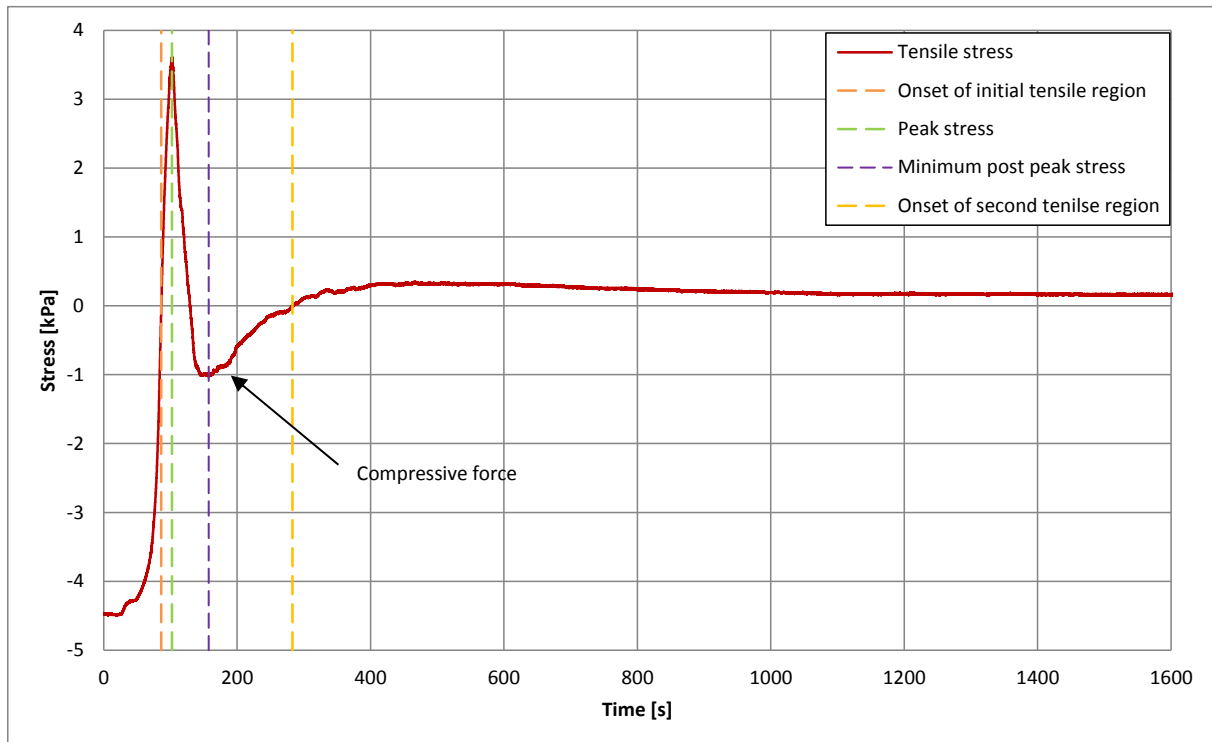
Figure 8.3: Tensile stress over time of the MR 4h specimen

As indicated in Figure 8.3, there is a significant region of the post-peak stress-time curve in which a compression force was measured by the load cell. This is a result of the excessive skewing of the specimen and mould which caused the compression of a portion of the specimen's cross-section, leading to the development of a measured compressive force. These negative regions were not taken into account when determining the fracture energy of test specimens.

As could be expected, when skewing occurred during testing it led to the underestimation of fracture energy, and subsequently also characteristic length. The behaviour shown by the 4h MR test specimen was not an isolated case. Similar behaviour was displayed by the following specimens, as can be seen by the negative stress indicated on their stress-strain curves in Appendix D:

- 4h MR
- 6h MR
- 5h MSA
- 6h MSR
- 3h MSA

119

The occurrence of skewing was not always as severe as that of the MR 4h specimen test and the negative displacement of one of the on mould LVDT's or the measurement of a compressive force by the load cell mostly did not occurred. Other specimens that underwent significant skewing during testing that influenced their post-peak stress-strain behaviour without displaying a compressive stress, and also shown in Appendix D, are:

- 5h MA9
- 3h MA19
- 6h MA19
- 4h MF1.8
- 6h MF1.8
- 4h MF0.6

A good example of skewing that significantly decreased the expected fracture energy of a sample is the 6h MF1.8 test specimen. The 5h MF1.8 test specimen displayed virtually no skewing and an extremely high fracture energy of 81.7 J/m^2. With the near linear relationship between fracture energy and tensile strength for specimens which have reached the initial setting time, as established in Section 8, it would be expected that the 6h MF1.8 test specimen, with increased strength and interfacial shear bond stress between its concrete paste and fibres, would have an fracture energy of approximately 110.3 J/m^2, as determined by means of linear regression. As a result of the moderate skewing, the fracture energy was instead determined to be 83.3 J/m^2. For this reason the effect of skewing should be taken into account when interpreting the results of the descending stress-strain properties of early age concrete.

8.3   Experimental results for Objective 2: Effect of coarse aggregate size on the tensile properties of fresh concrete

This section graphically presents the descending tensile properties for the MR, MA9 and MA19 concrete mixes.

8.3.1 Fracture energy

The fracture energy versus age of the MR, MA9 and MA19 concrete mixes are shown in Figure 8.4. All specimens displayed low fracture energy values before the initial setting time had occurred. However, after initial setting had occurred the fracture energy gradually increased with age. As described in Section 8.2, the values of the 4h and 6h MR test specimens, the 5h MA9 test specimen and the 3h and 6h MA19 test specimens were underestimated due to the skewing of moulds during testing. Taking this into account, it is evident that for specimens tested between the initial and final setting times, an increase in

coarse aggregate size resulted in an increase in the fracture energy of the early age concrete specimens. The explanation for this is that larger aggregates increase the size of the bridging zone, which is the weak interface between aggregates and cement paste after microcracking has occurred in the fracture process zone (FPZ), and this allows a greater degree of interlocking and toughening, as shown in Figure 2.16.

The fracture energy versus tensile strength of the MR, MA9 and MA19 concrete mixes are shown in Figure 8.5. Taking the effect of skewing into account and ignoring the specimens which can still be considered fresh concrete, and consequently have not reached the initial setting time, it is tentatively proposed that there exists a near linear relationship between fracture energy and tensile strength for the specimens who have surpassed the initial setting time. From the results presented it is tentatively suggested that as the aggregate size increases, so does the gradient of the fracture energy versus tensile strength curve.

8.3.2 Characteristic length

The characteristic length versus age of the MR, MA9 and MA19 concrete mixes are shown in Figure 8.6. The characteristic length typically increased with time to a maximum just prior to initial setting, after which it decreases with time as the degree of hydration and brittleness of the concrete increases. Taking into account the effect of skewing on the 4h MR test specimen, the 5h MA9 test specimen as well as the 3h and 6h MA19 test specimens, it is evident that an increase in coarse aggregate size leads to an increase in characteristic length and consequently ductility, once the initial setting time has occurred. As an increase in coarse aggregate size increases the length of the bridging zone and therefore also the FPZ, and keeping in mind that characteristic length is also representative of FPZ length, the characteristic length results agree with this logic. Karihaloo (1995) determined a similar trend for mature concrete, as shown in Table 2.2.

8.3.3 Concluding remarks for Objective 2

With an increase in aggregate size, the fracture energy of early age concrete specimens between the initial and final setting times increased as well. The increased bridging zone as a result of the larger aggregate is thought to be responsible for this increase in fracture energy. A near linear relationship between fracture energy and tensile strength is observed for the specimens between the initial and final setting times. It seems as though an increase in aggregate size increases the gradient of the fracture energy versus tensile strength curve. An increase in coarse aggregate size also leads to an increase in characteristic length, and consequently ductility. This is also a result of the increased bridging zone of the FPZ associated with an increase in coarse aggregate size and is in agreement with the trend for mature concrete (Karihaloo, 1995).
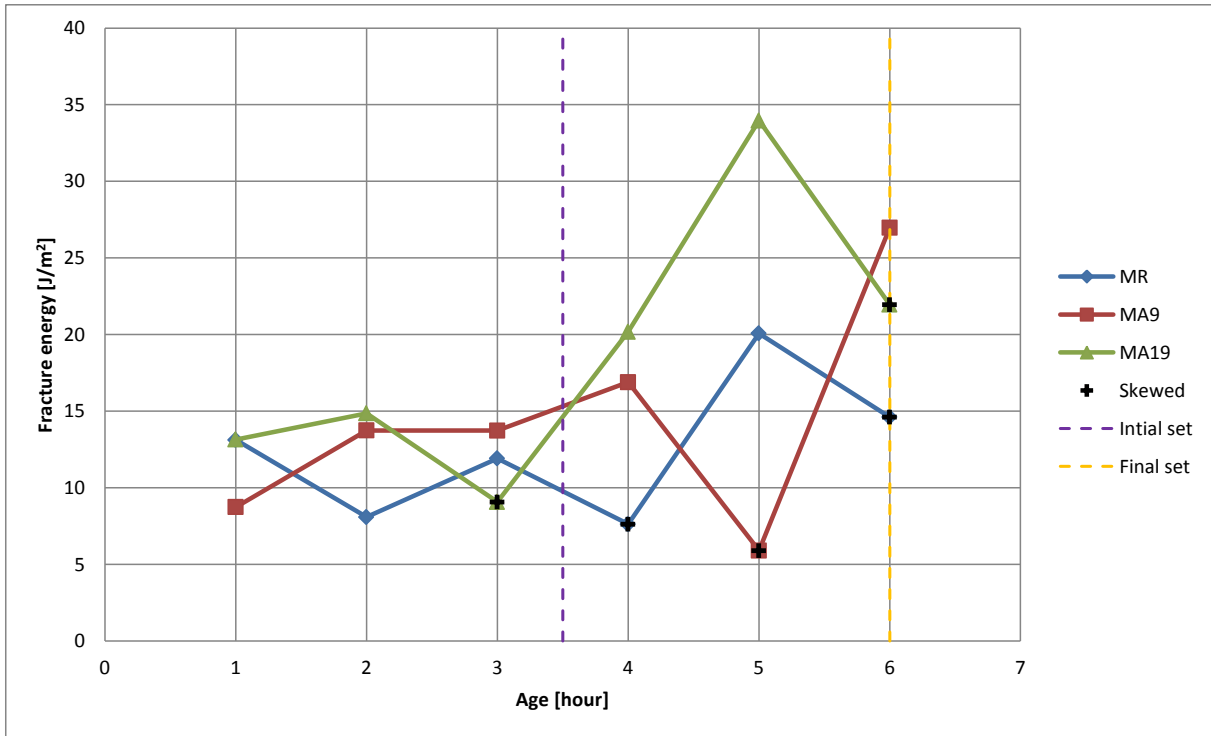
Figure 8.4: Fracture energy vs. age of MR, MA9 and MA19 mixes
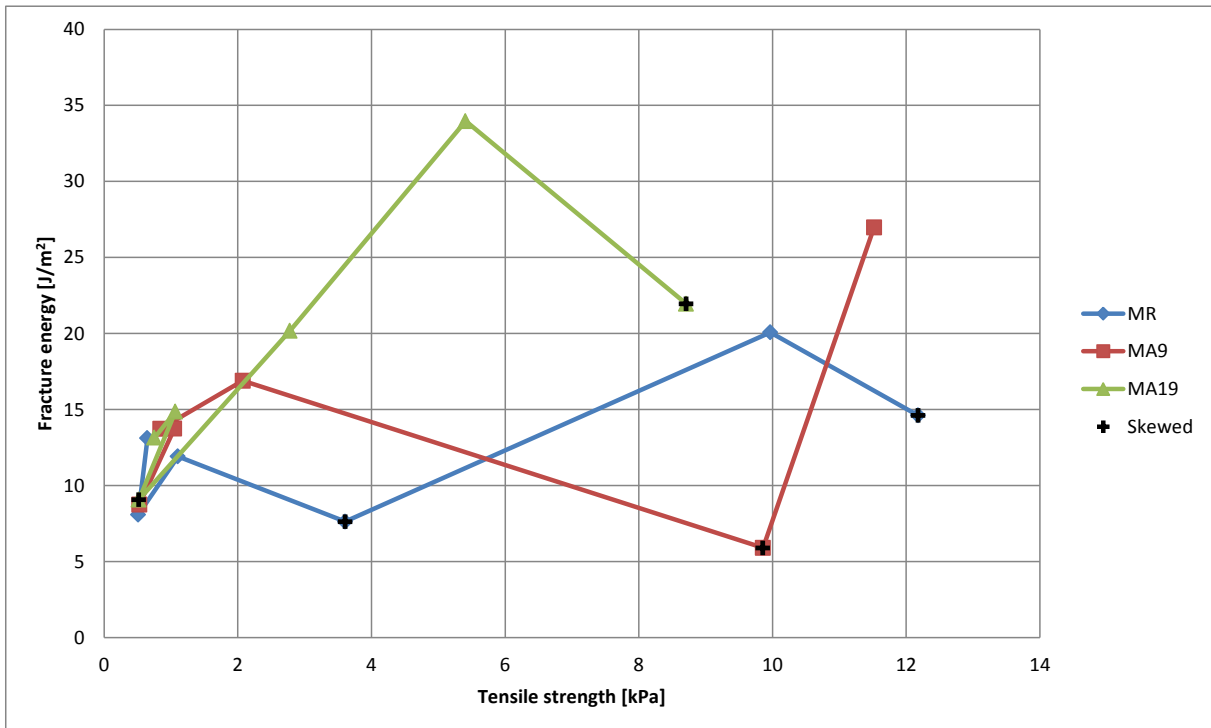
Figure 8.5: Fracture energy vs tensile strength of MR, MA9 and MA19 mixes

122
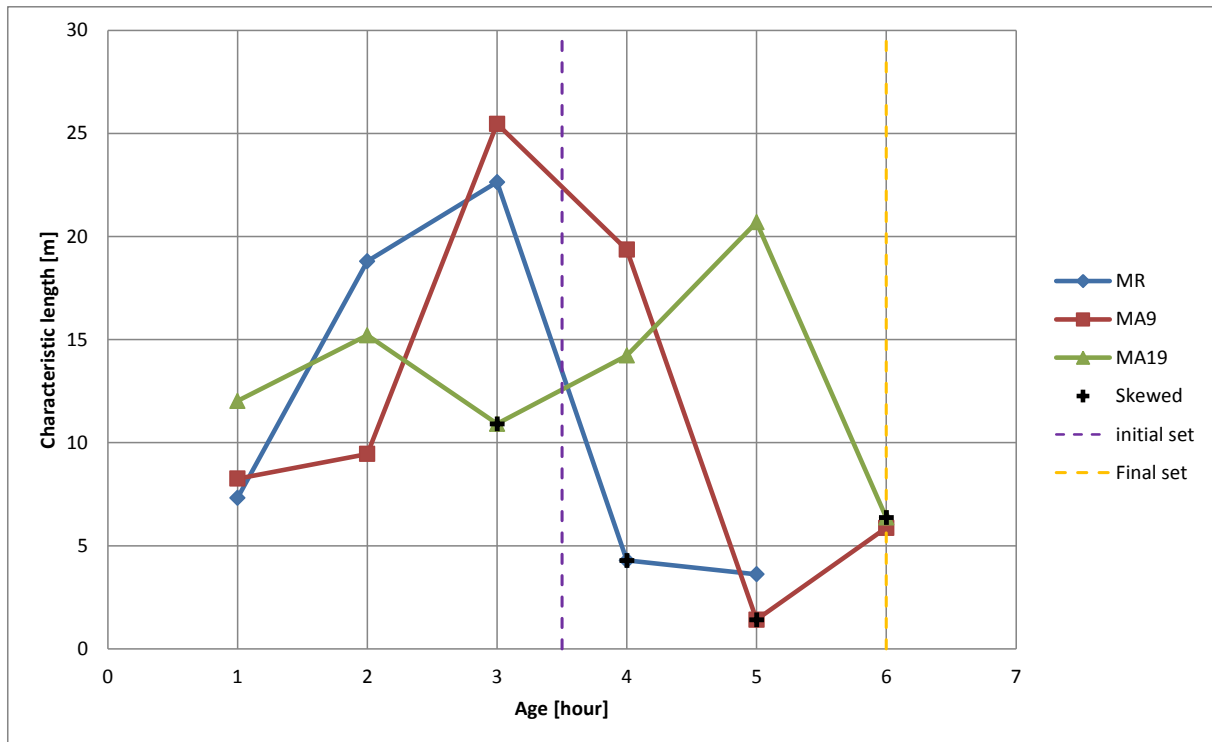
Figure 8.6: Characteristic length vs. age of MR, MA9 and MA19 mixes

8.4 Experimental results for Objective 3: Effect of the addition of microfibres on the tensile properties of fresh concrete

This section graphically presents the descending tensile properties for the MR, MF0.6 and MF1.8 concrete mixes. The addition of fibres has a significant effect on the post-cracking behaviour of early age concrete. The deformed specimens after 6.5 mm displacement over the 100 mm gauge length is indicated in Figure 8.7 for the 1h and 2h MF1.8 test specimens, and Figure 8.8 for the 5h and 6h MF1.8 test specimens.

The fresh concrete specimens shown in Figure 8.7 display a multiple crack pattern, similar to the typical fresh concrete deformation pattern to be described in Section 9.1. However, after the initial setting time, deformation localised in the form of a single discrete crack with fibres bridging over the crack plane, as shown in Figure 8.8. This added significant post-cracking tensile strength to the early age specimens, as is discussed in this section.

8.4.1 Fracture energy

The fracture energy versus age of the MR, MF0.6 and MF1.8 concrete mixes are shown in Figure 8.9. For the MF0.6 mix the 4h test specimen skewed significantly while for the MF1.8 mix both the 4h and 6h test specimen showed skewing, which led to an underestimation in the fracture energy of these specimens. From the results presented in Figure 8.9 it is clear that the MF0.6 test specimens have approximately twice the fracture energy of the MR test

123
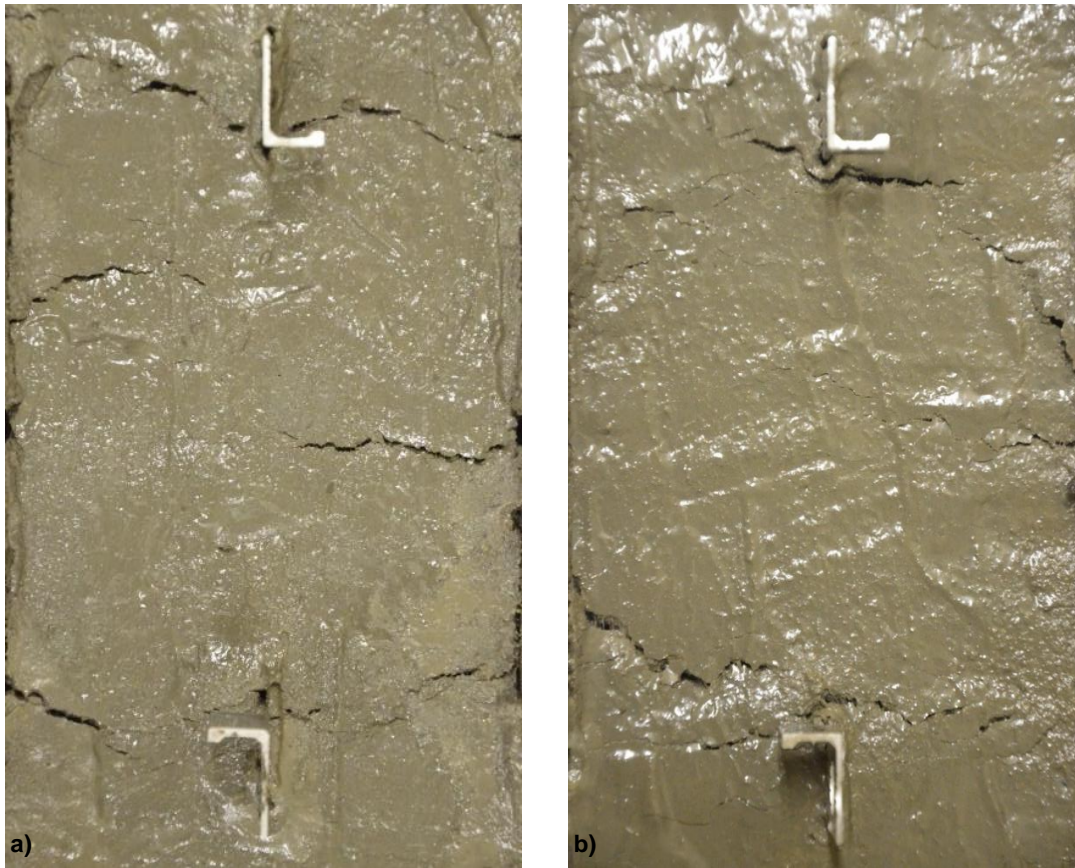
Figure 8.7: a) 1h MF0.6 test specimen and b) 2h MF1.8 test specimen
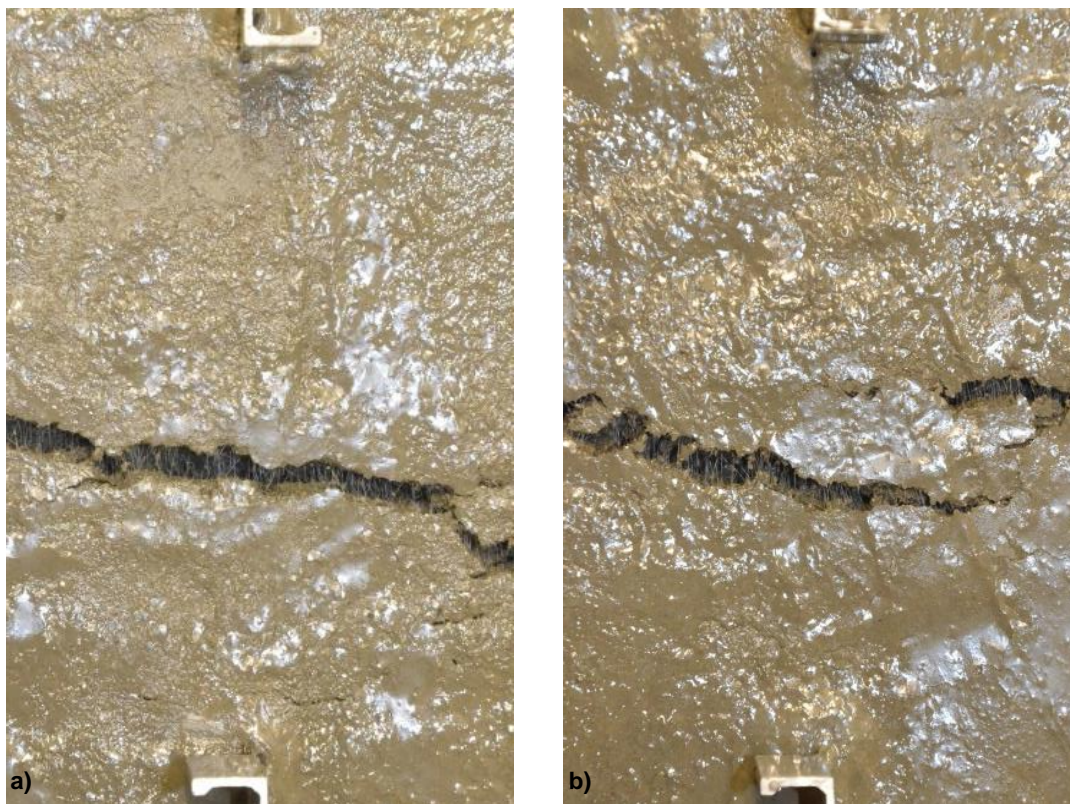
Figure 8.8: a) 5h MF1.8 test specimen and b) 6h MF1.8 test specimen

124

specimens at the same age. The MF1.8 test specimens have a fracture energy of approximately four times that of the corresponding MR test specimens, with the 1h test specimens being the exception. It can clearly be seen that the addition of microfibres leads to an increase in the fracture energy of an early age concrete specimen. The reason for this is that as hydration continues the interfacial bond strength between the concrete paste and fibres increase and therefore also the capacity of the bridging zone of the FPZ to transfer a tensile stress, leading to an increase in the fracture energy of the early age low volume fibre reinforces concrete (LV-FRC) specimens. The increased fracture energy measured for the fresh concrete specimens is believed to be a result of the increased stiffness and cohesion of LV-FRC mixes, which is also indicated by the lower slump values of the MF0.6 and MF1.8 mixes, rather than the interfacial bond strength that had developed before the initial setting time.

The fracture energy versus tensile strength of the MR, MF0.6 and MF1.8 concrete mixes are shown in Figure 8.10. Taking the effect of skewing into account and ignoring the specimens which can still be considered fresh concrete, it is apparent that a near linear relationship between fracture energy and tensile strength exists for the specimens which have surpassed the initial setting time. From the results presented it can be deduced that with an addition of microfibres to a concrete mix, an increase in the gradient of the fracture energy versus strength curve can be expected.
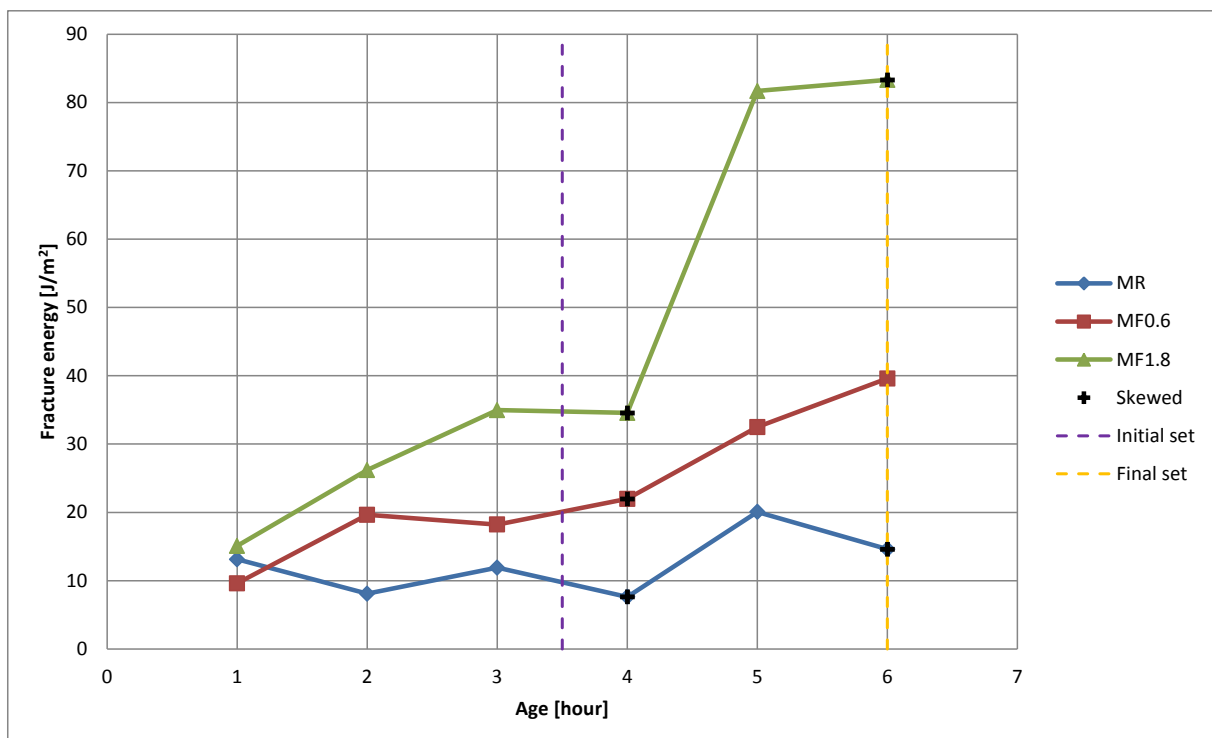
Figure 8.9: Fracture energy vs. age of MR, MF0.6 and MF1.8 mixes

125
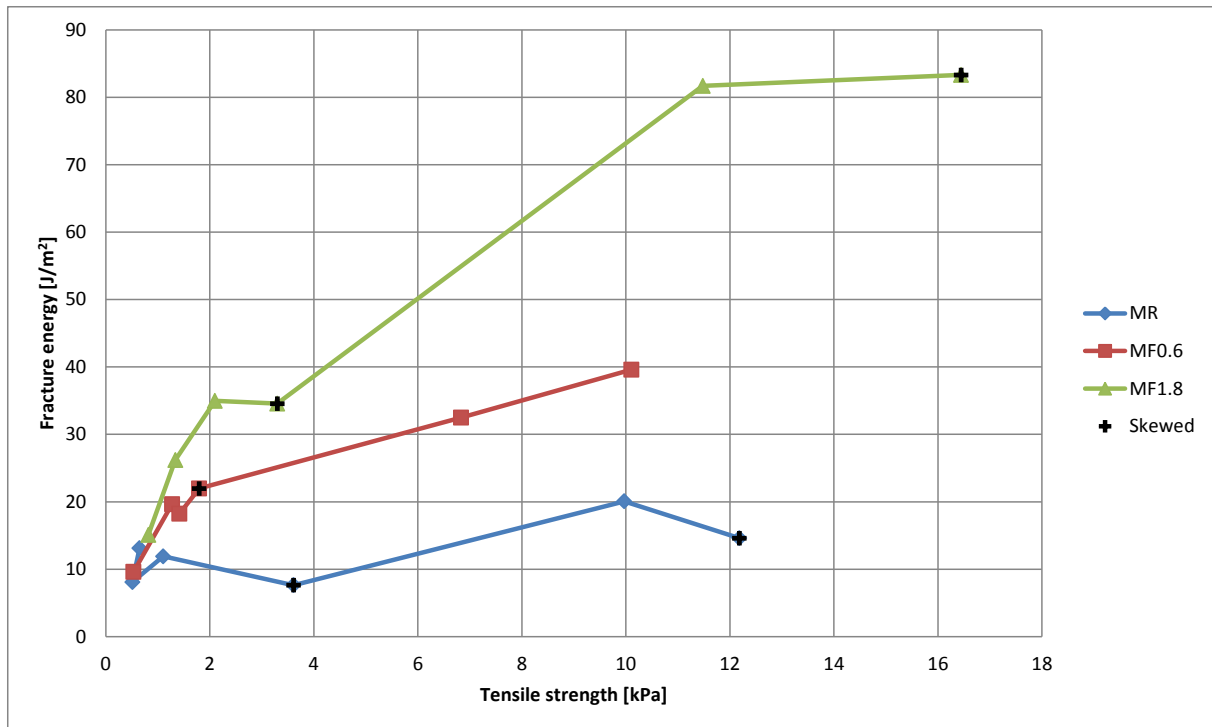
Figure 8.10: Fracture energy vs tensile strength of MR, MF0.6 and MF1.8 mixes

8.4.2 Characteristic length

The characteristic length versus age of the MR, MF0.6 and MF1.8 concrete mixes are shown in Figure 8.11. With regards to Young's modulus, that plays a significant role in the determination of characteristic length, the outliers, as described in Section 7.2, were the 5h MF1.8 test specimen, with an extremely high value, and the 6h MF0.6 test specimen ,with an extremely low value. If these outliers are ignored, it is clear that the addition of microfibres significantly increases the characteristic length and consequently the ductility of early age concrete between the initial and final setting times, while not having a significant effect on the characteristic length of fresh concrete. Once again this is a result of the significant interfacial shear bond strength between the concrete paste and fibres that develops after the initial setting time. Similar to the use of larger coarse aggregate, the addition of microfibres increase the length of the bridging zone of the FPZ and consequently also the characteristic length as it is indicative of the FPZ length. The increased length of the FPZ can easily be identified in Figure 8.8.

8.4.3 Concluding remarks for Objective 3

The addition of microfibres to concrete leads to a significant increase in the fracture energy of early age concrete specimens. For fresh concrete specimens this is believed to be as a result of the increased cohesion and stiffness associated with the addition of fibres. However, after the initial setting time has occurred the interfacial bond strength between the concrete

paste and fibres increases significantly, therefore also the capacity of the fibres to transfer a tensile load across the crack plane. A near linear relationship between fracture energy and tensile strength exists for the specimens that have surpassed the initial setting time. It was also found that the addition of microfibres increases the gradient of the fracture energy versus strength curve. The addition of microfibres also significantly increases the characteristic length and consequently the ductility of early age concrete after the initial setting time has occurred.
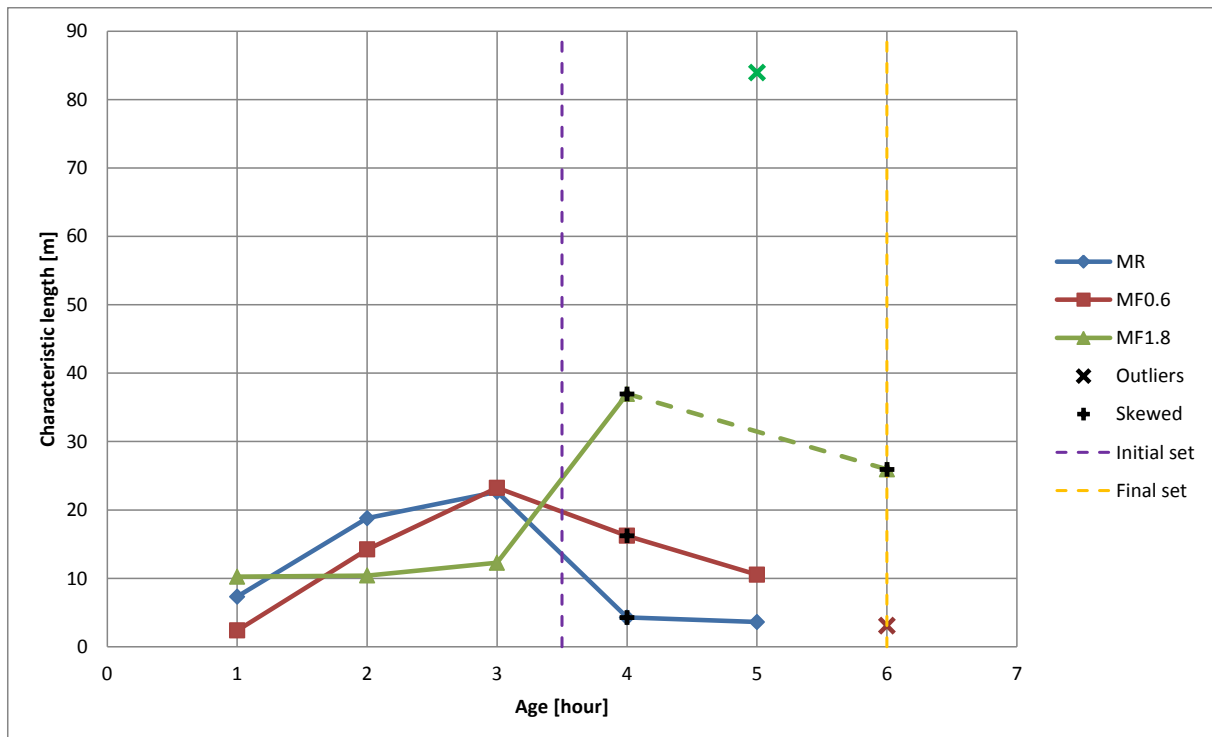
Figure 8.11: Characteristic length vs. age of MR, MF0.6 and MF1.8 mixes

8.5   Experimental results for Objective 4: Effect of setting time altering admixtures on the tensile properties of fresh concrete

This section graphically presents the descending tensile properties for the MR, MSA and MSR concrete mixes.

8.5.1   Fracture energy

The fracture energy versus age of the MR, MSA and MSR concrete mixes are shown in Figure 8.12. For the 3h and 5h MSA test specimens as well as the 6h MSR test specimen significant skewing occurred during testing and these tests consequently provided lower than expected fracture energies. All specimens exhibited low fracture energy values before the initial setting time had occurred. However, after initial setting had occurred the fracture energy values gradually increased with age. Both the MSA and MSR mixes displayed a rapid

increase in fracture energy at later ages, with the 6h MSA specimen showing a fracture energy of 35.71 J/m^2 and the 8h MSR a fracture energy of 61.74 J/m^2. When comparing these results to the MR mix and ignoring the test specimens that skewed, it can be concluded that this accelerator increases the fracture energy of early age concrete after the initial setting time had occurred, while the retarder significantly reduced the fracture energy since it delays setting and therefore also the formation of a FPZ.

The fracture energy versus tensile strength of the MR, MSA and MSR concrete mixes are shown in Figure 8.13. Taking the effect of skewing into account and ignoring the specimens which have not yet reached the initial setting time, a near linear relationship exists between the specimens which have already reached initial setting. The high fracture energies of the 5h MSA and MSR 6h test specimens are a result of the high tensile strength of these specimens, as described in Section 2.2.2. No physical toughening mechanism such as microfibres or larger coarse aggregate was present in these mixes that could account for the increased fracture energies of these specimens. The addition of setting time altering admixtures therefore has no significant effect on the gradient of the fracture energy versus tensile strength curves.
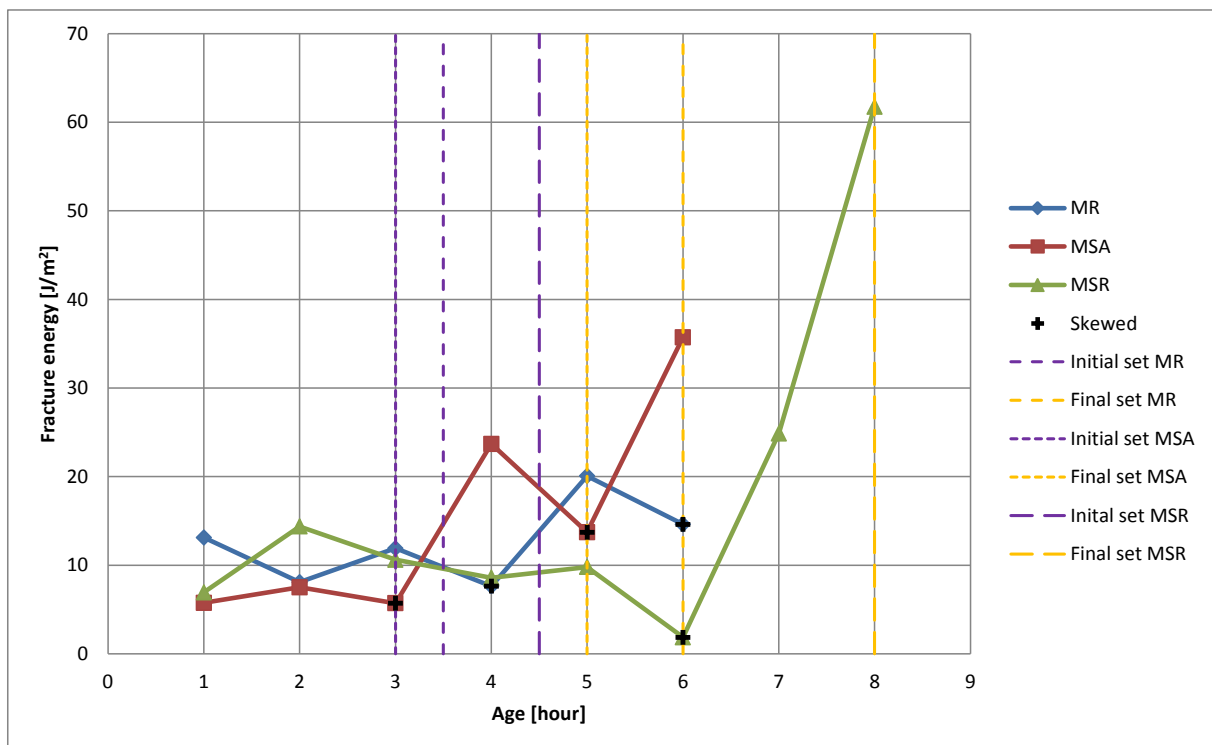
Figure 8.12: Fracture energy vs. age of MR, MSA and MSR mixes

8.5.2 Characteristic length

The characteristic length versus age of the MR, MSA and MSR concrete mixes are shown in Figure 8.14. The MSA test specimens demonstrated similar results as the MR test

specimens with regards to characteristic length. The characteristic length increased with time to a maximum at the point of initial set and then gradually decreased to a minimum at an age of 6 hours. The 3h and 5h MSR test specimens proved to be semi-outlier due to unusually high Young's modulus values and unusually low tensile strengths for fresh concrete specimens. This combination resulted in unrealistic characteristic length values. As discussed in Section 7.1, the 6h MSR specimen is seen as an outlier with regards to Young's modulus, also leading to an unrealistic characteristic length value for this specimen. Together with the skewing of the MSR 5h specimen, it is very difficult to draw a clear conclusion on the effect of the retarder on the characteristic length of early age concrete specimens. However, it is expected to display similar behaviour to that of the MR mix with the major difference being that the delay in the setting time of the specimens causes the characteristic length parameters to develop at a slower rate.
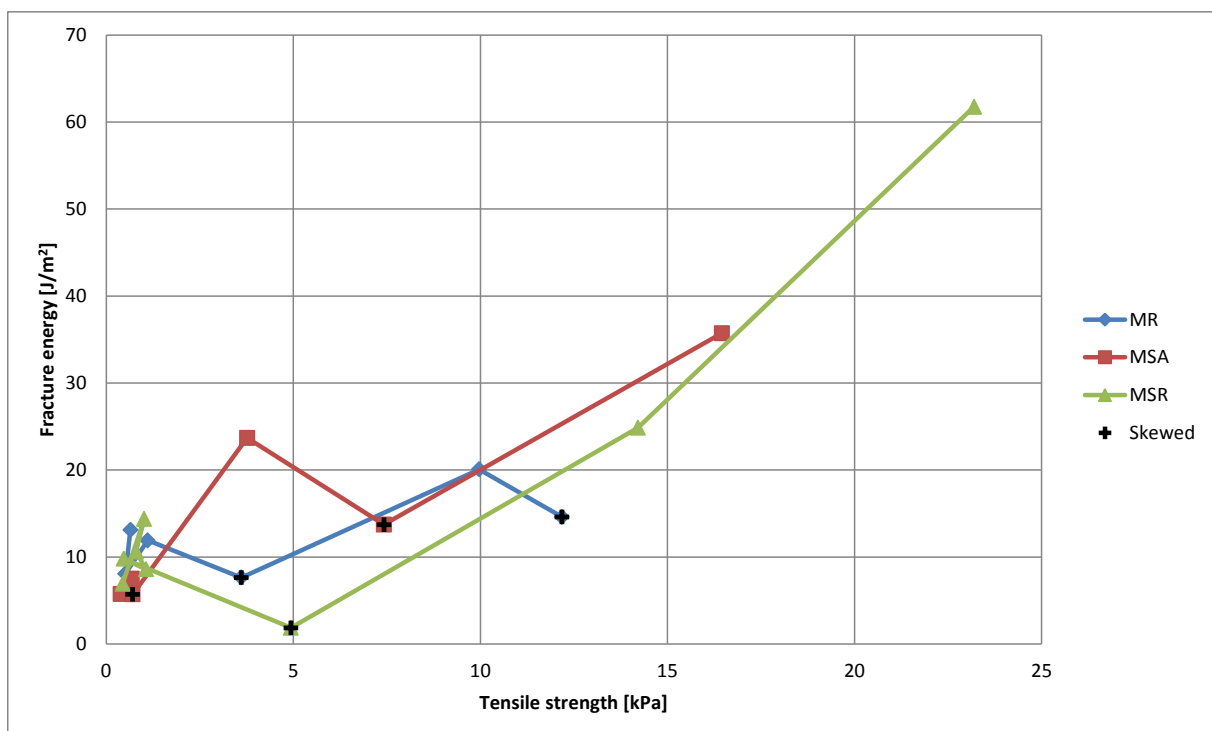
Figure 8.13: Fracture energy vs tensile strength of MR, MSA and MSR mixes

8.5.3 Concluding remarks for Objective 4

The addition of this accelerator to a concrete leads to an increase in the fracture energy of early age concrete after the initial setting time. Contrastingly the retarder used in this study significantly reduced the fracture energy of early age concrete specimens since it delays setting and therefore also the formation of a FPZ. A near linear relationship between fracture energy and tensile strength is observed for all test specimens. The addition of a setting time altering admixtures does not introduce additional physical toughening mechanisms such as

fibres or larger coarse aggregate and therefore has no effect on the gradient of the fracture energy versus tensile strength curve. The MSA test specimens displayed similar results as the MR test specimens with regards to characteristic length. No clear conclusion on the effect of the retarder on the characteristic length of early age concrete could be drawn. However, it is believed to display similar behaviour to the MR mix with the major difference being that the delayed setting times would cause the characteristic length of specimens to develop at a slower rate.
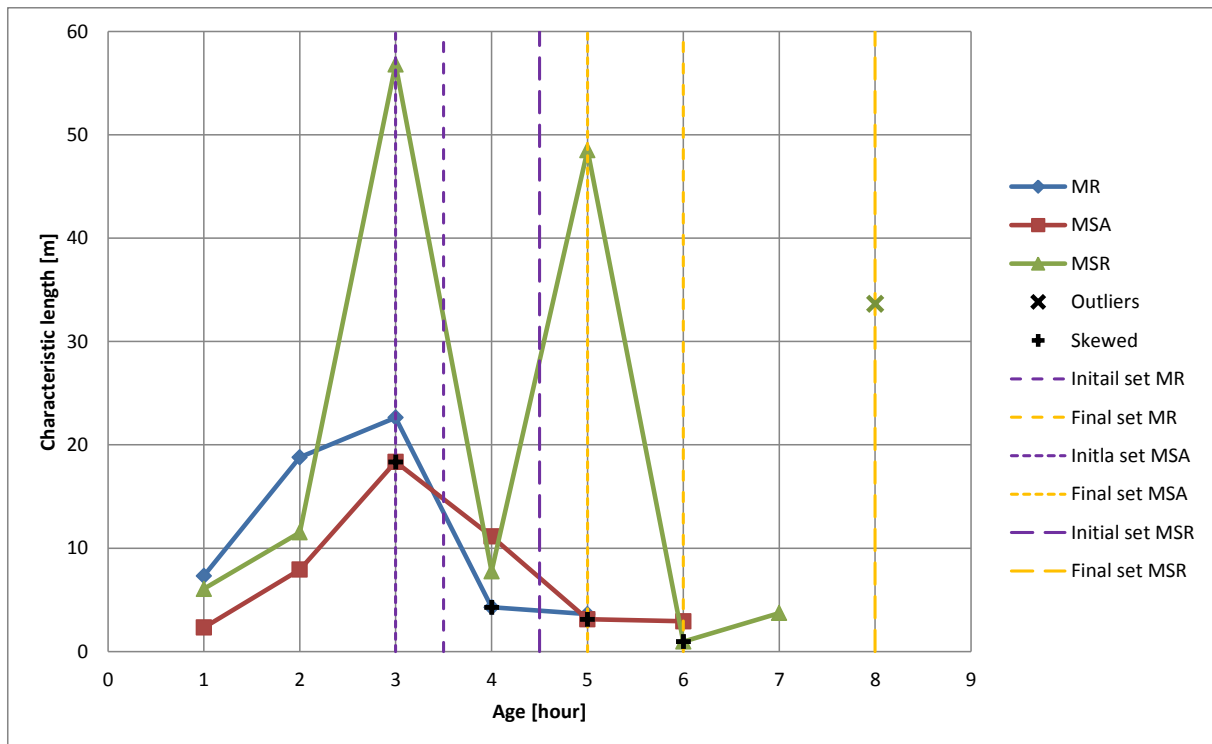
**Figure 8.14: Characteristic length vs. age of MR, MSA and MSR mixes**

8.6   Concluding summary

This chapter describes the descending portion of the stress-strain behaviour of early age concrete from the point of the peak stress, where the tensile strength of the specimen has been exceeded and cracking initiates, to the point of approximate full crack separation. Firstly, the data processing methodology is discussed. Next, the effect of skewing on the ascending stress-strain behaviour of early age concrete is discussed. Finally, the results are presented and discussed according to the objectives of the study: the effect of coarse aggregate size, the effect of the addition of microfibres and the effect of setting time altering admixtures on the tensile properties of early age concrete. The next chapter discusses the results presented in the previous as well as this chapter and focusses on cracking and material behaviour. A link between the result of this study and PShC is also made.

9. Cracking, material behaviour and the link with plastic shrinkage cracking

This chapter discusses the results presented in the previous three chapters with regards to cracking, material behaviour and the link between these results and plastic shrinkage cracking (PShC). Firstly, the cracking behaviour and state of setting of the specimens tested before and after the initial setting time is described. Next, the interpretation of the experimental results for the fresh concrete specimens, which are the specimens that have not yet reached the initial setting time, are discussed. The tensile properties of conventional early age concrete are then presented. Finally, results from a study on PShC are used to show the link between PShC and the results of this study. This not only validates the results of this study, but also indicates the great potential of LV-FRC to reduce the occurrence of PShC.

9.1 Cracking behaviour and state of setting

Images of the 1 to 6 hour test specimens of the MA9 mix are shown in Figure 9.1 to 9.6. These figures illustrate the specimens after the completion of a 6.5 mm displacement measured over the concrete gauge length during the tensile testing period. To provide a physical representation of the state of setting and the workability of the specimens, a tennis ball size sphere was moulded by hand for each early age concrete specimens directly after the completion of each test. This sphere is also indicated in the figures.

From the figures it is clear that for all tests conducted before the initial setting time has occurred, in this case the 1h, 2h and 3h test, multiple cracking and visible strain localisations within the gauge length as well as the initial section of the transitions curves were observed as a result of deformation. This was the case for all concrete mixes that were tested in this study. For extremely plastic test specimens, such as the fresh concrete MSA and MSR specimens, the zones of significant strain localisations or the presence of cracking over the gauge length were less pronounced. These specimens however displayed a noticeable loss of cross-section height over the gauge length, as displacement commenced. This behaviour is indicative of the plastic flowing of a Bingham fluid, as described in Section 2.1.1. It was also observed that a large amount of concrete paste adhered to the surface of the coarse aggregate particles of these fresh concrete specimens after testing, as can be seen in the fresh concrete spheres in Figure 9.1 to 9.3.

Figure 9.1: 1h MA9 test specimen

Figure 9.2: 2h MA9 test specimen

Figure 9.3: 3h MA9 test specimen

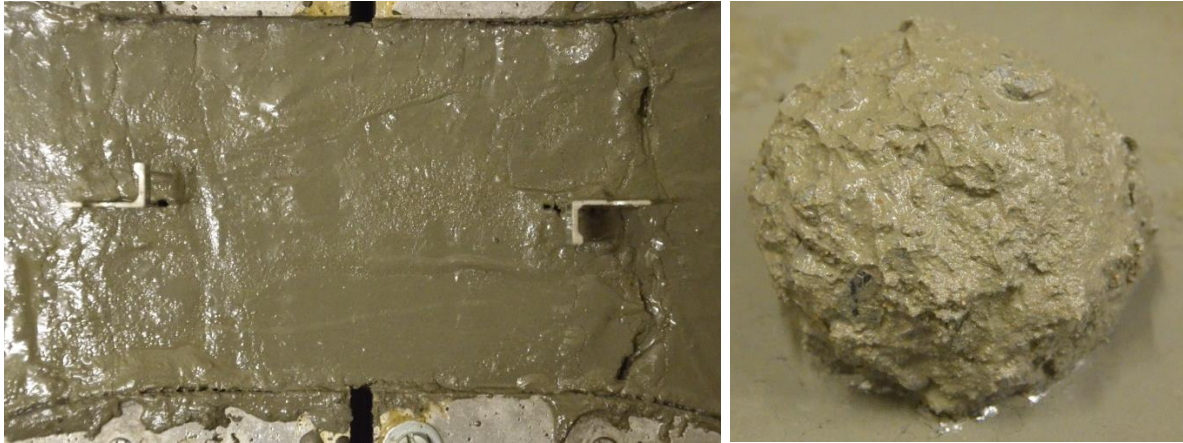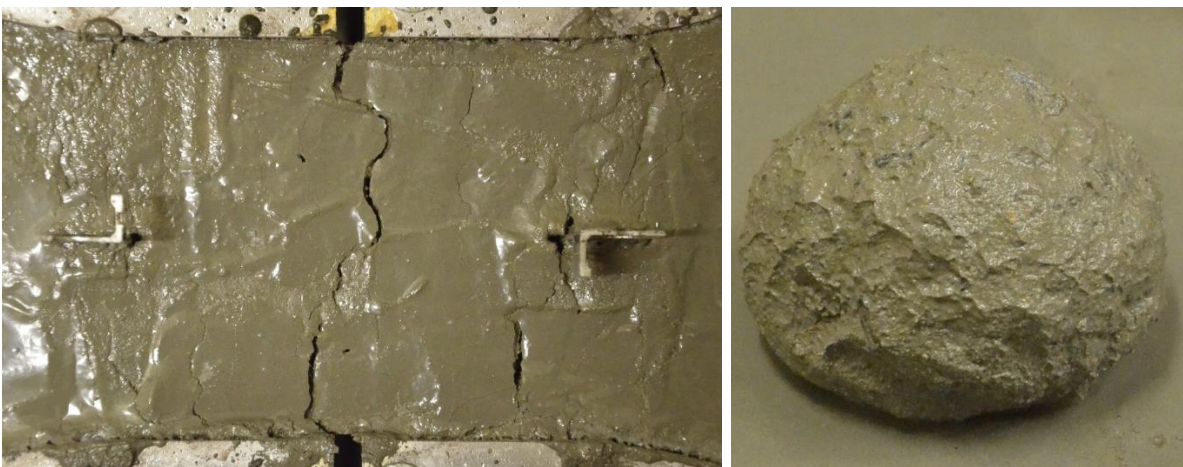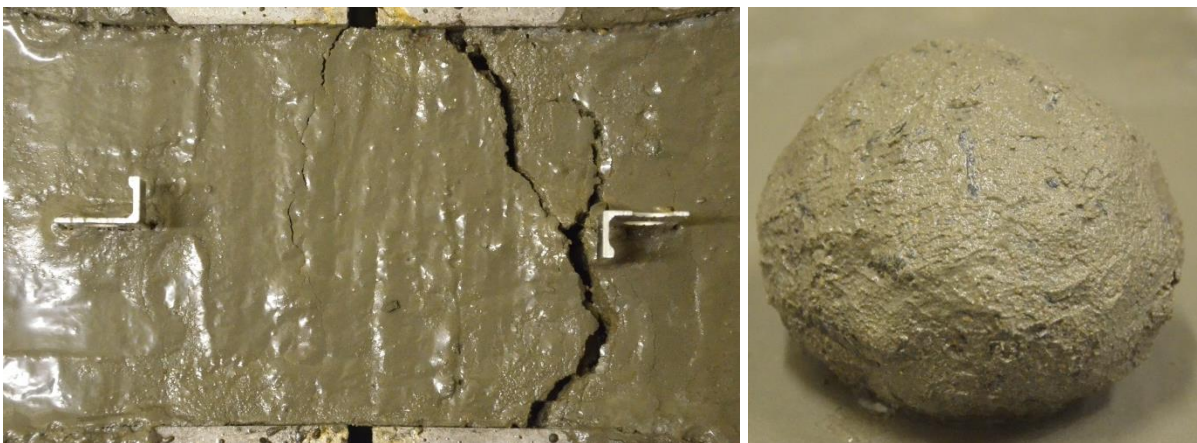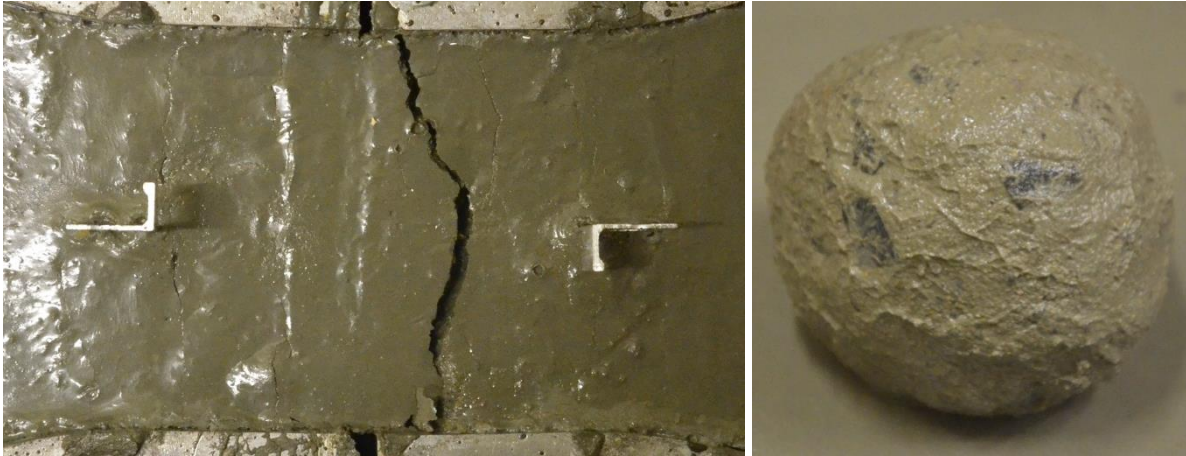**Figure 9.4: 4h MA9 test specimen**
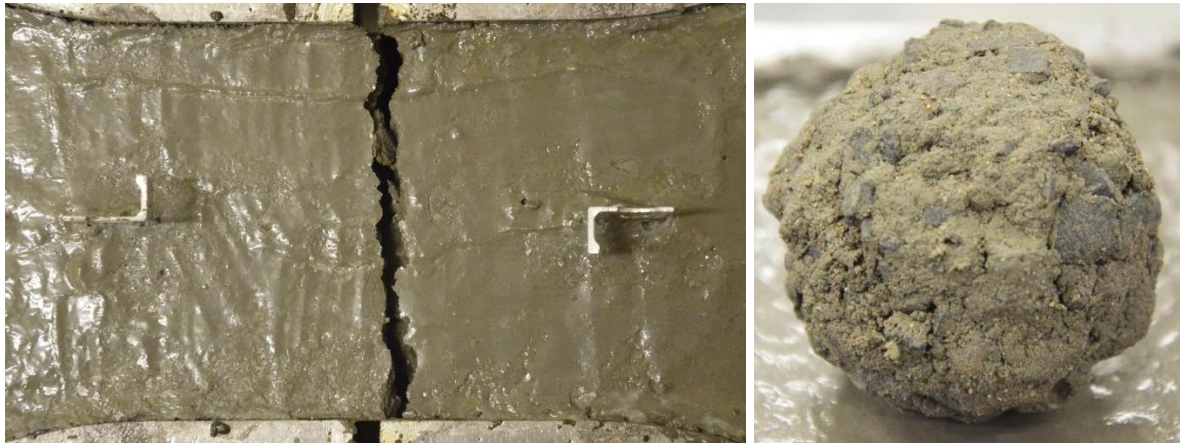
Figure 9.5: 5h MA9 test specimen
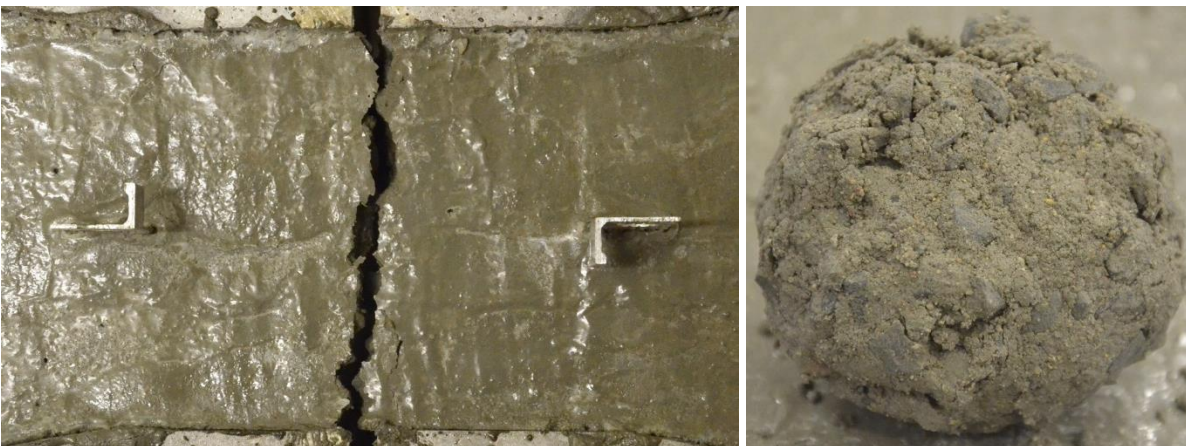
Figure 9.6: 6h MA9 test specimen

Once the initial setting time had occurred all tensile test were characterised by the presence of a single discrete crack through the cross-section of the gauge length, as shown in Figure 9.4 to 9.6. A typical example of a fully cracked surface area of a 5h test specimen is

133

shown in Figure 9.7. Considering the state of setting of the MA9 test specimens which have already reached initial setting, the 4h test specimen still proved to be mouldable by hand. However the 5h specimen became too stiff and lacked the presence of sufficient free water to be moulded into a sphere without causing the destruction of the material's paste structure. At an age of 5 hours the interlocking between the insitu aluminium pins and the concrete became so strong that they had to be removed with a hammer and chisel. From the early age concrete spheres shown in Figure 9.4 to 9.6, and the cracked surface area shown in Figure 9.7, it can be seen that the exposed coarse aggregate surface areas are relatively clean when compared to those of the fresh concrete specimens. From this it is deduced that the strength of the concrete paste rapidly becomes stronger than that of the bond between the coarse aggregate and concrete paste as the internal structure of the concrete paste develops. Branch, et al. (2002) made a similar observation in the study conducted on high strength concrete, as described in Section 2.2.1.

Figure 9.7: Fully cracked surface area of a 5h test specimen

9.2   Interpretation of experimental results for fresh concrete

In the previous chapters a plastic material, in the case of fresh concrete, was compared to a solid material, for the specimens that were tested after the initial setting time. The difference in the material behaviour of the fresh concrete specimens and the early age concrete specimens after the initial setting time is clearly illustrated by the failure modes during testing, as described in the previous section. No discrete fracture surface was present in the test conducted on specimens before the initial setting time had occurred. Rather, the strain behaviour was characteristic of a yield fluid, as described in Section 2.1.1. For a single

discrete crack to develop in a linear elastic material a load has to be induced to deform a body to the point that the strain stored in the body is sufficient to provide the required fracture energy to cause the tip stress of the crack to reach its tensile strength. The fictitious crack model (FCM) has the requirement that the bulk material behaviour of specimens is isotropic linear elastic, and thus defined by Young's modulus and Poisson's ratio. This was not the case for the fresh concrete specimens tested in this study, as can also be seen by their stress-strain curve in Appendix D.

As a result, the validity of fresh concrete results for Young's modulus, fracture energy and characteristic length are questionable as the fresh concrete specimens cannot be described as linear elastic with regards to their bulk modulus. The fracture energy determined for these specimens cannot be classified as fracture energy in the true sense of the word, but rather as the energy required to cause 30000 µ plastic straining of the material, per unit area. Although these parameters for the fresh concrete specimens still convey important information about early age concrete before its initial setting time, it is believed that rheological test methods holds more value in describing the material behaviour of these fresh concrete specimens.

9.3   Tensile properties of convention early age concrete

The aim of this section is to describe the typical tensile properties of conventional early age concrete. This was achieved by determining the average properties of specimens with corresponding ages for the MR, MA9 and MA19 mixes. A summary of the representative properties of early age concrete is presented in Table 9.1.

Table 9.1: Summary of the tensile properties of conventional early age concrete

Age [hour]	f_t [kPa]	ε_c [µ]	E [MPa]	G_F [J/m^2]	l_{ch} [m]
1	0.6	4443.3	0.3	11.6	9.2
2	0.8	3525.3	0.8	12.2	14.4
3	0.8	1400.6	1.3	11.5	19.6
4	2.8	758.3	5.9	14.8	12.6
5	8.4	518.7	19.6	19.9	8.5
6	10.8	662.5	25.4	21.2	6.1

The upper and lower limits of the average tensile properties presented in Table 9.1 are indicated in the figures presented in this section by error bars so as to give an indication of the variability of the results. As mentioned before, the heterogeneous nature of early age concrete leads to a large amount of variability in the results of these tests.

9.3.1 Tensile strength

The tensile strength versus age of a conventional early age concrete is shown in Figure 9.8. The tensile strength of the specimens is low before initial setting has occurred. However, after initial setting has occurred, the tensile strength increases rapidly. These results are in agreement with those discussed in Section 2.2.1.
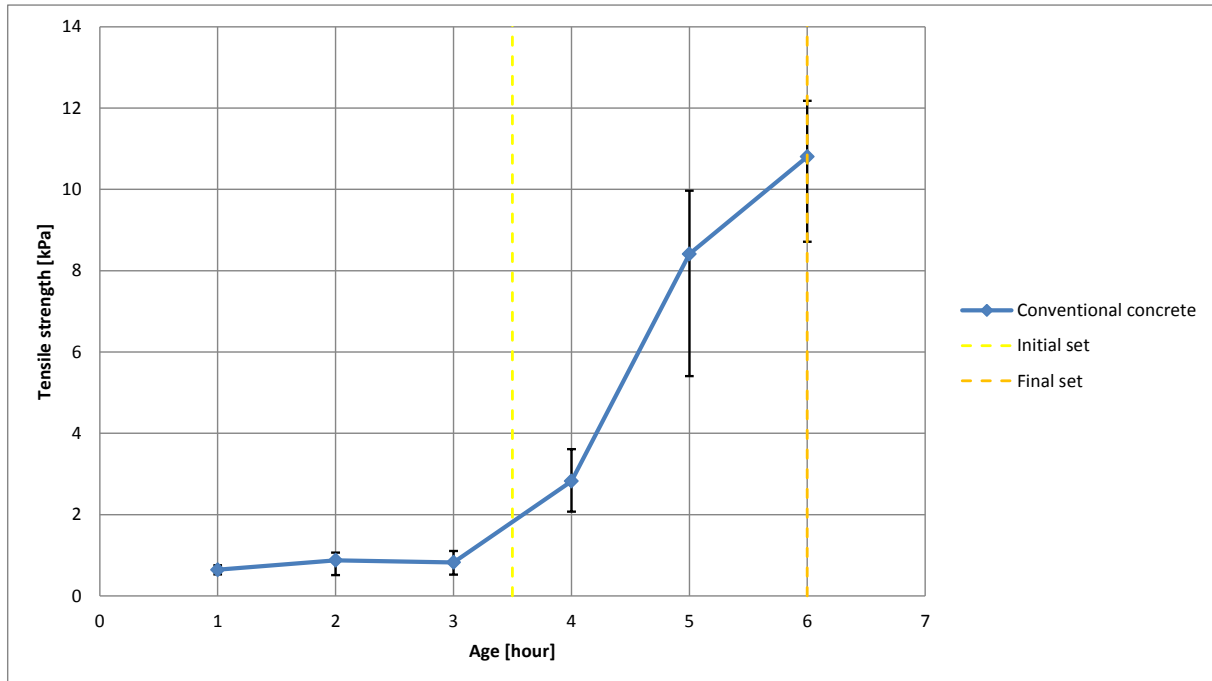
Figure 9.8: Tensile strength vs. age of a conventional early age concrete mix

9.3.2 Tensile strain capacity

The strain capacity versus age of a conventional early age concrete is shown in Figure 9.9. At an age of 1h the early age concrete has a strain capacity of approximately 4500 μ. The strain capacity decreases with time to a minimum value of approximately 500 μ at an age of 5 hours. It appears that the strain capacity starts to increase slightly from an age of 5 hours to and age of 6 hours, to an approximate strain capacity of 650 μ. These results agree with those of preceding studies, as discussed in Section 2.2.1, with the minor exception that the minimum strain capacities determined in this study, which correspond to the 5 and 6 hour specimens, are slightly higher than those determined in the studies of Branch, et al. (2002) and Dao, et al. (2009).

9.3.3 Young's modulus

The Young's modulus versus age of a conventional early age concrete is shown in Figure 9.10. Initially the Young's modulus of the specimens are very low and gradually increases with time up to the initial setting time. However, after initial setting has occurred, the Young's modulus increases rapidly.

The Young's modulus versus tensile strength of a conventional early age concrete is shown in Figure 9.11. The nearly straight line shown in this figure is indicative of a linear relationship between Young's modulus and tensile strength. The results presented for Young's modulus are in agreement with those determined by Branch, et al. (2002) and Dao, et al. (2009).
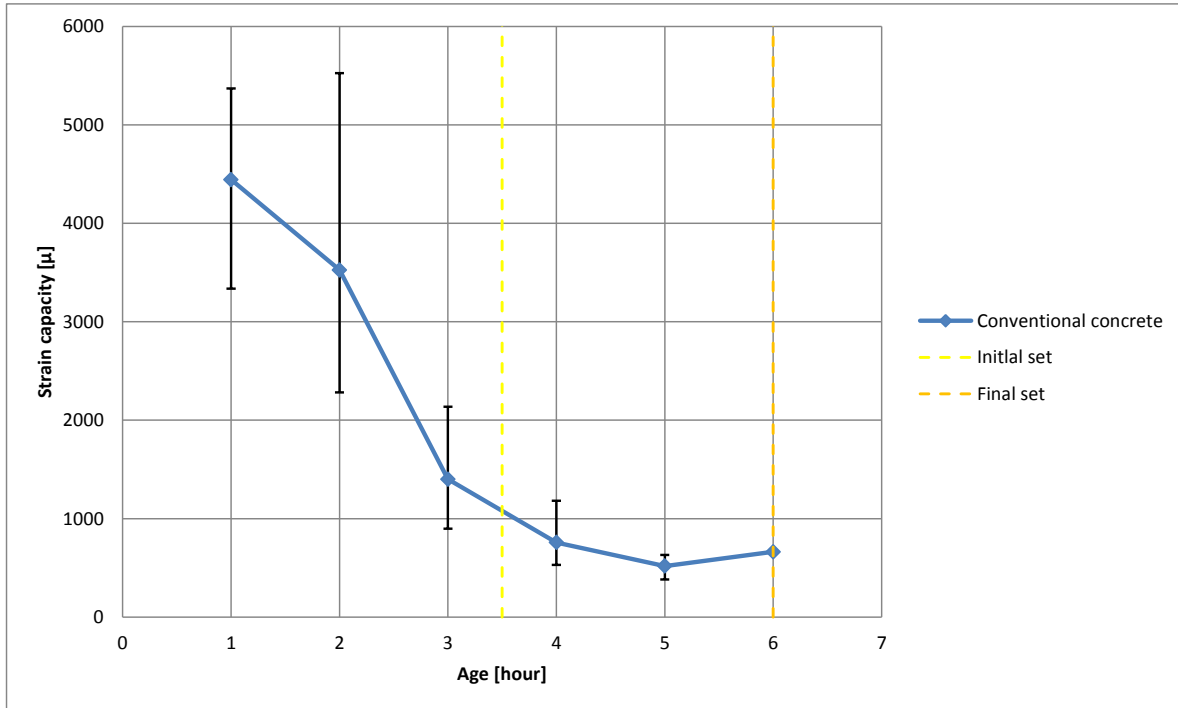
Figure 9.9: Strain capacity vs. age a conventional early age concrete mix
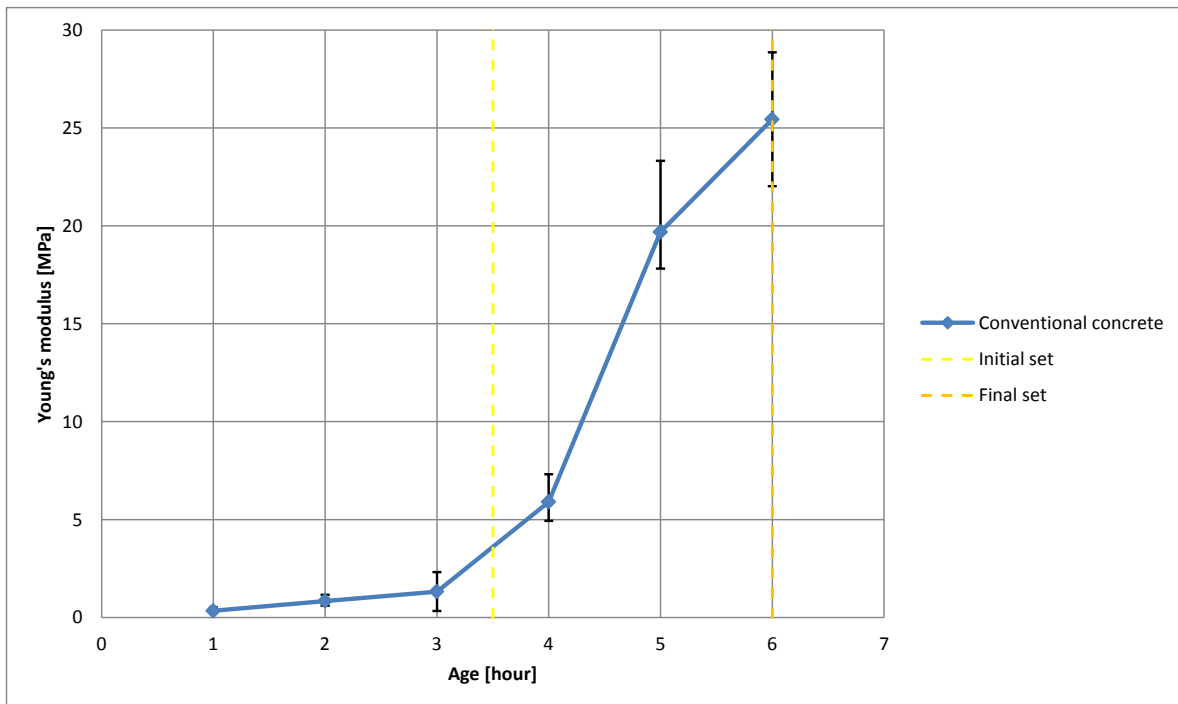
Figure 9.10: Young's modulus vs. age of a conventional early age concrete mix

137
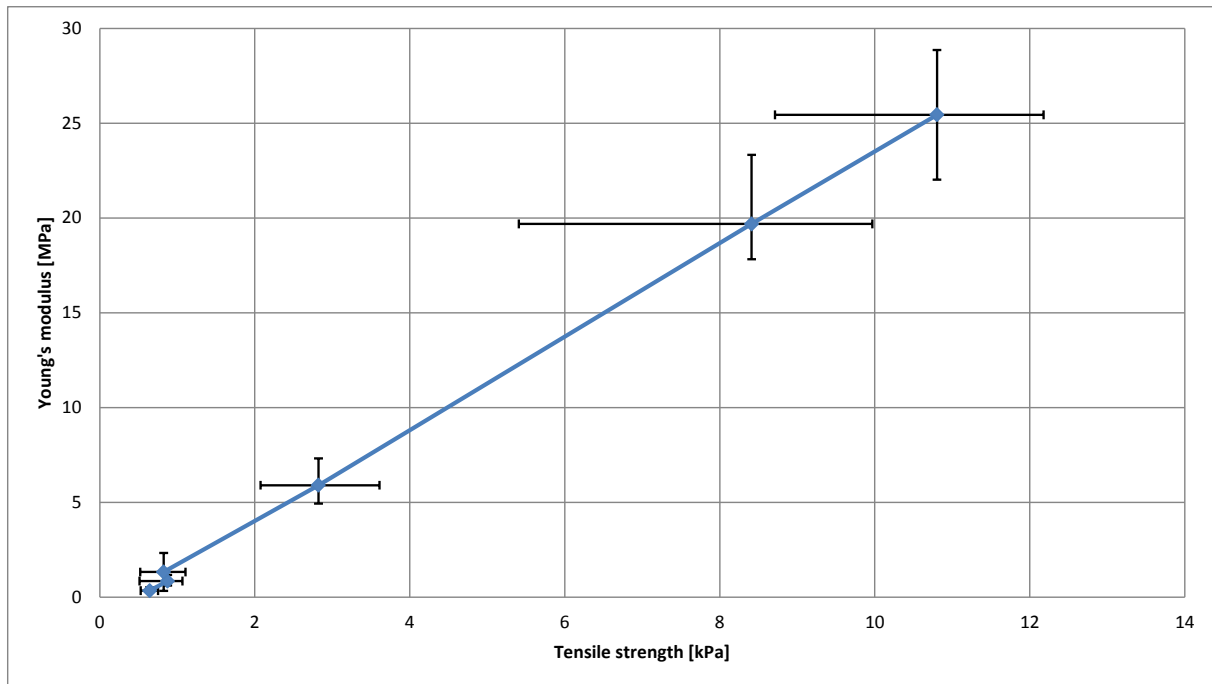
Figure 9.11: Young's modulus vs. tensile strength of a conventional early age concrete mix

9.3.4 Fracture energy

The fracture energy versus age of a conventional early age concrete is shown in Figure 9.12. The specimens have extremely low fracture energy before initial setting has occurred. An explanation for this is provided in the previous section. However, after the initial setting time has occurred the fracture energy gradually increases with age.

The Fracture energy versus tensile strength of a conventional early age concrete is shown in Figure 9.13. The nearly straight line, for the specimens tested after the initial setting time, is indicative of a near linear relationship between fracture energy and tensile strength. The results presented for fracture energy are in agreement with those of the study conducted by Doa, et al. (2009), as discussed in Section 2.2.2.

9.3.5 Characteristic length

The characteristic length versus age of a conventional early age concrete is shown in Figure 9.14. The characteristic length increases with time for the fresh concrete specimens to a maximum of approximately 20 m at an age of 3 hours. However, as initial setting commences, it decreases with time to approximately 6m at an age of 6 hours. The results presented for the characteristic length of early age concrete are in agreement with those of the study conducted by Doa, et al. (2009), as discussed in Section 2.2.2, although both studies display a large amount of variability in results.
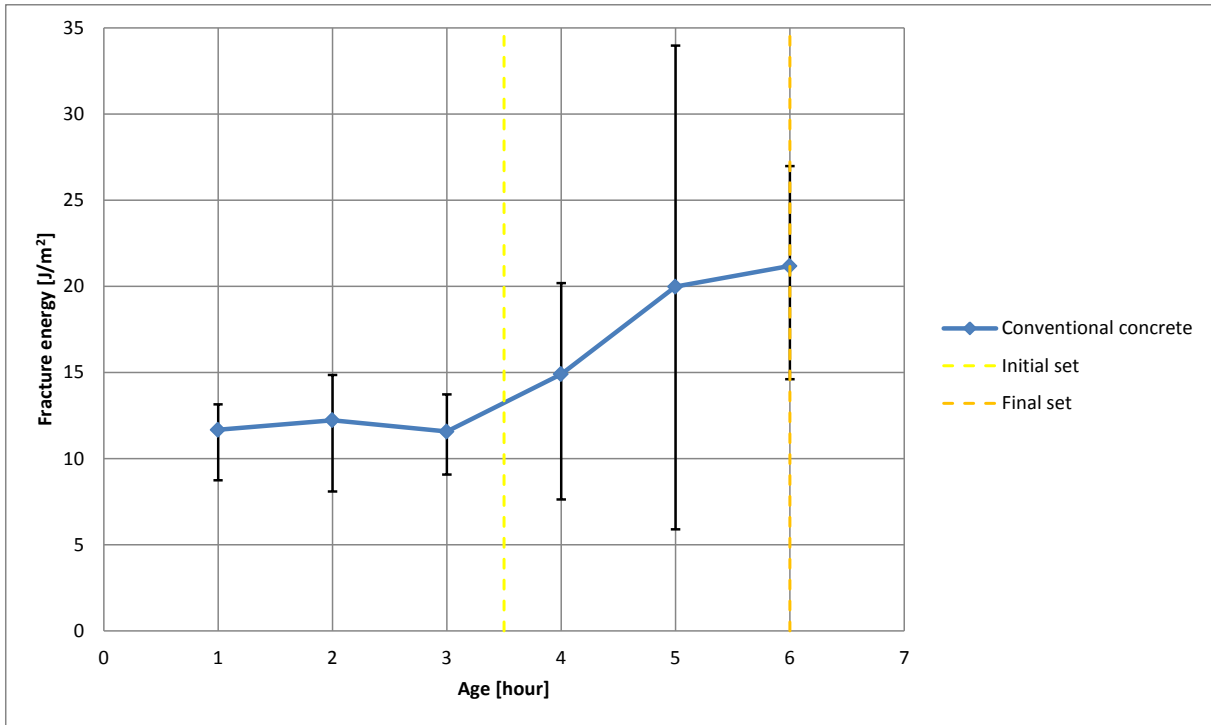
Figure 9.12: Fracture energy vs. age of a conventional early age concrete mix
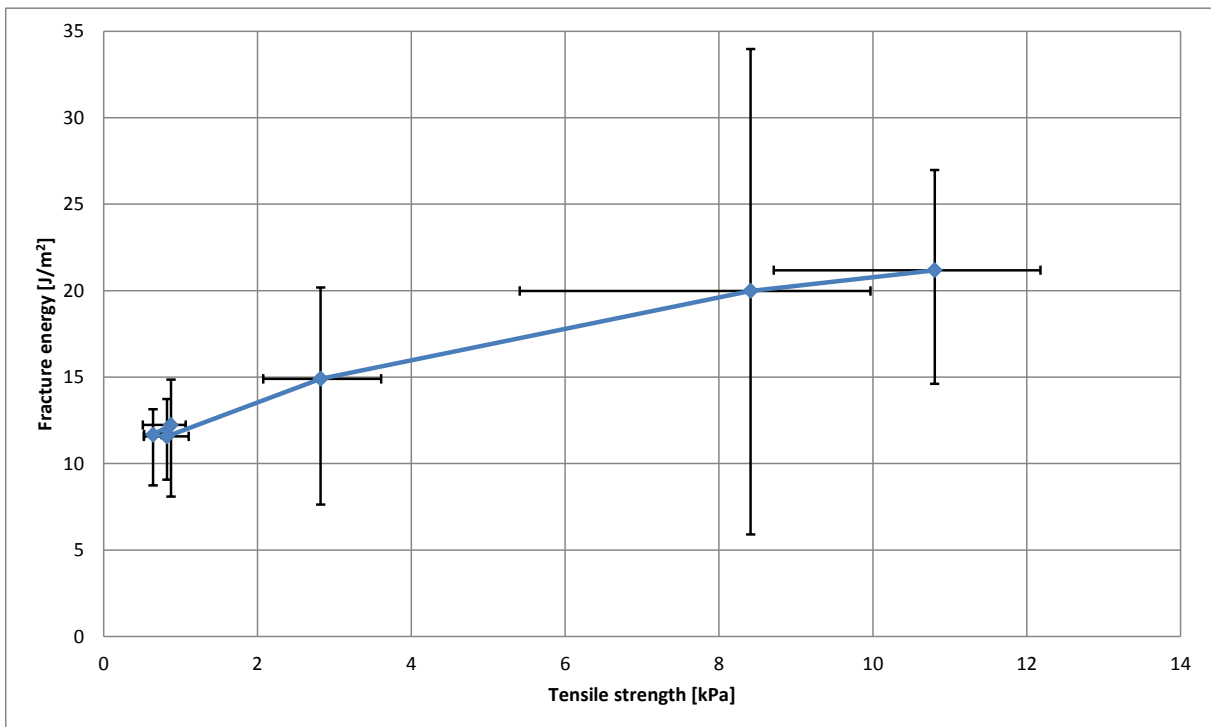
Figure 9.13: Fracture energy vs. tensile strength of a conventional early age concrete mix

139
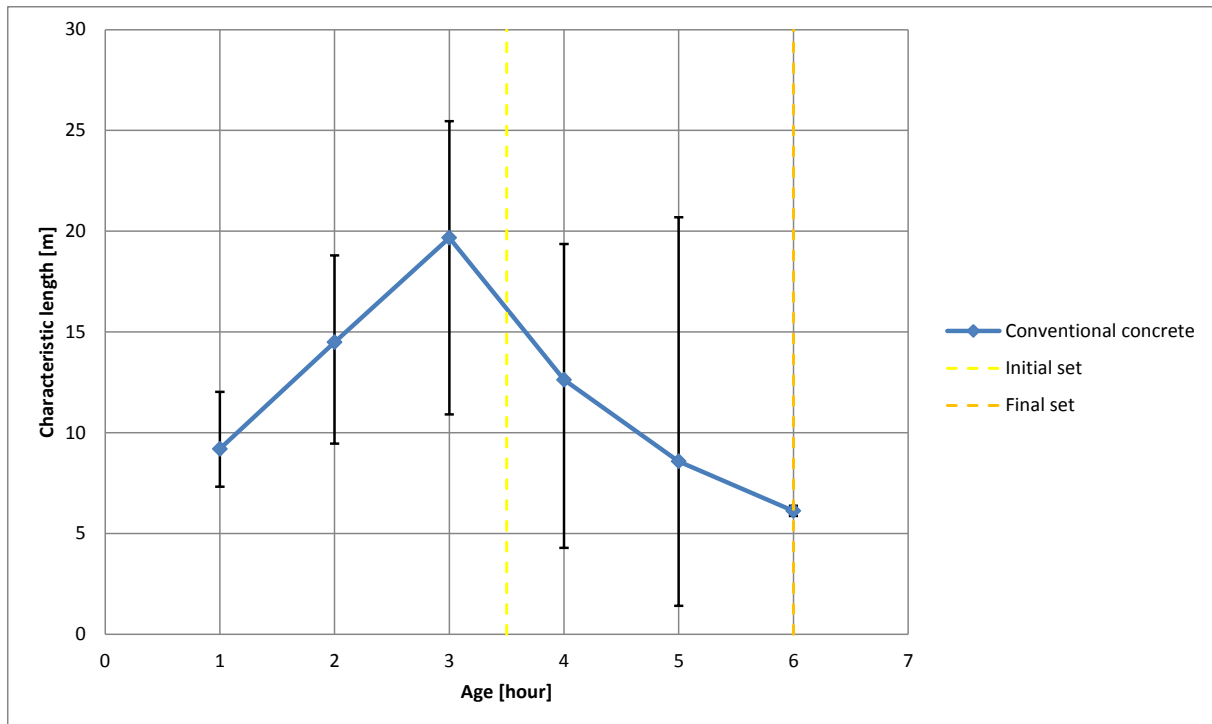
Figure 9.14: Characteristic length vs. age of a conventional early age concrete mix

9.4　PShC test results and tensile properties of early age concrete

The aim of this section is firstly to prove the validity of the tensile test results and also to show that the tensile properties determined from this study can potentially be used to predict and model PShC. In order to achieve this, results of a study conducted by Louw (2014), that utilised the MR mix to conduct PShC experiments, are used. The PShC experiments refer to tests that were conducted in a climate controlled chamber, as described by Combrinck (2011), at an ambient temperature of 40°C, a relative humidity of 10% and a wind speed of 22 km/h. The evaporation, bleeding, capillary pressure, horisontal shrinkage, vertical settlement, crack growth and setting times were all measured under these conditions.

The tensile tests were conducted under an ambient temperature of 23°C while the PShC tests were conducted at 40°C. As a result the hydration rates and consequently the setting times differed considerably for the MR mix as measured under the different ambient temperatures of these two test methods. The setting times of the MR mix as measured at the two different temperatures are shown in Table 9.2.

Table 9.2: Setting times of the MR mix exposed to different ambient temperatures

Temperature [°C]	Initial setting time [min]	Final setting time [min]
23	210	360
40	120	200

140

The development of the tensile strength, as determined in this study, along with the capillary pressure build-up and crack area, all as a function of time, are shown in Figure 9.15.

Figure 9.15: Development of tensile strength, capillary pressure and cracked area over time (unadjusted tensile strength)

Due to the different setting times of the MR specimens as tested under the two different test methods, the results of the tensile strength and capillary pressure build-up, as shown in Figure 9.15, are not comparable. Although it was shown in Section 7.5.1 that the initial and final setting time does not necessarily indicate a specific tensile strength of a specimen when utilising setting time alerting admixtures to alter the setting times of the mix, the assumption was made that the tensile material properties of the MR mix at a specific point in time was related to its measured setting times in order to make the results obtained by the two test methods more comparable. The MR mix takes 1.75 times longer to reach its initial setting time at 23°C than at 40°C and 1.8 times longer to reach its final setting time at 23°C than at 40°C. Consequently a factor of 1.775 was used to adjust the development of the tensile strength of the MR mix to account for the accelerated setting times as a result of the increased rate of hydration at 40°C. Figure 9.16 made use of this factor to adjust the tensile strength as shown in Figure 9.15. From the figure it can be seen that the capillary pressure exceeds the tensile strength of the specimen after approximately 93 minutes, at a stress of 0.98 kPa. Crack initiation takes place after approximately 115 minutes, which is relatively close to the time when the capillary pressure exceeded the tensile strength of the concrete. Crack initiation is defined as the time interval just before the first crack was observed.
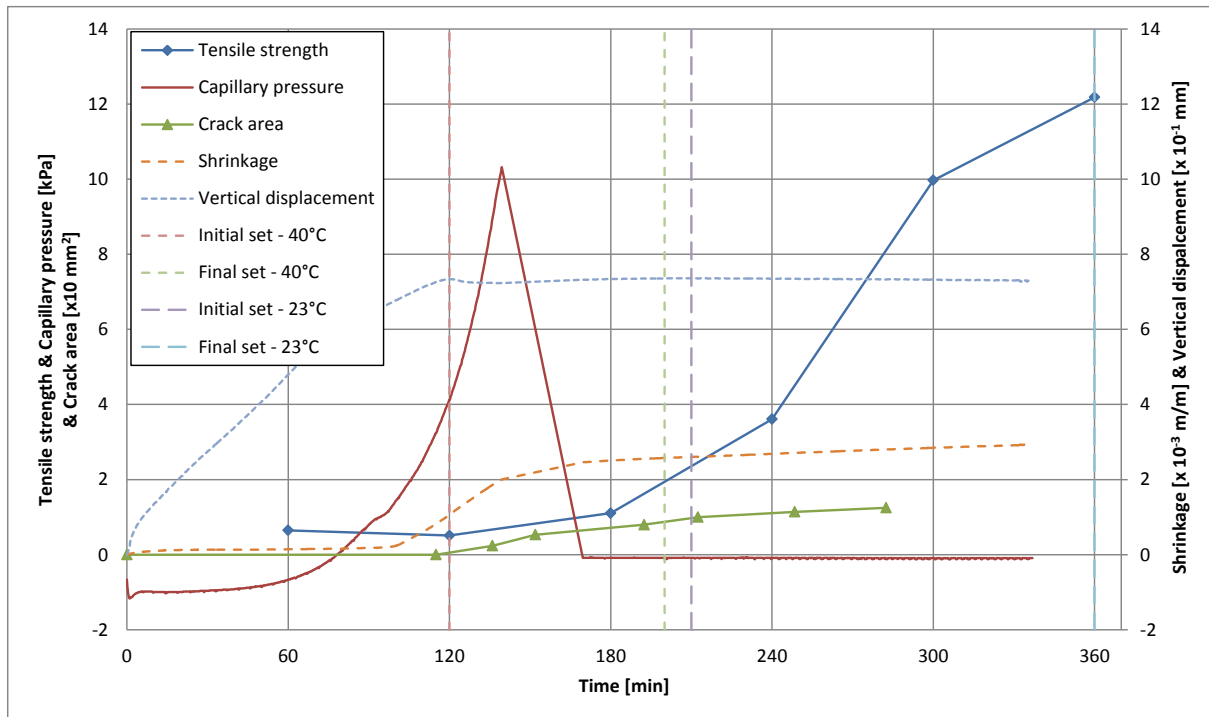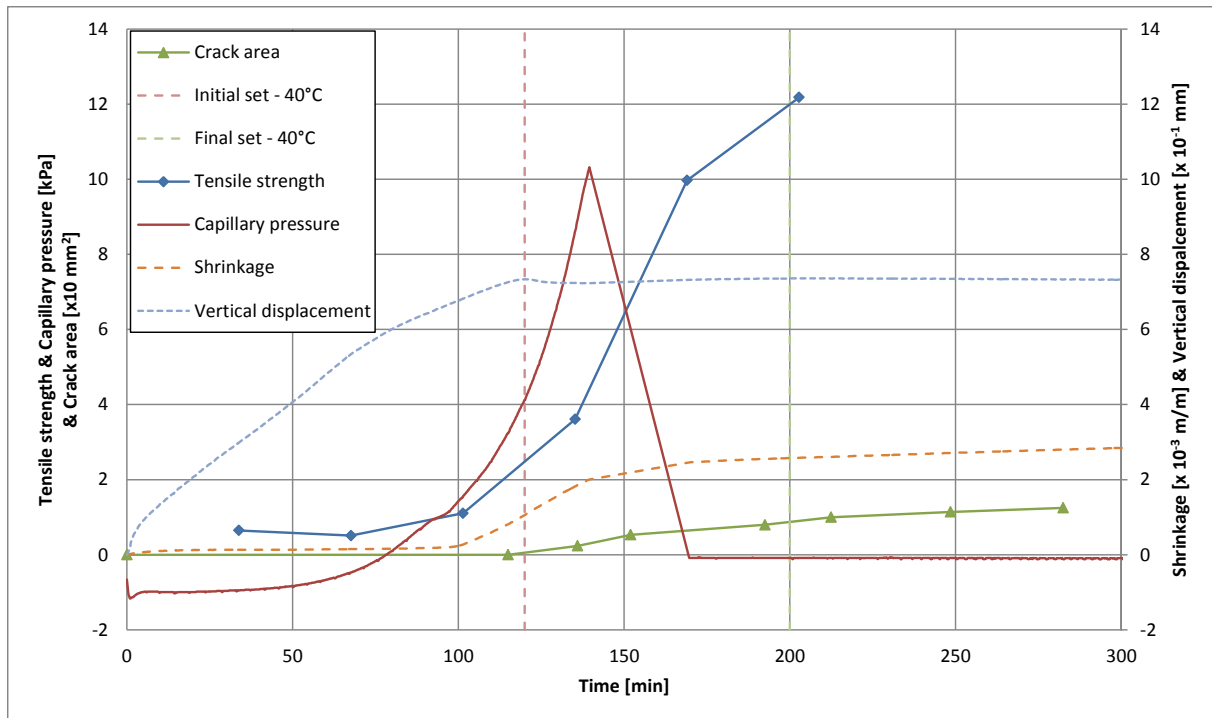
Figure 9.16: Development of tensile strength, capillary pressure and cracked area over time (adjusted tensile strength)

As mentioned in Section 2.2.1, cracking occurs if the tensile strength of the early age concrete specimen is exceeded, as indicated by Figure 9.16, or when the strain capacity is exceeded. Figure 9.17 shows the unadjusted strain capacity, as determined in this study, and shrinkage induced strain over time of the MR mix, determined from the unpublished PShC study. As described previously, the different setting times of the MR mix as determined for the two test methods, makes drawing a comparison difficult. For this reason the strain capacity was adjusted to account for the accelerated development of the tensile properties of early age concrete under a faster rate of hydration, as shown in Figure 9.18. After 114 minutes, at a strain of 787.5 µ, the strain capacity of the MR mix is exceeded by the shrinkage induced strain. This is almost the exact time crack initiation for the MR PShC specimen, which was at a time of 115 minutes, as indicated in Figure 9.16. Furthermore, the comparison between the results of the strain capacity and the tensile strength, as measured with the tensile test setup, with the results of measured cracks and shrinkage induced strain ,as determined with the PShC test setup, show great promise for further research. In fact, the results presented in this section suggest that these two different test methods can be used in combination to determine when and if cracks will occur.

As described in Section 7.4.2, the addition of fibres significantly increased the strain capacity of the test specimens just before and after the initial setting time. The increased strain capacity at this stage, along with the additional fracture energy associated with the addition

of fibres, is believed to be two of the main reason for the reduction in occurrence and severity of PShC in LV-FRC.
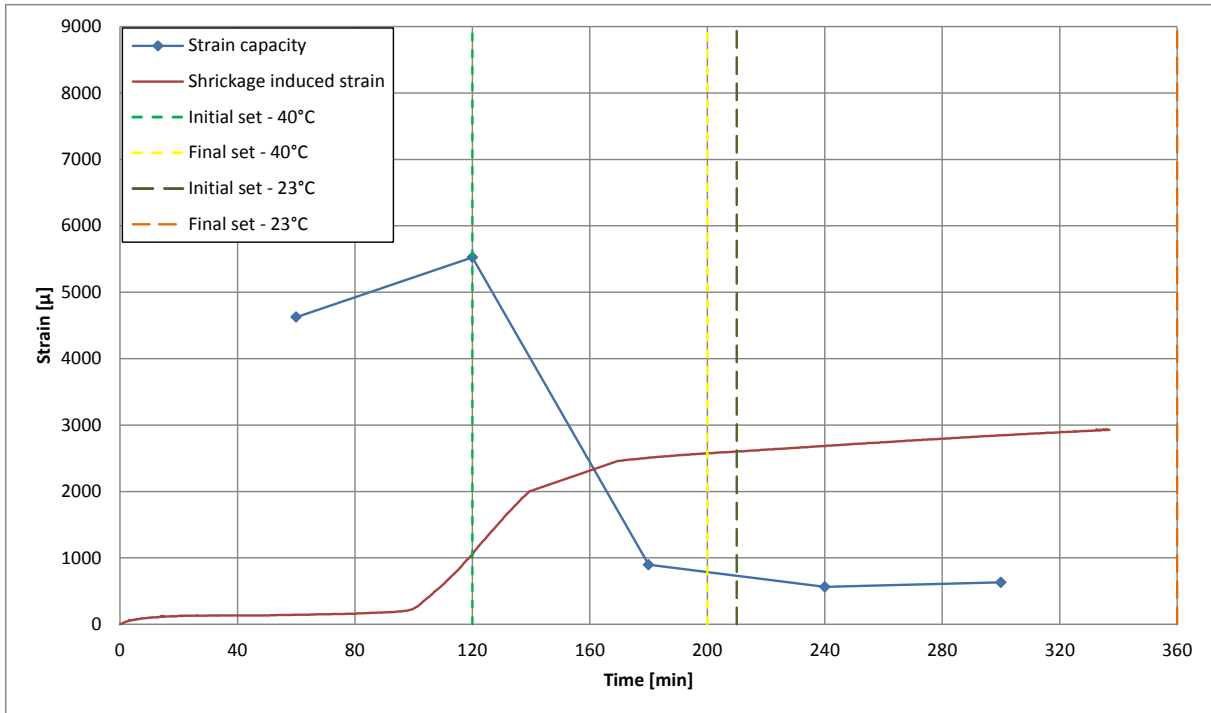
Figure 9.17: Strain capacity and shrinkage induced strain over time (unadjusted strain capacity)
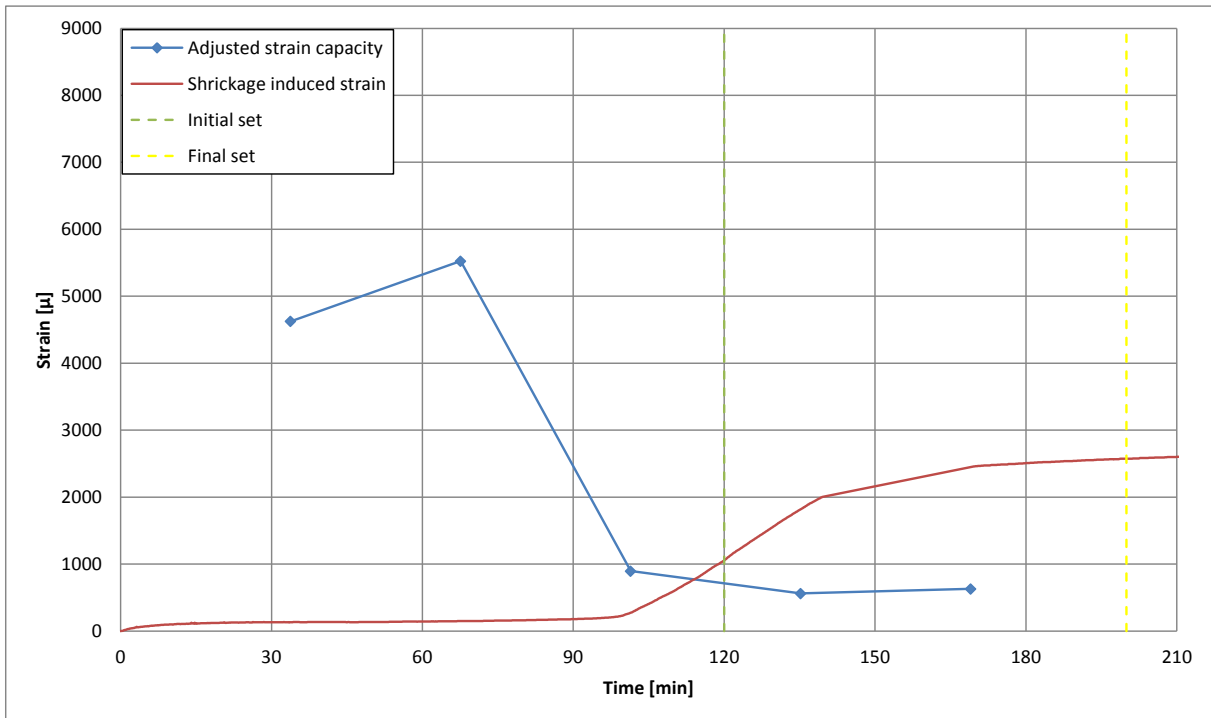
Figure 9.18: Strain capacity and shrinkage induced strain over time (adjusted strain capacity)

Section 7.5.2 stated that the addition of a retarder also increased the strain capacity of early age concrete during this period when compared to the MR mix. This is believed to be a possible explanation for the observed reduction in PShC severity observed by Combrinck & Boshoff (2012) in a retarded early age concrete mix, as stated before. Finally, allthough further research is needed for all the aspects mentioned, it can be concluded that the results of the tensile test setup can be used to shed light not only on the fundamental behaviour of PShC in concrete, but also more controvertial aspects such as the influence of fibres and admixtures on the occurence of PShC.

9.5   Concluding summary

This chapter discusses the results presented in the previous three chapters with regards to cracking, material behaviour and the link between these results and PShC. First the cracking behaviour and state of setting of the specimens tested before and after the initial setting time is described. Fresh concrete specimens display an arbitrary multiple cracking during failure, while after the initial setting time failure is characterised by a single discrete crack opening. Next, the interpretation of the experimental results for the fresh concrete specimens is discussed. As the bulk of the material modulus of the fresh concrete specimens could not be described as linear elastic, the results for Young's modulus, fracture energy and characteristic length determined for these specimens are thought to be questionable and the use of rheological test method are believed to be better in describing the material properties of early age concrete before the initial setting time. The tensile properties of conventional early age concrete are then presented. In this section the results of the MR, MA9 and MA19 mixes are used to determine the properties of a representative conventional early age concrete. Finally, results from an unpublished study on PShC are used to show the link between PShC and the result of this study. This not only validates the results of this study, but also indicates the great potential of LV-FRC to reduce the occurrence of PShC. The next chapter will present the significant conclusions of this study as well as recommendations for future studies.

10. Conclusions and recommendations

The main objective of this study was to reliably capture the full stress-strain behaviour of early age concrete specimens from one hour after casting and consolidation and onwards through the design and construction of a tensile testing setup. From achieving this main objective it is possible to derive all the tensile properties of interest. The secondary objectives of this study include the determination of the effect of coarse aggregate size, the effect of the addition of microfibres and the effect of setting time altering admixtures on the tensile properties of early age concrete. The following significant conclusions are drawn from this study:

The reliable capture of the full stress-strain behaviour of early age concrete:

- The tensile test setup and method used in this study reliably captured the full stress-strain behaviour of early age concrete. However, the insitu method of strain determination cannot be used to reliably determine the displacement over the specimen gauge length during the testing of specimen that have not yet reached their initial setting time. For this reason the method used in the study of Doa, et al. (2009) was adopted to determine the strain of these specimens. Although this method delivers a realistic approximation for the displacement over the gauge length for fresh concrete specimens, it was shown that it severely underestimates this displacement for specimens tested after the initial setting time.

The effect of coarse aggregate size on the tensile properties of early age concrete:

- The reduction of the coarse aggregate size in a concrete mix increases both the tensile strength and Young's modulus of early age concrete.

- The increase of the coarse aggregate size in a concrete mix increases both the fracture energy and characteristic length, and consequently the ductility, of early age concrete. The increased bridging zone in the fracture process zone (FPZ), due to a large degree of aggregate interlocking, is believed to be responsible for the increase in both fracture parameters. This is in agreement with the results for mature concrete specimens (Karihaloo, 1995).

The effect of the addition of microfibres on the tensile properties of early age concrete:

- For fresh concrete specimens the addition of fibres lead to an increase in both tensile strength and Young's modulus. This is believed to be a result of the lower slump

145

values and increased cohesion associated with an addition of fibres to concrete. The 3h and 4h specimens, of mixes containing fibres show increased strain capacity when compared to the reference mix (MR). As both the MF0.6 and MF1.8 mixes displayed similar strain capacities for these tests, it is believed that the fibre volume added to the reference concrete has an inconsequential effect on strain capacity within the range of fibre volume additions tested in this study. This is of great significance as it provides evidence of the increased strain capacity resulting from the addition of fibre at the initial setting time of a concrete. This is believed to be a reason for the increased resistance of low volume fibre reinforce concrete (LV-FRC) to the occurrence of plastic shrinkage cracking (PShC). Section 9.4 further substantiates this as it is shown that visible cracking appears right before the initial setting time of the MR mix nearly at the same time that the strain capacity of the concrete was exceeded by the shrinkage induced strain during the PShC experiments.

- The addition of microfibres to concrete significantly increases both the fracture energy and characteristic length, and consequently the ductility, of early age concrete. The MF0.6 test specimens displayed approximately twice the fracture energy of the MR test specimens at the same age while the MF1.8 mix had a fracture energy of approximately four times that of the corresponding MR specimens. After the initial setting time has occurred, the interfacial bond strength between the concrete paste and fibres significantly increases, therefore also the capacity of the fibres to transfer a tensile load across the crack plane. As with an increase in coarse aggregate size, the addition of fibres increase the bridging zone in FPZ due to the bridging of fibres across the crack plane. This is believed to be responsible for the significant increase in both fracture parameters and also explains how the addition of fibres decreases the severity of PShC once it has occurred.

The effect of setting time altering admixtures on the tensile properties of early age concrete:

- The addition of an accelerator slightly increases the development of the ascending tensile properties of early age concrete, while a retarder decreases it, as would be expected. The MSR mix displayed significantly more strain capacity when compared to the MR mix. This is a possible explanation for the reduction in PShC severity observed by Combrinck & Boshoff (2012) when comparing the induced PShC of a retarded mix with a reference mix.

- The addition of an accelerator slightly increases the development of fracture energy and characteristic length of early age concrete, while a retarder decreases it, as would be expected.

From the knowledge gained during this study, the following is identified as important aspects that require further investigation:

- A significant area of improvement was identified to be the strain measurement apparatus and method used in this study. Although the insitu method used to determine the displacement over the gauge length of specimens tested after the initial setting time was believed to be an improvement from the method used by Doa, et al. (2009), it cannot be used reliably on fresh concrete specimens. Non-intrusive optical methods of measuring the strain on the concrete surface can be a possible improvement. However, it should be noted that the constant presence of bleeding water on the concrete surface, a requirement to ensure that capillary pressure build-up and subsequent horisontal shrinkage does not occur, would make the use of optical methods troublesome. It is also believed that a displacement gradient exists over the depth of fresh concrete specimens. Irrespective of the strain measurement method used, it is cumbersome to reliably determine the strain of such specimens.

- Bazant (2002) suggested that a fully developed FPZ of mature concrete is in the order of 3 to 12 times that of the maximum aggregate size in the fractured concrete. This is confirmed by the characterise lengths of mature concrete presented in Table 2.2. However, this was not the case for early age concrete, particularly early age LV-FRC, as the characteristic lengths of these specimens were in the order of 100 times larger than that of mature conventional concrete. Although the tensile testing mould made provision for a fully developed fracture process zone, as prescribed by Bazant (2002), it would need to be scaled up 400 times to accommodate the formation of the fully developed FPZ of the 4h MF1.8 test specimen, given its characteristic length. Although this would be ideal, it is clearly unrealistic as the size and weight of the current tensile testing mould made its transportation and handling very troublesome.

- From the results of preceding studies, as described in Section 2.2.1, as well as those of this study, it is evident that concrete has its lowest strain capacity during the period that PShC typically occurs. It is believed that if the strain capacity during this period is increased, the occurrence and severity of PShC is significantly limited. As discussed in Section 9.4, the results of the tensile testing setup, with regards to the tensile

strength and strain capacity of early age concrete, can be used to better understand the fundamentals of PShC as well as more controversial aspects such as the influence of fibres and admixtures on the occurrence of PShC in concrete. This shows great promise for future studies.

11. References

Abel, J. & Hover, K., 1998. Effect of Water/Cement Ratio on the Early Age Tensile Strength of Concrete. *Transportation Research Record,* Volume 1610, pp. 33-38.

Bagherzadeh, R., Sadeghi, A. & Latifi, M., 2011. Utilizing polypropylene fibers to improve physical and mechanical properties of concrete. *Textile Research Journal,* 00(00), pp. 1-9.

Bazant, Z. P., 2002. Concrete fracture models:testing and practice. *Engineering Fracture Mechanics,* Volume 69, pp. 165-205.

Bentz, D. P., 2008. A review of early-age properties of cement-based materials. *Cement and Concrete Research,* p. 196–204.

Boshoff, W. P. & Combrinck, R., 2013. Modelling the severity of plastic shrinkage cracking in concrete. *Cement and Concrete Research,* p. 34–39.

Branch, Hannant, D. J. & Mulheron, M., 2002. Factors affecting the plastic shrinkage cracking of high-strength concrete. *Magazine of Concrete Research,* 54(5), p. 347–354.

Branch, J., Hannant, D. J. & Mulheron, M., 2002. Factors affecting the plastic shrinkage cracking of high-strength concrete. *Magazine of Concrete Research,* 54(5), p. 347–354.

Cement, Concrete & Aggregates Australia, 2005. *Plastic Settlement Cracking.* Sydney, Cement, Concrete & Aggregates Australia.

Chryso SA, 2007. *General Catalogue,* 1ste Edition: 2007. Boksburg: Chryso South Africa.

Combrinck, R., 2011. *Plastic shrinkage cracking in conventional and low volume fibre reinforced concrete,* Stellenbosch: Thesis presented in partial fulfilment of the requirements for the degree Master of Science in Engineering at the University of Stellenbosch.

Combrinck, R. & Boshoff, W. P., 2012a. *Influence of restraint on the early age cracking of concrete.* Guimarães, BEFIB2012.

Combrinck, R. & Boshoff, W. P., 2012b. Typical plastic shrinkage cracking behaviour of concrete. In: *Magazine of Concrete Research.* s.l.:ICE Publishing, pp. 1-8.

Combrinck, R. & Boshoff, W. P., 2014. *Fundamentals of plastic settlement cracking in concrete.* Stellenbosch, Department of Civil Engineering, Stellenbosch University.

Dao, V. T., Dux, P. F. & Morris, P. H., 2009. Tensile Properties of Early-Age Concrete. *ACI Materials Journal,* Volume November/December, pp. 483-492.

Doa, V. T., Morris, P. H. & Dux, P. F., 2010. *Fracture mechanics of early-age concrete.* Seoul, School of Civil Engineering, The University of Queensland, Australia, pp. 95-98.

Doa, V. T. N., Dux, P. F., Morris, P. H. & O'Moore, L. O., 2010. Plastic shrinkage cracking of concrete. *Australian Journal of Structural Engineering,* pp. 207-214.

Elfgren, L., 1989. *Fracture Mechanics of Concrete Structures: From Theory to Applications (Report of the Technical Committee 90-FMA Fracture Mechanics to Concrete Applications).* Londen: Chapman and Hall.

FAULHABER, 2012a. *Technical Information: Brushless DC-Servomotors with integrated Encoder,* Schönaich, Germany: FAULHABER.

FAULHABER, 2012b. *Technical Information: Encoders - Magnetic Encoders with Line Driver,* Schönaich, Germany: FAULHABER.

FAULHABER, 2012c. *Technical Information: Motion Controller - V2.5, 4-Quadrant PWM,* Schönaich, Germany: FAULHABER.

FAULHABER, 2012d. *Technical Information: Planetary Gearheads,* Schönaich, Germany: FAULHABER.

Ferraris, C. F. & de Larrard, F., 1998. *Testing and Modeling of Fresh Concrete Reology.* Gaithersburd: Building and Fire Reseach Laboratory, National Institute of Standards and Technology.

Griffith, A. A., 1920. The phenomena of rupture and flow in solds. *Philosophical Transactions of the Royal Society of London,* Volume A 221, pp. 162-198.

Gutsch, A. W., 2002. Properties of early age concrete- Experiments and modeling. *Materials and Structures/Materiaux et Constructions,* pp. 76-79.

Hannant, D. J., 1978. *Fibre Cements and Fibre Concretes.* New York: John Wiley & Sons.

Hannant, D. J., Branch, J. & Mulheron, M., 1999. Equipment for Tensile Testing of Fresh Concrete. *Magazine of Concrete Research,* 51(4), pp. 263-267.

Hillerborg, A., Modeer, M. & Petersson, P. E., 1976. Analysis of crack formation and crack growth in concrete by means of fracture mechanics and finite elements. *Cement and Concrete Research,* 6(6), pp. 773-781.

Holt, E. & Leivo, M., 2004. Cracking risks associated with early age shrinkage. *Cement & Concrete Composites,* p. 521–530.

Illston, J. & Domone, P., 2001. *Construction materials: their nature and behaviour.* New York: CRC Press.

Louw, J.P., 2014. *Influence of admixtures on the early age plastic cracking of concrete,* Stellenbosch: Final year project presented in fulfilment of the requirements for the degree Bachelor of Engineering at Stellenbosch University.

Johnston, C. D., 2001. *Fiber-Reinforced Cements and Concretes.* New York: Taylor & Francis.

Kanakubo, T., 2006. Tensile characteristics evaluation method for ductile fiber reinforced concrete. *Journal of Advanced Concrete Technology,* 4(1), pp. 3-17.

Karihaloo, B. L., 1995. *Fracture Mechanics and Structural Concrete.* Harlow: Longman.

Kasai, Y., Yokoyama, K. & Matsui, I., 1972. *Tensile Properties of Early-Age Concrete, Mechanical Behaviour of Materials - Proceedings of the International Conference on Mechanical Behaviour of Materials.* Kyoto, Japan: The Society of Materials Science.

Kim, J.-K., Lee, Y. & Yi, S.-T., 2004. Fracture characteristics of concrete at early ages. *Cement and Concrete Research,* 3(34), p. 507–519.

Kovler, K. & Roussel, N., 2011. Properties of fresh and hardened concrete. *Cement and Concrete Research,* p. 775–792.

Kronlöf, A., Markku, L. & Sipari, P., 1995. Experimental study on the basic phenomena of shrinkage and cracking of fresh mortar. *Cement and Concrete Research,* Issue 25, pp. 1747-1754.

Kwak, H. G. & Ha, S. J., 2006. Plastic shrinkage cracking in concrete slabs. Part II: numerical. *Magazine of Concrete Research,* 58(8), pp. 517-532.

Maritz, J.-L., 2012. *An Investigation on the Use of Low Volume - Fibre Reinforced Concrete for Controlling Plastic Shrinkage Cracking,* Stellenbosch: Thesis presented in fulfilment of the requirements for the degree Master of Science in Engineering at Stellenbosch University.

Mehta, P. K. & Monteiro, P., 2014. *Concrete: microstructure, properties, and materials.* Fourth edition. New York: McGraw-Hill Professional 2014.

NRMCA, 1998. *Concrete in Practice: CIP 5 Plastic Shrinkage Cracking.* [Brochure], Clobo.

Ostergaard, L., Lange, D. & Stang, H., 2004. Early-age stress-crack opening relationships. *Cement and Concrete Composites,* 5(26), pp. 563-572.

Owens, G., 2009. *Fulton's concrete technology.* Midrand, South Africa: Cement & Concrete Institute.

Owens, G., 2012. *Fundamentals of concrete.* 2nd ed. Midrand: Cement & Concrete Institute.

Planas, J., Elices, M. & Guinea, G. V., 1995. *The extended cohesive crack.* First Edition ed. Londen: E&FN Spon.

Powers, T. C., 1968. *The Properties of Fresh Concrete.* New York: John Wiley & Sons. Inc.

Qi, C., 2003. *Quantitative assessment of plastic Shrinkage cracking and its effect on the corrosion of steel reinforcement.* PhD thesis. Indiana, United States of America: Purdue University.

Ravina, D. & Shalon, R., 1968. Plastic Shrinkage Cracking. *ACI JOURNAL,* 65(4), pp. 282-292.

Reinhardt, H. W., 1984. Fracture Mechanics of an Elastic Softening Material like Concrete. *HERON,* 29(2), pp. 1-42.

SANS 10162-1, 2011. *Part 1: Limit-states design of hot-rolled steelwork.* Edition 2.1 ed. Pretoria: Standards South Africa.

SANS 1083, 2013. *Aggregates from natural sources - Aggregates for concrete,* Edition 2.3. Pretoria: Standards South Africa.

SANS 50196-3, 2006. *Methods for testing cement Part 3: Determination of setting times and,* 2nd ed. Pretoria: Standards South Africa.

SANS 50286-1, 1998. *Simple unfired pressure vessels designed to contain air or nitrogen.* First Edition ed. pretoria: Standards South Africa.

SANS 5861-1, 1994. *Concrete tests - Mixing fresh concrete in the laborator,* First revision. Pretoria: Standards South African.

SANS 5862-1, 2006. *Concrete tests - Consistence of freshly mixed concrete - Slump test,* Edition 2.1. Pretoria: Standards South Africa.

SANS 5863, 2006. *Concrete tests - Compressive strength of hardened concrete,* Edition 2.1. Pretoria: Standards South Africa.

SAPY, 2014. *Corehfil speciality fibres,* Hammarsdale: SAPY.

Shi, Z., 2009. *Crack Analysis in Structural Concrete - Theory and Application.* First Edition ed. Oxford: Elsevier Ltd.

Slocum, A. H., 1992. *Precision machine design.* Third Edition ed. Dearborn: Society of Manufacturing Engineers.

Slowik, V., Schmidt, M. & Fritzsch, R., 2008. Capillary pressure in fresh cement-based materials and identification of the air entry value. *Cement and Concrete Composites,* pp. 30:557-565.

Slowik, V., Schmidt, M., Hubner, T. & Villmann, B., 2009. Simulation of capillary shrinkage cracking in cement-like materials. *Cement & Concrete Composites,* Volume 31, pp. 461-469..

Swaddiwudhipong, S., Lu, H.-R. & Wee, T.-H., 2003. Direct tension test and tensile strain capacity of concrete at early age. *Cement and Concrete Research,* Volume 33, p. 2077–2084.

Telford, T., 1992. *Comite Euro-International du Beton, Durable Concrete Structures - Design Guide.* Second Edition ed. London: Thomas Telford Services Ltd.

Uno, P. J., 1998. Plastic Shrinkage Cracking and Evaporation Formulas. *ACI Materials Journal,* 95(4), pp. 365-375.

van Mier, J. & van Vliet, M., 2002. Uniaxial tension test for the determination of freacture parameters of concrete: state of the art. *Engineering Fracture Mechanics,* Volume 69, pp. 235-247.

Wittmann, F. H., 1976. On the Action of Capillary Pressure in Fresh Concrete. *Cement and Concrete Research,* pp. 6:49-56.

Wongtanakitcharoen, T., 2005. *Effect of Randomly Distributed Fibres on Plastic Shrinkage.* Michigan: The University of Michigan. (PHD-thesis).

Zeiml, M., Leithner, D., Lackner, R. & Mang, H. A., 2006. How do polypropylene fibres improve the spalling behaviour of in-situ concrete?. *Cement and Concrete Research,* Issue 36, pp. 929-942.

Zollinger, D. G., Tang, T. & Yoo, R. E., 1993. Fracture toughness of concrete at early ages. *ACI Materials Journal,* 90(5), pp. 463-471.

List of appendices

Appendix A: Tensile testing mould design and evaluation

This appendix describes the tensile testing moulds designed and used during this study. Firstly, an introduction that identifies the requirements of the tensile testing mould as well as a discussion regarding possible solutions will be presented. Next, two mould designs are introduced, after which the mould chosen for this study is described in more detail with regards to its connections between mould halves, weight, transportation and maintenance. Finally, the performance of both mould designs is evaluated.

A.1. Introduction

The primary aim of this study is to determine the tensile properties of early age concrete. This however cannot be achieved without the early age concrete specimens having a predetermined shape. Once again, in this study the term early age concrete describes concrete from the time it has been cast to the point of significant strength gain, which coincides with the final setting time. From the evaluation of the literature study on the tensile properties of early age concrete in Sections 2.2 and 2.3 and the tensile testing apparatus presented in Section 4.1, the following requirements regarding the moulding of early age concrete specimens for the purpose of tensile testing were identified.

- The moulds must be able to transfer a tensile force to the specimen. As established in Chapter 4, direct tensile methods are the only viable method of determining the tensile properties of early age concrete. As a result of the low degree of hydration present in early age concrete specimens at these early stages, demoulding cannot occur as the internal structure of the early age concrete is too weak and the concrete can still deform under its own weight in some cases.
- Localisation of deformations and cracking should occur over a constant gauge length to give a reliable reflection of the specimen's tensile material properties.

Dog-bone specimens are typically used in the direct tensile testing of mature concrete. The reduction in cross section in the neck of the specimen causes the localisation of deformation and cracking in this area as it is effectively under the greatest tensile stress. For this reason a dog-bone shaped mould, similar to that of the one used by Dao, et al. (2009), from here on referred to as the reference mould, was designed and is discussed in the following sections.

A.2. Tensile mould design and manufacturing

The curved transitions in the middle portion of the reference mould had the function of increasing the stress over the 70 mm constant gauge length ensuring that localisation of deformations and cracking occurs over the gauge length. Unlike the use of friction keys to transfer a tensile force to the specimen, as was the case with Hannant et al. (1999), the curved transitions eliminate significant stress concentrations that could lead to undesirable cracking along the length of the transitions. A main area of improvement identified in the reference mould was its neck area. These moulds have removable side inserts over the 70 mm gauge length, as shown in Figure A.1: Disassembled reference mould as used by Doa, et al.. From the interpretation of the literature describing the test procedure used by Doa and his co-workers, the removable base plate was not removed during testing on the air bearing. When removing these side inserts while a concrete specimen is still plastic, and able to exert a hydrostatic pressure on the mould, or even a weak solid, would unavoidably cause damage to its fragile internal structure
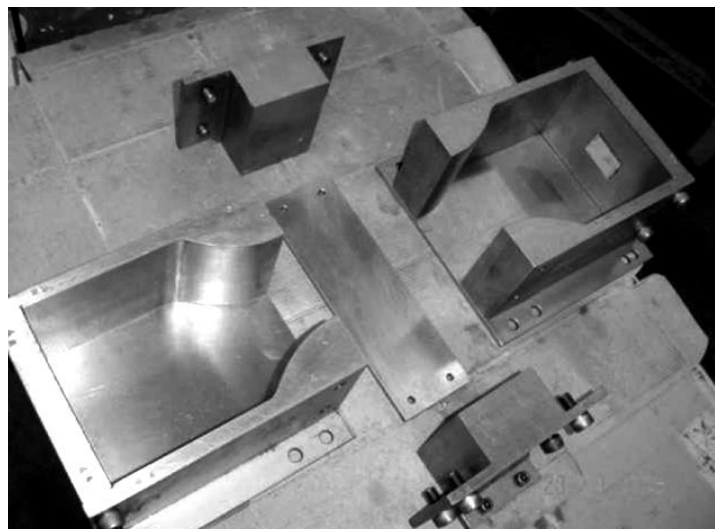

Figure A.1: Disassembled reference mould as used by Doa, et al. (2009)

To overcome this challenge, two variations of the reference mould were designed and manufactured, as shown in Figure A.2. These moulds had to be manufactured to a high accuracy. This is firstly necessary as they are to float on an air film of approximately 30 μm produced by an air bearing, as discussed in Appendix B. Secondly, this is required to ensure that the moulds' halves fit perfectly flush and do not leak concrete water during the specimen curing stage, as this could lead to the build-up of capillary pressure or insufficient water for hydration to take place. For this reason, all mould components were manufactured from grade 6082 aluminium using a computer numerical controlled (CNC) milling machine with an accuracy of 8 μm.
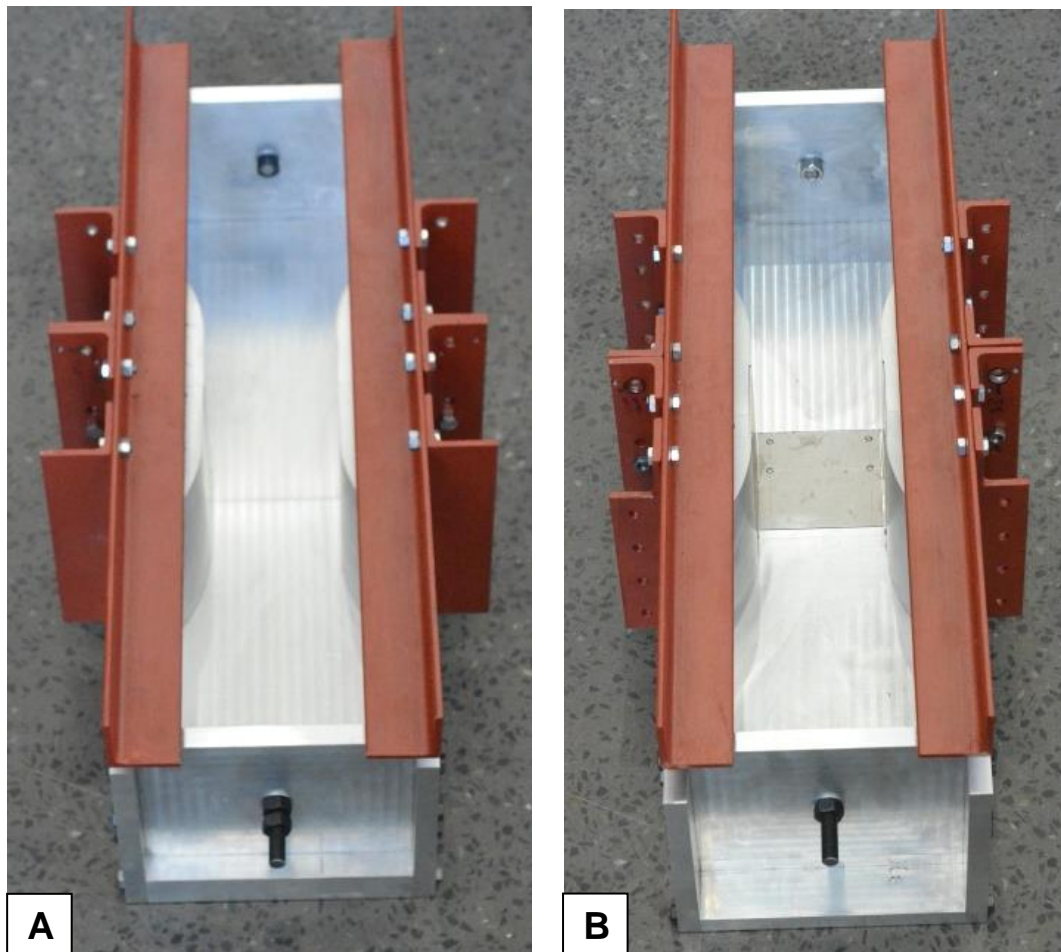
Figure A.2: Newly assembled tensile moulds

The shape of the dog-bone specimen inside both mould options were identical to that of the reference mould. The only difference was that the specimen size was scaled up by a factor of 1.43. This was done to allow for the testing of concrete mixes that utilise 19 mm aggregate, like those typically used in commercial concrete slabs. With the scaled up mould design, a complete Fracture Process Zone would most likely be able to form over the cross-section of the necked portion in this larger specimen, as discussed in Section 2.2.2 (Bazant, 2002).

Mould A omitted the removable side inserts and consists of two perfectly symmetrical mould halves as illustrated by Figure A.3.

Mould B, on the other hand made use of 1 mm thick steel plates on the sides and bottom of the 100 mm gauge length. The bottom plate was connected to the fixed mould half while the side plates were connected to the moving mould half, which displaced during testing, overlapping by 50 mm in the centre of the gauge length, as illustrated by Figure A.4.
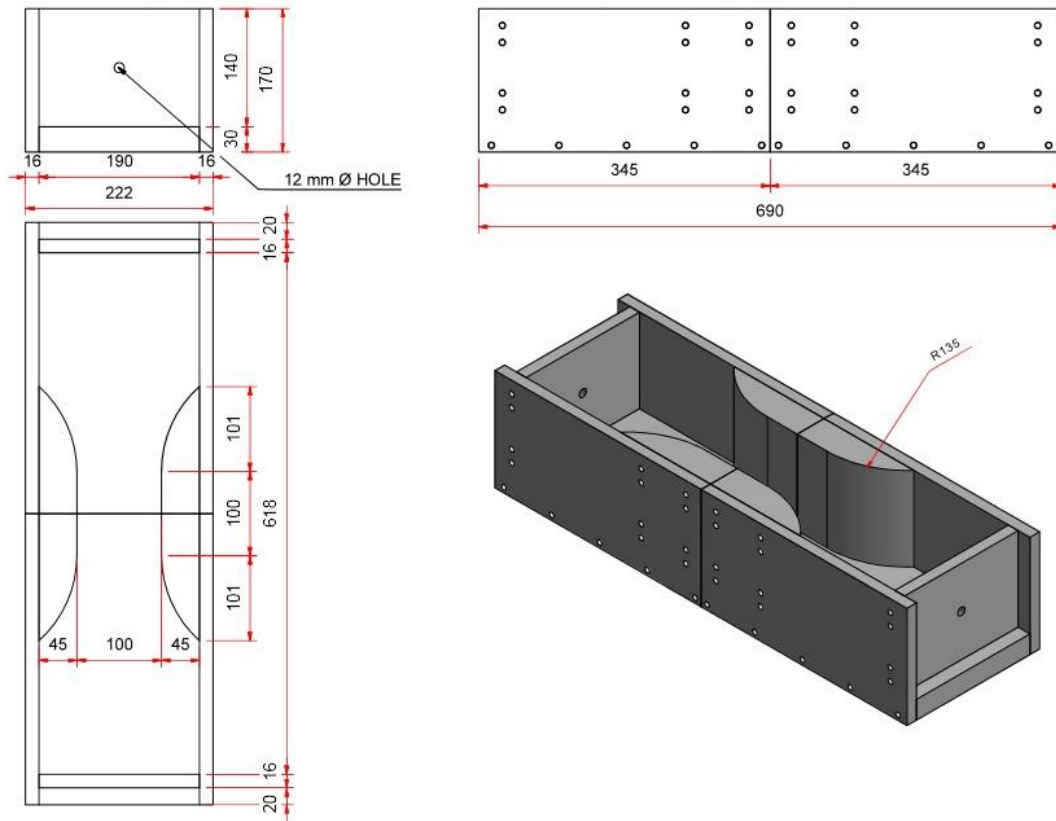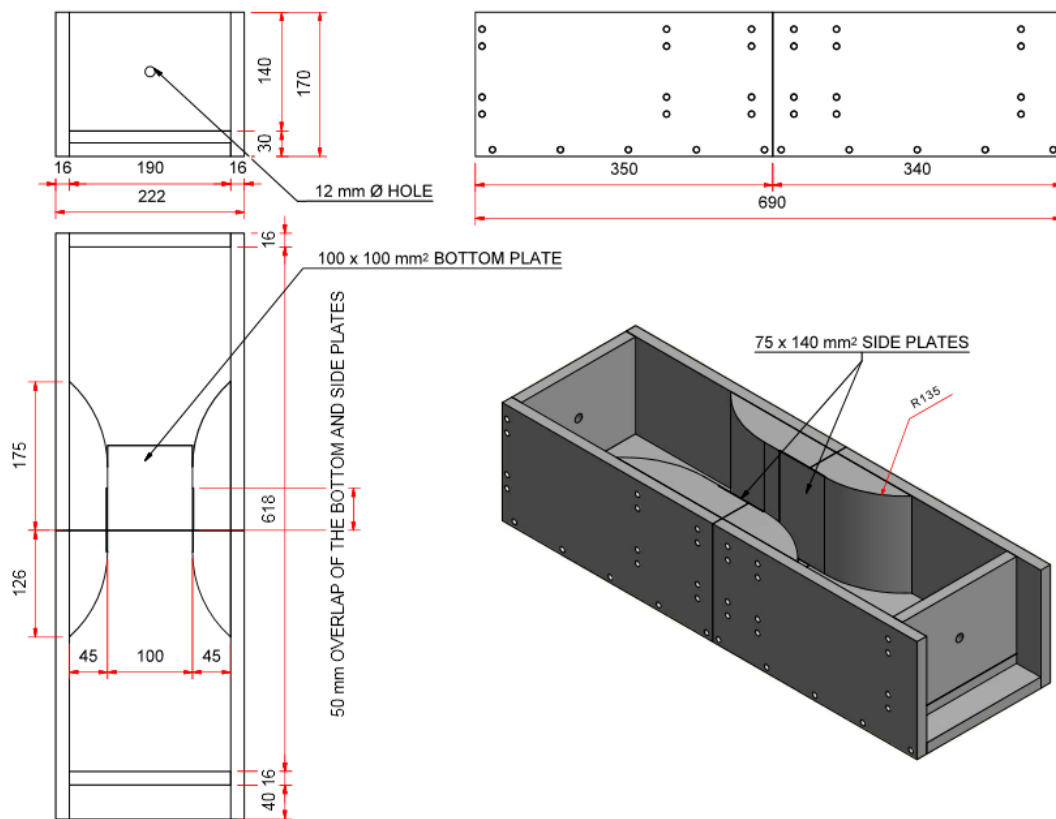
Figure A.3: Mould option A

Figure A.4: Mould option B

158

The purpose of the thin steel plates are to support the plastic fresh concrete against the effects of gravity and to keep the material intact while the two mould haves moved apart, as demonstrated in Figure A.5.

Figure A.5: Plates supporting fresh concrete

During the performance evaluation of the moulds, as discussed in Section A.3, it was found that Mould A was considerably better and would be used as the tensile testing mould in this study. Consequently, the rest of this section discusses Mould A.

A.2.1 Connecting mechanisms between mould halves

A steel angle profile structure was designed with the purpose of keeping the mould halves rigidly together during transportation and compaction and also provided handles for the two persons responsible for the transportation of the heavy specimen. Every mould utilised 80 x M8 class 8.8 bolts to keep all the mould components as well as the steel angle profile frame securely in place. The 68 bolts that were threaded into the aluminium mould itself were permanently fixed and check regularly to ensure that they were sufficiently tight. The two bolts on each side of the mould in its centre, as indicated by the yellow area in Figure A.6, are the positioning bolts that were fastened by hand once the mould halve faces were plush and perfectly lined up during the pre-test preparation on the air bearing. Once this was done, the large horisontal angle profiles were fastened by the bolts indicated by the blue area's in Figure A.6. These bolts were tightened as much as possible as to effectively create a rigid friction grip which could withstand handling and compaction without allowing any movement. The large stiffness of the thick horisontal angle profiles kept the mould halves together and flush during handling.
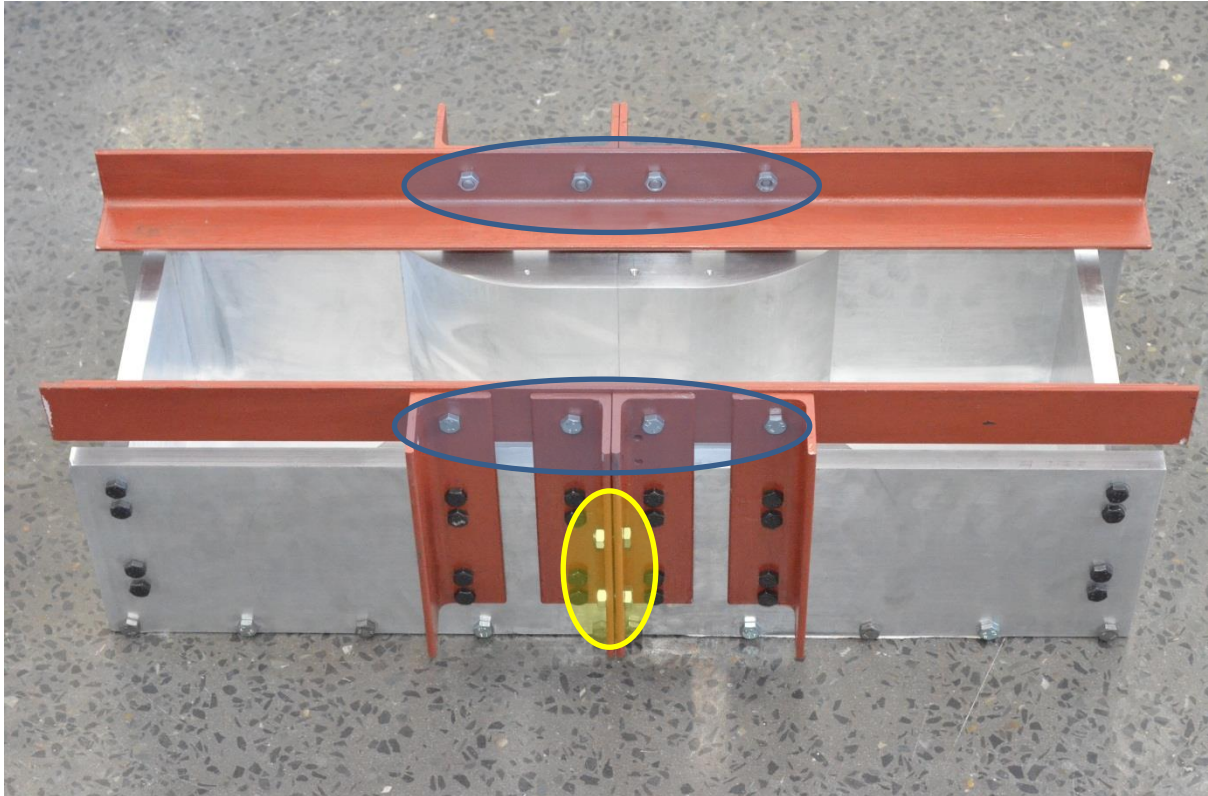
Figure A.6: Connections between mould halves

A.2.3 Weight, transportation and protective measures

The aluminium portion of the mould weighs 30.8 kg, the steel angle profile supporting structure 7.5 kg and the concrete specimen on the inside, 39.3 kg. A fully prepared early age specimen thus weighed approximately 77.6 kg. Apart from aluminium's exceptional corrosion resistance, the primary reason for choosing aluminium as the base material is that it is significantly lighter than steel. While retaining identical dimensions to the aluminium moulds, a fully loaded steel equivalent would have weighed 149.5 kg, making it completely unsuitable for handling.

Because of its immense weight, the mould was predominantly transported via trollies and handled as little as possible. It was of great importance to protect the bottom aluminium surface. If pronounced scratches occurred or any solid particles like fine aggregate or steel shavings adhered to it, it would not be able to glide without friction over the air bearing surface during testing. Consequently the mould halves were always placed on a clean protective plastic surface during storage, transportation and casting and compaction. During cleaning the bottom surface was never placed in contact with the ground. As a precautionary measure, to provide for the potential deformation of the bottom edges of the mould through the course of numerous tests, the mould was made wider (222 mm) than the air bearing (200

160

mm). This would ensure that in the event of a mould edge that deformed, the mould surface in contact with the bearing surface would not be damaged.

A.3. Performance evaluation

Tests were conducted on a reference concrete mix, as described in Section 5.4, to verify the performance of the two mould designs. The tests were conducted at hourly intervals from 1 to 4 hours after the concrete had been cast and compacted. This period was chosen as it incorporated the plastic phase as well as the initial setting time, at approximately three and a half hours, in which the early age concrete is in transition to a weak solid.

The results of the 1h and 4h tests are showed in Figures A.7 and A.8 respectively. From the 1h test it is clear that Mould B measured a considerably higher maximum tensile strength which also did not decrease over time as expected. The force displacement curve also indicated numerous sharp rises and sudden drops in the measured force. In contrast, the results of Mould A showed a tensile strength more than 3 times lower than what was found for Mould B. Its force displacement curve indicated a smooth rise to its peak tensile strength and then a gradual reduction as the specimen separated as would be expected. Keep in mind that full separation of the specimens is assumed to occur at a displacement of 6.5 mm, as measured over the concrete gauge length.
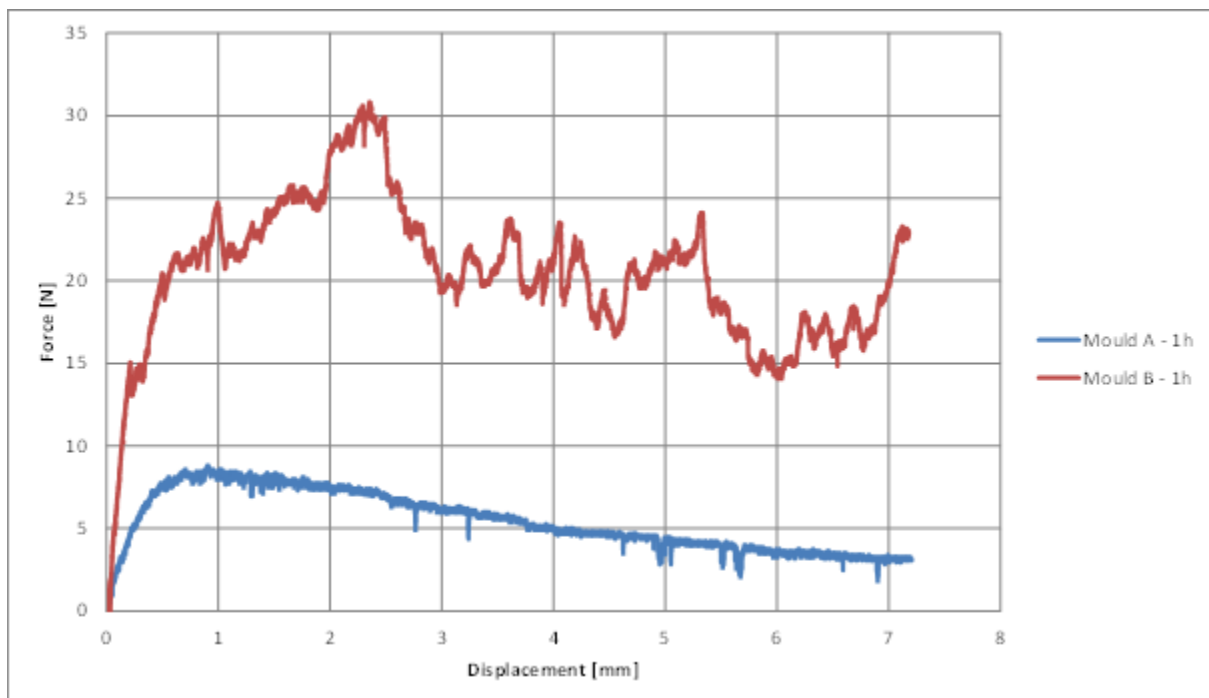

Figure A.7: Force-displacement curve of 1h specimens

For the 4h tests, the test conducted with Mould B once again resulted in a larger measured tensile strength, and consequently a steeper gradient of the force-displacement curve.

161

Similar to the 1h test, sharp rises and sudden drops in force were measured, with the measured force not decreasing at the rate as expected from literature (Section 2.2.1). In contrast, Mould A produced a smooth force-displacement curve with a significantly lower peak.
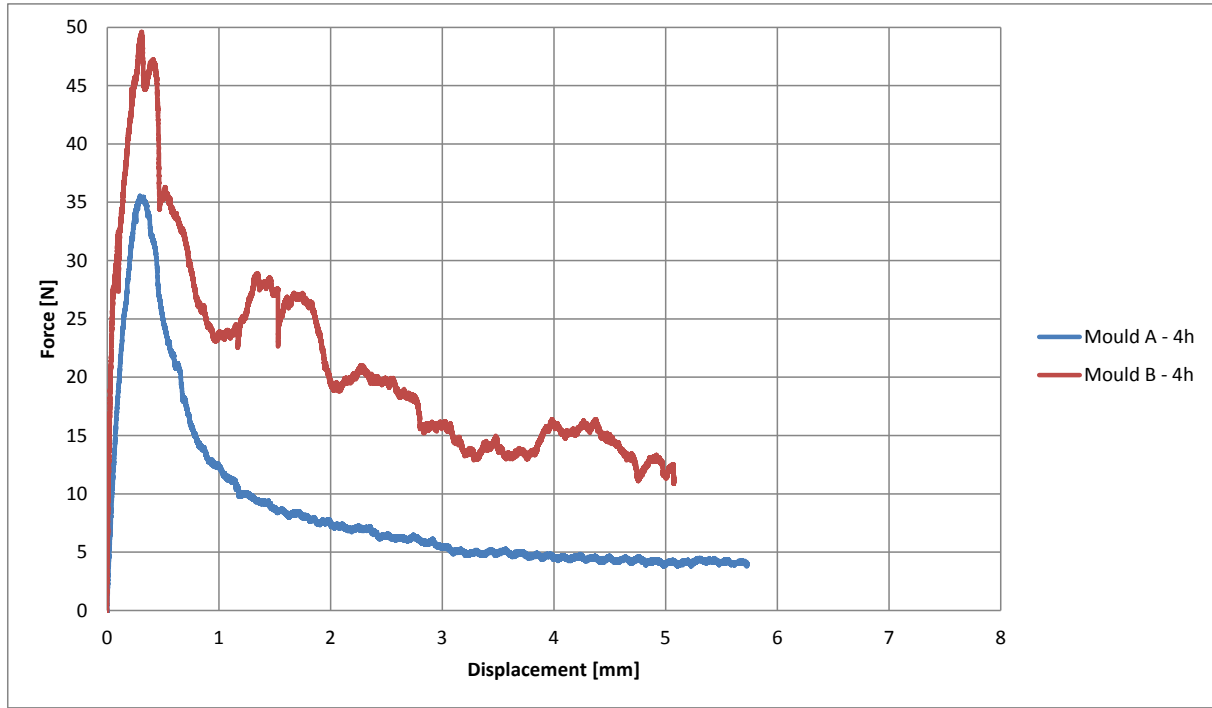

Figure A.8: Force-displacement curve of 4h specimens

It is believed that the use of the plates to support the fresh concrete was not effective since suspended fine particles in the plastic concrete could intrude into the interface between the plates and this caused significant friction. This led to an overestimation in the tensile strength as well as sharp rises and sudden drops in the force-displacement curve for both the plastic and semi-solid specimens. Mould A on the other hand provided adequate support to the early age concrete in its plastic state. When sufficiently lubricated it did not exert significant friction on the specimen in its semi solid state over the gauge length. Taking this into account, it was decided to used Mould A as the tensile testing mould in this study.

During this study its effectivity was confirmed by the formation of multiple cracks over its transition zone and neck for fresh concrete specimens and a single discrete crack over the cross section of the gauge length for specimens which had already reached the initial setting time.

A.4. Summary

This appendix describes the tensile testing mould design setup as used in this study. Firstly, an introduction, identifying the requirements of the tensile testing mould and discussing a

possible solution is presented. Next, two mould designs are introduced and discussed. Mould A is identified as the better choice and described in more detail with regards to its connections between the mould halves, weight, transportation and maintenance. Finally, this decision is verified and the performance of the two mould designs is evaluated. It is found that Mould A performed sufficiently and meets the requirements for a tensile testing mould as needed for this study.

Appendix B: Air bearing design and evaluation

This appendix describes the air bearing used in this study. Firstly, an introduction, identifying the specific requirement of the bearing system needed for this study is discussed. The air bearing is identified as the best option and a brief background study is presented. Next, the different facets of the air bearing design, regarding its load bearing capacity and structural integrity, are discussed. The key aspects of the manufacturing and construction processes are then elaborated on. The air pressure system is described briefly and finally, the performance of the air bearing is evaluated.

B.1. Introduction

From the evaluation of the literature study on the tensile properties of early age concrete in Section 2.2 and 2.3 as well as the tensile testing apparatus presented in Section 4.1 and the initial test setup and results discussed in Section 4.2, the following requirements regarding the bearing system for allowing linear motion during the displacement of the early age concrete test specimens, were identified.

- During linear motion friction must be eliminated as far as possible. This is because the tensile strength of early age concrete is so low, that the presence of friction during testing will result in an overestimation of the specimens' tensile strength, Young's modulus and fracture parameters.

- The bearing system must be able to level accurately and easily, and should be robust enough not to require re-levelling after testing. If insufficient levelling of the bearing system occurs, the effects of gravity play an unwanted role in the tensile test results. During the initial testing, the use of mechanical bearings proved very troublesome in this regard. It was not always possible to have the mould in contact with all the bearing surfaces during testing and this contributed to the unreliability of the initial results.

- The bearing should be robust, durable and provide repeatable performance. During the tensile testing of early age concrete, especially fresh concrete, there is usually concrete residue present after the testing process. The bearing system should be robust and durable enough not to let repeated testing influence its performance.

Taking this into account, the use of an air bearing, as utilised in the studies presented by Hannant, et al. (1999), Branch, et al. (2002) and Doa, et al. (2009) was determined to be the best bearing option for this study.

Air bearings, also known as aerostatic bearings, operate on the principle of a thin film of high pressure air to support a load and act as a lubricant medium. This air flows continuously from the bearing into the atmosphere. Since air has a very low viscosity, air bearing gaps are very small, usually from 1 to 50 μm. Although air bearings have a moderate load capacity and damping when compared to other types of bearings, their greatest advantage is that they offer absolutely zero static friction as well as negligible dynamic friction forces at speeds lower than 2 m/s. The only contributing factor to friction in an air bearing is viscous friction as a result of the shearing of the air film during motion (Slocum, 1992).

An air bearing's load capacity can be determined roughly by multiplying the effective projected bearing area by the entry pressure of the air as it enters the bearing clearance. The projected bearing area can be estimated as the area contained between the inlet orifices plus half the area situated outside the enclosed orifice area, towards the edge of the bearing. Thus, for the air bearing described in Figure B.1, the load capacity could be approximated as:

$$F = (b - a)(L - a)P_d$$

With F representing the bearing load capacity, P_d representing the orifice exit pressure and the projected bearing area dimensions as shown in Figure B.1.
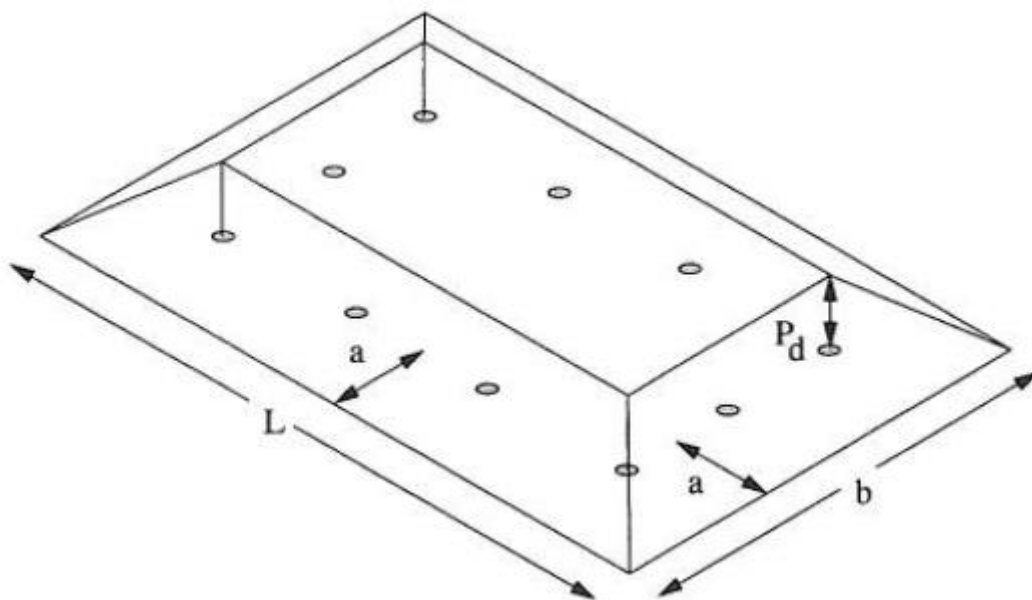

Figure B.1: Parameters for determining the load capacity (F) of air bearings (Slocum, 1992)

Air bearings are also very forgiving in the sense that they are able to average out local irregularities, which would usually result in an increase in friction. However, if the pressurised

air is not filtered and kept free from pollutants, the effectiveness of the air bearing will be impaired. The pressurised air supply is also required to be regulated. If this is not done, both the accuracy and repeatability of the bearing will be decreased. One of the biggest drawbacks associated with the use of air bearing is its use of an air pressure system and supporting equipment. The system must be kept exceptionally clean to prevent contaminants from clogging the flow regulating equipment. Generally it is required that the pressurised air be filtered to 1 µm. In some cases the use of a desiccant drier is also required to minimise condensation within the bearing as a result of the refrigeration effect that occurs when air expands and cools. Although it is prescribed to keep a cover over an air bearing when not in use in order to keep the bearing surface clean, air bearings can be considered self-cleaning, given that the air pressure system does not contain contaminants (Slocum, 1992).

With regards to the manufacturing of air bearings, the critical parameters to keep in mind are the maintaining of sufficient orifice and clearance dimensions. The orifice length should not be greater than four times its diameter and it is of critical importance that the orifice edges be as sharp as possible. Because of the small bearing clearance, tolerances are extremely small and high manufacturing quality is a necessity. If this is not achieved, the design load capacity will not be realised.

B.2. Air bearing design, manufacturing and construction

B.2.1 Load bearing theoretical design

The type of air bearing used in this study is called a rectangular flat pad bearing and is typically used in facilitation the linear motion of grinding machines, diamond turning machines and a variety of precision measuring instruments (Slocum, 1992). Figure B.2 shows a typical single-row-entry configuration on the left and a double-row-entry configuration on the right. For a standard single-row air bearing it is prescribed that $c/B = 0.5$ and for a double-row air bearing $a/B = 0.25$. Rectangular flat pad bearings are considered to be one of the most challenging pad bearings to design effectively as a result of the complex flow patterns from the inlet orifices to the bearing outlet, which occurs within the bearing clearance. Because of this it often occurs that insufficient pressure profiles are obtained within the bearing clearance. Many designers have found that simple analytical solutions and approximate models do not yield effective performance. To overcome this it is often necessary to use more sophisticated design approaches, such as finite difference calculations, to evaluate the load capacity, flow rate, and stiffness of a rectangular flat pad air bearing. The scope of this research project however did not allow for that. It was decided to use the approximate models presented in Precision Machine Design Section 9.3.5, by Slocum (1992), and to be very conservative in the entire design process.
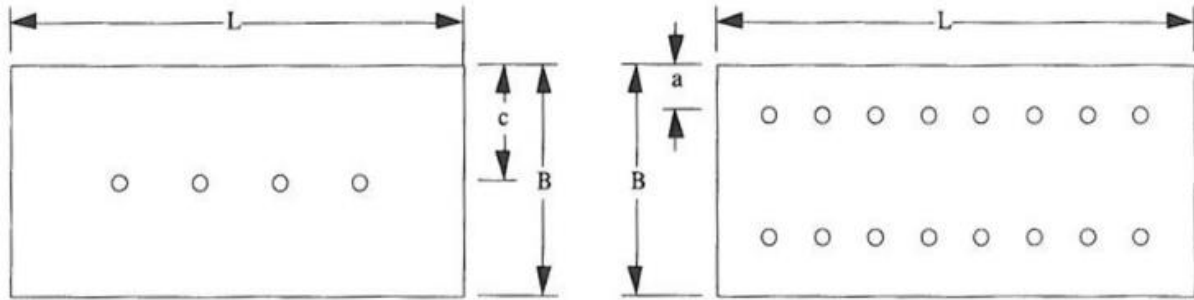
Figure B.2: Prescribed dimensions for single-entry and double entry air bearings (Slocum, 1992)

Taking into consideration the guidelines set out by Slocum (1992) in Precision Machine Design Section 9.3.5 for the design for rectangular flat pad bearings, the dimensions and weight of the early age concrete moulds that will be supported, and the capacity of the compressor that will provided the pressurised air supply, the following design requirements and parameters were determined:

- The design requirement for the bearing stiffness should be higher than 50 N/μm (Slocum, 1992)
- The design air clearance, h_0, will be taken as 30 μm.
- Two rows of eight orifices will be used to support the mould halves, thus n = 8 (the amount of orifice restrictors per row) and N = 16 (the total amount of orifice restrictors peasant on the air bearing). The double-row configuration, when compared to a single row, has the advantage that load capacity and air film stiffness is increased for an air bearing with the same surface area. The major disadvantage is that the rate of air flow is doubled. The double-row configuration also offers improved tilting resistance to the supported load
- The orifice type will be inherently compensated as it is the easiest to construct.
- With regards to the layout of the air bearing surface, as shown in Figure B.2, L = 690 mm, B = 200 mm and a = 50 mm, to satisfy a/B = 0.25. The orifice entries will be spaced 90 mm apart. This is in agreement with the dimensions of the tensile testing mould that is to flout on the air bearing surface.
- With regards to the pressure supply, although the available compressor can achieve a pressure of 0.7 MPa, it is not able to sustain this pressure for long periods of time. Thus a design supply pressure of P_0 = 0.5 MPa will be used, while P_a, the atmospheric pressure, will be taken as 0.1 MPa.
- The weight of the moulded concrete specimen that the air bearing will need to support is approximately 80 kg, as discussed in Appendix A.

The following design steps were taken using the above mentioned design parameters. (Slocum, 1992):

1. Calculate the bearing shape factor ξ from Equation 9.3.42.b:

$$\xi= \frac{\pi 2a}{L} = \frac{\pi \cdot 2 \cdot 50}{690} = 0.455$$

$$N\xi = 16 \cdot 0.455 = 7.28 \ldots \ldots \ldots \ldots \ldots \ldots \ldots \ldots \ldots \ldots \ldots \ldots \ldots \ldots \ldots \ldots \ldots \ldots \ldots \ldots \ldots . (A)$$

2. Calculate the diameter of the inherently compensated restricting orifice, d_0, from Equation 9.3.45.b and taking $A_s\xi = 0.55$ for optimal stiffness air film stiffness:

$$A_s\xi = \frac{32.55nd_0\pi B}{P_0 n_0^2 L}, \quad rearranged$$

$$d_0 = \frac{A_s\xi P_0 n_0^2 L}{32.55n\pi B} = \frac{0.55 \cdot 0.5 \cdot 30^2 \cdot 690}{31.55 \cdot 8 \cdot \pi \cdot 200} = 1.08 \approx 1\ mm$$

$$\frac{nd_0\pi}{L} = \frac{8 \cdot 1 \cdot \pi}{690} = 0.064 \ldots \ldots \ldots \ldots \ldots \ldots \ldots \ldots \ldots \ldots \ldots \ldots \ldots \ldots \ldots \ldots \ldots \ldots \ldots . (B)$$

3. Using the values determined in (A) and (B) and Figure 9.3.18, as shown below, $1/\lambda$ is determined to be = 0.4.

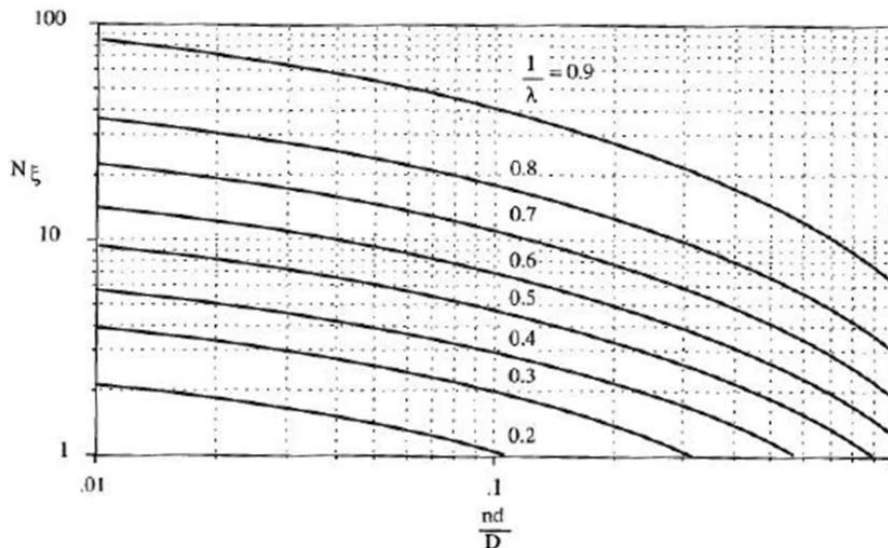$$\frac{1}{\lambda} = 0.4 \ldots \ldots \ldots \ldots \ldots \ldots \ldots \ldots \ldots \ldots \ldots \ldots \ldots \ldots \ldots \ldots \ldots \ldots \ldots \ldots \ldots \ldots \ldots \ldots . (C)$$

Figure 9.3.18 Determination of l/λ.

4. Calculate the stiffness of the air film, K: The term $\overline{K}$ was determined using Figure 9.3.32, as shown below, and the values $A_s\xi = 0.55$ and (C) to be 0.251:
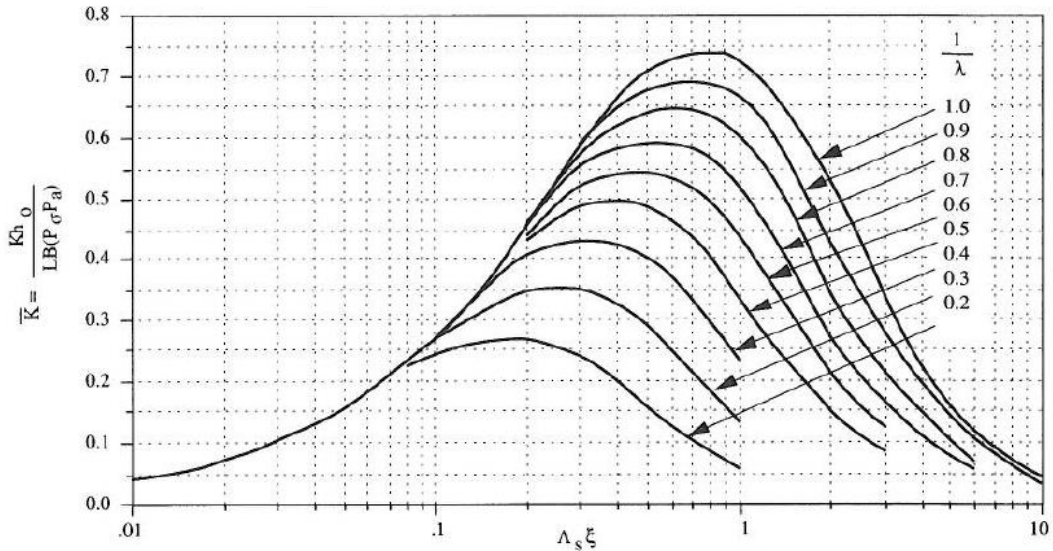
168

Figure 9.3.32 Stiffness parameter for rectangular double-entry thrust bearings with pocketed orifices where a/B = 0.25, P_0/P_a = 5, C_d = 0.8, and ν = 1.4. For inherently compensated orifices, multiply the ordinate by 0.67. For single-entry bearings, multiply the ordinate by 0.75.

$$K = \frac{\overline{K}LB(P_0 - P_a)}{h_0} = \frac{0.251 \cdot 690 \cdot 200 \cdot (0.5 - 0.1)}{30} = 462\,N/\mu m$$

5. Calculate the load capacity, W: The term $\overline{W}$ was determined using Figure 9.3.33, as shown below, and the values $A_s\xi$ = 0.55 and (C) to be 0.325.
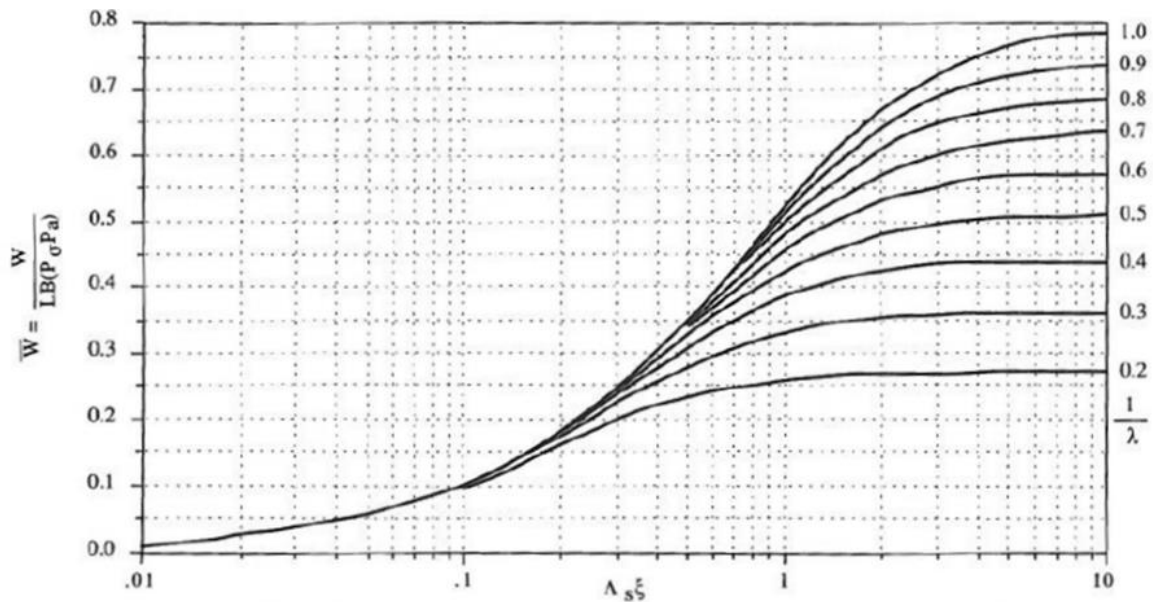

Figure 9.3.33 Load parameter for rectangular double-entry thrust bearings with pocketed orifices where ε = 0, a/B = 0.25, P_0/P_a = 5, C_d = 0.8, and ν = 1.4. For single-entry bearings, multiply the ordinate by 0.75.

$$W = LB(P_0 - P_a)\overline{W} = 690 \cdot 200 \cdot (0.5 - 0.1) \cdot 0.325 = 17900\,N$$

Even if a 50% reduction in the load capacity was assumed (8950 N = 895 kg) to take into account any errors that might have occurred during the design and manufacturing of the air bearing, it would still have more than sufficient load capacity to support the early age concrete specimens at a weight of approximately 80 kg. It should be noted that it is preferred that the air bearing does not operate close to the maximum capacity of the pressurised air system as this would be less stable, could lead to the disturbance of the early age concrete specimen and would leave no room for errors or unforeseen issues.

6. Finally, determine the flow rate of air required, G. The term $\overline{G}$ was determined using Figure 9.3.34, as shown below, and the values $A_s\xi = 0.55$ and (C) to be 0.24.

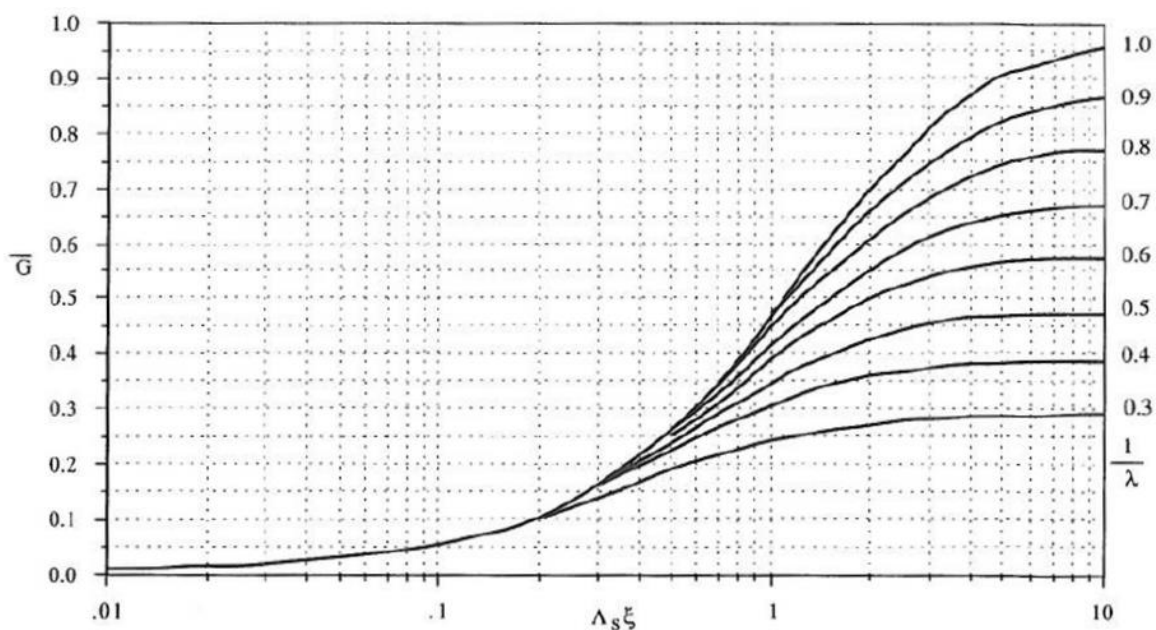
Figure 9.3.34 Nondimensional flow rate for rectangular double-entry thrust bearings with pocketed orifices where a/B = 0.25, P_o/P_a = 5, C_d = 0.8, and ν = 1.4. For single-entry bearings, multiply the ordinate by 0.5.

$$G = \frac{h_0^3 P_0^2 \overline{G}}{3.42 \cdot 10^6 \xi} = \frac{30^3 \cdot 0.5^2 \cdot 0.24}{3.42 \cdot 10^6 \cdot 0.455} = 62.5 \, l/min$$

This required flow rate, approximately determined, was also well within the capacity of the available compressor.

B.2.2. Structural design

After the bearing layout, orifice dimensions and load bearing capacity of the air bearing were determined, the physical structure of the air bearing needed to be designed. As an air bearing is a pressure vessel, it is of great importance to ensure that it has sufficient capacity to withstand its internal pressure. If not, the consequences could prove fatal. From a safety point of view, it was decided that steel would be used as the primary construction material

and where applicable, the SANS 50286-1 code was used to design the air bearing. The ultimate limit state design was done assuming an internal pressure of 0.7 MPa, the maximum pressure that the compressor system was able to generate.

However, the guideline, as stipulate in the SANS 50286-1 code, was not applicable to air bearing design from a serviceability point of view. The most important aspect to take into account was the surface deflections caused by the pressurised air. As the design bearing clearance was only 30 μm, the surface deflections caused by the bearing's internal pressure needed to be kept to a minimum. The serviceability limit state design was done assuming an internal pressure of 0.5 MPa, the maximum pressure at which the compressor could be operated in a stable manner for an extended period of time.

No standard design guidelines for rectangular pressure vessel could be found that deliver accurate approximations of stresses and displacements. As a result, the rectangular steel pressure vessels was analysed using finite element methods (FEM). The software package utilised for these analyses was Abaqus 6.12, developed by Simulia. A variety of air bearing structure designs were considered and numerous FEM analysis were performed under the ultimate limit state loading condition and the serviceability state loading condition. After substantial planning, taking into account the required surface rigidity of the bearing, the limitations of the CNC machines and the construction process as well as its functioning and maintenance, a final air bearing structure design was determined. The air bearing, consisting of two parts, a base and surface, is illustrated are Figure B.3 - B.7. The material decided to use to manufacture the air bearing parts was a class C 50 carbon steel. The reason for using this material was its favourable material properties, most significantly its high Young's modulus and harness, and its availability. The steel's material properties are:

- Tensile strength = 450 MPa
- Yield strength = 345 MPa
- Young's modulus = 205 GPa
- Poisson ratio = 0.27
- Density = 78000 kg/m^3
- Hardness = 181 – 269 HB

Through FEM analysis it was determined that the base and surface parts had more than sufficient capacity to withstand the ultimate limit state loading condition. The serviceability limit state proved to be the determining factor in the design process. It was decided that a maximum displacement of 1.2 μm on the surface of the air bearing, under the serviceability loading conditions, was acceptable as it would not decrease the bearing clearance

significantly and thus not influence the performance of the bearing to a great extent. The two longitudinal legs of the surface part, which would fit into the base part, were spaced as close as possible effectively decreasing the beam length over the width of the surface part. By adding more material to the bearing surface this displacement could be further decreased, with the penalty of added weight and manufacturing cost. Thus an optimum balance between the surfaces part's weight and its maximum displacement at its centre needed to be found. Because the air bearing would occasionally be handled, it could not weigh too much. It was decided that the total air bearing weight of 95 kg, that corresponds to a maximum surface deflection of 1.2 μm, was acceptable. The exaggerated deformations of one quarter of the air bearing surface, found from the FEM analysis, is shown in Figure B.3. The symmetry of the surface was taken into account during the analysis by modelling a quarter of the surface part with appropriate boundary conditions. The leg of the surface part, where it would fit into and be bolted to the base part, was modelled as fixed along its length.
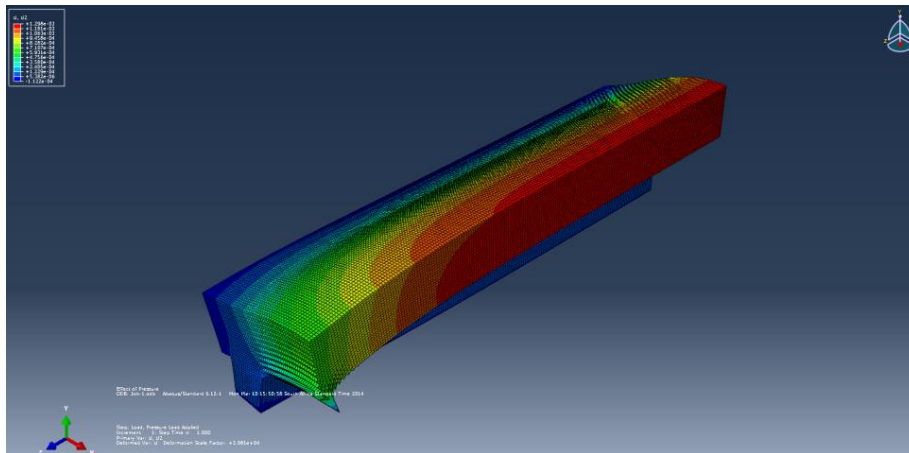

Figure B.3: Deformed shape of a quarter of the surface part

The final assembled shape along with significant dimensions of the rectangular air bearing box is shown in Figure B.4. The surface and base parts, shown in Figure B.5 and B.6 respectively, were designed to fit into each other. This was achieved by a rectangular interface zone with corresponding 2 and 5 mm radii on both the surface and base parts. These radii were adopted as the CNC machine in certain instances could not produce perfect sharp angles. As a result no cavities existed in the interface between the two parts when assembled and the pressurised air cavity was perfectly sealed. This was confirmed by means of a sectional analysis on the Inventor AutoCAD software package. In effect, the assembled air bearing box could be viewed as a solid continuous structure with an internal cavity.
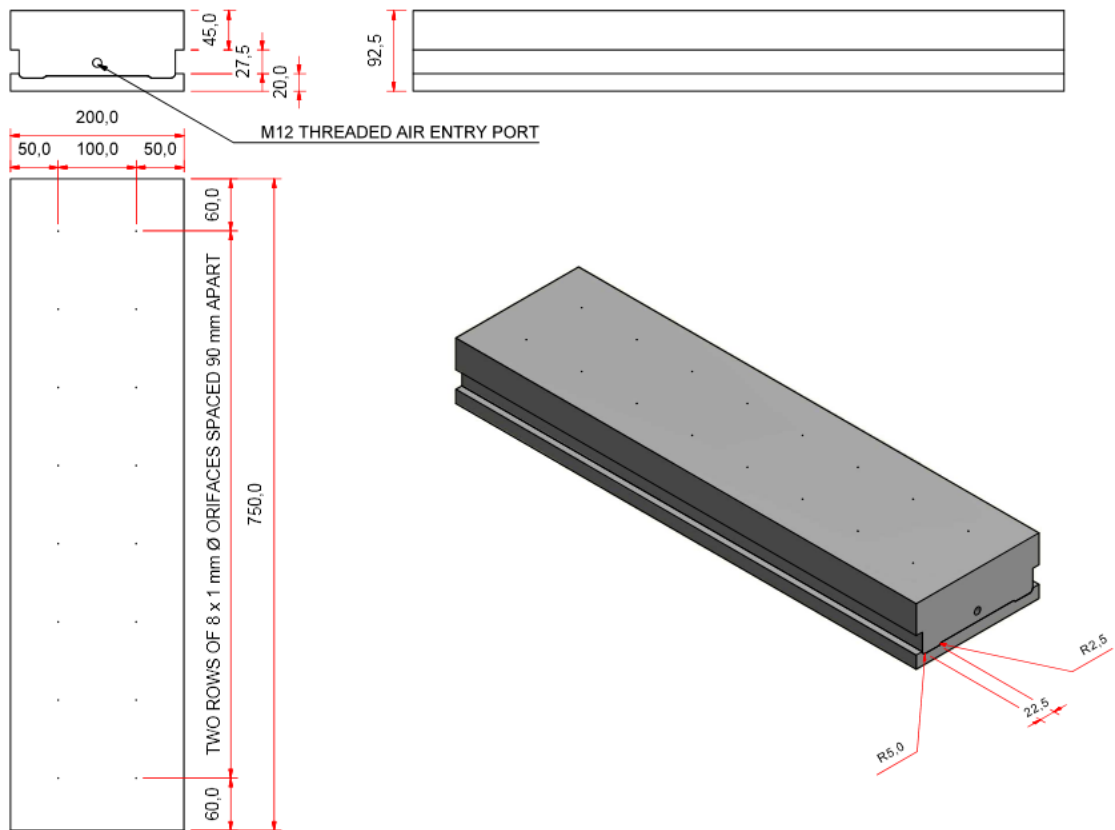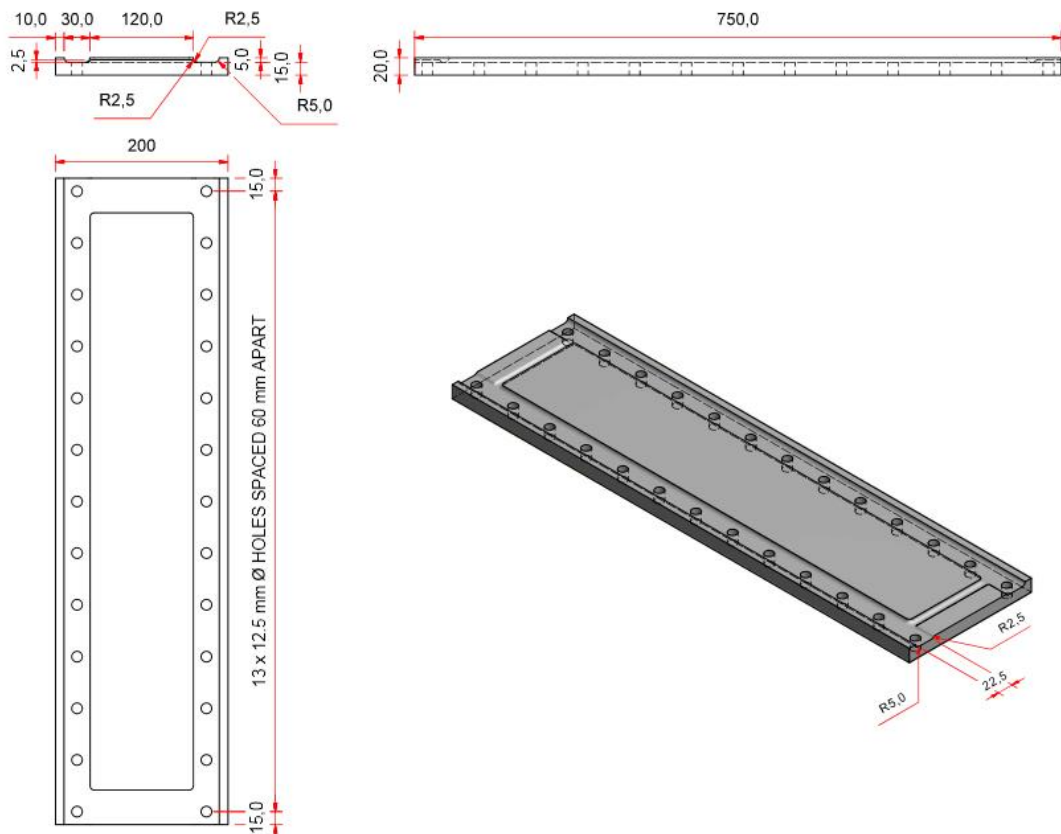
172

Figure B.4: Assembled air bearing
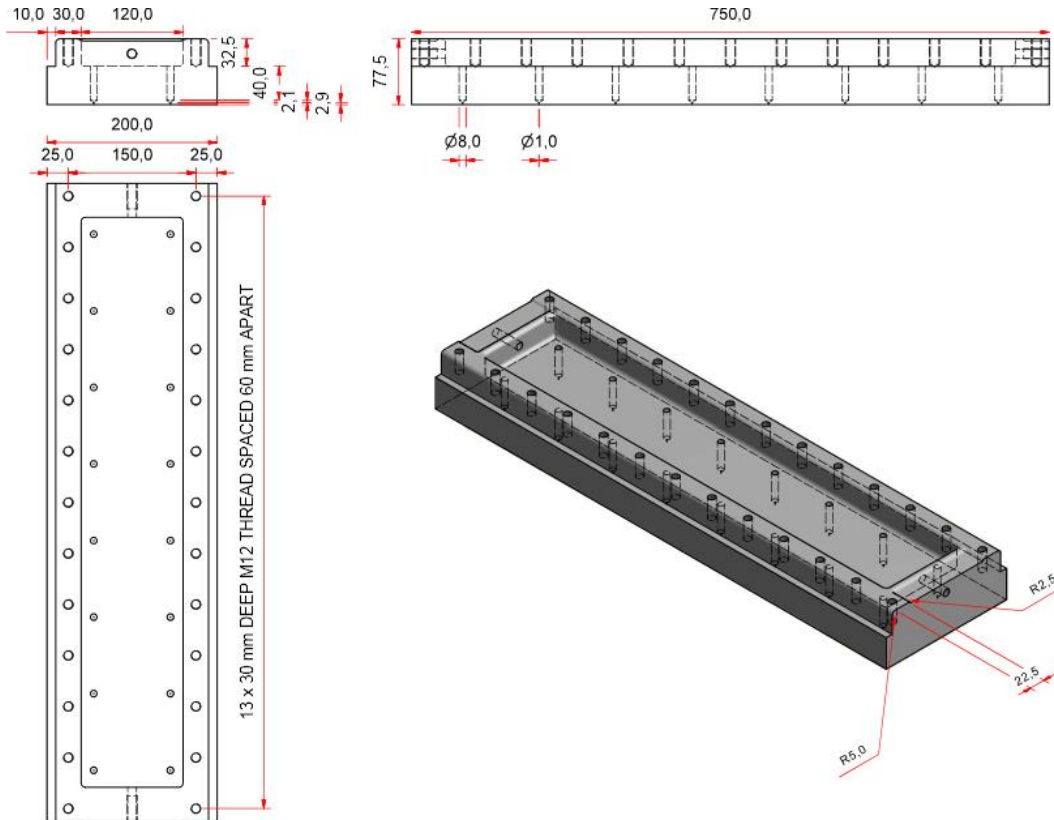
Figure B.5: Base part

173

Figure B. 6: Surface part –upside down

B.2.3. Air bearing construction

Due to the small bearing clearance and the accuracy and tolerances required in the manufacturing of the air bearing, a CNC milling machine was used to manufacture its parts from two solid C 50 steel blocks. This allowed for an extremely smooth surface finish and a production accuracy of 8 μm. With regards to the manufacturing of the restricting orifice, a 40 mm long 8 mm diameter hole with an approximately 2.1 mm long taper at its end was first drilled into the inside of the air bearing surface. After this, a 1 mm hole was drilled from the surface, meeting the centre of the 8 mm hole. The surface was then given a smooth milling finish and the 1 mm orifice holes were cleared to ensure that they have as sharp as possible edges. The end product was a 1 mm diameter orifice which was approximately 2.9 mm long, meeting the requirement stating that the orifice length must not be greater than four times its diameter as stipulated in Precision Machine Design (1992). This orifice design is shown in the top left corner of Figure B.6. The manufactured base and surface parts are shown in Figure B.7.The rectangular interface zone can easily be identified on both parts. Under the influence of an internal pressure, the interface allowed for the fixing of the parts in the horisontal direction, but not the vertical direction. Consequently, the parts had to be securely fixed to keep them from moving apart in the vertical direction during operation.
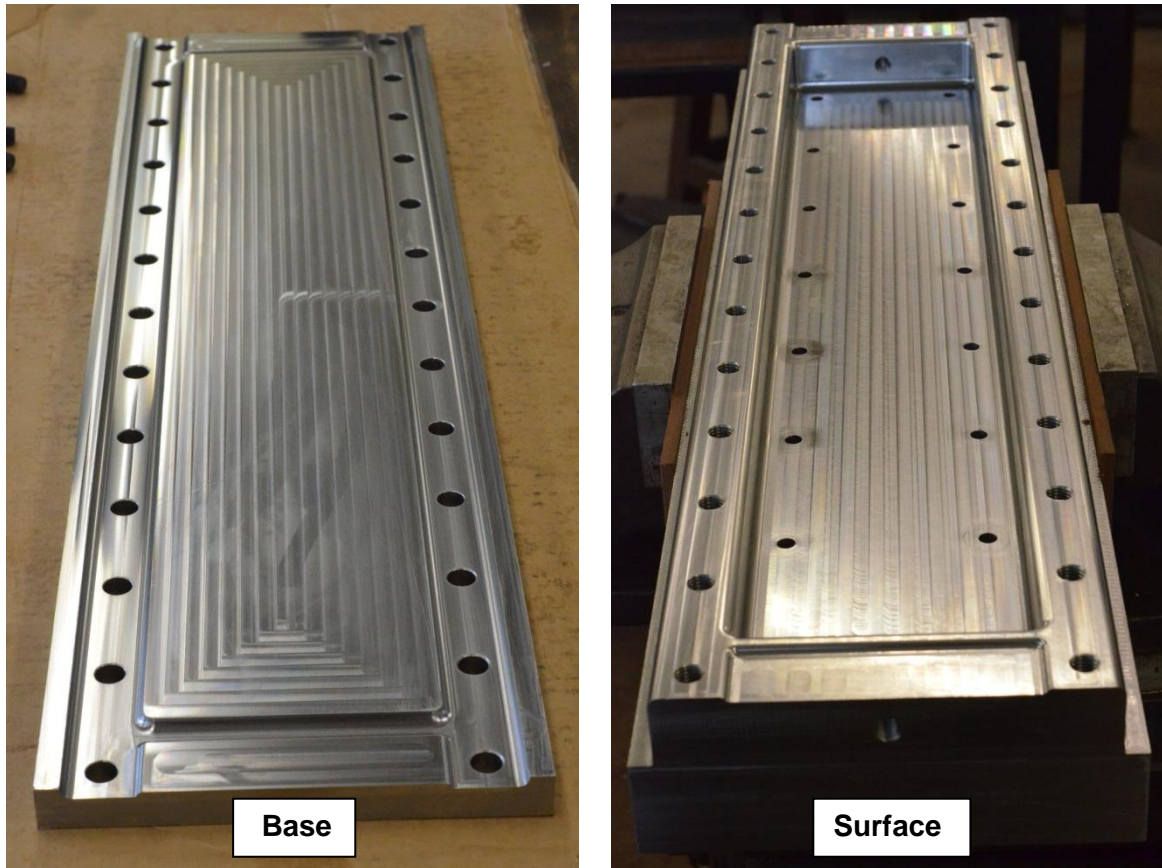
Figure B. 7: Air bearing parts with interface zone shown

SANS 50286-1 (1998) prescribes welding as the preferred method of assembly and bonding for pressure vessels. The heat generated during welding would however lead to warping and deformation of the air bearing parts, causing the interface not to fit seamlessly, the surface not to be perfectly level and ultimately the air bearing not to perform effectively. For this reason the two air bearing parts were bonded and sealed using a combination of pre-tensioned bolts and gasket sealing compound. Note that the air bearing base has 26 x 12.5 mm diameter holes, while the air bearing surface has a corresponding 26 x 30 mm long M12 threaded holes to allow for the use of bolts. Once again, the design approach was very conservative as the ultimate tensile force per bolt was $T_u = 2.88$ kN and the capacity of the M12 class 10.9 bolts used were $T_r = 67.5$ kN per bolt (SANS 10162-1, 2011).

With regards to the assembly procedure, the bearing surface was first clamped firmly with its interface at the top and surface protected from scratching at the bottom, as shown in Figure B.7. Next a non-corrosive, oil resistant gasket sealant, Loctite SI 5980, was applied to the interface zone as prescribed. After the base was placed on the surface, a small amount of appropriate lubricant was applied to the surface thread, hardened washers were place over the air bearing base hole and 22 x M12 class 10.9 bolts were inserted in the centre holes and systematically tightened until the snug-tight condition was achieved with an

175

ordinary spanner. To ensure the air bearing stays air tight under pressure, the bolts were preloaded using the torque method specified in ISO 898-1. For a given preload tension, $T_{u\ =}$ 50 kN, a bolt diameter, d = 12 mm, and a known friction factor, in the case where lubricant is used k = 0.15 to 0.18, the following simplified formula was used to determine the needed torque:

$$T = kdT_u$$

$$T = 0.18 \cdot (12 \cdot 10^{-3}) \cdot (50 \cdot 10^3)$$

$$T = 108 \, N.m$$

Using a torque wrench, the bolts were systematically fastened to an ultimate torque of 108 N.m.

To create a robust and accurate adjustable levelling system, four 90 mm long M12 threaded rods were screwed into tho corner holes. Two nuts and a dome nut, as shown in Figure B.8, were attached to each leg. The top nut locked the M12 thread, and once the bearing surface had been perfectly levelled, the bottom nut locked the dome nut in its position.

Figure B.8: Threaded levelling system

B.2.4. Air pressure system

A schematic representation of the pressurised air supply system is shown in Figure B.9. Pressurised air was supplied to the air bearing from both sides so that a pressure differential would not occur over its length. A FR1M, manufactured by Air System Pneumatic, was used

176

to both filter and regulate the pressurised air supply. All particles larger than 20 μm were filtered, and this proved to be more than sufficient for the 1 mm diameter orifice restrictors. Initial testing confirmed that the use of a dryer was not required as no condensation of water was witnessed in the area of the bearing surface after sustained periods of operation.
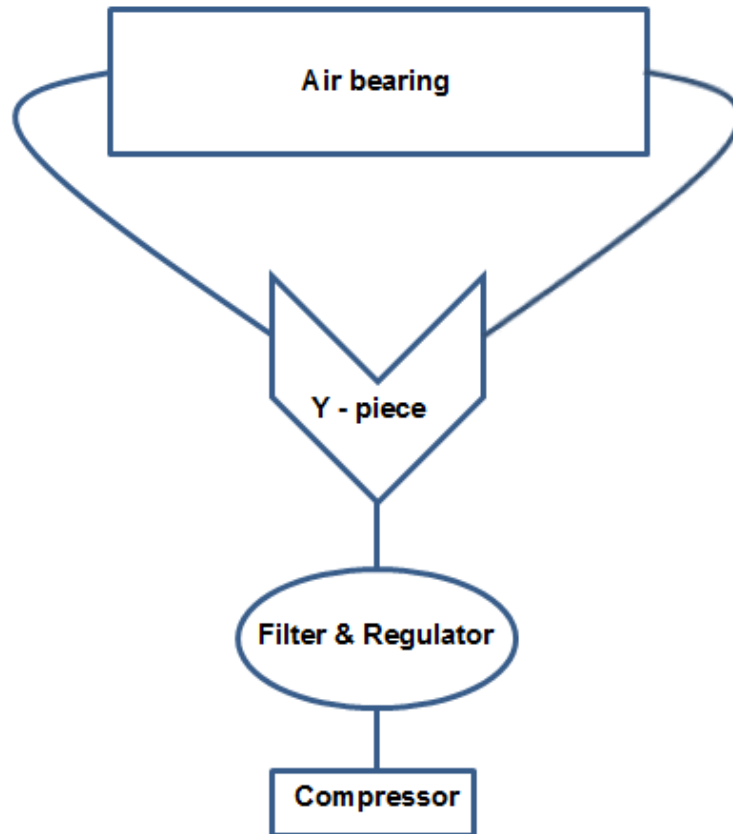

Figure B. 9: Air pressure system schematic

B.3. Performance evaluation

The completed air bearing, set up for consistent usage, is shown in Figure B.10. It was found that the air bearing could float a complete specimen, weighing approximately 80 kg, at a pressure of 1.2 bar. During linear motion the air bearing offered practically zero friction. The levelling system proved to be sufficient and robust, as it never had to be adjusted during the testing period after it was set up correctly. During the duration of the testing period, the performance of the air bearing and its supporting equipment remained effective and constant, contributing to the consistency of all experiments conducted.
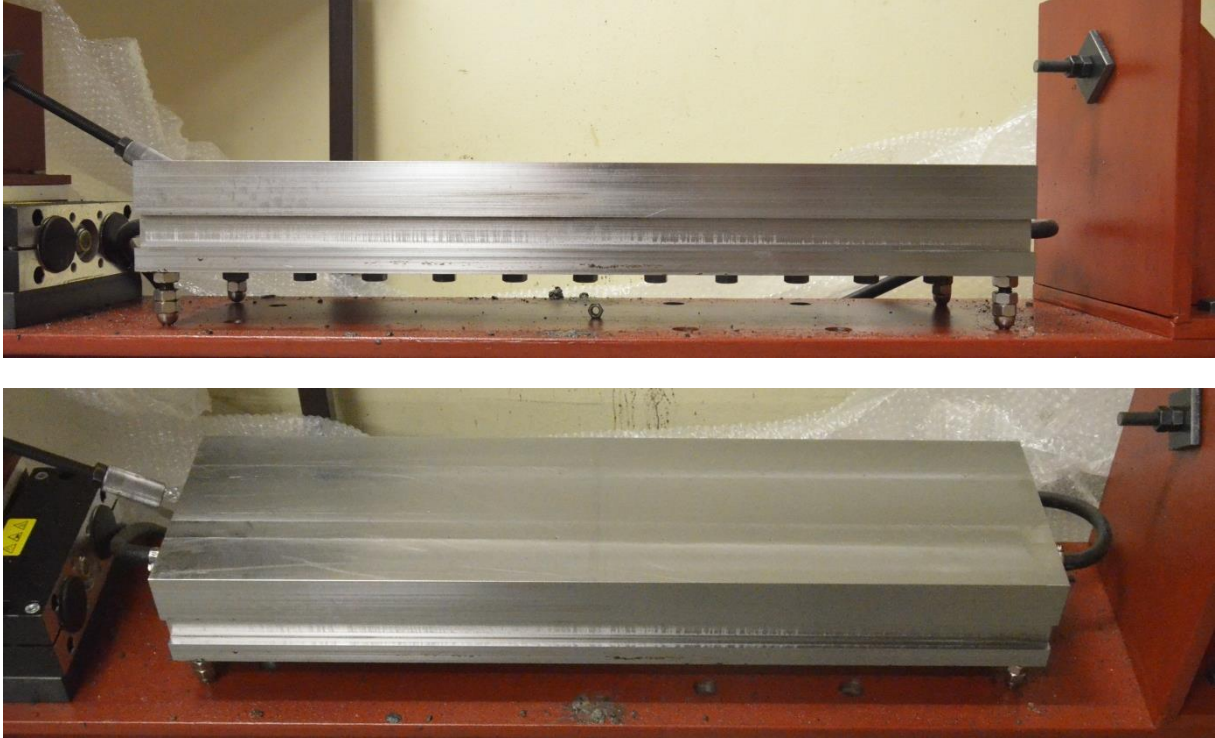
Figure B.10: Complete air bearing set up for operation

B.4. Summary

This appendix describes the air bearing used in this study. Firstly, the requirements of the bearing system are discussed, whereafter the most viable option is identified as an air bearing. Next, the design process in terms of load bearing capacity and structural integrity is described. The key aspects of the manufacturing and construction processes are elaborated on and the air supply system is briefly discussed. Finally, the performance of the air bearing is evaluated and it is found to satisfy all the requirements of this study.

Appendix C: Linear actuator design and evaluation

This appendix describes the linear actuator used in this study. Firstly, an introduction, identifying the specific requirements of the load application method for this study is discussed where after the most viable options are introduced. Next the components of the linear actuator setup and the design and construction process are described. Finally, the performance of the actuator is evaluated.

C.1. Introduction

From the evaluation of the literature study on the tensile properties of early age concrete in Sections 2.2 and 2.3, the tensile testing apparatus presented in Section 4.1 and the initial test setup and result discussed in Section 4.2, the following regarding the means of load application for the direct tensile testing of fresh concrete was identified.

- The means of loading must be displacement controlled, in other words; it must be able to exert an actively varying tensile force at a constant displacement rate.

- In order to obtain reliable post-peak behaviour of the early age concrete specimens, an extremely slow displacement rate is required. Doa, et al. (2009) used a displacement rate of 0.05 mm/min as to attain sufficient resolution of the post-peak stress-displacement curve.

- The apparatus must be able to exert a tensile force of 1.5 kN. This was determined by assuming the maximum tensile strength of a specimen to be 90 kPa, as was the case for convention early age concrete of the same age as determined by Doa, et al. (2009). Taking into consideration that the neck of the tensile test mould has a cross sectional area of 100 x 140 mm^2, a maximum required force of 1.26 kN is expected.

- The means of load application must be rigid as to keep the mould halve from moving apart and disturbing the fragile concrete specimen just prior to testing, when the supporting frame of the moulds are detached. In the case of concrete mixes with high slump values at extremely early ages, the effect of the hydrostatic pressure on the inside of the tensile testing mould caused the separation of the specimen while a pulley system was used for load application for the initial test setup.

- The apparatus used for the load application must be portable to allow for the testing of specimens under different climatic conditions during later studies.

With this in mind, various linear actuators utilising a variety of mechanisms to generate linear motion were identified as possible options. The only two financially feasible options that satisfy the above mentioned requirements were found to be the following: First, the Zaber

NA34C60-T4 which made use of an incremental stepper motor. The second was a multi component actuator assembly proposed by Horne Technologies in Pretoria. After critically evaluating both options, it was decided that the effect of the incremental displacements, although just 0.198 μm in size, produced by the stepper motor, would cause unwanted accelerations and consequently disturbances of the early age concrete specimen.

C.2. Linear actuator setup design and construction

C.2.1. Motor assembly

The electrical motor assembly, together with its motion controller, was manufactured by FAULHARBER, in Germany. The motor used is a 3268G024BX-3692 brushless DC-servomotor, capable of exerting 92 mNm, with an additional encoder (FAULHABER, 2012a). The IE3-1024-L encoder is built into the motor, creating a closed loop feedback system. This encoder option offers 1024 lines per revolution, the highest possible rate of all available encoder options. This ensures that the motor revolves at as stable as possible constant rate under a varied load (FAULHABER, 2012b). To achieve the extremely slow displacement rate required a 32A-2076:1 planetary gearhead was fitted to the front portion of the brushless DC-servomotor. The reduction ratio of this planetary gearhead is effectively 2076:1 (FAULHABER, 2012d). Although the motor unit on its own could exert 92 mNm, with the effect of the gearhead, this would translate to 19 Nm (0.092 X 2076). As the gearhead has a maximum capacity of 4.5 Nm, a torque limit of 4.5 Nm was placed on the assembly motor upon manufacturing. The motor unit with planetary gearhead is shown in Figure C.1.
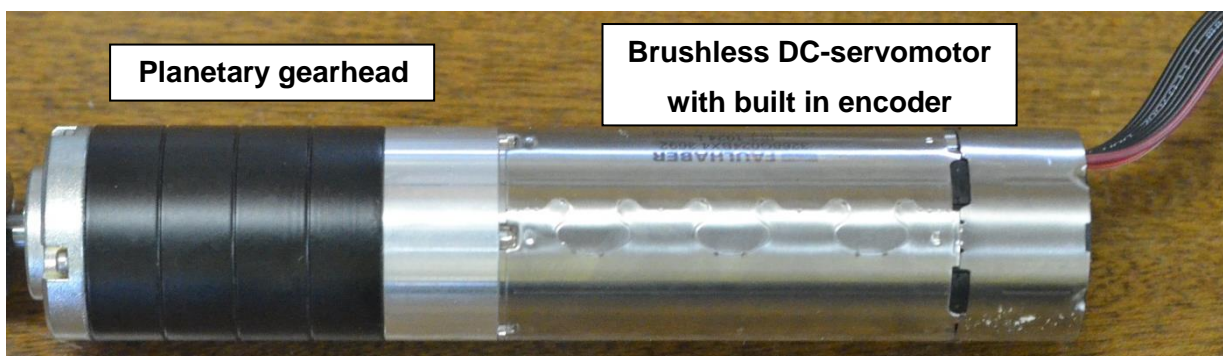

Planetary gearhead

Brushless DC-servomotor with built in encoder

Figure C.1 Brushless DC-servomotor with planetary gearhead

The last component of the motor assembly is the MCBL 3006, specifically designed to be used in combination with FAULHARBER brushless DC-servomotor. All commands with regards to rotational velocity, duration, current limits, etc. were programmed onto the motion controller using the FAULHARBER Motion Manager 5.2 software package (FAULHABER, 2012c). A 24 Volt power supply was connected to the motor assembly in order to convert nominal 220 Volt power to the needed 24 Volts of the assembly. The motion controller and

the 24 Volt power supply are shown in Figure C.2. This rotary actuator assembly allowed for the accurate angular positioning and velocity required.
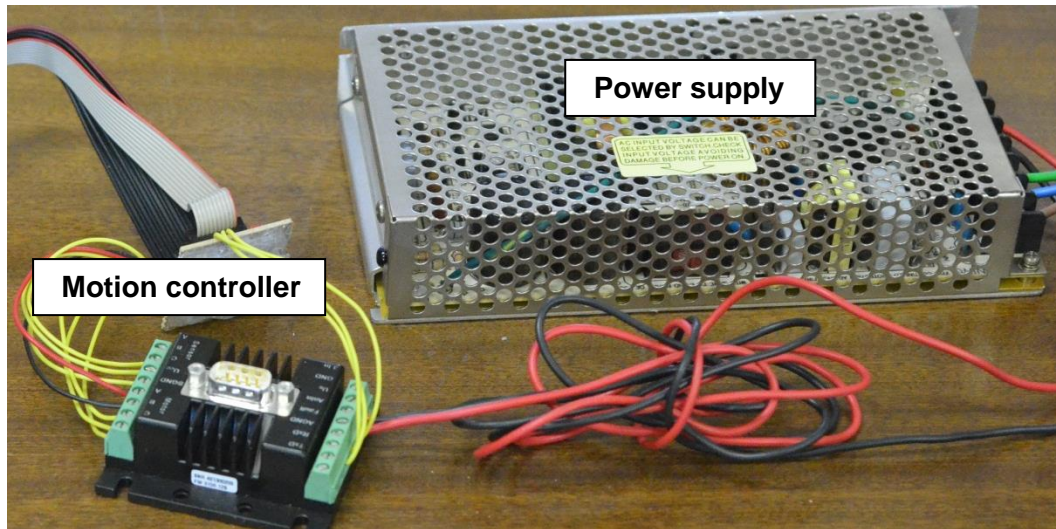

Figure C.2: Motion controller and power supply

C.2.2. Leadscrew linear actuator

In order to translate the rotation into linear motion, a mechanical linear actuator, manufactured by ROSE+KIEGER, was used. The EPX 50, as shown in Figure C.3, was the smallest model that could provide the needed loading conditions as stipulated in the Section C.1. This actuator makes use of two carriages, connected by a stainless steel fixing plate that slides over two robust steel tubes. The first carriage facilitates linear motion by means of a ball bearing leadscrew unit fitted around the rotating thread. The second free running carriage has the sole purpose of increasing the leadscrew actuator's resistance to bending moments during loading. A loading platform was bolted to the fixing plate and the test specimen mould would then be connected to the loading platform. This leadscrew actuator unit was securely bolted to the rigid 254x254x107 H-profile base.

With regard to the loading capacity of the linear actuator unit, its leadscrew unit could exert a maximum force of 1.7 kN (F_{max}), while the maximum moment that it could be resisted as a result of the maximum applied force was 345 Nm (M_{max}). Conservatively assuming a screw efficiency of 25%, the 4.5 Nm motor assembly would be able to generate a force of 2.3 kN through the leadscrew actuator, greatly exceeding its capacity. It was suggested by Horne technologies that an ampere limit be placed on the motor assembly, affectively limiting the torque to under the leadscrew actuator's capacity. However, this could not be achieved without altering the linear actuator's performance in an undesired manner. During this study, this was not an issue as a maximum force of 245 N was needed to be exerted to cause the failure of the strongest specimen during testing. This can however lead to difficulties in later

studies on stronger concrete specimens. It is thus of great importance that all people using this linear actuator are aware that the motor assembly can exceed the physical capabilities of the leadscrew actuator. When determining the maximum height at which the tensile force could be applied to the specimens through the loading structure, it was assumed that the maximum tensile force would also be applied simultaneously. The height of force application is indicated by a blue arrow in Figure C.3. Taking z as the distance from the centroid of the leadscrew actuator, where the leadscrew is situated, to the height at which the tensile force is applied to the specimens, z_{max} can be determined as follows:

$$z_{max} = {M_{max}}/{F_{max}}$$

$$z_{max} = {345}/{1700}$$

$$z_{max} = 0.203 \, m$$

By using steel spacers to lift the leadscrew actuator, the point of load application was kept well within this maximum height, as indicated in Figure C.3.
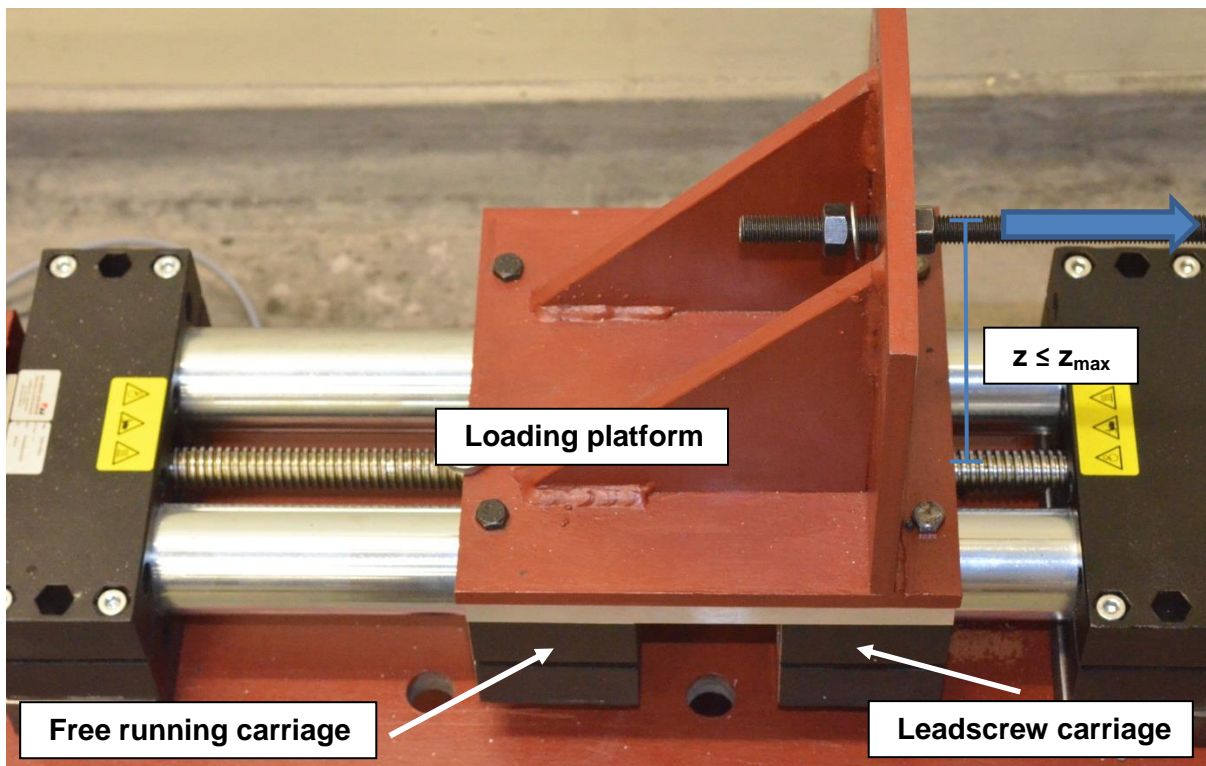

Figure C.3: Brushless DC-servomotor with planetary gearhead

C.2.3. Connecting flange, axial coupling and protective cover

Since the motor and actuator system were not from the same manufacturer, a standard connecting flange was not available. Thus it had to be designed and manufactured in order for the rotation of the motor assembly to be transmitted to the threaded axis of the linear actuator. This flange connection is shown in Figure C.4. It comprises of three aluminium components; one motor connector flange, as shown in Figure C.5 and Figure C.6, and two actuator connector flanges as shown in Figure C.7. Four M8 threaded steel rods were screwed into the leadscrew actuator in existing threaded holes to approximately a maximum depth. An actuator connector flange was then slid over both the bottom and top two threaded rods. The motor connector flange was securely screwed onto the motor-gearhead assembly, with the axial coupling being fastened earlier. The motor connector flange was then slid into the four steel rods as to connect both the axis of the motor and the leadscrew actuator with the axial coupling. Finally, the flange was systematically tightened to ensure a secure and flush fit.
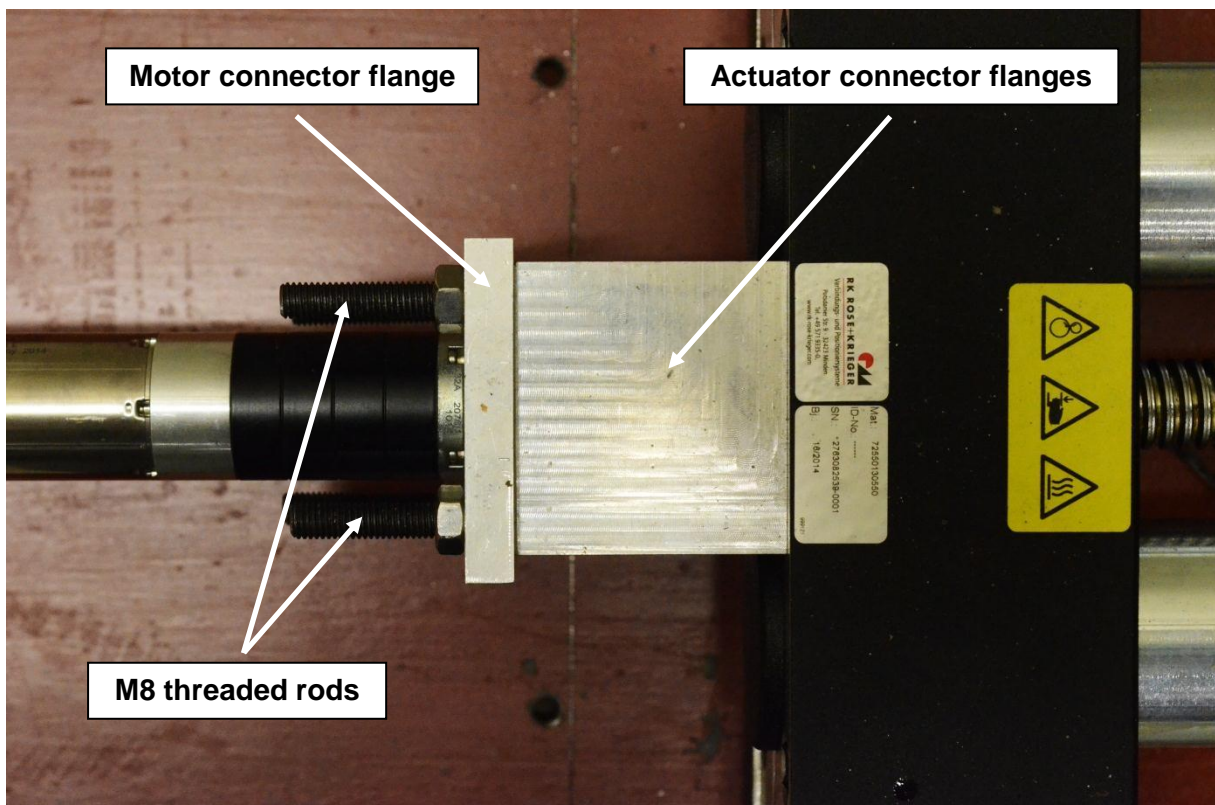

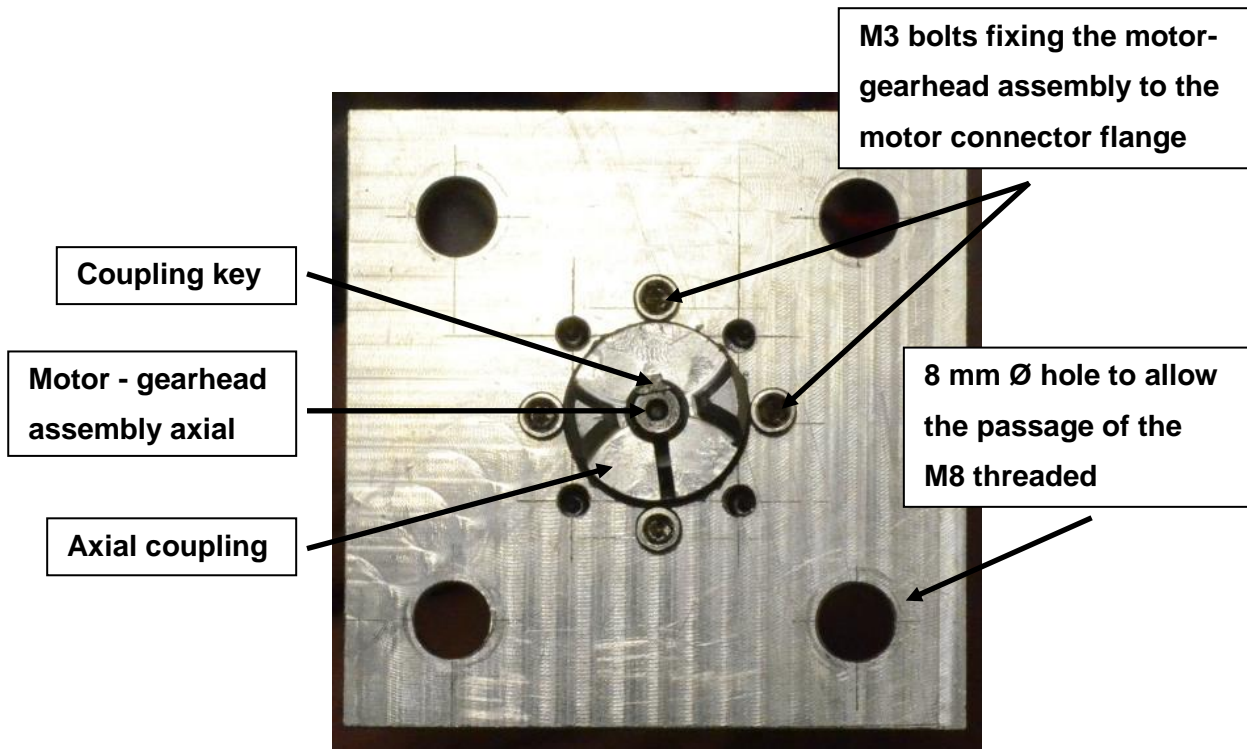**Figure C.4: Flange connecting the motor assembly and leadscrew actuator**

Figure C.5: Actuator connector flange screwed onto the motor assembly with the axial coupling and coupling key shown
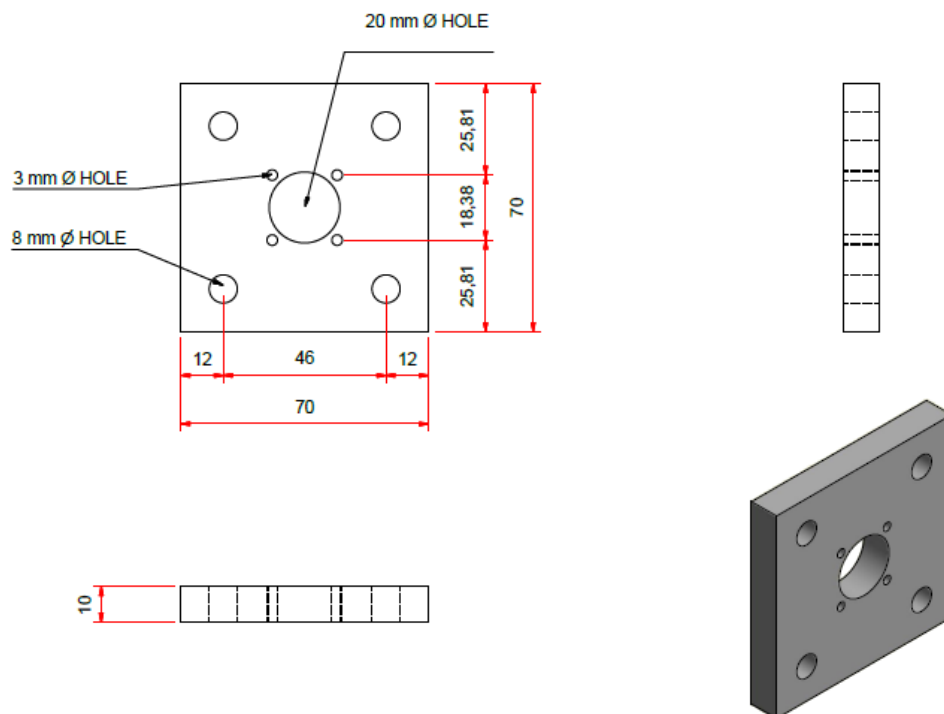

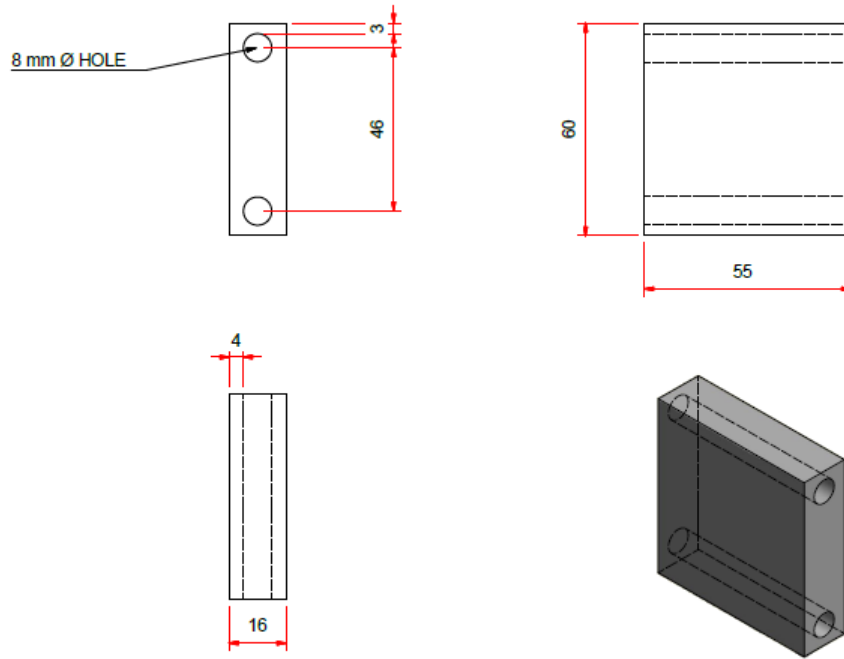**Figure C.6: Motor connector flange**

184

Figure C.7: Actuator connector flange

With regards to the axial coupling, a standard ROSE+KIEGER coupling was used. It was a perfect fit for the ROSE+KIEGER actuator axis; however, it was not entirely compatible to the FAULHARBER motor axis. To overcome this, a coupling key, as shown in Figure C.8 and Figure C.9, was used. Because of the part's size and small tolerances required, the key was manufactured by a CNC machine. A perfect snug fit was achieved, as illustrated in Figure C.5, and the axis of the motor and leadscrew actuator was lined up and connected effectively.
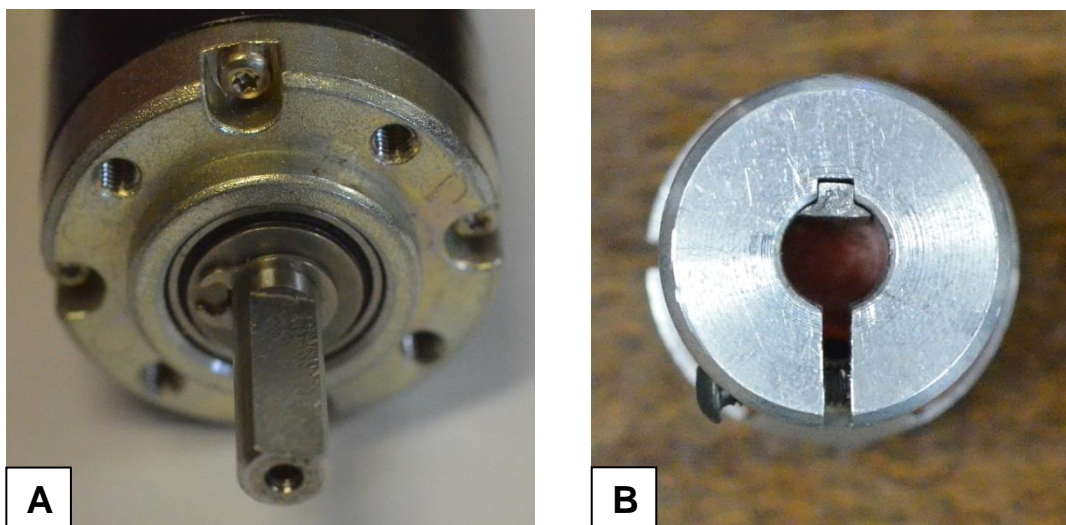

Figure C.8: (A) The axis of the motor with a flat segment, (B) The axial coupling with the coupling key inserted
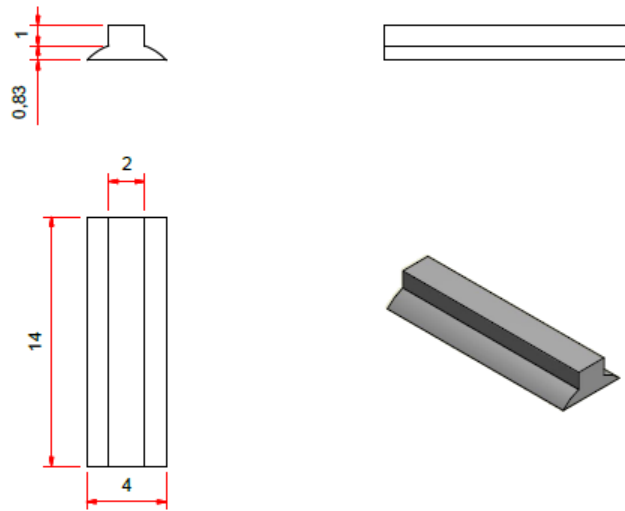
185

Figure C.9: Actuator connector flange

After all the linear actuator components were in place and connected, a steel protective cover, as shown in Figure C.10, was installed to protect the motor assembly and wiring from potential damage.
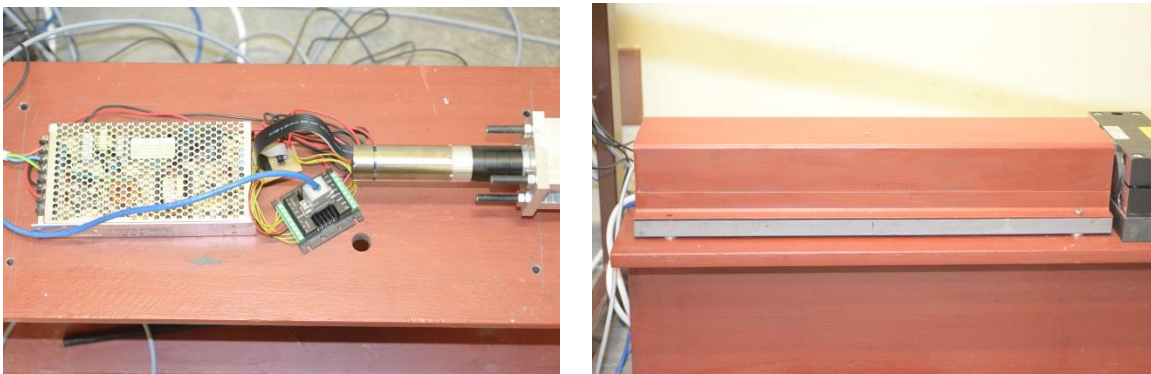

Figure C.10: Installed motor assembly and protective cover

C.3. Performance evaluation

As the displacement rate of the linear actuator could only be specified in terms of rotational velocity in the Motion Manager 5.2 software package, the following conversion was done in order to determine the required rotational velocity to result in a specific displacement rate required.

$$\frac{Rotational\ velocity\ [rpm]}{Reduction\ factor\ of\ gearhead} = \frac{Displacement\ rate\ [mm/min]}{Screw\ lead\ [mm]}$$

The screw lead is defined as the linear displacement of the actuator carriage for one full rotation of the actuator axial. This was 4 mm for the EPX 50 actuator. Thus to achieve a constant displacement of 0.25 mm/min, as was used for the experimental tests in this study, the required rotational velocity was determined as follows:

$$Rotational\ velocity\ =\ \frac{0.25\ \times\ 2074}{4}$$

$$Rotational\ velocity\ =\ 129.6\ rpm$$

Preliminary tests using a variety of displacement rates from 0.05 to 2 mm/min was conducted. The linear actuator proved to perform excellently for all displacement rates that were tested. Figure C.11 indicates the displacement and stress recorded over time for a typical early age concrete specimen with a relatively high strength and Young's modulus for early age concrete. The maximum tensile stress translates to 138.4 N. The displacement was measured by two linear variable differential transformers (LVDT's) mounted on the outside of the tensile test mould, from which the average was determined. A capture rate of 50 Hz was utilized. The practically perfectly straight line, with a gradient of 0.25 mm/min, gives an indication of how accurate and effective the linear actuator performed while exerting an actively varying tensile force.
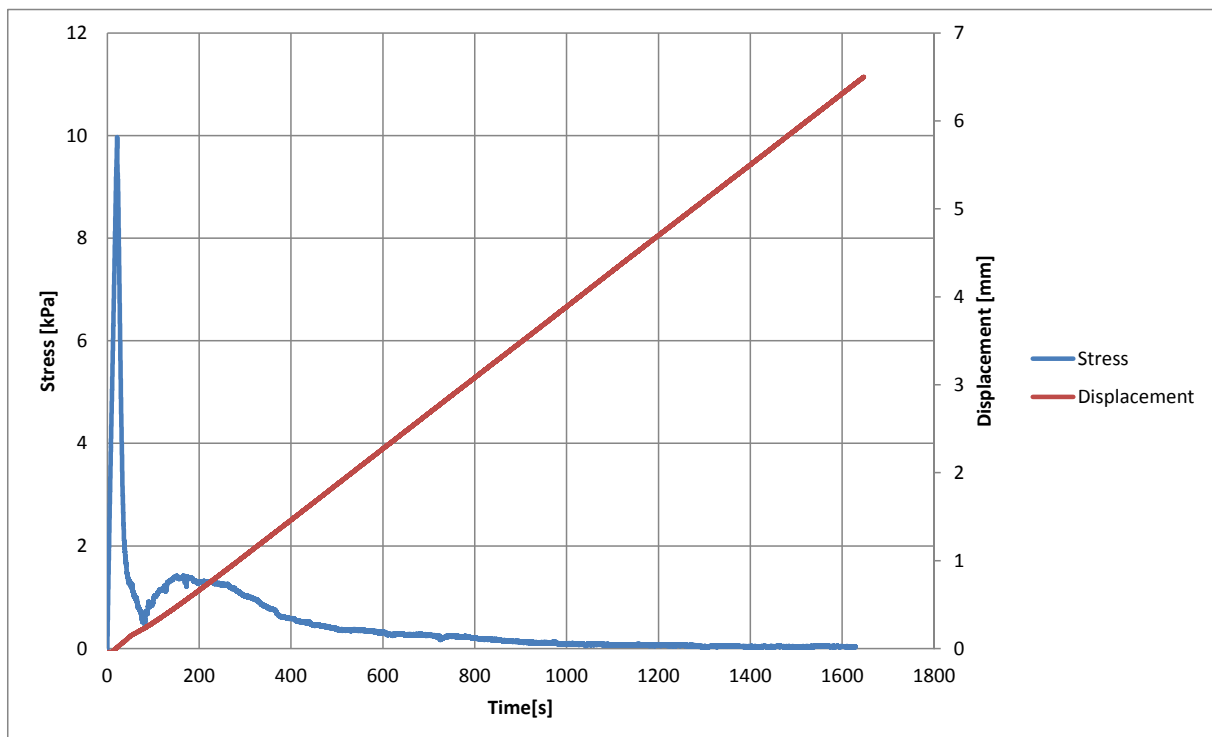

Figure C.11: Typical displacement and stress over time curve for an early age concrete specimen

From Figure C.11 it is clear that the initiation of displacement coincides with the increase in the measured load. This is in stark contrast to the displacement and stress over time curve, as shown in Figure 4.8, of initial tensile test setup. Although the displacement rate remained constant, the load application system was not rigid enough to capture the ascending portion of the specimen's stress-strain behaviour, as described in Section 4.2.

C.4. Summary

This appendix describes the linear actuator setup used in this study. Firstly, the requirements of the load application method are discussed, whereafter the most viable option is identified. Next the components of the linear actuator setup are described as well as the design and construction processes. Finally, the performance of the actuator is evaluated and it is found to satisfy all the requirements of this study.

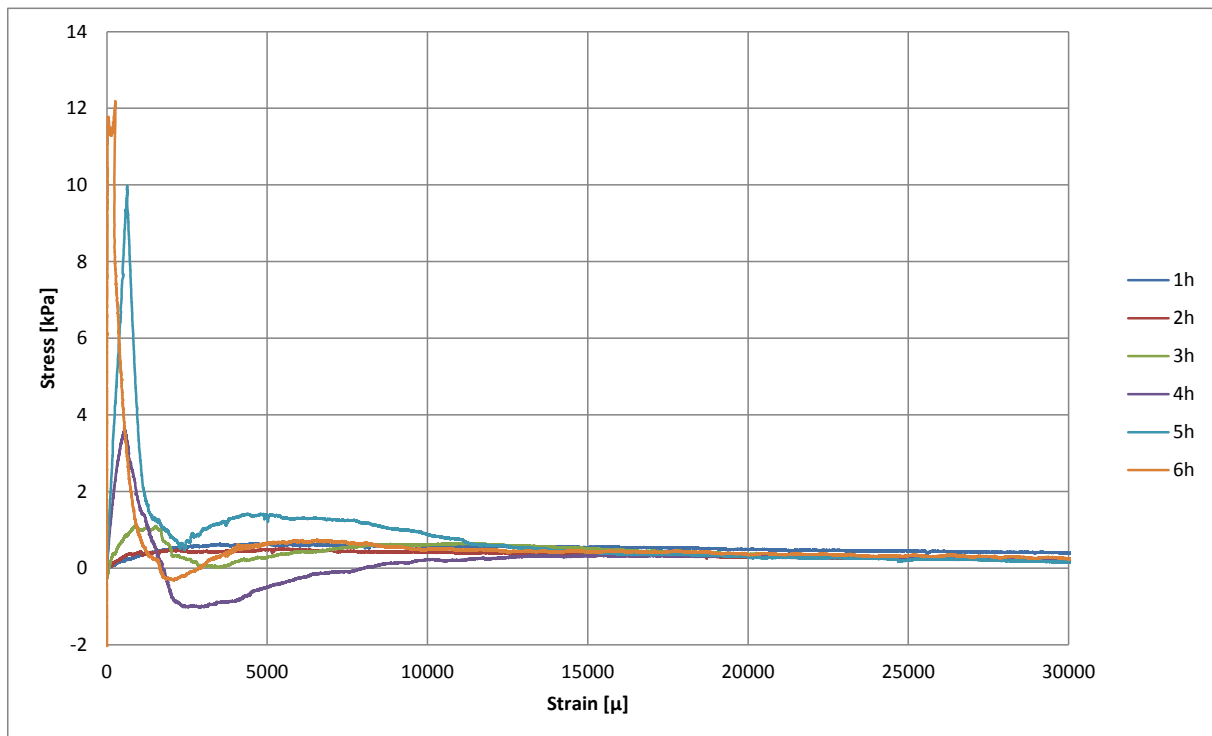# Appendix D: Stress-strain curves of early age concrete

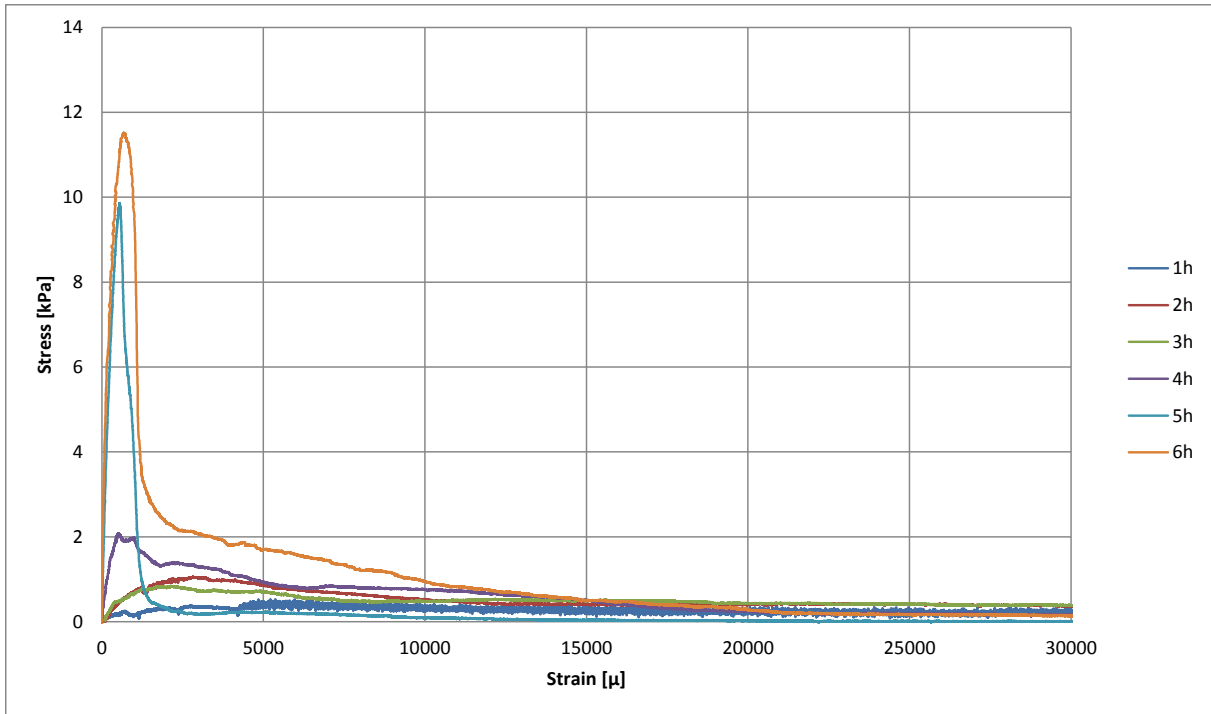**Figure D.19: Reference mix (MR)**

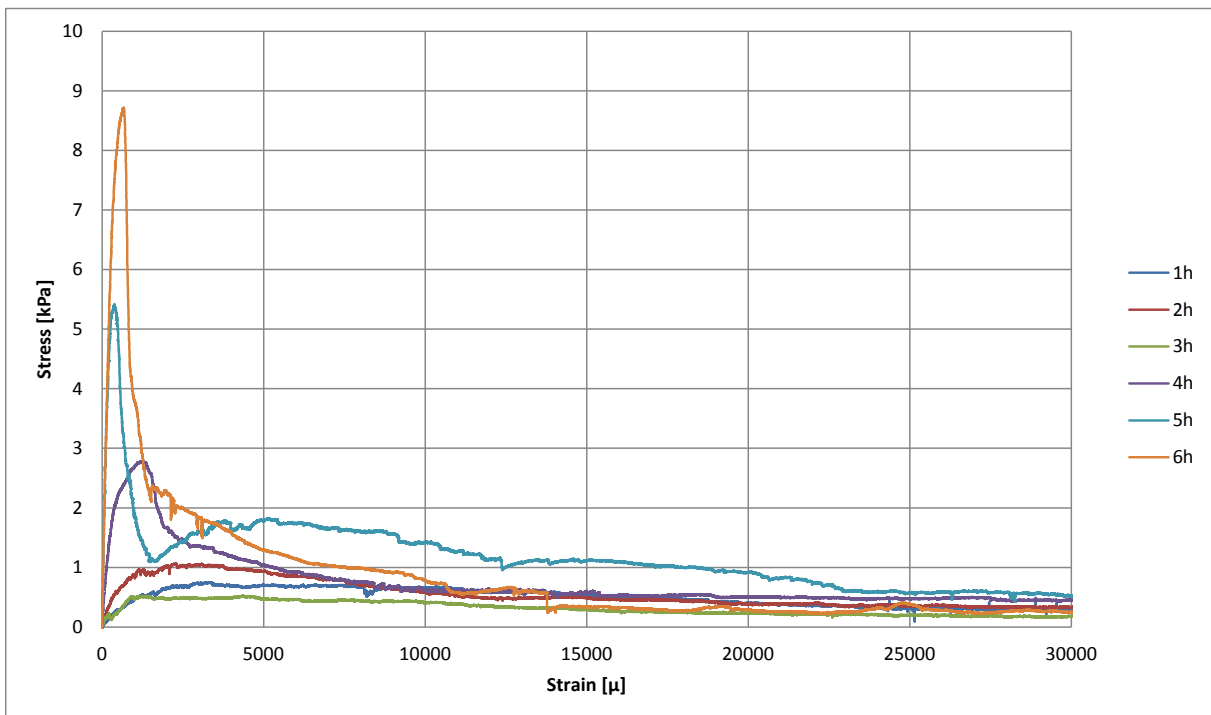**Figure D.2: 9 mm aggregate mix (MA9)**

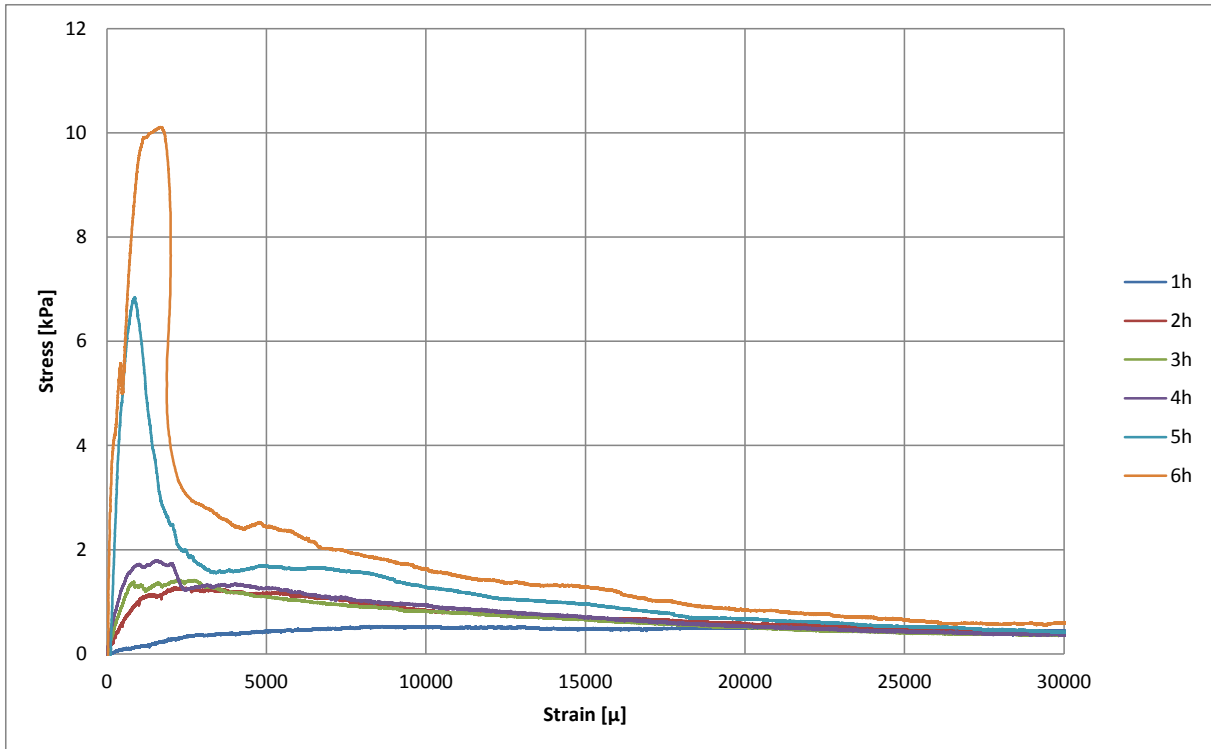**Figure D.3: 19 mm aggregate mix (MA19)**

190

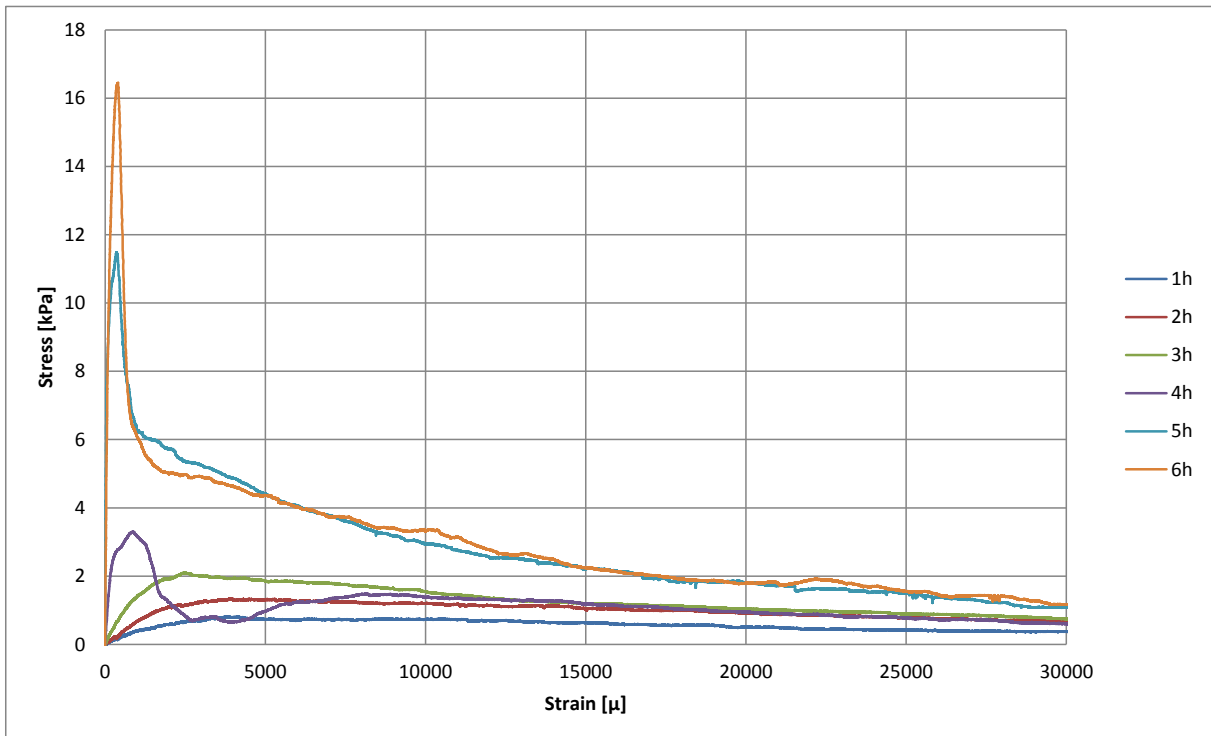**Figure D.4: 0.6 kg/m^3 polypropylene microfiber mix (MF0.6)**

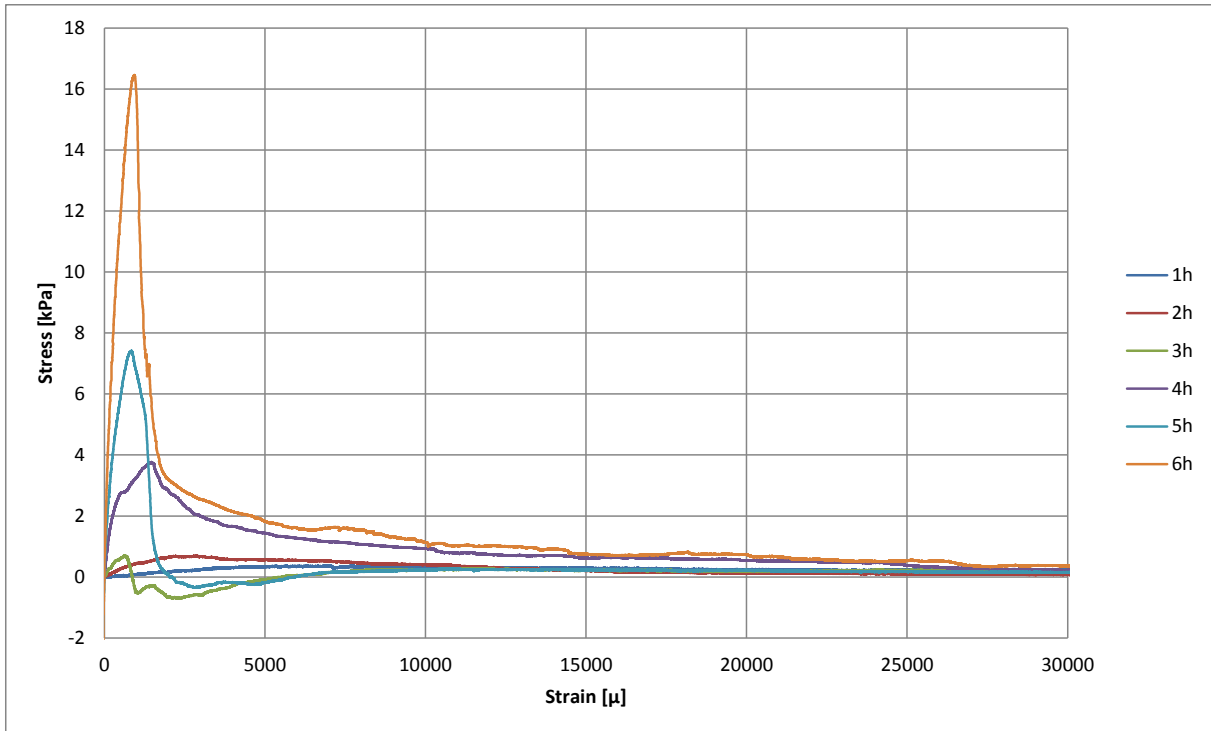**Figure D.5: 1.8 kg/m^3 polypropylene microfiber mix (MF1.8)**

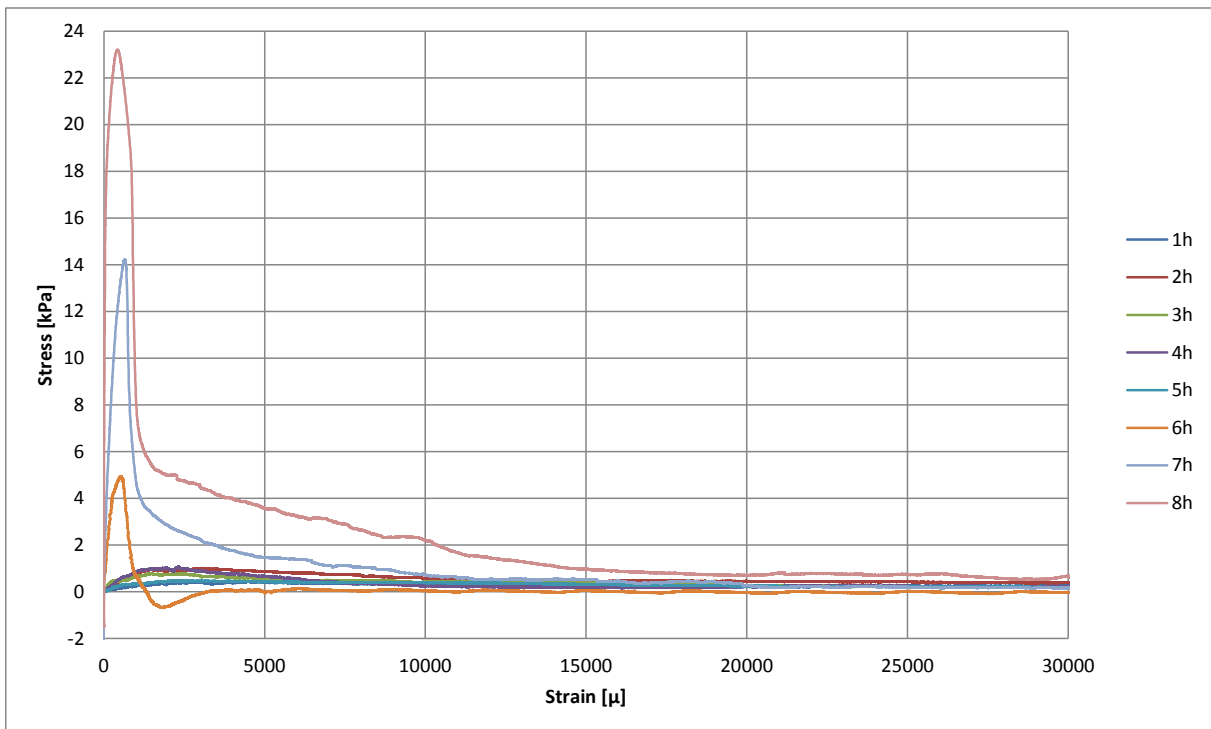**Figure D.6: Accelerated mix (MSA)**

Figure D.7: Retarded mix (MSR)

192

Appendix E: Tensile properties of early age concrete

Table E.1: Ascending stress-strain tensile properties of early age concrete

Mix	Age [hour]	f_t [kPa]	ε_c [µ]	E [MPa]
MR	1	0.64899	4624.6	0.23496
	2	0.51130	5525.6	0.60778
	3	1.1056	897.18	2.3236
	4	3.6085	562.50	7.3146
	5	9.9675	631.25	17.917
	6	12.178	-	-
MA9	1	0.52654	5370.3	0.26192
	2	1.0501	2768.7	0.75880
	3	0.8441	2135.9	1.3214
	4	2.0739	531.25	4.9318
	5	9.8578	543.75	23.322
	6	11.519	675.00	28.857
MA19	1	0.75280	3335.0	0.51831
	2	1.0657	2281.5	1.1629
	3	0.52142	1168.8	0.32704
	4	2.7817	1181.3	5.4549
	5	5.4078	381.25	17.816
	6	8.7114	650.00	22.023
MF0.6	1	0.53284	8062.5	0.07025
	2	1.2741	2755.3	1.1755
	3	1.4145	2733.8	2.5516
	4	1.7959	1600.0	2.3807
	5	6.8328	875.00	15.131
	6	10.108	1637.5	7.9573
MF1.8	1	0.81941	3817.1	0.45622
	2	1.3379	3882.2	0.71172
	3	2.0983	2479.1	1.5463
	4	3.2968	881.25	11.629
	5	11.479	356.25	135.43
	6	16.446	406.25	84.221
MSA	1	0.38677	8293.8	0.06038
	2	0.68074	2154.4	0.48867
	3	0.70475	618.75	1.5985

	4	3.7671	1462.5	6.6772
	5	7.4217	843.75	12.563
	6	16.455	931.25	22.2246
MSR	1	0.43912	4462.5	0.16899
	2	1.0147	3045.3	0.82596
	3	0.79443	1494.1	3.3792
	4	1.0626	2324.1	1.0220
	5	0.47157	2064.1	1.1021
	6	4.9380	531.25	12.698
	7	14.210	650.00	30.269
	8	23.1965	418.75	293.19

Table E.2: Descending stress-strain tensile properties of early age concrete

Mix	Age [hour]	G_F [J/m^2]	l_{ch} [m]
MR	1	13.1248	7.3218
	2	8.08638	18.799
	3	11.9103	22.638
	4	7.6311	4.2866
	5	20.072	3.6198
	6	14.613	-
MA9	1	8.7372	8.2540
	2	13.741	9.4557
	3	13.732	25.464
	4	16.888	19.363
	5	5.8979	1.4154
	6	26.976	5.8659
MA9	1	13.147	12.024
	2	14.854	15.208
	3	9.0721	10.912
	4	20.179	14.225
	5	33.967	20.693
	6	21.950	6.3701
MF0.6	1	9.6087	2.3775
	2	19.636	14.219
	3	18.229	23.242
	4	21.982	16.229
	5	32.491	10.530

194

	6	39.593	3.0833
MF1.8	1	15.082	10.248
	2	26.195	10.415
	3	34.958	12.278
	4	34.553	36.968
	5	81.685	83.954
	6	83.304	25.938
MA9	1	5.7424	2.3178
	2	7.5104	7.9197
	3	5.7006	18.348
	4	23.688	11.146
	5	13.721	3.1298
	6	35.712	2.9312
MA19	1	6.9213	6.0655
	2	14.372	11.528
	3	10.608	56.796
	4	8.5823	7.7669
	5	9.7869	48.502
	6	1.8634	0.97045
	7	24.845	3.7240
	8	61.744	33.644